Role of Synthetic and Dimensional Synthetic Organic Chemistry in Block Copolymer Micelle Nanosensor Engineering

Ek, Pramod Kumar

Publication date:
2012

Document Version
Publisher's PDF, also known as Version of record

Technical University of Denmark

Role of Synthetic and Dimensional Synthetic Organic Chemistry in Block Copolymer Micelle Nanosensor Engineering

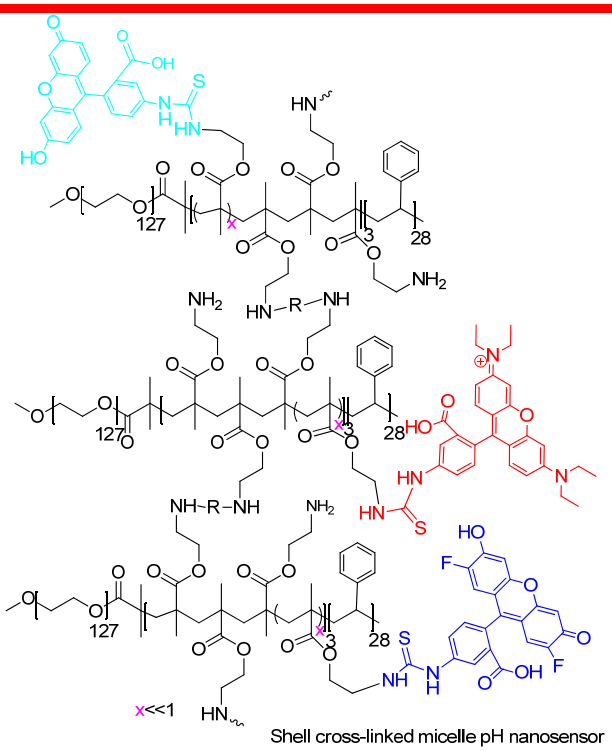

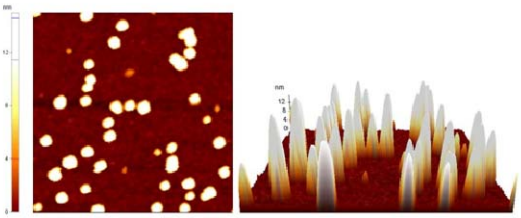

PhD thesis

Pramod Kumar EK

2012

DTU Nanotech
Department of Micro- and Nanotechnology

Role of Synthetic and Dimensional Synthetic Organic Chemistry in Block Copolymer Micelle Nanosensor Engineering

Pramod Kumar EK

Ph.D. Thesis

January 2012

Department of Micro- and Nanotechnology (DTU Nanotech)

Technical University of Denmark

DK-2800 Kgs. Lyngby

Denmark

Acknowledgement

The thesis is the result of my Ph.D project carried out in Department of Micro- and Nanotechnology at the Technical University of Denmark (DTU) from 2009 to 2012. The project was financed by Kræftens Bekæmpelse and the Danish Research Council for Technology and Production (Grant 274-07-0172). The project has been supervised by Associate Professor Thomas L. Andresen and Professor Kristoffer Almdal

First and foremost I express my profound gratitude to my supervisor Professor Thomas L. Andresen for giving me the opportunity of working on this interesting interdisciplinary project. I have always appreciated your constant encouragement, support and guidance throughout the project. I owe my sincere thankfulness to my supervisor Professor Kristoffer Almdal for the helpful discussions and suggestions especially during my thesis writing. This dissertation would not have been possible without the support from both of you.

I am thankful to Dr. Jonas R. Henriksen and Dr. Sokol Ndoni for the kind helps they have offered during fluorescence and GPC measurements.

I would like to thank Lotte Nelsen, Ole Kristoffersen and Lene Hubert for all the technical assistance they have provided during my study

There are few of my lab mates I would like to mention individually. I am obliged to Dr. Honghao Sun for maintaining a good working environment in the synthesis lab and the office, Lise N. Feldborg for the AFM and TEM measurements, Dr. Thomas P. Etzerodt and Dr. Rasmus I. Jølck for the training they offered in peptide synthesis, Nynne M. Christensen, Rikke V. Benjaminsen for the cell experiments, and Andreas I. Jensen for his help in CMC measurements. All my other colleagues are also acknowledged for many pleasurable experiences throughout the last three years.

I would like to thank my entire extended family, and friends all over the world who have always given the help and support whenever wherever it was needed. Basil Uthuppu and his wife Dr. Susan Kurian is especially acknowledged for all the helps they have provided for the last one year.

Last, but not at all least, I would like to thank my parents, my mother's sister and my brother for their love, prayers and support throughout this journey.

Kgs. Lyngby, 27th December 2011. Pramod Kumar EK

Abstract

This thesis investigated the role of amphiphilic triblock copolymer micelle nanomaterials in nanosensors, with emphasis on the synthesis of micelle particle sensors. The thesis is focused on the role of synthetic and dimensional synthetic organic chemistry in amphiphilic triblock core-shell-corona micelle based ratiometric fluorescence pH nanosensor fabrications. Two synthetic strategies such as post micelle modification and mixed micellisation (co-micellisation) were employed for pH nanosensor synthesis.

In the post micelle modification strategy, dimensional synthetic modifications on polymer micelles were performed. The structural potential of amphiphilic functional triblock copolymer self-assembly to provide regioselective functionalization and cross-linking was the key factor for this approach. Initially, functional amphiphilic triblock copolymers (functional unimers) were prepared by synthesis based on isolated macroinitiator ATRP of protected functional monomers. Self-assembly of these functional unimers in water resulted in functional core-shell-corona micelles. The functional micelles were stabilized by covalent cross-linking at the distinct functional shell or core domains of the micelle. The cross-linked micelles were converted into ratiometric pH nanosensors by conjugating pH sensitive and reference fluorophores at the shell region.

The amphiphilic triblock copolymers, PEG-*b*-PAEMA-*b*-PS, PEG-*b*-PAEMA-*b*-PES and PEG-*b*-PAEMA-*b*-PCMA, were used for the preparation of functional micelles. Shell cross-linking on PEG-*b*-PAEMA-*b*-PS micelles was performed by amidation reactions between the amino groups of PAEMA blocks using a di-carboxylic acid cross-linker. Also a dendritic cross-linker based click chemistry was used to stabilize the PEG-*b*-PAEMA-*b*-PES micelle having click readied PES core. In another study, UV radiation was used to induce non-reversible and reversible photo core cross-linking of core-shell-corona functional micelles were also investigated. A PEG-*b*-PAEMA-*b*-PES micelle core was photo cross-linked by UV induced oxidative coupling between alkyne groups present at the micelle core. In a different system, reversible photo dimerization of coumarin was used to construct reversibly photo core cross-linked PEG-*b*-PAEMA-*b*-PCMA micelle. By conjugating pH sensitive and reference fluorophores at the shell regions of the shell and core cross-linked micelles, pH nanosensors were synthesized with sensitivity ranges that were appropriate for pH measurements in living cells. The sensitivity ranges of the nanosensors were simply altered by changing the fluorophores conjugated to the shell region.

Nanosensors having targeting capabilities were synthesized by mixed micellisation or co-micellisation strategy. In this approach, the amphiphilic triblock copolymers synthesized by ATRP were further modified, and conjugated with targeting ligands and fluorophores. The co-micellisation of this functionalized amphiphilic triblock copolymers resulted in functionalized mixed micelle nanosensors. Post polymer modifications were easier to implement and quantify than post micelle modifications; hence the co-micellisation strategy provided more precise knowledge about the composition of the nanosensor.

Targeted non-cross-linked and targeted cross-linked ratiometric pH nanosensors were prepared by mixed micellisation or a co-micellisation strategy. Fluorophores and octaarginine conjugated amphiphilic triblock copolymers were synthesized by post-polymer modifications of PEG-*b*-PHEMA-*b*-PMMA and NH_2-PEG-*b*-PHEMA-*b*-PMMA. Co-micellisation of these functionalized triblocks resulted in octaarginine surface functionalized mixed micelle pH nanosensors. Similarly, a cross-linked cyclic RGD peptide targeted mixed micelle nanosensor was also prepared. The cyclic RGD peptide (cRGDfK) and fluorophores were conjugated to the amphiphilic triblock copolymers, NH_2-PEG-*b*-PAzEMA-*b*-PMMA and PEG-*b*-PAzEMA-*b*-PMMA. Mixed micellisation of these functionalized unimers followed by dendritic click shell cross-linking resulted in a stable cRGDfK targeted mixed micelle pH nanosensor.

Thus, the engineerability of triblock core-shell-corona micelle was utilized for the synthesis of ratiometric pH nanosensor having desired pH sensitivity ranges.

Contents

List of Figures

List of Schemes

List of Tables

List of Abbreviations

2D	2-Diamensional
3D	3-Diamensional
AFM	Atomic Force Microscopy
Alexa	Alexa Fluor
ATRP	Atom Transfer Radical Polymerization
-*b*-	block
BCECF	2′,7′-bis- (2-carboxyethyl) -5-(and-6) carboxyfluorescein
Boc	*tert*-Butoxycarbonyl
ca.	Approximately
cm^{-1}	Wavenumber
CMC	Critical Micelle Concentration
CMT	Critical Micelle Temperature
CuAAC	Copper Catalyzed Azide-Alkyne Cycloadditions
DCM	Dichloromethane
D_h	Hydrodynamic diameter
DLS	Dynamic Light Scattering
DMF	Dimethylformamide
DMSO	Dimethyl sulfoxide
DP_n	Degree of Polymerization
FA	Fluorescein
FRET	Fluorescence Resonance Energy Transfer
FT-IR	Fourier Transform Infrared
GPC	Gel Permeation Chromatography
h	hours
MeOH	Methanol
mL	Milliliters
mg	Milligram
LCST	Lower Critical Solution Temperature
M_n	Number-average Molecular Weight
mV	Millivolt

M_w	Weight Average Molecular Weight
MWCO	Molecular Weight Cut-off
nm	Nanometer
NMP	Nitroxide-Mediated Polymerization
NMR	Nuclear Magnetic Resonance
OG	Oregon Green
PAEMA	Poly (2-aminoethyl methacrylate)
PAzEMA	Poly (2-azidoethyl methacrylate)
PCMA	Poly (coumarin methacrylate)
PEG	Poly (ethylene glycol)
PES	Poly (ethynyl styrene)
PHEMA	Poly (hydroxyethyl methacrylate)
PMMA	Poly (methyl methacrylate)
PS	Poly (styrene)
RAFT	Reversible Addition Fragmentation Chain Transfer
RhB	Rhodamine B
RT	Room Temperature
SEC	Size-Exclusion Chromatography
TEM	Transmission Electron Microscopy
Teoc	2-Trimethylsilylethyl Carbamate
T_g	Glass Transition Temperature
THF	Tetrahydrofuran
TLC	Thin Layer Chromatography
TM	Transition Metal
TMS	Trimethylsilane
vs	versus
UV	Ultraviolet
W	Watt
δ	Chemical shift
λ	Wavelength
µl	Microliter
ξ	Zeta potential

Outline

The thesis is primarily concerned with the role of synthetic and dimensional synthetic chemistry in the fabrication of amphiphilic triblock copolymer micelles based nanosensors. Nanosensors are specifically designed for fluorescence based ratiometric intracellular pH monitoring.

The first chapter gives a brief introduction of controlled radical polymerization techniques, synthesis of amphiphilic block copolymers by ATRP, block copolymer self-assembly in water, chemistry behind the functionalization and cross-linking of polymeric micelles, and polymeric pH nanosensors in biology.

Chapter 2 describes the transformation of stabilized amphiphilic triblock copolymer micelles into ratiometric pH nanosensors *via* post micelle modifications. This chapter is divided into two sections. Section 2.1 introduces the synthesis of the intermediate layer cross-linked ratiometric PEG-*b*-PAEMA-*b*-PS micelle nanosensors. Section 2.2 deals with the synthesis of dendritic click core cross-linked ratiometric pH nanosensors from PEG-*b*-PAEMA-*b*-PES micelle.

The third chapter deals with the use of UV radiation in polymeric micelles based pH nanosensor fabrications. In this chapter, section 3.1 describes the transformation of photo core cross-linked PEG-*b*-PAEMA-*b*-P(SC≡CH) micelle into ratiometric pH nanosensor. Section 3.2 describes the synthesis of reversibly photo core cross-linked ratiometric pH nanosensors from PEG-*b*-PAEMA-*b*-PCMA micelle.

The chapter 4 deals with the preparation of pH nanosensors by co-micellisation of functionalized amphiphilic triblock copolymers having similar composition. The chapter is divided into two sections. Section 4.1 deals with the synthesis of targeted ratiometric pH nanosensors by co-micellisation of functionalized R-PEG-*b*-PHEMA-*b*-PMMA. Section 4.2 demonstrates the synthesis of the intermediate layer cross-linked and targeted ratiometric pH nanosensors from functionalized R-PEG-*b*-PAzEMA-*b*-PMMA *via* mixed micellisation and dendritic click shell cross-linking.

A general summary and outlook are given in chapter 5.

All references used in the thesis can be found in chapter 6 under bibliography.

After bibliography, the papers published (or under communication) as a part of the PhD study can be found in the following appendices:

Appendix A deals with part of the work presented in the section 2.1 of the thesis
Appendix B demonstrates the work presented in section 2.2 of the thesis
Appendix C explains the work presented in section 3.1 of the thesis
Appendix D illustrates the work presented in section 3.2 of the thesis
Appendix E shows part of the work presented in section 4.1 of the thesis
Appendix F represents part of the work presented in section 4.2 of the thesis

Chapter 1

Introduction

Linear amphiphilic block copolymers are schizophrenic macromolecules having two or more polymer blocks of different chemical composition joined together by covalent bonds in a single main chain, in which one part of the macromolecule likes the solvent (water) while the other part does not. Microphase separation of block copolymers in the melt and solutions is examples of block copolymer self-assembly. In the melt, the repulsive interactions between the monomers of different blocks are the driving forces for their self-assembly, where as in solutions, selective segmental solubility of block copolymers also contributes to the self-assembly. The structure, symmetry and flow characteristic of the resulting supramolecular aggregates in solution depends the block copolymer composition and architecture.[1] Therefore, the recent developments in synthetic polymer chemistry are focused on ease and efficient ways of synthesizing block copolymers having well defined architecture, precisely controlled molecular weight and narrow molecular weight distribution.[2] Spontaneous nanoscale phase separation of such block copolymers in block selective solvents can provide nanotechnology in its inexpensive bottom up approach. The introduction chapter is concerned with controlled radical polymerization in amphiphilic block copolymer synthesis, amphiphilic block copolymer self-assembly in water, dimensional synthetic modifications of polymeric micelles and polymeric pH nanosensors in biological sensing.

1.1 Controlled radical polymerization

In recent years, controlled radical polymerization (CRP) has emerged as the method of choice for the synthesis well defined polymeric materials having molecular, compositional and structural homogeneity. Previously this can only be achieved by living ionic polymerization.[3, 4] In ideal living polymerization, initial initiator concentration $[I_0]$ is equal to the number of growing chains hence the theoretical molecular weight or degree of polymerization (Dp_n) increases with the decrease in initiator concentration ($Dp_n = [M_0]/[I_0] \times$conversion). As a result, the apparent molecular weight (M_n) of the polymers increases with monomer conversion and the polydispersity (M_w/M_n) decreases with the monomer conversions. Living ionic polymerization is divided into anionic and cationic, in which the anionic polymerization is known as ‘true living’ polymerization. In anionic polymerization, hetrolytic scission of monomer double bond occurs *via* conjugate addition of

anionic initiator to the monomer. The anionic chain then propagates and results in living polymers (**Scheme 1.1**). Broadly cationic polymerization is mechanistically similar to anionic except the fact that the active anions are replaced by the reactive cations. The anionic polymerization is highly sensitive to moisture, oxygen and other acid base impurities. Though, the cationic polymerizations are comparatively less sensitive to the oxygen, carbon dioxide and water; unwanted intrinsic termination and chain transfer reactions reduces the polymerization control as compared to the anionic polymerizations. In addition to the practical difficulties, monomers that can be polymerized by living ionic polymerization are limited to number of vinylic and cyclic monomers.

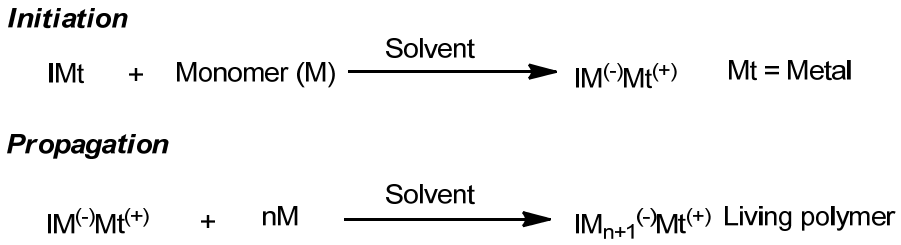

Scheme 1.1. Mechanism of anionic polymerization.

Conventional radical polymerization (RP) is a robust technique applicable to a wide range of monomers and operation conditions (even in water-emulsion polymerization) with the advantages of functional group tolerance. The application of this technique in block copolymer synthesis is limited by highly non-selective reactions and non-trivial product control. The basic difference between a conventional living ionic polymerization and radical polymerization is that, for living ionic polymerization the rate of initiation (Ri) is faster or comparable with the rate of propagation (Rp). Hence all the chains initiate and propagate at the same time and results in the same degree of polymerization (Dp_n). In radical polymerization, the chain propagation is faster or comparable with the initiation ($Ri \leq Rp$). This helps to keep radical concentration low (ppm or ppb) and hence reduces the diffusion controlled radical reaction. The fast propagations rate prevents the modifications or functionalization of the growing chains and end up with high molecular weight homo dead polymers.[5] This limits its scope in block copolymer synthesis.

The controlled radical polymerization (CRP) combines the advantages of radical polymerization and living polymerization by introducing equilibria between the dormant species and the propagating radicals. During the chain growth, the propagating radical can be deactivated to dormant species, which are resistant towards termination. The dormant species can be reactivated

again to the propagating radical. This reversible living radical process considerably reduces the concentration of free radicals and hence the proportion of terminated chains during the polymerization. The 3 main controlled radical polymerization techniques are nitroxide mediated (NMP), reversible addition fragmentation chain transfer (RAFT) and atom transfer radical polymerization (ATRP). The first report of CRP is dithiauram disulphide based iniferter polymerization.[6]

NMP is a stable free radical mediated controlled radical polymerization. The polymerization can be initiated by a bimolecular initiating system composed of a radical source (*e.g.* benzyl peroxide (BPO)), and a stable free radical[7] (*e.g.* 2,2,6,6-tetramethyl-1-piperidinyloxy (TEMPO) or by a unimolecular initiating system (alkoxy amine initiators).[8] The unimolecular initiator system (reactive radical and stable radical on the same molecule, **1**) have the advantage of complete control over the initiation but the temperature required for the polymerization is higher than that of bimolecular NMP. Mechanistically NMP is reversible deactivation of the reactive radical **2** by coupling with stable nitroxide radical **3** (**Scheme 1.2**).

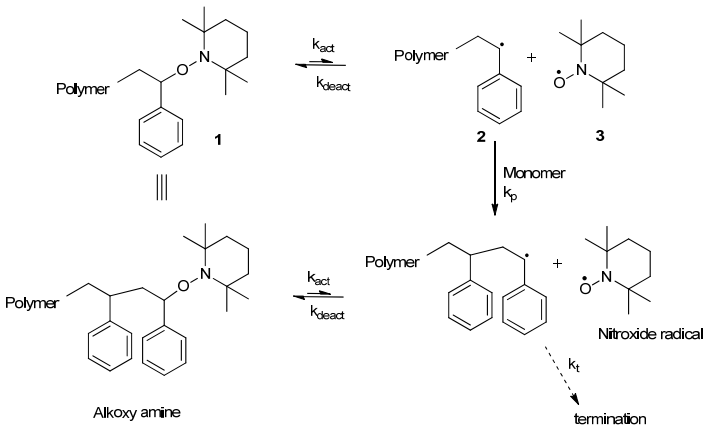

Scheme 1.2. Unimolecular nitroxide mediated copolymerization.

Wide variety of monomers can be copolymerized by NMP, but methacrylates are the exception. This due to the degradation of the methacrylate propagating radical *via* β-hydrogen abstraction by the nitroxide results in the formation of hydroxyl amine. The hydroxylamine thus formed will act as a chain transfer agent and terminate another propagating chain. One of the other disadvantages of NMP is the requirement of library of alkoxyamine initiators for polymerization.[9, 10]

Reversible addition fragmentation chain transfer[11] is another example of CRP technique that provides living characteristics to radical polymerization. The main difference of RAFT over the conventional radical polymerization is the presence of degenerative chain transfer (addition fragmentation) equilibria (S**cheme 1.3**). Like conventional radical polymerization, the reaction is initiated by an external radical source **4**, but the propagating chain **5** are then added to a RAFT chain transfer agent (RAFT-CTA) **6** in degenerative manner and maintain pre-chain transfer equilibria. A RAFT chain transfer agent (RSC(=S)Z) composed of a decent homolytic living group capable to reinitiate the polymerization ($R^{\cdot}$), a reactive C-S double bound and an Z group which controls the reactivity of the C-S double bond and hence influences the rate of radical addition and fragmentation. The fragmentation of the pre-chain transfer equilibria (k_{β}) can generate a new free radical **9** which is capable of re-initiating the polymerization and generate new propagating radicals **10**. In the main chain transfer equilibria, the macro-radical **10** is reacting with the polymeric RAFT agent **11** in a degenerative manner and maintain equilibrium between the dormant and living chains, thus allowing all the chains to grow at the same rate. The termination reactions are not suppressed in RAFT. Retention of thiocarbonylthio groups in the final polymers shows the living nature and possibilities of block copolymer synthesis.

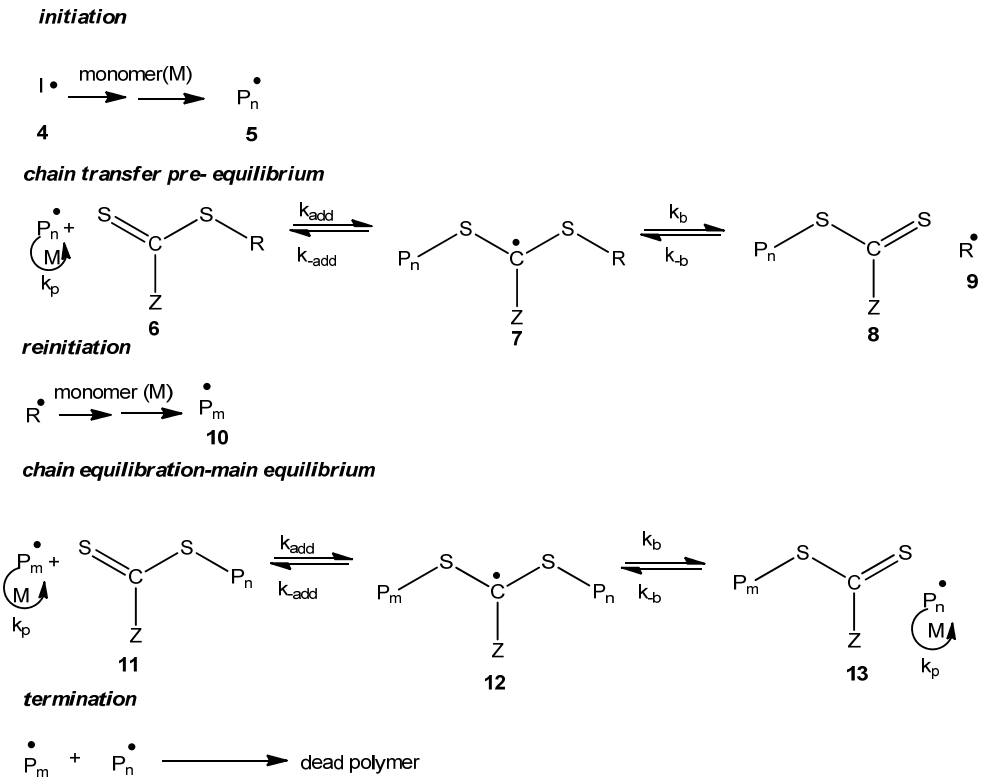

Scheme 1.3. Mechanism of RAFT polymerization.

Synthesis of well defined polymers by RAFT required a fast attainment of pre-equilibrium and high re-initiation capability of (R·). The total number of propagating chains **5** or **10** must be lower than the dormant species **8** or **13** and/or the intermediate radicals **7** or **12**. RAFT polymerization can easily be performed by classical radical polymerization equipments with a wide range of monomers even having unprotected functional groups. Additional catalyst removal steps are not necessary, and RAFT can be employed to all the radical polymerization procedures (solution, emulsion and suspension) with the rate of polymerization comparable with the free radical polymerization. To polymerize wide range of monomers by RAFT, access to numerous RAFT agents is necessary. This is because the nature of monomers and the RAFT-CTA together decides the rate of propagation, control over the molecular weight and polydispersity of the polymers.[12] Synthesis of RAFT-CTA can be difficult and may require anaerobic and anhydrous reaction conditions and multistep purification procedures.[13] Another disadvantage of the RAFT technique is the color and smell of the polymer products due to the chain transfer agents.

Atom transfer radical addition (Kharasch reaction)[14] is the basis for the development of transition metal catalyzed controlled radical polymerization technique called atom transfer radical

polymerization (ATRP).[15, 16] Mechanistically standard ATRP is an inner sphere electron transfer process. The process involves a reversible homolytic (pseudo) halogen transfer between a dormant species (alkyl halide)-an added initiator (RX)-macroinitiator **14** (P_nX), or dormant propagating chain end ($R\text{-}P_nX$); and a transition metal complex in the lower oxidation state called activator **15** (Mt^zL_m) (Mt is a transition metal with oxidation state z, L is the ligand). This results in the reversible formation of propagating radical **16** ($R^{\cdot}$/ $P_n^{\cdot}$), and a higher oxidation state transition metal complex with coordinated halogen ligand **17** ($XMt^{z+1}L_m$) (deactivator). The active radical form with a rate constant k_{act}, subsequently propagate with the rate constant k_p and are reversibly deactivated - k_{deact}. Since ATRP is radical process, the active radical can also terminate with a rate constant k_t (**Scheme 1.4**).

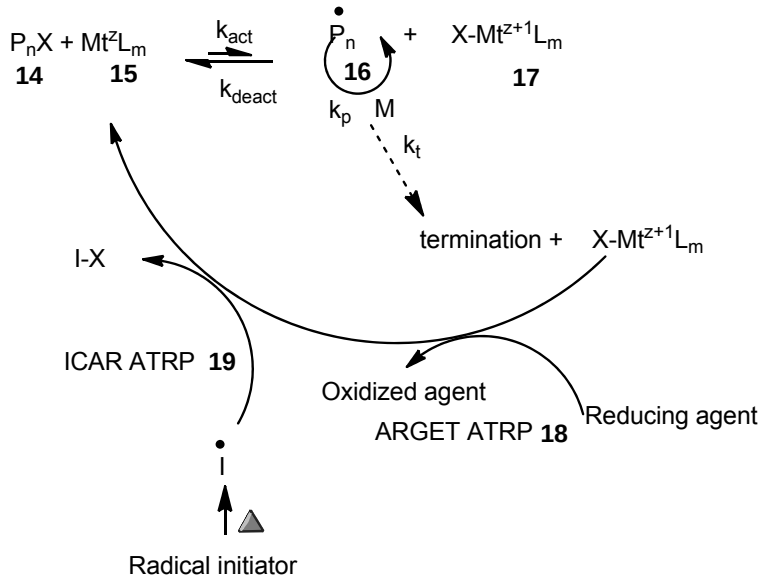

Scheme 1.4. Mechanism of ATRP. Mt = Cu (most common), Fe, Ru, Rh, Ni, Pd, Co, Os, Re, Ti *etc*., L depends on the nature of the transition metal, for copper it is multidenate ligands based on amine, imines or pyridine.[17]

Standard or normal ATRP uses excess amount of catalyst (typically 0.1-1 mole% of the monomer) to overcome the irreversible transformation of activators **15** into deactivators **17** resulting from the inevitable bimolecular radical termination reactions (1 to 10 % of the total chains). Therefore, additional purification steps are required to remove the excess catalysts from the final products. The equivalent of persistent radical (PRE)[18] (the higher oxidation state transition metal) can be added directly to the reaction prior to initiation. This increase the efficiency of initiation by reducing the fraction of low molecular weight radical termination reaction initially required to generate PRE (can also be formed *in situ* by reaction with dissolved oxygen). As a result of this, the equilibrium will

strongly shift towards the dormant species ($k_{act} << k_{deact}$). The ATRP equilibria ($K_{(ATRP)} = k_{act} / k_{deact}$) depends on the redox potential of the TM, also the halidophylicity ($X...Mt^{z+1}L_m$ bond strength) of the TM complex. Kinetics of ATRP shows the effect of kinetic parameters and reagent concentrations on rate of polymerization and polydispersity (**equation 1, 2**).[17] The rate of polymerization (R_p) is controlled by the ratio of activator **15** and deactivator **17**, and not the absolute amount of catalyst present in the reaction medium (**equ.1**). Polydispersity (M_w/M_n) is lower for the polymerization having higher deactivation (k_{deact}) rate or deactivator concentration. Polydispersity also decreases with the monomer conversion (Conv) and lower initiator concentration ($[RX]_0$) (**equ.2**).

$$R_p = K_{ATRP}\, k_p \frac{[M][RX][Mt^z L_m]}{[X\text{-}Mt^{z+1}L_m]} \quad \text{----------} \quad (1)$$

$$\frac{M_w}{M_n} = 1 + \left[\frac{k_p[RX]_0}{k_{deact}\,[X\text{-}Mt^{z+1}L_m]} \right] \left[\frac{2}{Conv} - 1 \right] \quad \text{------} \quad (2)$$

Since ATRP do not depend on the absolute activator or deactivator concentration, by keeping the activator/deactivator ratio constant, ATRP can be operated at extremely low (ppm level) catalyst concentration.[19] The first reverse ATRP technique based on this idea is activators regenerated by electron transfer (ARGET)[20] ATRP (**18**). In ARGET ATRP excess of reducing agents (*e.g*.tin^{II}2-ethylhexanoate, glucose, ascorbic acid, amines, Cu^0 *etc*) are used for constantly regenerating the ATRP activator (Cu^I) from the deactivator (Cu^{II}) formed during radical terminations. The same process can be achieved by a radical initiator, called initiators for continuous activator regeneration (ICAR)[21] ATRP (**19**). In ICAR ATRP, a source of organic free radical (*e.g*.AIBN) is used for continuously regenerate the activator; which is otherwise, consumed in termination reaction-when catalysts are used at extremely low concentration. These low catalyst concentration techniques (**18, 19**) reduces the catalyst related side reactions[22] and offers almost catalyst free well defined polymers.

1.2 ATRP in amphiphilic block copolymer synthesis

Living ionic and living radical polymerization are the main techniques used for the synthesis of well defined block copolymers. The development of functional group tolerant metathesis catalyst by

Grubb also facilitated the block copolymer synthesis by ring opening metathesis polymerization (ROMP).[23] Ionic (anionic and cationic) polymerizations require extremely pure reagents and inert environment to prevent the accidental terminations of the living chains due to impurities. Recent achievements in control over radical polymerizations (CRP) overcome the synthetic difficulty of making well defined block copolymers. Among the living radical polymerization techniques, the transition metal complex catalyzed reversible redox process-ATRP has been used most extensively for the synthesis of block copolymers. ATRP do not demand any unique initiators as like (NMP) or group transfer agents as like in RAFT; all the reagents for ATRP are commercially available.

Conservation of livingness of the polymer chains and control over composition and molecular weight distribution facilitate the application of ATRP in block copolymer synthesis. First application is the synthesis of (polystyrene)-*b*-poly(methylacrylate) block copolymer.[15] Block copolymer synthesis by ATRP can be performed by two different methods, one pot sequential and isolated macroinitiator method.[24-27] In which, step wise isolation of macroinitiator can provide more pure block copolymers than adding the monomers sequentially in continuous ATRP process. The first amphiphilic block copolymer synthesized by ATRP is the synthesis of di and tri block copolymers of *n*-butyl acrylate with 2-trimethylsilyloxyethyl acrylate (HEA-TMS).[28] The sequence and control of block formation is dependent on the rate constant for cross propagation and propagation rate of the added monomers. For efficient block copolymer synthesis, the product of rate and equilibrium constant for the addition of macroinitiator to the added monomer should be comparable with the monomer propagation rate. If the rates are not comparable, then halogen exchange of the macroinitiator can change the equilibrium constant of cross propagation, this can provide control over the uncontrolled propagation rates of added monomers.[29] The control in block copolymer synthesis may also be achieved by sequential addition of a more reactive co-monomer to the less reactive propagating monomer block. The presence of less reactive monomer during the propagation of more reactive monomer can provide kinetic control by preventing uncontrolled propagation of the second block, but this process can affect the purity of the blocks.[30] Polymer synthesized by different mechanisms can be incorporated into ATRP block copolymer synthesis *via* converting them into macroinitiator. In which polyethylene glycol (PEO/PEG/POE) macroinitiator are extensively used for the synthesis of amphiphilic di and tri block copolymer synthesis. The PEG block has a wide range of application in medical and biotechnology field.[31] PEG can provide a hydrophilic block in the synthesis of amphiphilic block copolymers. PEG macroinitiator is first

used in ATRP by a Danish group, for the synthesis of poly(styrene)-*b*-poly(ethylene glycol)-*b*-poly(styrene) (PS-*b*-PEG-*b*-PS) as di-functional macroinitiator.[32] Nowadays mono and difunctional α-haloesters of polyethylene glycol have been extensively used in the di and tri block copolymerization of styrenic and acrylic monomers.[33-36]

Monomers having substituent that can stabilize the propagating radicals can be polymerized by ATRP. For polymerizations of each monomer, the corresponding alkyl halide chain end has its own unique redox potentials. Therefore, the polymerization of different monomers under same catalyst and identical conditions show different ATRP equilibrium constant (K_{ATRP}) and/or different propagating radical concentration. Due to this intrinsic propagation rate for each monomer the optimum value for K_{ATRP} may be obtained by tuning the other factors affecting the ATRP equilibria such as the amount and reactivity of transition metal catalysts, solvents, reaction temperature *etc*. For the synthesize of block copolymers having narrow molecular weight distribution, in copper catalyzed ATRP, the carboxylic acid, amino and alkynyl functionalities present in macroinitiators or monomers (**Figure 1.1** b, d, e, f, g, i) should be protected.[25, 37-39] The carboxylic acid in the monomer can cause catalytic poisoning by coordination with the transition metal, or can be protonate the nitrogen containing ligands. This affects the metal ligand coordination ability of the TM complex. The free amino groups in the monomers can also participate in complexation with the transition metals and alter the catalyst activity. The unprotected alkynyl moiety on the monomer can also suffer from undesirable side reaction such as acetylenic proton abstraction, nucleophilic addition to C≡C and thermal stability.

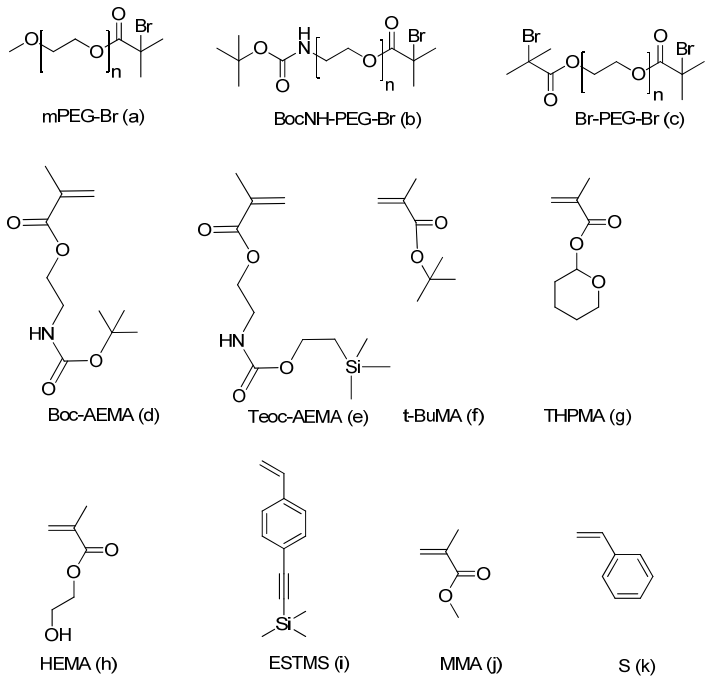

Figure 1.1. Representative PEG macroinitiators and monomers for ATRP.

1.3 Amphiphilic block copolymer self-assembly

Polymeric micelles are amphiphilic colloidal dispersion having the size range of 5 to 100 nm formed by the free energy driven spontaneous self-assembly[40-42] of amphiphilic block copolymers in dispersion media (water). When an amphiphilic block copolymer is placed in a solvent (water), difference in block solubility and solution-block(s) interactions enables the self-assembly of block(s). In details, the hydrophilic blocks forms hydrogen bonds and organizes the surrounding water molecules. Conversely, the hydrophobic blocks decrease the conformational entropy of water molecules by changing (decreasing) hydrogen bonding dynamics of water molecules as a result of hydrophobic hydration. The hydrophobic blocks are then stick together (dehydrations effects) to reduce the surface area exposed to water. This hydrophobic effect[43, 44] reduces the number of water molecules that are suffering from a decrease of conformational entropy. Experimentally this is achieved by dissolving the amphiphilic block copolymers in a common solvent for all the blocks and then slowly displacing the common solvent by selective solvent for the hydrophilic block (normal micelle) or the hydrophobic block (reverse micelle). The micelles are then kinetically trapped by the complete replacement of the common solvent by selective solvents. The concentration at which the first micelle is formed is called the critical micelle concentration (CMC)

and the number of unimers presents in this supramolecular aggregate to be aggregation number[45] of the micelle (**Figure 1.2**).

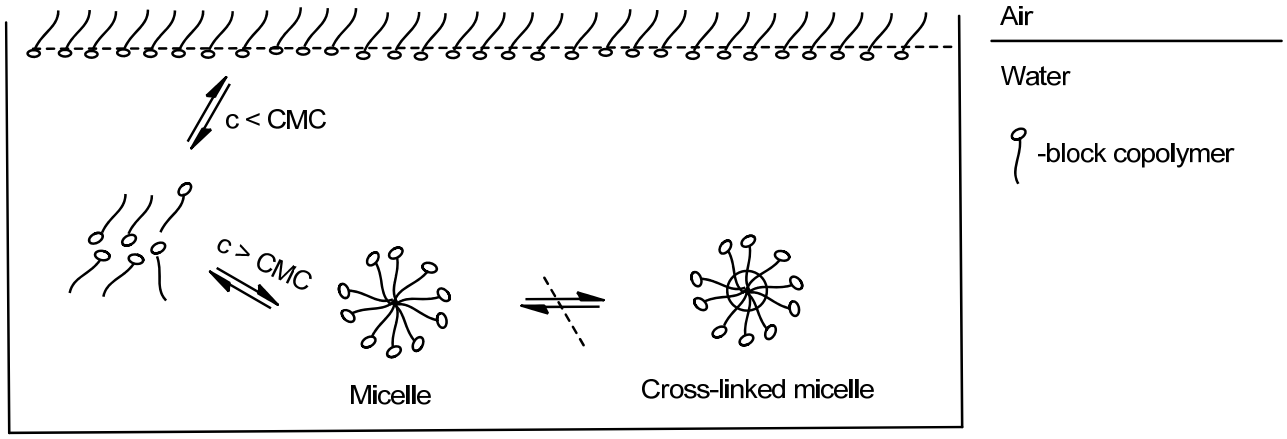

Figure 1.2. Schematic representation of self-assembly of amphiphilic molecules in water, at a concentration (c), above its critical micelle concentration (CMC).

The morphologies of the block copolymer aggregate are not only depends up on the conditions of self-assembly, but also the block copolymer compositions (packing parameters).[46, 47] Packing parameters *(p)=v/al*, *a* is the surface area of the hydrophilic block or head groups, *v* an *l* are volume and length of the hydrophobic blocks respectively. The packing parameters relate the properties of the molecule to the preferred curvature property of the aggregates. The symmetry of the aggregates increases with the decrease in packing parameters. For highly symmetric aggregates (spherical micelles), the packing parameter is 0.33, when *(p)* close to unity planar bilayers can be formed.[44]

The recent advances in block copolymer synthesis enable polymer self-assembly with precision and complexity as shown in natural systems like enzymes and viruses.[48] Amphiphilic diblock copolymers (AB) in block selective solvent can be self assembled into spherical core-shell micelle.[49] This well defined phase separated core-shell micelles have been extensively studied. This is due to its morphological and synthetic simplicity, entropically favorable diblock copolymer architecture in micellar state,[50] and a wide range of potential applications such as pharmaceutical carriers for therapeutics and molecular imaging agents.[51-54] Introductions of a third block (C) to the diblock (AB), and the resulting linear ABC triblock copolymers in bulk show number of morphologies.[55, 56] In which, core-shell-corona spheres and core-shell-corona cylinders are the common morphologies.[57, 58] ABC triblock copolymer self-assembly in block selective solvent can be classified into two center of symmetric micelles. Types 1- The micelles with compartmentalized core-two blocks (A, B) are insoluble in selective solvent, but C is soluble. Type 2-The micelles with

radially compartmentalized corona-two blocks (B, C) are soluble in water, and A is an insoluble block, in this micelle the heterogeneity in micellar corona is observed in the radial direction. These ABC triblock copolymer micelles (type 1 and 2) are known as 'core-shell-corona' or 'onion' type micelle or '3 layer' micelles. In addition to these, a non-center of symmetric triblock copolymer micelles like Janus micelles[59] has also achieved significant research attentions. Janus micelles are BAC type micelle, in which the cross-linked core (A) is surrounded by two different coronal hemispheres (B, C). In this micelle, the heterogeneity in coronal chain is observed in lateral dimensions. However, there are no examples for linear ABC triblock copolymer micelles having B is a soluble block, and A and C are insoluble blocks in block selective solvents. Compared to the block copolymer, because of the less mobile and loosely packed hydrophobic domains of amphiphilic graft-copolymers micelle favors inter micelle interactions and thus results in micelle aggregates.[60-62]

Polymeric micelles are highly tunable nanomorphologies with respect to their size, shape, mechanical and material properties. Properties can be simply altered by changing the composition of the core forming blocks. The core can be even removed to get solvent filled nanocages or can be hydrolyzed to fully hydrophilic structures.[63-66] The polymeric micelles are more stable and have lower CMC than the surfactant micelles. CMC measurements can be performed by different methods (HPLC, small angle scattering, fluorescence *etc*), in which techniques based on the partitioning of pyrene fluorophores in hydrophobic and aqueous environments are more sensitive and precise one.[67] The polymeric micelles can be characterized by dynamic light scattering, static light scattering, transmission electron microscopy, atomic force microscopy, analytical ultracentrifugation (AU), viscometry, size exclusion chromatography, and small-angle neutron scattering *etc*.

1.4 Dimensional synthetic modifications of polymeric micelles

Inspired from nature[41] and by combining strong covalent and week none covalent interactions, self-assembly has emerged as one of the few strategies available for the making of ensembles of nanostructures. Synthetic organic chemistry can play a key role in the preparation and modifications of the self-assembled polymeric nanoparticles by balancing the weak and strong interactions such as van der Waals, hydrophobic, electrostatic interactions, hydrogen, coordinate and covalent bonds *etc*. Amphiphilic block copolymer self-assembly is thermodynamic, consequently reversible and

entropically driven process. Due to the dynamic nature of the resulting polymeric micelle, micelles are unstable at lower concentration (CMC) and higher temperature (CMT). Stability of the micelles can be enhanced by changing the dynamic equilibrium to static *via* providing reinforcement to the weak interactions responsible for the micelle existence. This is often achieved by covalent cross-linking throughout a selective domain of the polymeric micelle (**Figure 1.3**). The first report on micelle cross-linking is through the core domain of a diblock copolymer micelle in 1979 by Prochaska group *via* photochemical irradiation.[68]

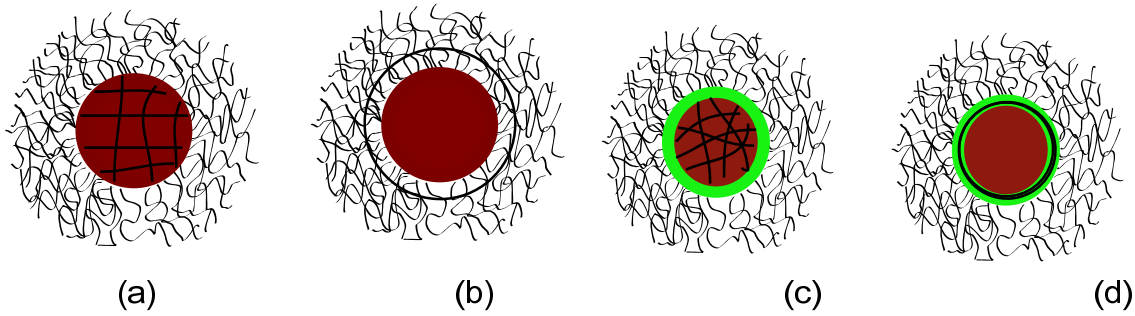

Figure 1.3. A schematic representation of core (a) and shell (b) cross-linked diblock core shell micelle and core (c) and shell (d) cross-linked triblock core-shell-corona micelle.

In recent years, role of synthetic and dimensional synthetic chemistry in the preparation, regioselective functionalization and cross liking of block copolymer micelles has achieved significant research attentions. In which, pioneering works of K.L Wooley's group on diblock copolymer core–shell micelles and S.P Armes group work on triblock core-shell-corona micelles are the two main contributions in this area. In 1996 Wooley's group has prepared shell cross-linked diblock spherical polymeric micelle (SCK) *via* radical oligomerization of the pendant styrene group attached to the Poly(4-vinyl pyridine) block of the amphiphilic diblock copolymer polystyrene-b-poly(4-vinyl pyridine) (PS-*b*-PVP) under high dilution conditions.[69] This group further utilized carbodimide coupling[70] and 'click'reactions[71] in the preparation of shell (SCK) and core cross-linked spherical micelles. Group of Armes has utilized a hybrid of core shell cross-linking *via* cross-linking at the central layer of the amphiphilic triblock copolymer micelle. They prepared 3 layer onion type micelle from a poly-[ethylene oxide-*b*-2-(dimethylamino) ethyl methacrylate-*b*-2-(*N*-morpholino) ethyl methacrylate] (PEO-*b*-DMA-*b*-MEMA) triblock copolymer. The reactive groups on central block (DMA) of the polymer micelle is then cross-linked (quaternized) to afford a central core of MEMA, which is surrounded by a cross-linked layer that is further surrounded by PEG corona. In contrast to the shell cross-linked diblock core-shell micelle (SCK), cross-linking of onion micelles can be performed at higher polymer concentrations in the absence of intermicellar cross-

linking and/or aggregations. The presence of PEG corona offer steric stabilization and confined inner shell cross-linking.[72] It is also necessary to mention about the reversible cross-linking in micelles. The reversible cross-linking in micelles is significant especially for the controlled drug delivery. The reversible strategy can offer structural stabilization and stable encapsulation of cargoes in the pharmaceutical carriers followed by destabilization and selective cleavage (release) under the condition in the desired targeted cells.[73, 74]

Similar to regioselective cross-linking, various functionalities can be introduced at core, shell or corona of the micelles (**Figure 1.4**). This allows tailoring of these nanoparticles for applications such as targeted drug delivery, diagnosis, sensing *etc*. Attachment of biological molecules on the surface of polymer micelle (bioconjugation) is an essential requirement for tuning the polymeric micelle for pharmaceutical applications. Preparation of these natural and synthetic-hybrid materials required more complex synthetic strategies such as use of functionalized initiators, chemistry of protection and deprotection and other post polymer modifications. The functional initiator strategy is first used in 1999 by Kataoka by preparing polymer micelle from sugar chain end functionalized poly(ethylene glycol)-*b*-poly(D,L lactide) block copolymers.[75] In 2004, Wooley has prepared sacharide,[76] biotin,[77] and antigen,[78] conjugated shell cross-linked (SCK) polymeric nanoparticle from corresponding functionalized poly(acrylic acid)-*b*-poly(methyl acrylate) (PAA-*b*-PMA) and non functionalized PAA-*b*-PMA by mixed micelle methodology and studied the ligand-receptor interactions. Though, those efforts tune the amount of targeting ligands presents at the surface of the mixed micelle, there is considerable decrease in the actual surface available functionalities than expected from the theoretical studies. This shows the uncertainty in predicting exact amount of available molecular recognition elements present at the surface of the micelle due to the steric inhibitions from the polymeric chains, density and spatial distribution of the ligands or due to burying of the ligand beneath the surface of the micelle by various conformation of the polymer chain segments. Recently Gillies showed the enhanced receptor binding efficiency of dendritic surface functionalized polymeric micelles.[79] Still surface functionalization strategies are limited by synthetic challenges and degree of control over the actual bio availability of the chain end functionalities.

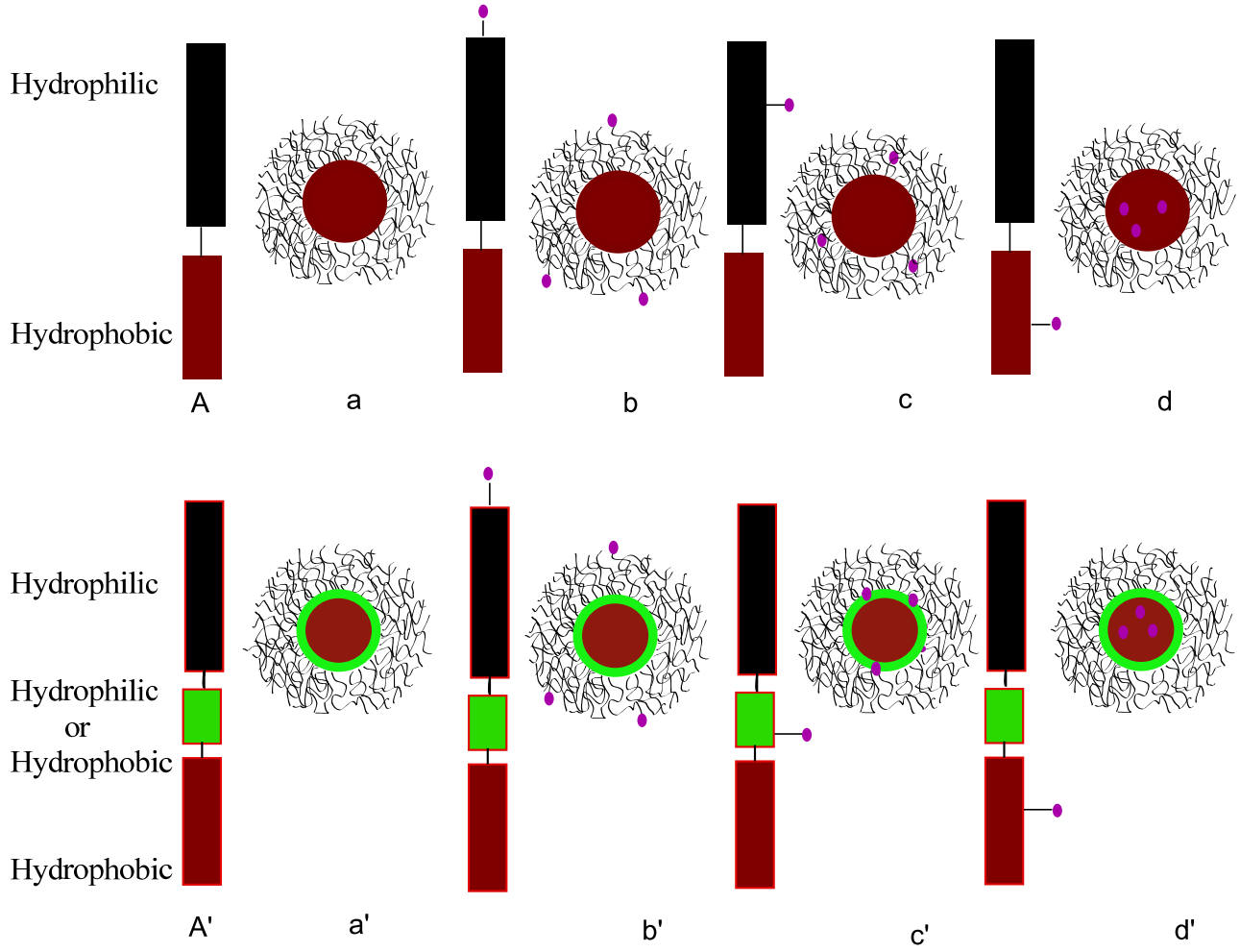

Figure 1.4. Schematic representation of possible locations for functionalization on amphiphilic diblock (A) core-shell micelle (a) and triblock (A') core-shell-corona micelle (a'). Surface functionalization (b, b'), shell functionalization (c, c'), and core functionalization (d, d') on diblock and triblock copolymer micelle respectively.

One of the highly efficient regioselective functionalization reactions, 'click' reaction,[80] briefly click reaction represents a group of high yielding and nearly substrate insensitive reactions by gaining enthalpy of at least 20 kcal/mol. The azide alkyne click reaction represent a metal catalyzed variant of Huisgen 1-3 dipolar cyclo addition reaction between the terminal alkyne and azides (CuAAC)[81, 82] and results in 1,4-triazoles over 1,5-adducts (**Scheme 1.5**). These reactions are insensitive to solvents (highly reactive in water), substrate (only sensitive to free thiols (by Staudinger reaction),[83] electronically activated alkenes,[84] and cyanides[85]) and can be performed in heterogeneous and homogeneous conditions. In addition, strained alkynes can be clicked even in the absence of metal catalysts.[86, 87] Due to the compatibility and orthogonality towards other functional groups, the click reactions, can be utilized in post-polymer modifications of unimers and stabilization and functionalization of its self-assembly in aqueous media.

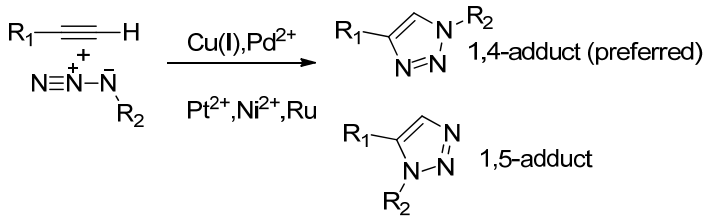

Scheme 1.5. Schematic representations of regioselective click reaction.

The shell layer of a diblock core-shell micelle can be considered as a swollen hydrogel that reinforces the pre-assembled structures. For triblock core-shell-corona micelle, the intermediate shell layer may be hydrophilic or hydrophobic and decide the compartmentalization in core or corona of the micelles. The selective functional modifications and cross-linking at the shell domain are achieved by chemical modification of the backbone groups on the shell domains. The first report on shell functional modification is reported by Wooley *et al*. They have used solid phase synthesis strategy to couple protein transduction domain (PTD) to Fluorescein 5-thiosemicarbazide (FTSC) labeled shell cross-linked (SCK) nanoparticles. Cleavage from the solid support and excavation of the nanoparticle core domain yield FTSC-labeled PTD nanocages.[88] Number of studies is reported about functionalization and cross-linking at the micelle shell domain.[89-91] In 2005 Wooley's groups have introduced click reactive groups to the shell backbone of the poly(acrylic acid)-*b*-polystyrene micelle (PAA-*b*-PS) by amidation reaction of a portion of the acrylic acid residues. They have performed the shell functionalization and cross-linking both step wisely and simultaneously by amidation reactions. Bioavailability and reactivity of the click reactive groups on the particles shell is confirmed by click reaction with complimentary click reactive groups bearing fluorophores.[92] This orthogonal approaches based on the functional group tolerance of click reaction do not require each unique initiator for the functionality to be introduced. But the disadvantages of this orthogonal shell functionalization strategy are requirements of primary amino groups, compatibilities of functionalities other than click towards the amidation reactions. Consumption of the large amount of hydrophilic carboxylate groups may also decrease the hydrophilicity of the shell. This may lead to detrimental effects on the structure and stability of the shell functionalized and cross-linked micelles. The same group modified the above two step functionalization cross-linking strategy to one step process by introducing click reactive dendritic cross-linkers. The dendritic cross-linker can provide a large number of reactive functionalities under a well defined molecular architecture. The click readied polymeric micelles prepared from (PAA-*b*-PS) having some of the PAA is modified with click reactive groups, are cross-linked with complimentary dendritic cross-linkers. The

polyvalent cross-linkers thus provide a new generation of shell click cross-linked nanoparticles (SCCKs) by single step click cross-linking strategy. The excessive click reactive groups on the micelle can be utilized for the functional modification of the shell domain. The compatibility of the dendritic cross-linkers with aqueous shell domain is the crucial parameter which decides the success of the shell cross-linking.[71] Reports on shell functionalization and cross-linking of triblock core-shell-corona micelles are mentioned in chapter 2.

Functionalization and cross-linking at the micelle core domains enhances the applications of these pharmaceutical carriers especially for the transport of hydrophobic drugs to the hydrophilic physiological environments. The covalent attachments of functionalities at the hydrophobic environments are protected from chemical degradation (hydrolysis). Presences of protective shell (in the case of diblock core shell micelle), shell and corona (in the case of triblock core-shell-corona micelle) around the hydrophobic core are capable to prevent its interactions with the external surroundings. Functional modifications at the core domain face two fundamental issues such as transfer of reagents and substrate across the shell, core shell interface and its solubility and reactivity at the nano hydrophobic environment of the core. These issues are addressed with the help of fluorescence spectroscopy. Wooley's group have synthesized shell cross-linked poly(acrylic acid)-*b*-polystyrene micelle having some of the styrene block containing azide groups (PAA-*b*-[PS-*co*-PS(N_3)]). Alkynyl functionalized dansyl fluorophores are then introduced to the swollen core domain of the micelle by click reactions in organic media (mixture of water and THF). The covalent attachment rather than the physical sequestration of the fluorophores on the core is confirmed by analytical ultracentrifugation analysis.[92] The covalent functionalization at the core domain is further confirmed by the generation of fluorescence of coumarin azide during click reactions. For that, a shell cross-linked polymeric micelle having alkynyl functionalized core is prepared. The covalent attachment of coumarin azide to the alkynyl functionality present at the micelle core was achieved by click reactions. The covalent attachment is confirmed by the fluorescence generated by the alteration of electronic structure of coumarin during the fluorogenic click reaction.[93] These results confirm the permeability of the shell layer and availability of reactive functionalities at the core domain. The same group has further extended the scope of orthogonal click reaction for the synthesis of core click cross-linked nanoparticle. For that, they have synthesized amphiphilic diblock copolymer poly(acrylic acid)-*b*-poly(styrene) (PAA-*b*-PS) with some of the hydrophobic

polystyrene blocks having the alkynyl group. The click readied hydrophobic core of the micelles is then cross-linked with a hydrophobic poly benzyl ether dendritic azide cross-linkers.[94] Preparation of this robust nanostructure is further confirmed the accessibility of functional groups at the hydrophobic micelle domains. Functionalization and cross-linking at the core domain of a core-shell-corona micelle has not been investigated yet.

1.5 Polymeric pH nanosensors for biological sensing

Fluorescence microscopy and flow cytometry are the two most popular cellular analysis techniques used for biological studies in single cellular level.[95, 96] Fluorescence microscopy can provide continuous real time observation of cells over a time; whereas, in flow cytometry, only cells are observed when it flows through the detection region. Both of these complimentary techniques are associated with fluorescence probes, to label the observed cells. The applications of fluorescence probes for cellular studies are limited by their cytotoxicity and perturbations to the cellular functions.

One of the significant achievement in the field of nanotechnology and nanofabrication in biology is the development of nanosensors for the probing of microscopic environments. Simply nanosensors for intracellular studies are optical devices having nanometer dimensions, and capable to insert into single-living cell for real time tracking of cellular processes. Due to large surface-to-volume ratios and small sizes of nanoparticles can have unique properties; consequently, they have some potential as sensors in medicine and biotechnology. The important requirements for the selection of nanoparticles for biological applications (drug delivery, imaging and sensing) include, long circulating half life for the particles in blood, ability to deliver hydrophilic and hydrophobic drug molecules, imaging agents, proteins, and genes into the desired locations, ease of surface functionalization, biocompatibility and biodegradability *etc*.

Fast response, high signal to noise ratio and the simple instrumental setups made molecular probe based fluorescence nanosensor techniques as a perfect method for real-time measurements in cells.[97] The developments in nanotechnology can provide different nanoparticles as a platform for the construction of bioanalytical nanosensors.[98] Most of the nanoparticles available are nontoxic and hence chemical interference to the cell will be less. Probes attached on nanoscaffolds can possess several advantages over small molecule sensors. First, multiple indicators can be attached to single particles; hence, the localized brightness of the system is increased. Second, particles can

simultaneously support sensitive and insensitive dyes to facilitate ratiometric measurements. Third, nanoparticles may be less vulnerable to leakage through cell membranes and to cellular compartmentalization. Fourth, some nanoparticles are more photostable than small organic dyes. Finally, the physical properties of the nanoparticles can be modulated and manipulated.[99] The challenge ahead is to minimize the factors affecting the reliability of the intracellular fluorescence measurements. Factors include perturbation and cytotoxicity of fluorophores to the cell process, effective accumulation of the sensor at the location of interest, photon penetration distance (for deep tissue monitoring near infrared (NIR) fluorophores[100] (NIR regions are free from auto fluorescence of the cellular environment) must be used *etc*.

Intracellular pH measurements can provide not only new knowledge about the cellular biology, but also give deep insight about how we can utilize the pH changes in the intracellular compartment to release a drug from an engineered drug delivery system during endocytosis. From early reports on pH sensors, nanoparticle fluorescence based sensors[101, 102] are superior over the submicron fluorescence optical fiber sensors[103] and microelectrode techniques[104, 105] based sensors. The nanoparticle sensor offers ease of miniaturization, minimum effect on cell viability and functions, increased pH sensitivity, and greater spatial sampling capabilities. The first polymeric nanoparticle based sensor is reported by sasaki *et al*., they entrapped pH sensitive Fluorescein dye in polyacrylamide nanoparticle and measured the pH distribution in water glass interfaces.[101] Kopelmen prepared 20-200 nm diameter Probe Encapsulated By Biologically Localized Embedding (PEBBLE) nanosensors for the intracellular measurements of pH, molecular oxygen, calcium ions, glucose and nitric oxides in macrophages. The sensors showed high selectivity, fast response time, reversibility and reversible analyte detections.[102] The first ratiometric pH submicron sensor for intracellular measurement is prepared by Rosenzweig *et al*. for site specific intracellular pH measurements in Murine Macrophages. They improved the accuracy of the nanosensors, by covalently incorporating succinimidyl derivatives of pH sensitive Oregon Green and pH insensitive reference dye-Texas red to the amino modified surface of polystyrene beads *via* amide bonds.[106] The main advantage of ratiometric intensity measurement over the absolute intensity measurement is that this method eliminate the distortion of data caused by photo bleaching, variations in probe loading and source fluctuations. The same group has also introduced phospholipid based biocompatible liposome[107] and lipobead pH nanosensors.[108] Liposome based sensors allows the encapsulation of fluorophores in the aqueous media of the liposomes and provide solution based

characteristics to the sensors. Whereas the lipobead sensor is composed of fluorescence indicators immobilized on a polystyrene beads, which is encapsulated by phospholipids membranes. The lipobead sensors thus provide much more resistant to biological degradations and maintain the solution characteristics as like liposome sensors. In addition to this, numbers of polymeric nanoparticle systems are used for the fabrication of ratiometric pH nanosensors. This includes polyacrylamide nanosensors[109-113] and polysaccharide nanoparticle.[114]

The size and morphologies of the nanoparticle formed by block copolymer self-assembly is depending up on hydrophilic to hydrophobic mass ratios or block lengths. For micelle morphology, the lengths of hydrophilic blocks are slightly higher or comparable with the hydrophobic blocks. Block copolymers with too long hydrophilic block exist as unimers and too long hydrophobic block results in other morphologies such as rods and lamellae.[115] Compatibility of hydrophobic drug with the hydrophobic core of the polymer micelle provides high loading capacity and controlled release profile of the encapsulated hydrophobic cargoes. The hydrophilic coronas provide steric protection to the micelle and are un-reactive towards the blood and tissue components. The un-reactive coronal chains (PEG) allow micelle to stay rather long in the blood/tissue without being recognized by the phagocytic cells and certain proteins(opsonization).[116] This prolonged circulation of optimum sized (5 to 100 nm) nanocarriers enhances their accumulations in pathological sites having leaky vasculature (tumors, inflammation and infracted areas) by so called enhanced permeation and retention effect (EPR)[117, 118] or *via* targeted drug delivery.[119] The coronal chain also determines the hydrophilicity, charge and density of surface functionalization on the micelle. Thus, block compositions of the amphiphilic copolymer micelle controls its biological characteristics such as biodistribution, pharmacokinetics, biocompatibility, longevity, surface adsorption of biomacromolecules, adhesion to biosurfaces and targetability.[120, 121] Even with biological advantages and excellent engineerability, polymeric micelles are not yet investigated in nanosensor fabrications.

Chapter 2

Nanosensors Fabrications by a Post Micelle Modification Strategy

Recent developments in radical polymerization enable the synthesis of well defined block copolymers; previously this could only be achieved by living ionic polymerizations. Among the 3 well known living radical polymerization techniques, NMP,[122] ATRP,[17] and RAFT,[123] the transition metal catalyzed ATRP is emerged as the main technique used in block copolymer synthesis. This is due to its simple experimental set up, commercially available monomers initiators and catalysts; excellent control over the block copolymer composition and molecular weight distributions of the resulting polymers. ATRP in block copolymer synthesis can be performed by two different methods such as one pot sequential and isolated macroinitiator method.[24-27] In both of these methods, the propagating chains of monomers having higher equilibrium constant ($K_{ATRP} = k_{act}/k_{deact}$) can initiate the polymerization (cross propagation) of monomers with lower equilibrium constant for activations. The macroinitiator method can provide more pure living block(s) by precipitating the polymers at lower monomer conversions. In one pot sequential method, the propagation of the second monomer includes un-reacted first monomer along with the second, which result in contaminated random block copolymers.

The basic idea behind the pH nanosensors fabrications *via* post micelle modification strategy is based on the dimensional synthetic modifications on the functional core-shell-corona micelle; which is resulting from the self-assembly of functional triblock (ABC) copolymers. Isolated macroinitiator ATRP can be used for the synthesis of functional triblock (unimers) from protected functional monomers. The synthetic methodologies used for functional modification and cross-linking on the self assembled functional unimers should be facile under milder condition (ambient temperature and in aqueous solution), non-toxic, cost effective, minimum or no by-products formations (minimizes the purification steps) *etc*. The ability to calculate the degree of dimensional synthetic modifications is also highly desirable. Covalent cross-linking at the core or shell region of the triblock copolymer self-assembly can provide reinforcement to the hydrophobic interactions responsible for the micelle existence. The resulting stabilized robust micelles can prevent its dissociations under infinitely diluted condition (below CMC value) and hence enhances its potential in biomedical applications.[51] Number of methods reported for the shell cross-linking of ABC

triblock core-shell-corona micelle; which include, UV induced photo cross-linking,[124, 125] pH sensitive reversible imine cross-linking,[126] disulphide based reversible cross-linking using DTBP (dimethyl 3,3′-dithiobispropionimidate),[127] and cystamine,[73] cross-linking by amidation reactions on micelle having activated esters,[128] quaternization using bis(2-iodoethoxy)ethane (BIEE),[129, 130] cross-linking using glutaraldehyde,[131] genipin,[132] Michael addition *via* divinyl sulfone (DVS),[133] cross-linking by polyelectrolight complexation,[134] and click cross-linking.[135] In contrast to the diblock (AB) core-shell micelle, The presence of PEG corona on a triblock core-shell-corona micelle can provide exclusive intramicellar cross-linking at higher block copolymer concentration *via* steric stabilization mechanism.[72] The conformation of the corona chains entropically favors the repulsive PEG-PEG interactions. The enthalpically more favorable PEG-water interactions dominate the unfavorable PEG-PEG interactions and prevent aggregation during the Brownian motions of these amphiphilic aqueous colloidal dispersions.

The covalent bond formations at the hydrophobic core of the amphiphilic block copolymer self-assembly in water are rather difficult. Core cross-linking required the transverse of reagents and substrates through hydrophilic-hydrophobic micelle interfaces and should soluble in the hydrophobic nanodomains. Core cross-linking of diblock copolymer micelles are extensively studied; that includes the transverse of reagents to the core domain,[94, 136] and by radiation induced core cross-linking.[39, 74, 137] Syntheses of core cross-linked core-shell-corona ABC triblock micelle in aqueous media has not been reported yet.

This chapter explaining the conversion of core or shell cross-linked core-shell-corona micelle into ratiometric pH nanosensors *via* second generation dimensional synthetic modification on the core/shell stabilized micelle. The chapter is divided into two sections. Section 2.1 describes the shell cross-linked micelle nanosensor synthesis, and section 2.2 explains the synthesis of core cross-linked micelle nanosensors.

2.1 Amidation Shell Cross-linked Micelle Nanosensors

2.1.1 Introduction

Intracellular pH measurements give information about the pH gradients maintained by the intracellular organelles (which varies from 4 to 8 among varies organelles). Exploitation of this intracellular pH gradient[138] allows the developments of pH sensitive drug release or drug/drug carrier partitions in the desired cellular compartments. There are a number of nanosensors developed for pH measurement.[97, 106, 108, 110, 113, 114, 139-142] In order to have effective intracellular pH monitoring, the sensors have to overcome effective sequestration from the blood by macrophages of the mononuclear phagocyte system (MPS)[143] located in the liver and spleen. This MPS system prevents long-circulation and efficient accumulation of above mentioned particle sensors in relevant cells. Though, the well-known pharmaceutical carrier, polymeric micelles, can provide long-circulation requirements,[144] polymeric micelles in nanosensor fabrications have not been investigated considerably. Difficulties in synthesizing well-defined functional unimers and the instability of their self-assembly under infinitely diluted biological conditions are the two main reasons for excluding polymeric micelles.

Controlled radical polymerization, especially the redox-active transition metal complex catalyzed atom transfer radical polymerization (ATRP)[17] can nowadays fulfill the well defined polymer pre-requests for designing advanced functional materials. Nanoscale phase separations of well defined amphiphilic block copolymers in block selective solvents gives verities of morphologies such as spherical micelles, lamellae, tube, rode *etc*.[1, 145] In biology, the micellar morphology provides a set of unbeatable advantages over the others. They have a long circulating half life in the blood, which provides their gradual accumulation in the required area *via* enhanced permeability and retention effect (EPR).[117, 118, 146] The surface functionalization chemistry is easy and hence provides a platform for efficient biological targeting *etc*. In recent years, block copolymer micelles have attracted increasing research attention due to its numerous biological applications such as imaging, labelling, sensing, and drug delivery.[77, 147-151] Often these diverse spectrums of applications require robust and stabilized structures, which can be achieved *via* covalent cross-linking between the functional unimers of these nanoparticle scaffolds.[152, 153] Fluorescent labelled micelles for sensing applications are divided into two main classes. Fluorescent dyes or quantum dot encapsulated

micelles[154, 155] and micelles with chemically conjugated fluorescent dyes.[156, 157] The chemical conjugation can overcome the problems like cytotoxicity and leakage into cellular environments.

Well defined core-shell-corona micelle resulting from the amphiphilic triblock copolymer self-assembly in water have the potential to provide more diversity in regioselective functionalization and cross-linking, than an amphiphilic diblock core-shell micelle. This structural potential is used in this section for the fabrication of stabilized ratiometric pH nanosensors.

2.1.2 Experimental: Synthesis of shell cross-linked micelle nanosensor

Materials: Styrene (99.5%) obtained from Fluka and radical inhibitors was removed by passing through a column filled with basic alumina. 2-Aminoethyl methacrylate hydrochloride (AEMA.HCl) (90%), Bis(*tert*-butyl) dicarbonate (99%), triethylamine (TEA) (99.5%), 2-bromo-isobutyryl-bromide (98%), CuCl (99.995%), 2,2'bipyridyl (bpy) (99%), PMDETA (99%), $CuCl_2$ (99.995%), trifluoroacetic acid (TFA) (99%), dialysis tubing (MWCO = 12 kDa), N-(3-Dimetylaminopropyl)-N'-ethylcarbodiimide methiodide (EDC.MeI), Rhodamine B isothiocyanate (RhBITC) and Fluorescein 5(6)-isothiocyanate (FITC) (90%) were purchased from Sigma Aldrich and used as obtained. 3,6,9-Trioxaundecandioic acid (TUDA) was purchased from iris biotech GMBH, Oregon Green 488 isothiocyanate (F_2FITC) was purchased from Invitrogen, and CH_3O-PEG-OH (poly (ethylene glycol) monomethylether (M_n = 5000) was from Fluka. Solvents used for atom transfer polymerization (ATRP) were purified by distillation over the drying agents indicated in parentheses, stored under molecular sieves (MeOH 3Å and DMF 4Å) and transferred under argon; MeOH ($Mg(OMe)_2$), and DMF (CaH_2). Other solvents and commercially available chemicals were used as obtained. Water used was collected from Millipore; aqueous buffer solutions were prepared from the reported procedures.

Instrumentation details: ^{1}H-nmr spectra were recorded on a Bruker 250 MHz in solvents as indicated, chemical shifts (δ) were given in ppm relative to TMS. The residual solvent signals were used as a reference, and the chemical shifts converted into TMS scale ($CDCl_3$: δ_H = 7.24 ppm, ^{6}d-DMSO: δ_H = 2.50 ppm, D_2O: δ_H = 4.79 ppm). Infrared spectra's were recorded by Perkin Elmer FT-IR Spectrometer (KBr pellets method), and the wave numbers of recorded IR signals were quoted in cm^{-1}. The number-average molecular weight (M_n) weight average molecular weight (M_w) and polydispersity (M_w/M_n) of block copolymers were determined by GPC analysis based on poly styrene calibration standards. Measurements were carried out by using Mixed-D GPC column from

Polymer Laboratories (7.4 × 300 mm) and RID10A-SHIMADZU refractive index detector. DMF with 50mM LiCl solution was used as eluent (0.5 mL / min.) at 25 ^{0}C. Hydrodynamic diameters (D_h) and size distributions of the amphiphilic colloidal dispersion in MilliQ water at 25 ^{0}C were determined by Brookhaven ZETA PALS instrument. Calculation of the particle size distribution and distribution averages were performed with the ISDA software package (from Brookhaven) through CONTIN particle size distribution analysis routines. All determinations were made in triplicate and duration of 2 minutes each. Zeta potential measurements were carried out by using Brookhaven ZETA PALS analyzer. The measurements were made in MilliQ water at 25 ^{0}C, and the zeta potential (ξ) was calculated using Smoluchowski equation. Electrophoretic mobility (μ) = $\boldsymbol{\xi \epsilon/\eta}$, where η and ϵ are the absolute viscosity and dielectric constant of the medium respectively. Mean value of ξ was chosen from 10 determinations of 10 data accumulations. Fluorescence measurements were carried out by using EDINBURGH F-900 fluorometer. PSIA XE-150 scanning force microscope was used for AFM measurements. Argon atmosphere (99.9999 %) used in the reactions was provided by AGA Denmark

Synthesis of $PEG_{5000}Br$: The macroinitiator was synthesized by using a slightly modified procedure from that reported in the literature.[158] CH_3O-PEG-OH, M_n = 5000 (5 gram, 1 mmol) was dissolved in 60 mL of toluene. After azeotropic distillation of 10 mL of toluene under reduced pressure to remove traces of water, TEA (0.278 mL, 2 mmol) was added, and the solution was cooled to room temperature. 2-bromoisobutyryl bromide (0.185 mL, 1.5 mmol) was added drop wise to the mixture, and the reaction mixture was stirred at 40 ^{0}C for 2 days under a calcium chloride guard tube. The solution was filtered, and most of the toluene was removed by rotary evaporation prior to precipitation into 10 fold excess of cold ether. The crude polymer was dried under vacuum, dissolved in water at pH 8-9 and then extracted with DCM. The organic layers were collected and dried over anhydrous sodium sulfate. The removal of the solvent under reduced pressure afforded the purified macroinitiator in a yield of 5.1 g (99 %). ^{1}H-NMR (250 MHz, $CDCl_3$): δ = 3.63 (s, -C**H**$_2$C**H**$_2$O-), 1.91 (s, -C(C**H**$_3$)$_2$) ppm; FT-IR: υ = 2887, 1737, 1466, 1359, 1342, 1279, 1241, 1148, 1107, 1060, 963, 841 cm^{-1}.

Synthesis of 2-[N-(tert-Butoxycarbonyl)Amino]ethyl methacrylate (AEMA(Boc)): AEMA(Boc) was synthesized by a slightly modified procedure than reported.[38] AEMA HCl (2.5 g, 15.15 mmol) was dissolved in 40 mL of dry DCM and cooled to 0 ^{0}C in an ice water bath. Anhydrous triethylamine (4.2 mL, 30.3 mmol) was added drop wise to the ice cold solution and stirred for 20

minutes. Bis(*tert*-butyl) dicarbonate (5.22 mL, 22.725 mmol) dissolved in 10 mL of dry DCM was slowly added to the reaction mixture, warmed to room temperature and stirred for 24 h under argon atmosphere. The organic layer was washed with water (2 × 25 mL), 1M HCl (2 × 25 mL), saturated aqueous sodium bicarbonate (2 × 25 mL) and with saturated brine solution (2 × 20 mL). The organic layer was dried over anhydrous sodium sulphate; this was followed by removal of the solvent under reduced pressure gave crystalline solid 3.3 g (95%). ^{1}H-NMR (250 MHz, $CDCl_3$): δ = 6.11 (1H, Vinylic **H**), 5.58 (1H, Vinylic **H)**, 4.76 (broad (br), 1H, -N**H**), 4.20 (2H, -COOC**H**$_2$CH$_2$), 3.42 (2H, -COOCH$_2$C**H**$_2$), 1.94 (s, 3H, -C**H**$_3$), 1.44 (s, 9H, -C(C**H**$_3$)$_3$) ppm; FT-IR: υ = 3386, 2981, 1692, 1633, 1521, 1453, 1423, 1388, 1364, 1323, 1158, 1107, 1042, 998, 957, 915, 880, 853, 818, 777, 756, 653, 597 cm^{-1}.

PEG$_{127}$-b-P(AEMA(Boc))$_{12}$Cl: PEG-Br (2 gram, 0.36 mmol) AEMABoc (852 mg, 5 mmol), 2,2'bipyridyl (122 mg, 0.76 mmol) and 10 mL dry MeOH were added to 25 mL schlenk flask equipped with a stirrer bar. The flask was frozen in liquid nitrogen, and CuCl catalyst (40 mg, 0.40 mmol) was added. The reaction mixture was degassed with 3 freeze-pump-thaw cycles (each 15 minute long) to remove the oxygen, and the polymerization was carried out at 40 ^{0}C for 24 h under argon atmosphere. The dark brown reaction solution was passed through a silica gel column to remove the copper catalyst using MeOH as solvent. On exposure to air, the solution turned to blue, which indicated the areal oxidation of the Cu(I) catalyst. After the removal of most of the MeOH by rotary evaporation, the polymer precipitated into excess cold diethyl ether. It was then isolated by filtration, and the precipitate was dried under vacuum to yield 1.86 g (62%) of the diblock copolymer. ^{1}H-NMR (250 MHz, $CDCl_3$): δ = 5.50 (br s, -N**H**), 4.0 (br s, -OC**H**$_2$CH$_2$NH), 3.63 (s, -C**H**$_2$C**H**$_2$O), 3.37 (br m, -OCH$_2$C**H**$_2$NH, -OC**H**$_3$), 1.82 (br, -C**H**$_2$ backbone), 1.43 (s, -C(C**H**$_3$)$_3$), 1.11-0.81 (m, -C(C**H**$_3$)$_2$, -C**H**$_3$ backbone) ppm; FT-IR: υ = 3387, 2892, 1716, 1520, 1466, 1391, 1361, 1342, 1279, 1241, 1150, 1112, 1060, 996, 965, 843 cm^{-1}; M_n (NMR) = 8340; M_n (GPC) = 5600, M_w = 6460, PD (M_w/M_n) = 1.15.

Synthesis of PEG$_{127}$-b-P(AEMA(Boc))$_{12}$-b-PS$_{28}$ (20): PEG-*b*-PAEMA(Boc)-Cl (1 g, 0.12 mmol), Styrene (0.48 mL, 4.2 mmol), $CuCl_2$ (13 mg, 0.096 mmol), PMDETA (0.087 mL, 0.42 mmol) and 3 mL of DMF were taken in 25 mL schlenk flask equipped with a stirrer bar. The flask was frozen in liquid nitrogen, and CuCl catalyst (12 mg, 0.12 mmol) was added to it. After being degassed with 3 freeze-pump-thaw cycles (each cycle 15 minute long) to remove the oxygen, the polymerization was carried out at 130 ^{0}C for 27 h under argon atmosphere. The reaction mixture was concentrated

under vacuum, and the polymer was precipitated into cold diethyl ether. The precipitate was dried under vacum yielded 0.74 mg (55%) of the triblock copolymer. ^{1}H-NMR (250 MHz, ^{6}d-DMSO): δ = 7.3-6.5 (m, Ar**H**), 3.80 (br, -OC**H**$_2$CH$_2$NH), 3.50 (s, -C**H**$_2$C**H**$_2$O), 3.20 (br s, -OCH$_2$C**H**$_2$NH), 2.00-1.50 (br, C**H**$_2$ and -C**H** backbone), 1.40 (s, -C(C**H**$_3$)$_3$), 1.20-0.70 (m, -C**H**$_3$ backbone) ppm; FT-IR: υ = 3370, 3025, 2887, 1716, 1602, 1518, 1496, 1466, 1451, 1391, 1361, 1342, 1279, 1243, 1146, 1105, 961, 841 cm^{-1}; M_n (NMR) = 11250; M_n (GPC) = 9280, M_w = 11800, PD (M_w/M_n) = 1.27. ^{1}H-NMR spectra is given in **appendix A**.

PEG-b-PAEMA-b-PS (21): The triblock copolymer, PEG-*b*-PAEMA(Boc)-*b*-PS (1g, 0.088 mmol) was dissolved in 4 mL of DCM, followed by 4 mL TFA was added drop wise, and stirred at room temperature for 10 hours. After evaporating most of the solvent under reduced pressure; the polymer was precipitated into excess of cold diethyl ether, and dried under vacuum. The complete deprotection of amino group was confirmed by the disappearance of Boc group signal at δ 1.40 (s, -C(C**H**$_3$)$_3$) ^{1}H-NMR (250 MHz in ^{6}d-DMSO), and qualitatively by conducting Kaiser test.[159] ^{1}H-NMR spectra is given in **appendix A**.

Shell cross-linked micelle nanosensor (24) fabrication: The de-protected amphiphilic triblock copolymer PEG-*b*-PAEMA-*b*-PS (100 mg, 0.0088 mmol) was dissolved in 10 mL DMF by stirring overnight. To the polymeric solution under stirring, 2 mL of MilliQ water was added drop wise within 30 minutes followed by 20 mL more MilliQ water added drop wise. The cloudy micelle solution was then transferred into dialysis tube of molecular weight cut off (MWCO = 12 kDa) and dialysis against MilliQ water for 5 days. Hydrodynamic diameter (D_h) and zeta potentials (ξ) were found to be 29 ± 2 nm and 29 ± 1 mV respectively. The final block copolymer concentration after dialysis was 2 mg/mL. To the micelle solution 25 mL (50 mg, 0.0044 mmol, 0.053 mmol of amine), 3,6,9-trioxaundecandioic acid (3.6 mg, 0.016 mmol) and 1-[3-(dimethylamino)propyl]-3-ethylcarbodiimide methiodide (9.5 mg, 0.032 mmol) was added and stirred at room temperature for 10 h. The reaction mixture was then dialyzed against MilliQ water for 3 days (D_h = 24 ± 1 nm and ξ = 18 ± 2), then against carbonate buffer (pH = 9.8) for another 3 days. To the basic amphiphilic colloidal dispersion, RhBITC (0.014 mg, 0.0264 μmol), FITC (0.026 mg, 0.066 μmol) and F_2FITC (0.028 mg, 0.066 μmol) were added and stirred in the absence of light at room temperature for 12 hrs. The reaction mixture was transferred into dialysis tube (MWCO = 12 kDa); and dialysis was conducted against carbonate buffer for 3 days, then against MilliQ water for another 5 days (D_h =

25±2 nm and ξ = 16±2 mV). The final nanosensor concentration was 1.9 mg of polymers/mL of water.

2.1.3 Results and Discussion

Synthesis of a ratiometric nanosensor for intracellular pH measurement is schematically represented in **Figure 2.1**. The sensor is based on an intermediary layer cross-linked polymeric micelle and was fabricated as follows. The amphiphilic triblock copolymer, poly (ethylene glycol)$_{127}$-*b*-poly2-[N-(*tert*-Butoxycarbonyl)Amino]ethyl methacrylate)$_{12}$-*b*-poly(styrene)$_{28}$ (PEG$_{127}$-*b*-PAEMA(Boc)$_{12}$-*b*-PS$_{28}$) (**20**), was synthesized by isolated macroinitiator atom transfer radical polymerization technique[27] (**Scheme** 2.**1**). The triblock copolymer was characterized by NMR and FT-IR spectroscopy. From ^{1}H-NMR data, the number-average degree of polymerization (DP$_n$) was determined. GPC analysis was used to calculate the polydispersity index (M$_w$/M$_n$) of the amphiphilic triblock copolymers. The NMR-GPC results are summarized in **Table 2.1**. The Boc groups from PEG-*b*-PAEMA(Boc)-*b*-PS were de-protected by TFA in DCM, and the complete deprotection was confirmed by the disappearance of Boc group signal at δ 1.4 ppm (s, -C(C**H**$_3$)$_3$) ^{1}H-NMR (250 MHz, ^{6}d-DMSO).

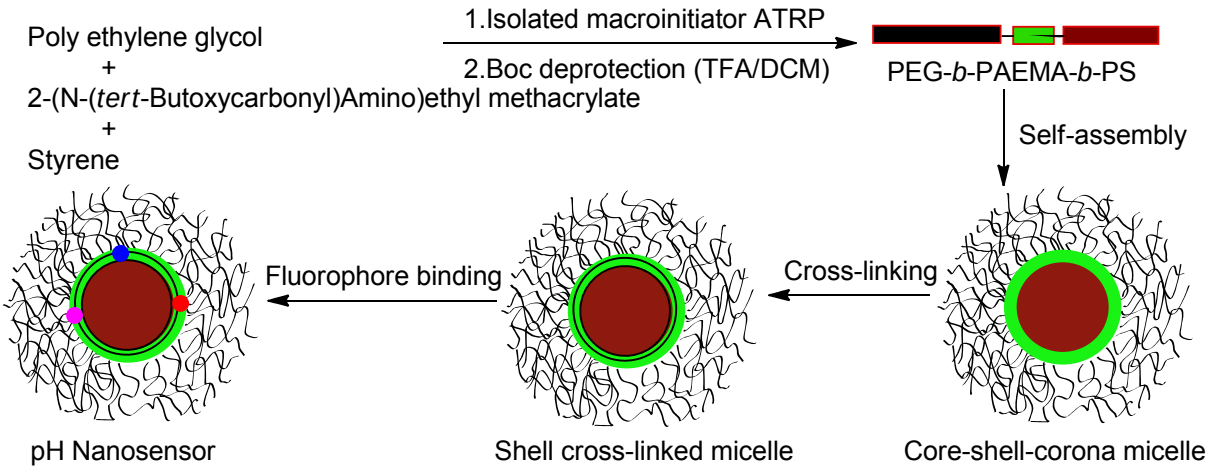

Figure 2.1. Schematic representation of a shell cross-linked core-shell-corona micelle nanosensor.

Table 2.1. Molecular weights of triblock copolymer, PEG$_n$-*b*-PAEMA(Boc)$_m$-*b*-PS$_p$ (**20**).

M$_n$[a]	M$_w$[a]	M$_w$/M$_n$[a]	M$_n$[b]	n[c]	m [c]	p [c]
9280	11800	1.27	11250	127	12	28

[a] Determined by GPC, [b] Determined by NMR, [c] Number of repeating units of PEG block(n), PAEMA(Boc) block (m) and PS block(p).

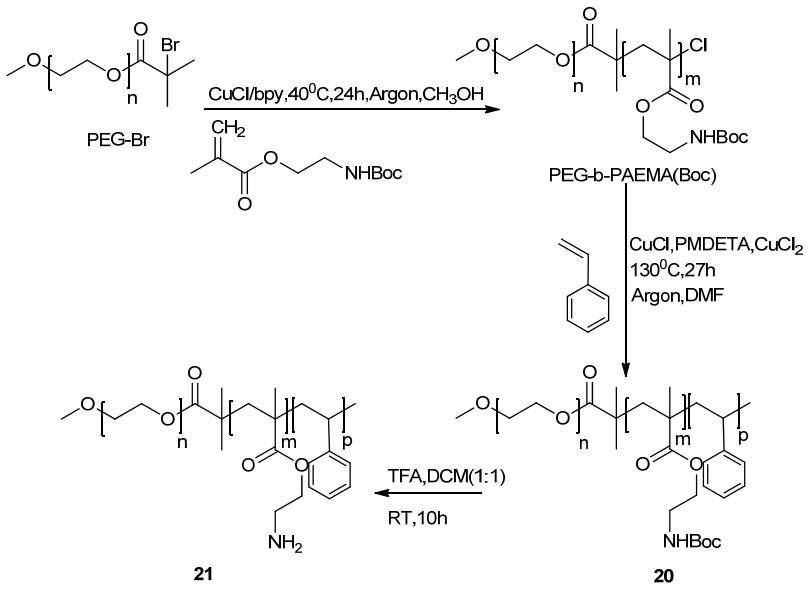

Scheme 2.1. Synthesis of PEG-*b*-PAEMA(Boc)-*b*-PS (**20)** by isolated macroinitiator ATRP and PEG-*b*-PAEMA-*b*-PS (**21**) by deprotection of **20**. bpy = 2,2'bipyridyl, PMDETA = N,N,N',N'',N'-Pentamethyldiethylenetriamine.

Synthesis of shell cross-linked core-shell-corona micelle nanosensor is given in **scheme 2.2**. First, the entropy driving nanoscale phase separation of PEG-*b*-PAEMA-*b*-PS (**21**) in water was achieved by dissolving the triblock copolymer in DMF, and the common solvent for the triblock was slowly displaced by selective solvent for the hydrophilic blocks (water). The resulting polymeric micelle was then kinetically trapped by complete displacement of common solvent by selective solvent *via* dialysis against MilliQ water. The stabilization of the PEG-*b*-PAEMA-*b*-PS micelle (**22**) in water was achieved by covalent cross-linking between the unimers *via* amidation shell cross-linking. Water soluble 3,6,9-trioxaundecandioic acid was used as a cross-linking agent. The diacid cross-linker was first converted into o-Acylisourea by reacting it with 1-[3-(dimethylamino)propyl]-3-ethylcarbodiimide methiodide (EDC.MeI). This active ester was then reacted with the free amino groups present at the intermediate layer (PAEMA shell) of the polymer micelle. Stoichiometrically, 60 % of the amino groups were used for the amidation shell cross-linking. The shell cross-linked micelles **23** was first dialyzed against MilliQ water, to remove the urea by-products and then against carbonate buffer at pH 9.6. The cross-linked micelle dispersion in basic buffer was converted into ratiometric pH nanosensors **24** by covalent conjugation of pH sensitive Fluorescein isothiocyanate (FITC) and Oregon Green isothiocyanate (F_2FITC), and pH insensitive reference fluorophore-Rhodamine B isothiocyanate (RhBITC). Some of the remaining free amino groups at the

intermediate layer (shell) of the shell cross-linked micelle were nucleophilically attacked the central electrophilic carbon of the fluorophores isothiocyanate (ITC) groups and made thiourea linkage.

The concentration of fluorophores on the sensor was adjusted to get maximum fluorescence intensities with minimum distance dependent excited state interactions (Förster resonance energy transfer, FRET)[160] between the pH sensitive and reference fluorophores and to have minimum self quenching.[161] The amount of fluorophore attached can be quantified from first derivative UV-Visible measurements as reported.[162] The morphology and distributions of the micelle nanosensor were investigated by atomic force microscopy (AFM) under ambient conditions (**Figure 2.2**). AFM images of the air dried nanosensor shows the particles are uniformly distributed and have a round shape. The spherical morphology can be seen clearly in the phase image (**Figure 2.2b**), which depicts the phase shift of the cantilever oscillation and visualizes differences in material properties of the sample. AFM image also confirms the absence of intermicellar cross-linking or aggregation in the nanosensor.

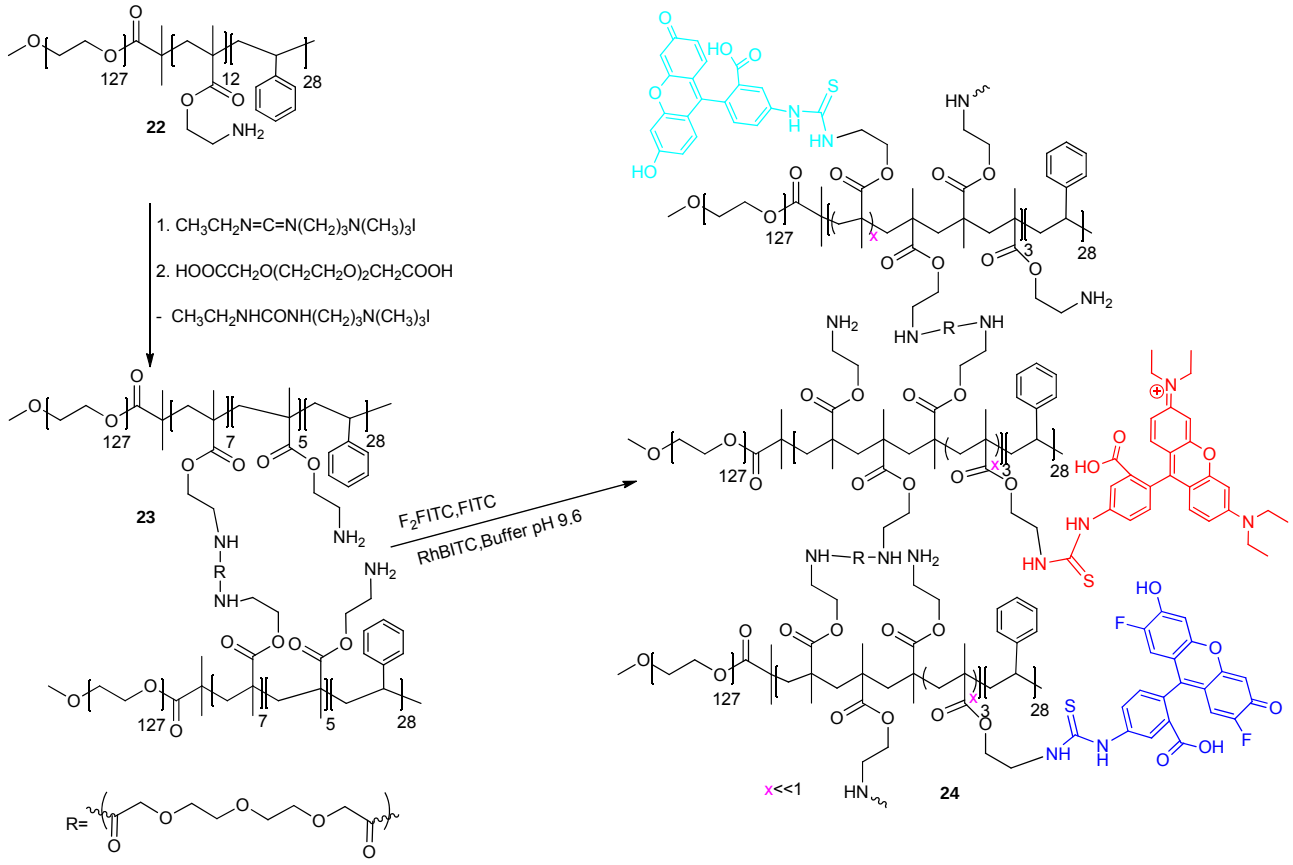

Scheme 2.2. Synthesis of shell cross-linked ratiometric micelle nanosensor.

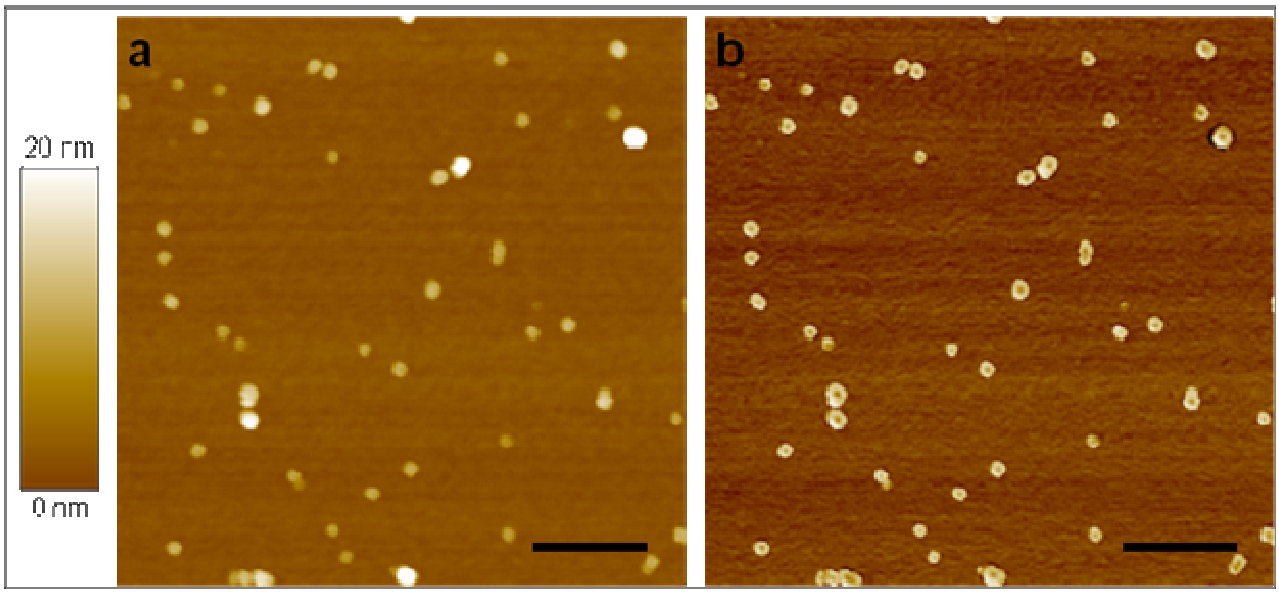

Figure 2.2. AFM images of shell cross-linked micelle nanosensor **24**, (**a)** Topographic image and (**b)** Phase image. Scale bar 1 μm.

Characterization of the shell cross-linked core-shell-corona micelle by ^{1}H-NMR was not possible due to solubility problems in deuterated solvents. In D_2O, the hydrophobic core of the lyophilized micelle was invisible, and the particles were totally invisible in ^{6}d-DMSO. FT-IR spectra of the lyophilized micelle after cross-linking showed additional overlapped amide I and II bands appeared approximately at 1640-1550 cm^{-1}. This confirmed the amide bond formation at the shell region of the micelle (**Figure 2.3**).

The inner shell stabilization did not affect the outer coronal mobility considerably. Hence was not entropically impaired the stabilizing capability of the hydrophilic micelle domains. As a result, the exclusive intramicellar cross-linking occurred. The intramicellar cross-linking was confirmed by dynamic light scattering (DLS) and zeta potential (ξ) measurements. DLS and ξ-potential measurement showed decreases in hydrodynamic diameter (D_h) and ξ-potential after micelle cross-linking. DLS and ξ measurements ensured that the cross-linking made more robust nanostructure with a decrease in surface charge density. This decrease in charge density also confirmed the participation of free amino groups of the shell domain in amidation cross-linking. The concentration of fluorophores in the nanosensor was extremely small, so that the binding of fluorophores to the cross-linked micelle did not show any significant change in hydrodynamic diameter and ξ-potential (**Table.2.2**).

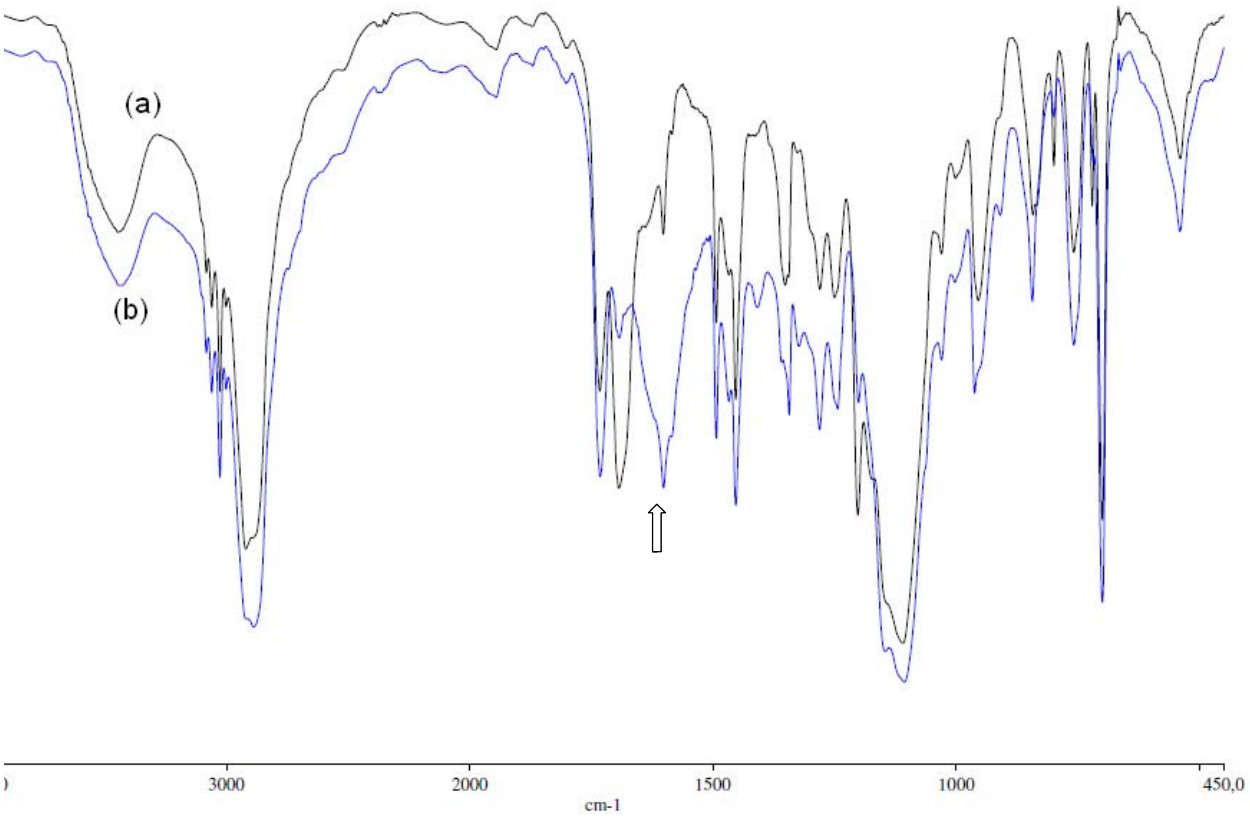

Figure 2.3. FT-IR spectra of PEG-*b*-PAEMA-*b*-PS micelle **22** (a) and **23** (b), arrow in (b) indicates the overlapped amide I and II bands after cross-linking.

Table 2.2. DLS and Zeta potential Measurements of Nanoparticles at 25 ^{0}C in MilliQ Water.

Particles	DLS(D_h)[a] (nm)	Zeta(ξ)[b] (mV)
22	29±2	29±1
23	24±1	18±2
24	25±2	16±2

[a] Number-averaged hydrodynamic diameters of nanoparticles by dynamic light scattering, [b] Zeta potential from 10 determinations, each having 10 cycles.

Micelle shell cross-linking was further confirmed by size exclusion chromatography (SEC). Lyophilized cross-linked and non cross-linked micelles showed different solubility in THF. The non cross-linked micelle was readily soluble in THF, whereas the cross-linked micelle was sparingly soluble only by ultasonication for 1h at 60 ^{0}C. SEC studies of these solutions showed different

elution time for cross-linked and non cross-linked micelles (**Figure 2.4**). This indicated that the micelle morphology in organic solvent was preserved after cross-linking.

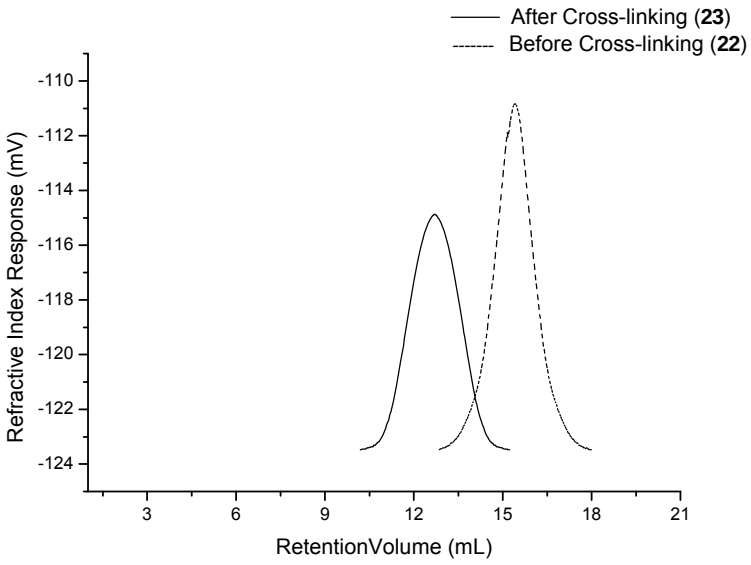

Figure 2.4. Size exclusion chromatogram of the micelles **22** and **23**.

The critical micelle concentrations (CMC) of the micelles are especially valuable when it is designed for biological applications. In infinitely diluted biological conditions, below its CMC values, the nanosensors can be dissociated into unimers. The micelle stabilization by covalent cross-linking throughout a domain can provide reinforcement to the weak hydrophobic interactions and hence prevent its dissociation below CMC. The sensitivity towards the microenvironment polarity of the hydrophobic probe pyrene was used to measure the CMC value of the micelles before and after cross-linking. A blue shift of the (0, 0) absorption band from 340 nm to 334 with a decrease in peak intensity ratio I_{340} / I_{334} (**Figure 2.5a**) indicated that the pyrene was moving from nonpolar to polar environment. Comparing the decrease in intensity ratio I_{340} / I_{334} of the micelles before and after cross-linking showed that, before cross-linking the decay was faster than after cross-linking. This demonstrates the presence of a hydrophobic environment in cross-linked micelle even below the CMC of the non cross-linked micelle (10 mgL^{-1}) (**Figure 2.5b**). Experimental procedure for CMC measurements can be found in **section 3.1.2**.

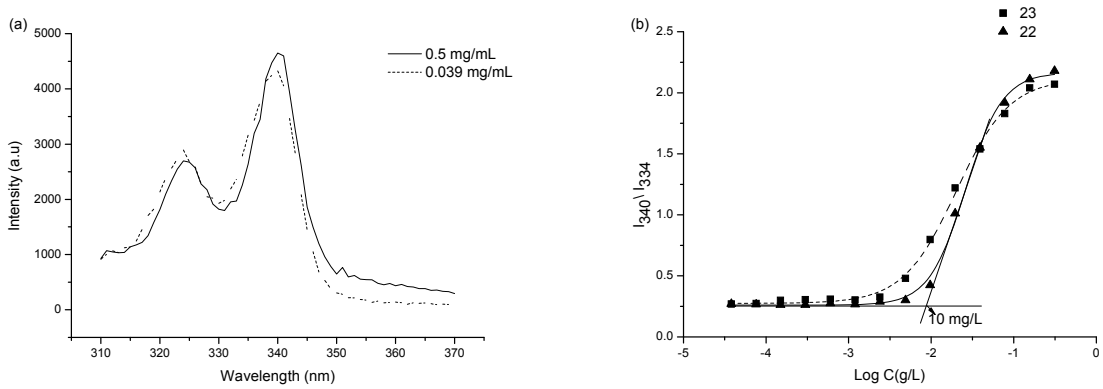

Figure 2.5. (a) Excitation spectra monitored at λ_{em} = 390 nm, representative spectra for the blue shift of (0,0) absorption band of pyrene with the decrease in block copolymer concentration (micelle concentration); (b) Plot of intensity ratio I_{340} / I_{334} (from pyrene excitation spectra) *vs* PEG-*b*-PAEMA-*b*-PS concentration of cross-linked (**23**) (■) and non-cross-linked (**22**) (▲) micelle, for each measurement [pyrene] = 6×10^{-7}M.

The pH sensitive Oregon Green (OG), Fluorescein (FA) and insensitive reference dye Rhodamine B (RhB) presented at the shell region of the shell cross-linked micelle dispersion in aqueous buffer of different pH, was excited at (λex) 488 nm and 543 nm respectively (**Figure 2.6a**). Fluorescence intensity ratios (I_{OG} + I_{FA}) / I_{RhB} were plotted against the pH corresponding to the fluorescence intensities to get the pH calibration curve. The pH calibration curve confirmed the covalent conjugation of pH sensitive and reference fluorophore at the shell region of the shell cross-linked micelle. The calibration curves (**Figure 2.6b**) show that the sensor is sensitive between the pH *ca.* 4 to 7.5. Time for response and reversibility of the pH nanosensor was also tested by fluorescence measurements (**Figure 2.7a** and **2.7b**). This show the nanosensors are quickly responding (with in micro seconds) towards the change in pH and are reversible between any two pH within the pH range 4 to 7.5. (Detailed procedure for the fluorescence measurements can be found in **appendix A**)

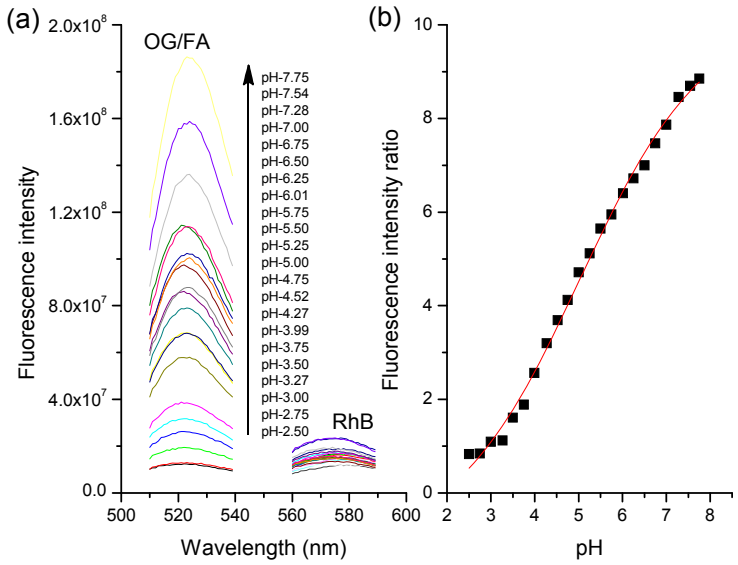

Figure 2.6. (a) Fluorescence emission curve for the pH nanosensor. b) pH calibration curve of the nanosensor made by plotting fluorescence intensity (I) ratios (I_{OG} + I_{FA} / I_{RhB}) against pH. OG = Oregon Green, FA = Fluorescein, RhB = Rhodamine B.

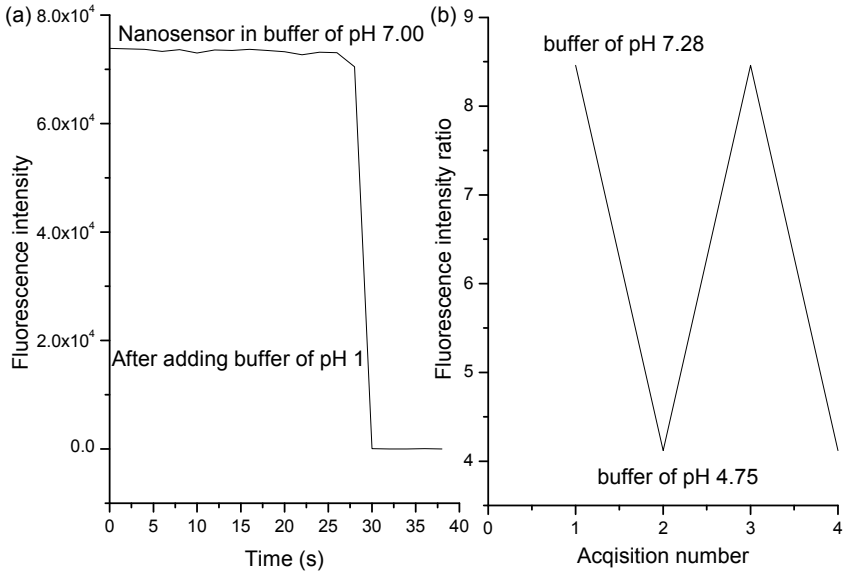

Figure 2.7. (a) Time for response of the nanosensor towards the change in pH. (b) Reversibility of the nanosensor, tested by repeatedly measuring the fluorescence intensity ratio (I_{OG} + I_{FA} / I_{RhB}) between two different pH.

The sensors can be easily tuned by changing the fluorophores, which can reconfigure its Π electron system during protonation. Binding of pH sensitive Fluorescein along with Rhodamine B to the cross-linked micelles can give ratiometric nanosensors for the pH range *ca.* 6 to 8. Incorporation of

Oregon Green expands the sensitivity from *ca.* pH 4 to 7.5. Ratiometric measurements minimized the errors due to excitation source fluctuations and sensor concentrations. The PEG corona of the core-shell-corona micelle sensors can enhances its biological advantages such as prolonged circulations of the nanosensors in blood. The PEG corona provided exclusive intramicellar shell cross-linking *via* steric stabilization mechanism.[163] The functionalities introduced in the shell region can be protected by the PEG corona. If protected from the light, the shell cross-linked micelle nanosensors appeared to be clear and remain stable for several months.

The cell uptake experiments of the nanosensor by HeLa cells were performed. The result showed that the nanosensor was capable of monitoring the intracellular pH in HeLa cells. Details of cell uptake experiments are given in **appendix A**.

2.1.4 Conclusion

The first synthesis and characterization of a shell cross-linked core-shell-corona micelle based ratiometric pH nanosensors for intracellular measurements is demonstrated. ATRP and principle of self-assembly is used to prepare polymeric micelles having well defined core-shell-corona morphology. The reinforcement of the weak hydrophobic interactions is achieved by covalent shell cross-linking using amidation reaction. The shell cross-linked core-shell-corona micelle is converted into ratiometric pH nanosensor by binding pH sensitive and reference fluorophores at the shell region. *In vitro* pH calibration curve by fluorescence measurement shows the broad pH sensitivity range for this shell cross-linked tripple labelled micelle nanosensor. Fluorescence measurements also confirm the quick response and reversibility of the ratiometric pH nanosensors towards the change in pH. AFM and DLS measurement confirms the exclusive intramicellar shell cross-linking in the nanosensor. GPC and CMC measurements show the difference in solution characteristics of cross-linked and non-cross-linked micelles.

2.2 Click-chemistry based Core Cross-linked Micelle Nanosensor

2.2.1 Introduction

The combination of controlled radical polymerization and click chemistry is nowadays extensively used for the preparation of polymeric nanomaterials.[164-166] Recent achievements in giving living characteristics to the radical polymerization[6, 7, 9, 11, 15, 16] have been able to provide easy and efficient ways of synthesizing amphiphilic block copolymers with well defined composition, as well as, narrow molecular weight distributions. Controlling the block copolymer composition (packing parameters)[46, 167] and conditions for assembly in solution, a wide range of morphologies[168-170] can be achieved by the spontaneous self-assembly of amphiphilic block copolymers. The amphiphilic diblock copolymers in block selective solvents give polymeric micelles having a spherical core-shell morphology,[49] whereas the amphiphilic linear triblock (ABC) copolymers give core-shell-corona spheres or cylinders.[57, 58] Many of the potential biomedical applications of these well known pharmaceutical carriers[171, 172] require stabilization by covalent cross-linking; enabling the resulting robust nanomorphology to maintain its structural integrity under various conditions.[48, 152, 153] Copper(I) catalyzed Huisgen 1,3-dipolar cycloadditions between azides and alkynes to yield triazoles are extensively used for functional modifications and cross-linking of diblock copolymer micelles due to its orthogonality and compatibility with other functional groups.[92, 93] As a result of the risks of intermicellar cross-linking or aggregation, the click cross-linking at the core[173] or shell region[71] of the diblock micelles are reported under very dilute conditions. In the case of triblock copolymer micelles, the presence of polyethylene glycol (PEG) coronal chains on a well defined core-shell-corona micelle will ensure primarily shell intramicellar cross-linking[72, 129] at high block copolymer concentration due to steric stabilization mechanisms.[163] The PEG corona will also protect the functionalities introduced at the shell or core regions of the micelle from the external surroundings. The protective PEG corona of this well known pharmaceutical carriers[174] can also provide prolonged circulation in blood and hence improve the effective accumulation in desired regions by the enhanced permeation and retention effect (EPR).[116, 175]

Compared to the diblock core-shell micelle, even with the potential to provide diversity in applications, regioselective functionalization, and stabilization; the three layer core-shell-corona-micelles are not yet investigated considerably. This is due to its structural complexity and synthetic difficulties in unimers synthesis. Synthesis of functional core-shell-corona micelles required the

synthesis of functional triblock copolymers. The functional block copolymers (unimers) can be synthesized by controlled radical polymerization, in which transition metal catalyzed ATRP provides an effortless way.[17] ATRP in functional block copolymer synthesis is associated with protection and deprotection chemistry. The two main reasons for incorporation of protection chemistry in block copolymer synthesis are the sensitivity of the functional monomer towards the transition metal catalyst, as well as the stability of the monomer under ATRP conditions.[25] Selection of monomer protecting groups for the synthesis of block copolymers having more than one functional block is a critical issue, as the protecting groups should be stable throughout the ATRP process and should be cleaved easily and simultaneously under mild conditions. In addition to this, functional modification and covalent cross-linking at the hydrophobic core domains of the amphiphilic triblock copolymer self-assembly require accessibility of reactants and catalysts into this domain. Hence the reagents should transverse the corona, shell and core-shell interface of the micelle and should be soluble in the hydrophobic core domain.[152]

Intracellular pH measurements provides information about the pH dependant cellular process[176] and pH sensitive drug delivery.[177] As a consequence of this number of nanoparticle especially polymeric nanoparticles based nanosensors for ratiometric pH measurements are developed.[97, 110, 113, 114, 142] It is fascinating but not surprising that even with the excellent pharmaceutical advantages[144] of polymeric micelle, are not yet utilized in pH nanosensor fabrication due to synthetic difficulties and structural instability under infinitely diluted biological conditions. This section elucidate the first synthesis of click core cross-linked core-shell-corona functional polymeric micelles based ratiometric pH nanosensors by ATRP, self-assembly and dimensional synthetic organic chemistry.

2.2.2 Experimental: Click-chemistry based core cross-linked micelle nanosensor synthesis

Materials and measurements: Poly (ethylene glycol) monomethylether (M_n = 5000), 2-Bromo-isobutyryl-bromide (98 %), Dichlorobis(triphenylphosphine)palladium(II) (98 %), copper(I) iodide (98%), (Trimethylsilyl)acetylene (98 %), 4-Bromostyrene (98 %), 2-Aminoethyl methacrylate hydrochloride (AEMA HCl) (90 %), 1-[2-(Trimethylsilyl)ethoxycarbonyloxy] pyrrolidin-2,5-dione, 2,2'-bipyridyl (bpy) (99 %), anisol (anhydrous) (99.7 %), 4,4′-Dinonyl-2,2′-dipyridyl (dNbpy) (97%), N,N-Diisopropylethylamine (DIPEA) (99.5 %), Dialysis tube (MWCO = 12kDa),

Tetrabutylammonium fluoride (1M THF solution), Methanesulfonyl chloride (MsCl) (99.7 %) and Sodium azide were purchased from Sigma Aldrich and used as obtained. CuCl (99.995 %) was washed with glacial acetic acid, followed by absolute ethanol and diethylether, dried and stored under argon. Triethylamine (TEA) was distilled from calcium hydride and stored under molecular sieves (4 Å). MeOH used for ATRP was purified by distillation over the drying agent $Mg(OMe)_2$, stored under molecular sieves (3 Å) and transferred under argon. $CuBr(PPh_3)_3$ and Dendritic alcohol $(OH)_4$-[G-1] (**26**) were synthesized by literature procedures[178, 179]. Argon atmosphere (99.9999 %) used in the reactions was provided by AGA Denmark. All other solvents and chemicals were purchased from Sigma Aldrich and used as obtained. NMR spectra were recorded by using a 300 MHz Varian Mercury 300 BB spectrometer. IR spectra were recorded by Perkin Elmer Spectrum 100 FT-IR Spectrometer. GPC measurements were carried out with a Viscotek refractive index detector and PL Gel Mixed-C+D column with a flow rate of 0.5 mL/min at 25 ^{0}C using THF as eluent. Fluorescence measurements were carried out by the Olis Line of SLM based Spectrofluorometer. Samples for atomic force microscopy (AFM) were prepared by placing a 5 µl drop of the nanoparticle suspension on a silicon wafer. The particles were allowed to settle for 30 minutes, before excess liquid were removed using the corner of a lens-cleaning tissue. AFM images were obtained by PSIA XE-150 scanning force microscope using non-contact tapping mode close to resonance frequency of the silicon cantilever (Nanoworld, pointprobe type, force constant 42 N/m and tip radius <12 nm) of around 320 kHz. All images were recorded under atmospheric conditions. Dynamic light scattering (DLS) and zeta potential measurements were carried out by Brookhaven Zeta PALS instrument.

Synthesis of 2-(((2-(trimethylsilyl)ethoxy)carbonyl)amino)ethyl methacrylate(AEMA-Teoc): 2-Aminoethylmethacrylate hydrochloride (AEMA HCl) (590 mg, 3.56 mmol) was dissolved in 15 mL of dry DCM. Anhydrous triethylamine (1.080 mL, 10.68 mmol) and 1-[2-(Trimethylsilyl)ethoxycarbonyloxy]pyrrolidin-2,5-dione (1015 mg, 3.916 mmol,) were added and stirred at room temperature under argon atmosphere for 7h. The progress of the reaction was monitored by TLC (Ethylacetate : Hexane (1:1) $R_{f(product)} = 0.56$). The reaction mixture was diluted with 50 mL of DCM, then washed with 5 % HCl (2 × 20 mL) followed by saturated sodium bicarbonate (2 × 20 mL) and brine (2 × 20 mL). The organic layer was dried over anhydrous sodium sulfate, filtered, and removal of solvent under reduced pressure gave a pale pink crystalline solid. Isolated yield 0.8 g (82 %). ^{1}H-NMR (300 MHz, $CDCl_3$): δ = 6.08 (d, 1 H; vinylic), 5.55 (d, 1

H; vinylic), 4.84 (br s, 1 H; -N**H**), 4.20 (t, 2 H; -NHCH$_2$C**H**$_2$O), 4.12 (t, 2 H; -NHCOOC**H**$_2$CH$_2$), 3.44 (m, 2 H; -NHC**H**$_2$CH$_2$O), 1.91 (s, 3 H; -C**H**$_3$), 0.97 (t, 2 H; -NHCOOCH$_2$C**H**$_2$), 0.001 (s, 9 H; -Si(C**H**$_3$)$_3$) ppm; FT-IR: υ = 3344, 1701, 1636, 1524, 1453, 1246, 1158, 1042, 833 cm^{-1}.

Synthesis of 4-(Trimethylsilylethynyl) styrene(ESTMS): The monomer was synthesized by modifying the previously reported reaction[180]. To a solution of 4-Bromostyrene (2.357 mL, 18 mmol) in 165 mL of TEA, small amounts of hydroquinone (to prevent polymerization), (Trimethylsilyl)acetylene (3.415 mmol, 24 mmol), Bis(triphenylphosphine)palladium(II) dichloride (0.252 g, 0.36 mmol), and copper(I) iodide (33 mg, 0.18 mmol) were added. The reaction mixture was then stirred for 6h at 55 °C under argon atmosphere. The progress of the reaction was monitored by TLC ($R_{f(product)}$ = 0.28 in hexane). The reaction mixture was filtered, and the solvent was evaporated under vacuum. The residue was washed with water, extract with hexane, and dried over anhydrous sodium sulfate. After filtration and evaporation, a pale yellow liquid product was isolated by column chromatography on silica gel using hexane as eluent; yield: 1.810 g (50 %). ^{1}H-NMR (300 MHz, $CDCl_3$) δ = 7.45 (d, 2H; o-ArH), 7.33 (d, 2H; m-ArH), 6.69 (dd, J = 11.2, 17.6 Hz, 1H; CH_2=CH), 5.79 (d, J = 17.6 Hz, 1H; trans CH_2=CH)), 5.29 (d, J = 11.2 Hz, 1H; cis CH_2=CH), 0.22 (s, 9 H; -Si(CH_3)$_3$) ppm; FT-IR: υ = 3085, 2958, 2896, 2155, 1627, 1503, 1400, 1249, 1113, 1013, 986, 910, 856, 833 cm^{-1}.

Synthesis of PEG$_{5000}$-Br: The macroinitiator was synthesized by a procedure explained in **Section 2.1.2** also in **appendix B**.

Synthesis of Diblock Copolymer (PEG-b-PAEMA(Teoc)-Cl): PEG-Br (1 gram, 0.189 mmol), AEMA(Teoc) (516 mg, 1.89 mmol), 2,2'-bipyridyl (59 mg, 0.378 mmol), and 5 mL of dry MeOH were added to a 25 mL schlenk flask equipped with a stirrer bar. The flask was frozen in liquid nitrogen, and CuCl (21 mg, 0.20 mmol) catalyst was added. The reaction mixture was degassed with three freeze-pump-thaw cycles (each 15 minute long) to remove the oxygen, and the polymerization was carried out at 40 ^{0}C for 18 h under argon atmosphere. The resulting polymer was passed through a silica gel column to remove the copper catalyst using MeOH as eluent. Most of the MeOH was removed by rotary evaporation, and the polymer was precipitated into excess cold diethyl ether, isolated by filtration, and the precipitate dried under vacuum; yield 0.9 g (63 %). ^{1}H-NMR (300 MHz, $CDCl_3$): δ = 4.11-3.72 (-NHCH$_2$C**H**$_2$O, -NHCOOC**H**$_2$CH$_2$), 3.60 (s, -C**H**$_2$C**H**$_2$O), 3.41-3.30 (-NHC**H**$_2$CH$_2$O), 2.00-1.73 (-C**H**$_2$ of the polymer backbone), 1.33-0.82 (-C**H**$_3$ of the

polymer backbone, -NHCOOCH$_2$C**H**$_2$), 0.001 (s, -Si(C**H**$_3$)$_3$) ppm; FT-IR: υ = 3341, 1718, 1642, 1529, 1464, 1341, 1240, 1104, 960, 839 cm^{-1}.

Synthesis of triblock copolymer (PEG-b-PAEMA(Teoc)-b-P(ESTMS)) (25): The diblock copolymer PEG-PAEMA(Teoc)-Cl (500 mg, 0.067 mmol), 5 mL anisole, 4,4′-Dinonyl-2,2′-dipyridyl (55 mg, 0.134 mmol) and ESTMS (402 mg, 2.01 mmol) were added to a 25 mL schlenk flask equipped with a stirrer bar. The reaction mixture was frozen under liquid nitrogen; CuCl (7.2 mg, 0.073 mmol) was added, and degassed with three freeze-pump-thaw cycles followed by stirred under argon at 130 ^{0}C for 30 h. After removing most of the solvent under vacuum, the polymer was precipitated into excess cold diethyl ether and dried under vacuum; yield 0.5 g (58 %). The polymer was further purified by dissolved it in THF (10 mg/mL) and dialyzed (MWCO = 12 kDa) against MilliQ water. From dynamic light scattering (DLS) of the micelle dispersion, number-averaged hydrodynamic diameter (D_h) was found to be 23±3 nm and zeta potential measurement showed (ξ) = -16±2 mV. The micelle solution was lyophilized to get the pure polymer. ^{1}H-NMR (300 MHz, $CDCl_3$): δ = 7.47-6.22 (m, Ar**H**), 4.18-3.72 (-NHCH$_2$C**H**$_2$O, -NHCOOC**H**$_2$CH$_2$), 3.60 (s, -C**H**$_2$C**H**$_2$O), 3.50-3.31 (-NHC**H**$_2$CH$_2$O), 2.04-0.60 (PAEMA and PES backbone, -NHCOOCH$_2$C**H**$_2$), 0.22 (s, -Si(C**H**$_3$)$_3$ of PESTMS), 0.00 (s, -Si(C**H**$_3$)$_3$ of PAEMA(Teoc)) ppm; FT-IR: υ = 3300, 2160, 2106, 1719, 1504, 1448, 1342, 1248, 1103, 962, 840 cm^{-1}. Kaiser test of the polymer was performed the colorless solution indicate fully protected amino groups.

.***PEG-b-PAEMA-b-PES micelle (28):*** The triblock copolymer PEG-*b*-PAEMA(Teoc)-*b*-P(ESTMS) (150 mg, 0.011 mmol) was dissolved in 9 mL of THF, followed by 1M TBAF in THF (0.318 mL, 1.1 mmol) was added and stirred at room temperature for 5h. The reaction mixture was diluted drop wise with 40 mL MilliQ water. The resulting cloudy micelle solution was transferred to a dialysis tube (MWCO = 12 kDa) and dialyzed against MilliQ water for three days. The final micelle concentration was 2.5 mg/mL (D_h = 20±1 nm and (ξ) = 11±2 mV). A portion of the micelle was lyophilized for characterization. ^{1}H-NMR (300 MHz, $CDCl_3$): δ = 7.50-6.10 (m, Ar**H**), 4.25-3.45 (-COOC**H**$_2$CH$_2$NH$_2$, -C**H**$_2$C**H**$_2$O), 3.45-3.31 (-CH$_2$C**H**$_2$NH$_2$), 3.27-2.85 (br s, -C≡C-**H**), 1.90-0.70 (PAEMA and PES backbone); FT-IR: υ = 3500, 3289, 3241, 2106, 1725, 1501, 1450, 1342, 1241, 1103, 961, 840 cm^{-1}. Positive Kaiser test (blue color) indicated the presence of free amino groups.

Synthesis of Dendritic cross-link***er ((N$_3$)$_4$-[G-1]) (27):*** The dendritic alcohol (HO)$_4$-[G-1] (**26**) (500 mg, 0.73 mmol) and triethylamine (0.610 mL, 4.35 mmol) were dissolved in 5 mL of DMF in a 25

mL round-bottom flask, and allowed to stir for 15 min at room temperature. The mixture was cooled to 0 ^{0}C, and Methanesulfonyl chloride (0.340 mL, 4.35 mmol) was added drop wise, warmed to room temperature, and stirred for 12 h under argon. After 12 h, NaN_3 (570 mg, 8.75 mmol) was added, and the reaction mixture was allowed to stir at 90 ^{0}C for another 18 h under argon. The progress of the reaction was monitored by TLC (10 % MeOH in DCM, $R_{f(product)}$ = 0.56). The reaction mixture was poured into brine and extracted with DCM (3×20 mL) and washed with saturated sodium bicarbonate (2×20 mL). The combined organic layer was dried over anhydrous sodium sulfate, filtered, concentrated *via* rotary evaporation and the residue was dried under vacuum; yield 0.45 g (90 %). ^{1}H-NMR (300 MHz, $CDCl_3$): δ = 7.78 (s, 2H; 2-triazole **H**), 6.93 (s, 4 H; Ar**H**), 6.92 (s, 2 H; Ar**H**), 5.24 (s, 4 H; traizole-C**H**$_2$O), 4.53 (t, J = 5 Hz, 4 H; triazole-C**H**$_2$CH$_2$OCH$_2$), 4.34 (s, 8 H; -C**H**$_2$N$_3$), 3.85 (t, J = 5 Hz, 4 H; triazole-CH$_2$C**H**$_2$OCH$_2$), 3.56 (s, 4 H; triazole-CH$_2$CH$_2$OC**H**$_2$); FT-IR: υ = 3150-2850, 2090, 1597, 1453, 1293, 1116, 1048, 839 cm^{-1}.

Synthesis of cross-linked micelle (29): 30 mL (75 mg, (2.5 mg/mL) of the PEG_{120}-*b*-$PAEMA_8$-*b*-PES_{26} micelle solution was transferred into dialysis tube (MWCO = 12 kDa) and dialyzed against 4:1 buffered water: THF for three days. The micelle solution (75 mg, 0.153 mmol of alkyne equivalent) was transferred into 100 mL round-bottom flask, added $CuBr(PPh_3)_3$ (42.78 mg, 0.046 mmol), DIPEA (80 µL, 0.46 mmol), Cu wire (to prevent oxidation of the catalyst) (*ca.* 100 mg), and the cross-linker $(N_3)_4$-[G-1] (in 2.5 mL of THF) (52.6 mg, 0.077 mmol). The reaction mixture was stirred for 3 days at room temperature and then transferred to a dialysis tube of (MWCO = 12 kDa) and dialyzed against MilliQ water and THF (4:1) for 4 days and then against MilliQ water for another 4 days. The final concentration of the micelle was 2 mg/mL (D_h = 22±2 nm and zeta potential (ξ) = 10±2 mV). A portion of the micelle was lyophilized for characterization. ^{1}H-NMR: Solubility of the cross-linked micelles in deuterated solvents was extremely low. FT-IR: υ = 3460, 3138, 2872, 2099, 1721, 1600, 1453, 1346, 1290, 1101, 948, 833 cm^{-1}.

Synthesis of click core cross-linked micelle nanosensors (30): The cross-linked PEG_{120}-*b*-$PAEMA_8$-*b*-PES_{26} micelle solution (**29**) (15 mL, 30 mg, 0.0023 mmol) in MilliQ water, was dialyzed against carbonate buffer (pH = 9) for three days. The micelle dispersion was transferred into 100 mL round-bottom flask; FITC (0.020 mg, 0.0525 µmol), Oregon Green ITC (0.022 mg, 0.0525 µmol) and RhBITC (0.01 mg, 0.021 µmol) were added and stirred at room temperature for 12 h in the absence of light. The reaction mixture was transferred to dialysis tube (MWCO = 12 kDa), dialysis against carbonate buffer (pH = 9) for three days and then against MilliQ water for

another three days (D_h = 23±1 nm, ξ = 7±3 mV). The sensor solution was covered with aluminum foil to protect it from the light. If protected from the light, the sensor was capable to maintain same pH sensitivity for several weeks.

2.2.3 Results and Discussion

Schematic representation of the polymeric micelle based core cross-linked ratiometric pH nanosensor fabrication is shown in **Figure 2.8**. The amphiphilic triblock copolymer poly(ethylene glycol)$_{120}$-*b*-poly([((trimethylsilyl)ethoxy)carbonyl] aminoethyl methacrylate)$_8$-*b*-poly((trimethylsilylethynyl) styrene)$_{26}$ (PEG$_{120}$-*b*-PAEMA(Teoc)$_8$-*b*-PES(TMS)$_{26}$ (**25**) was synthesized by isolated macroinitiator atom transfer radical polymerization (ATRP) (**Scheme 2.3**). The presence of Teoc and TMS protecting groups on the polymer were confirmed by NMR (^{1}H-NMR, $CDCl_3$), δ = 0.00 ppm and 0.22 ppm respectively (**Figure 2.9a**). FT-IR spectroscopy confirmed the carbonyl and aromatic (C=C) stretching of PAEMA(Teoc) and PES(TMS) blocks *ca.* 1700 cm^{-1} and 1500 cm^{-1} respectively. The number-average molecular weight (M_n) of the polymers measured by gel permeation chromatography (GPC) in THF with polystyrene as standard (**Figure 2.10**) was higher than that calculated from ^{1}H-NMR spectroscopy. The GPC analysis and ^{1}H NMR spectroscopic results are summarized in **Table 2.3**.

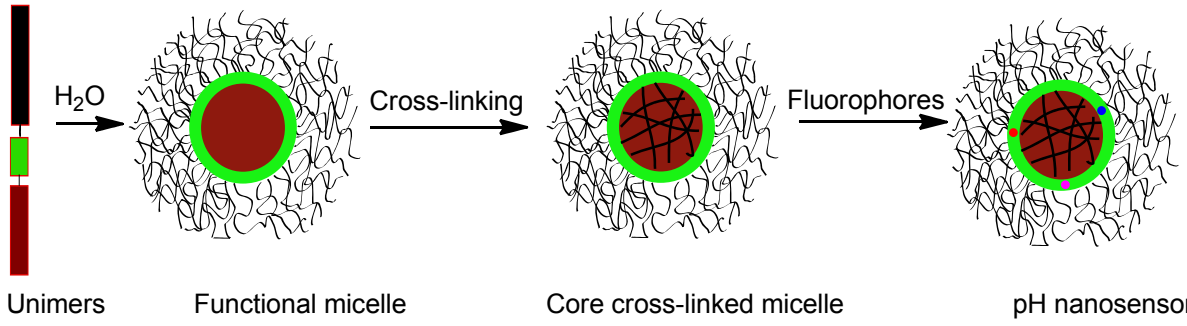

Figure 2.8. Click core cross-linked ratiometric pH nanosensor fabrication from functional amphiphilic triblock copolymer self-assembly.

Table 2.3. Molecular weights of PEG$_n$-*b*-PAEMA(Teoc)$_m$-*b*-PES(TMS)$_p$ (**25**).

M_n[a]	M_w[a]	M_w/M_n[a]	M_n[b]	n[c]	m [c]	p [c]
13700	16850	1.23	12670	120	8	26

[a] Determined by GPC, [b] Determined by NMR, [c] Number of repeating units of PEG block (n), PAEMA(Teoc) block (m) and PES(TMS) block (p).

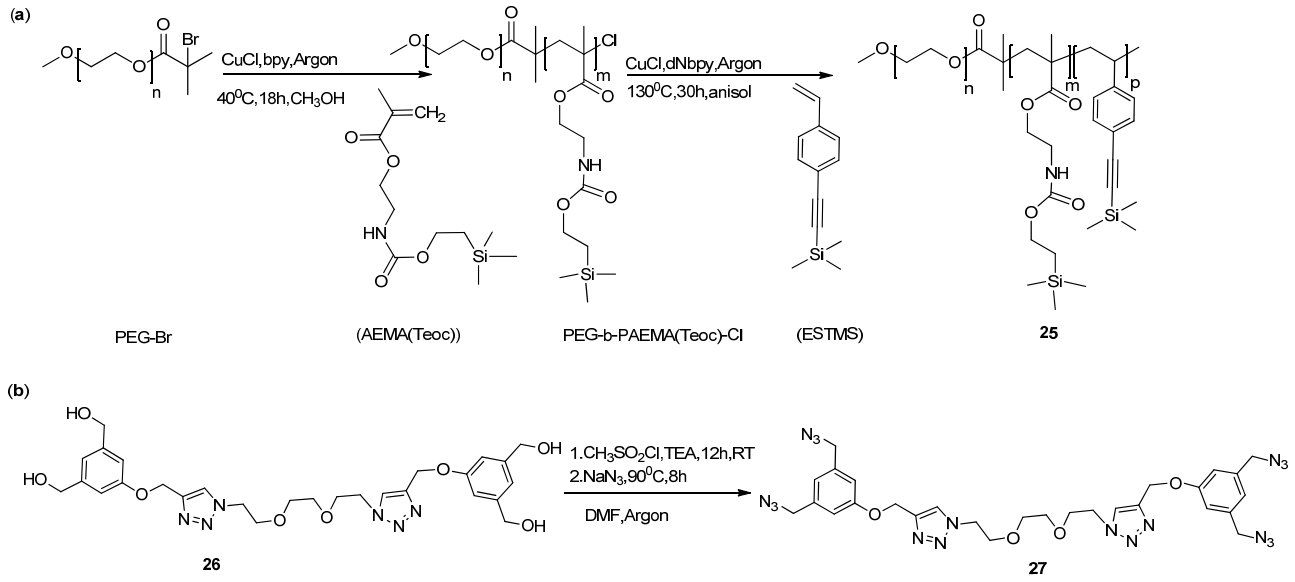

Scheme 2.3. a) Synthesis of PEG-*b*-PAEMA(Teoc)-*b*-PES(TMS) (**25**). b) Synthesis of dendritic azide benzyl ether cross-linker, **27**. bpy = 2,2'bipyridine, dNbpy = 4,4′-Dinonyl-2,2′-dipyridyl, TEA = triethylamine.

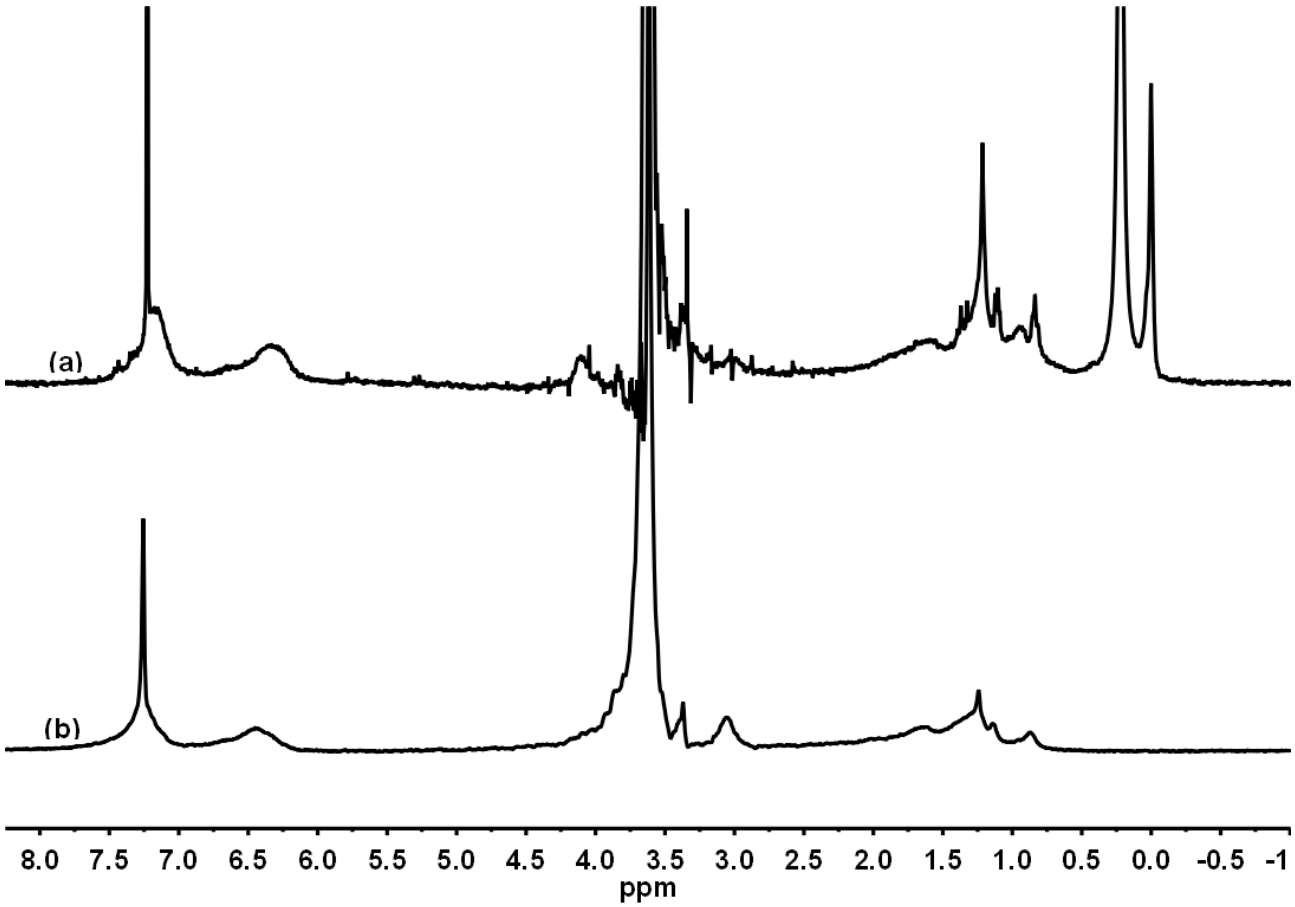

Figure 2.9. ^{1}H-NMR spectra of a) PEG_{120}-*b*-$PAEMA(Teoc)_8$-*b*-$PES(TMS)_{26}$ (**25**) and b) the lyophilized PEG_{120}-*b*-$PAEMA_8$-*b*-PES_{26} micelle (**28**), in $CDCl_3$ without containing tetramethylsilane as an internal standard.

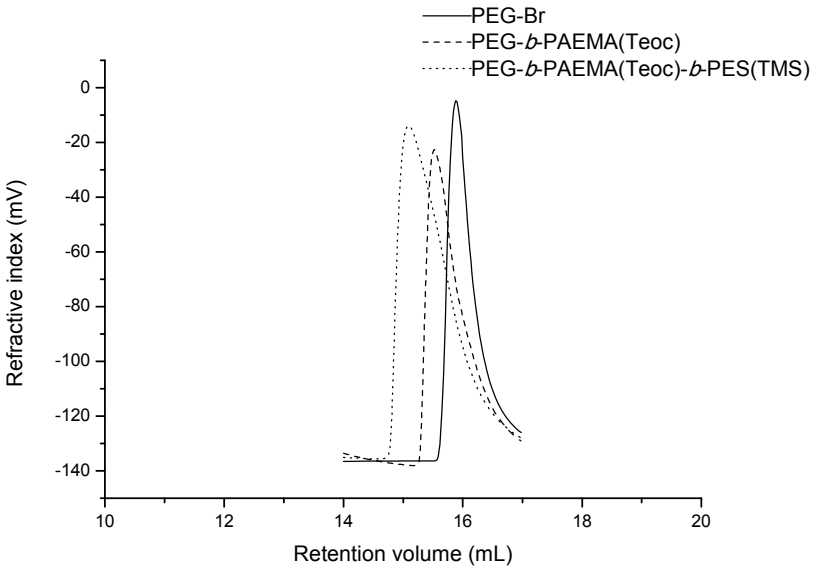

Figure 2.10. GPC spectra of macroinitiator, diblock and triblock copolymers.

The silyl protecting groups of the amphiphilic triblock copolymers were removed by treatment with 1M tetrabutylammonium fluoride (TBAF) in THF. The common solvent (THF) was gradually displaced by a selective solvent (water) for the hydrophilic blocks. The micelles were kinetically trapped by complete displacement of common solvent by selective solvent *via* dialysis against MilliQ water. A portion of the micelles **28** was lyophilized for characterization. The complete deprotection of TMS and Teoc groups was confirmed by the disappearance of nuclear magnetic resonance of the –SiC(C**H**$_3$)$_3$ at δ 0.22 ppm and 0.00 ppm respectively (**Figure 2.9b**). Appearance of alkyne (-C≡C**H**) proton resonance at 3.06 ppm in NMR and -C≡**C-H** stretching at *ca.* 3280 cm^{-1} in FT-IR further confirmed the TMS de-protection. Positive Kaiser test[159] for the lyophilized micelle (appearance of blue color), and the increase in zeta potential of the micelle solution after Teoc deprotection of the amino groups; further confirmed the presence of free amino groups at the shell region of the micelle (**Table 2.4, micelle 25 & 28**).

Table 2.4. Characterization Data for Micelles **25**, **28**, **29** and pH Nanosensors **30**.

Micelle	DLS[a] D_h(nm)	AFM[b] H_{av}(nm)	Zeta(ξ)[c] (mV)
25[d]	23±3	…….	-16±2
28	20±1	05±1	+11±2
29	22±2	13±3	+10±2
30	23±1	14±3	+7±3

*[a] Number-averaged hydrodynamic diameter of the polymeric micelles in MilliQ water by dynamic light scattering, [b] Average height of the micelles are calculated from the values of ca. 100 particle by tapping mode AFM, [c] Zeta potential from 10 determination of 10 cycles and [d] Micelle of **25**.*

Synthesis of the click core cross-linked ratiometric pH nanosensors is shown in **Scheme 2.4**. The poly(4-ethynyl styrene) (PES) core of the de-protected PEG-*b*-PAEMA-*b*-PES micelle (**28)** was swollen by dialyzing against 4:1 buffered water : THF. The swollen solvent filled core enhances the solubility of the hydrophobic dendritic azide benzyl ether cross-linker **27** in the hydrophobic nanodomain. The dendritic azide benzyl ether cross-linker **27** was synthesized *via* nucleophilic substitution of benzyl mesylate of the dendritic benzyl alcohol **26** by sodium azide (**Scheme 2.3b**). The click reaction was performed between the click readied hydrophobic core of the micelle and the dendritic cross-linker using $CuBr(PPh_3)_3$/DIPEA as a catalyst in high block copolymer concentrations (2.5 mg/mL). The click core cross-linked micelle **29** was purified by dialysis. DLS measurement of the cross-linked micelle in MilliQ water showed no significant change in the hydrodynamic diameter after cross-linking. DLS measurements confirmed intramicellar core cross-linking of the confined core-shell-corona micelle at high block copolymer concentration (**Table 2.4, micelle 29**). Comparison of FT-IR spectra of the lyophilized PEG-*b*-PAEMA-*b*-PES micelle before and after core cross-linking showed the disappearance of -C≡C-**H** stretching absorption at *ca.* 3280 cm^{-1} and the appearance of a strong -N≡N asymmetric stretching absorption from the azide at *ca.* 2100 cm^{-1} after cross-linking (**Figure 2.11**). This confirmed the consumption of alkyne functionality at the core domain and the presence of excess azide groups on the cross-linker of the core cross-linked micelle. Characterization of the cross-linked micelle by NMR was unsuccessful due to solubility problems in deuterated solvents.

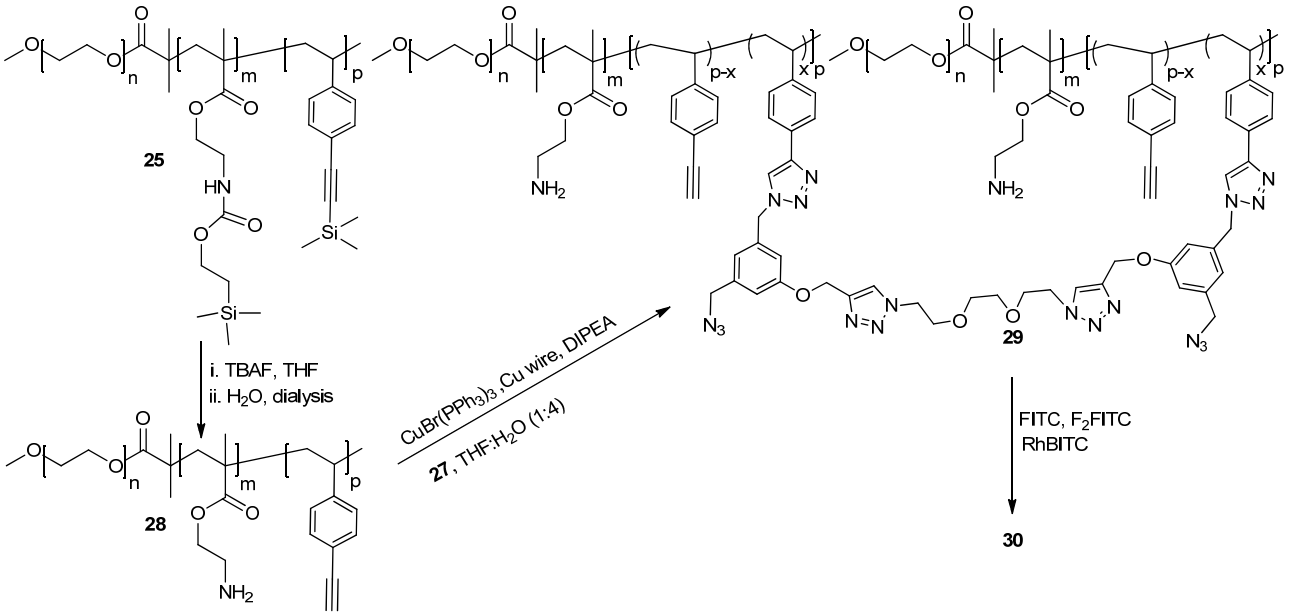

Scheme 2.4. Synthesis of click core cross-liked micelle ratiometric pH nanosensors (**30**). The cross-linking reaction was performed by dendritic azide cross-linker **27** (0.5 equiv). The minimum click core cross-linking potential of the cross-linker molecule is shown in the scheme. TBAF = Tetrabutylammonium fluoride, DIPEA = N,N-Diisopropylethylamine, FITC = Fluorescein isothiocyanate, F_2FITC = Oregon Green 488 isothiocyanate, RhBITC = Rhodamine B isothiocyanate; at 100% cross-linking, p = x.

The core cross-linked micelle was converted into a ratiometric pH nanosensor **30** by binding pH sensitive (Fluorescein and Oregon Green) and reference (Rhodamine B) fluorophores at the shell region of the micelle. In an alkaline buffer, few of the free amino groups present at the PAEMA shell of the core cross-linked micelle were nucleophilically attacked at the central elctrophilic carbon atoms of the pH sensitive and reference fluorophore-isothiocyanates. The un-reacted free fluorophores from the thiourea product were removed by extensive dialysis against carbonate buffer followed by dialysis against MilliQ water. DLS measurements showed that the nanosensor **30** in MilliQ water had approximately same hydrodynamic diameter as that of the cross-linked micelle **29**. The zeta potential measurements showed a slight decrease in surface charge density as a result of fluorophore binding (**Table 2.4, micelle 30**).

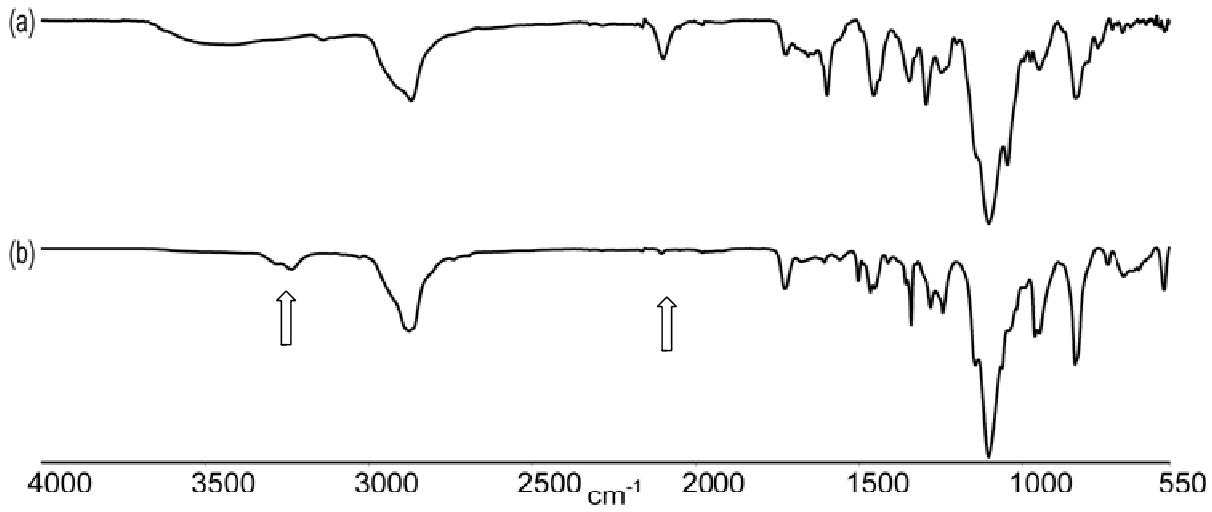

Figure 2.11. FT-IR spectra of PEG-*b*-PAEMA-*b*-PES micelle; (a) after cross-linking, **29** and (b) before cross-linking, **28**. The arrows in (b) indicate the presence of acetylenic groups and absence of azide groups; y-axis is % of transmittance in arbitrary units.

2D and 3D Atomic force microscopic (AFM) images of micelle **28**, **29** and **30** absorbed on a hydrophilic silica surface are shown in **Figure 2.12**. Compared to the non-cross-linked micelle **28**, the robust cross-linked micelle **29** and nanosensor **30** shows a significant increase in average height (H_{av}) calculated by AFM measurements (**Table 2.4**). The significant increase in nanoparticle heights (H_{av}) during core cross-linking indicates that the extent of interaction between the spherical nanoparticles and the silica substrate changed considerably after cross-linking. Core cross-linking using the hydrophobic benzyl ether cross-linker enhances the hydrophobicity of the polystyrene core *via* covalent reinforcement to the hydrophobic interactions at the core domain. The resulting hydrophobic core of the robust micelle strongly repels the hydrophilic silica surface (less flattening on the surface) and as a result of this hydrophobic hydrophilic repulsion, the nanoparticle height increases. The fluorophores binding to the core cross-linked micelles do not show further significant increase in the height of the resulting nanosensors. Thus, the AFM studies reveal the effect of core cross-linking on the core-shell-corona micelle-surface interactions.

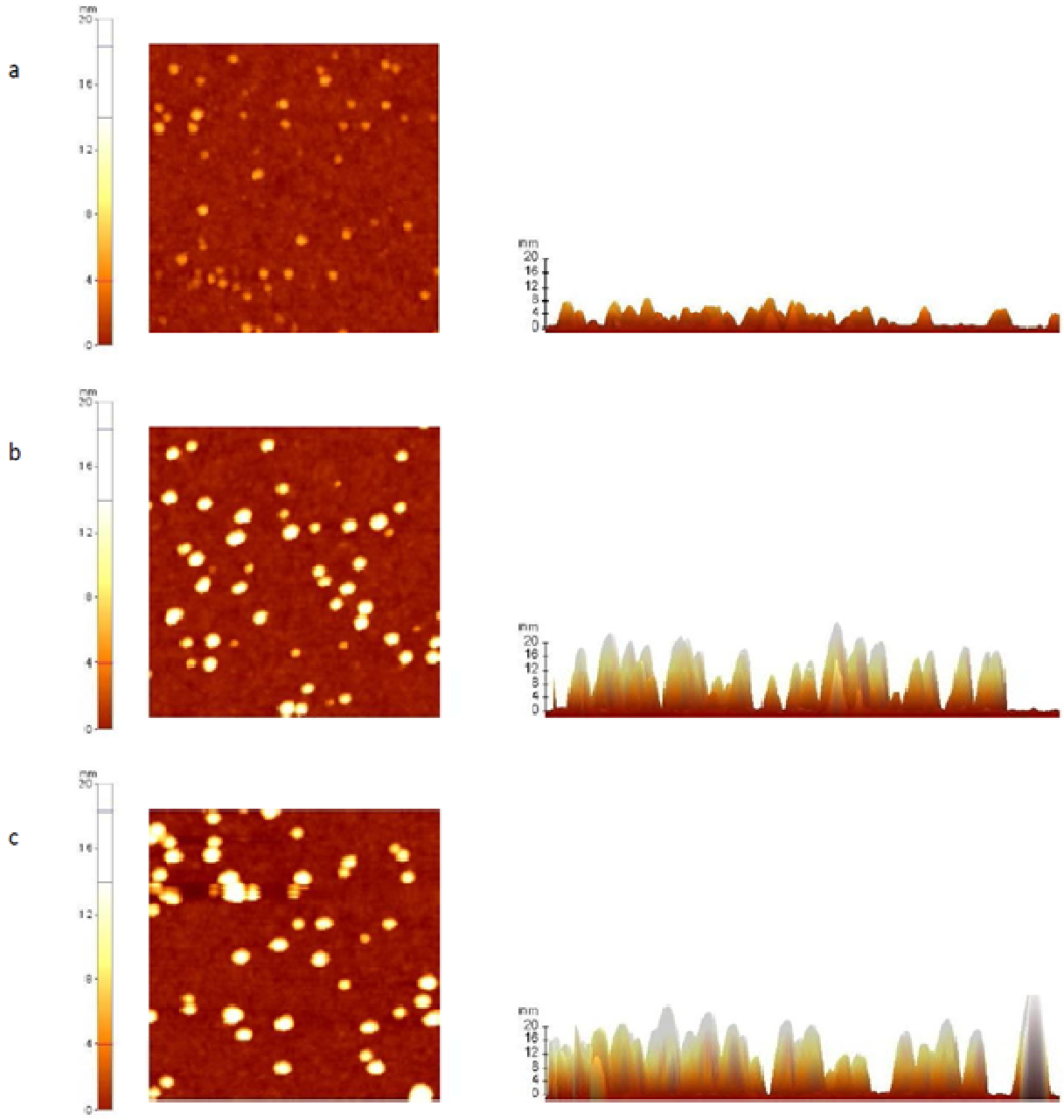

Figure 2.12. Representative tapping-mode 2D and 3D AFM images of nanoparticles; a) non-cross-linked micelle **28**, b) cross-linked micelle **29**, and c) pH nanosensors **30**. XY scan size is 1 μm x 1 μm.

DLS measurements of aqueous micelle solutions at different temperature were performed to confirm the solution stability of this block copolymer self-assembly. Incubating the micelle solutions from 25 ^{0}C to 70 ^{0}C, followed by DLS measurements showed thermodynamically favored micelle dissociation of non-cross-linked micelle **28** occurred *ca.* 65 ^{0}C, and there after no self-assembled structures were detectable. But the cross-linked micelle **29** and nanosensor **30** were maintained their structural integrity throughout the experiments. This provided an additional

evidence for the covalent cross-linking between the unimers of this nanoparticle scaffolds (**Figure 2.13**).

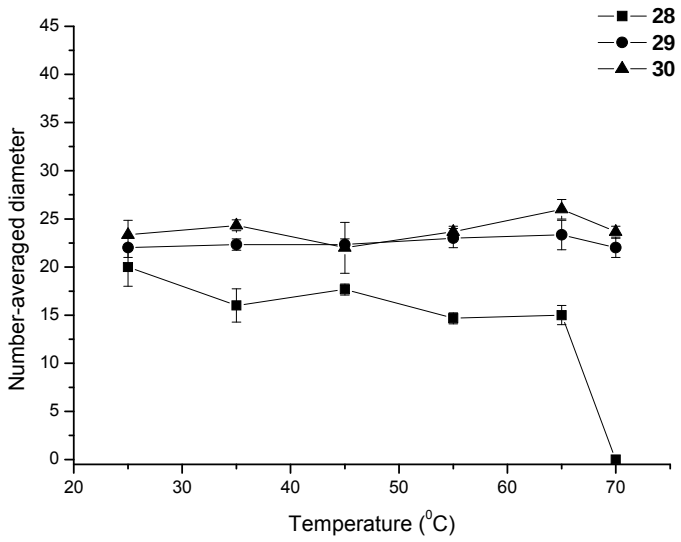

Figure 2.13. Variation of number-averaged hydrodynamic diameter (D_h) with temperature is determined from DLS measurements; non-cross-linked micelle (■) **28**, cross-linked micelle (●) **29**, and cross-linked nanosensor (▲) **30**.

A pH calibration curve for the nanosensors was constructed by fluorescence measurements. The pH sensitive Oregon Green and Fluorescein (OG and FA) and reference fluorophore Rhodamine B (RhB) of the nanosensors were excited in buffer of different pH. The fluorescence intensity ratios ($(I_{OG} + I_{FA}) / I_{RhB}$) were then plotted against the corresponding pH. Resulting calibration curve confirmed the covalent attachments of pH sensitive and reference fluorophores to the PAEMA shell of core cross-linked core-shell-corona micelle, and demonstrated that the resulting pH nanosensor is sensitive between the pH *ca.* 4.5 to 7.5 (**Figure 2.14**). Reversibility and time for response for the nanosensor was also measured by fluorescence spectroscopy (**Figure 2.15**). The measurements show that the sensors are reversible between any two pH within the broad pH sensitivity range and are quickly responding (with in micro seconds) towards the change in pH.

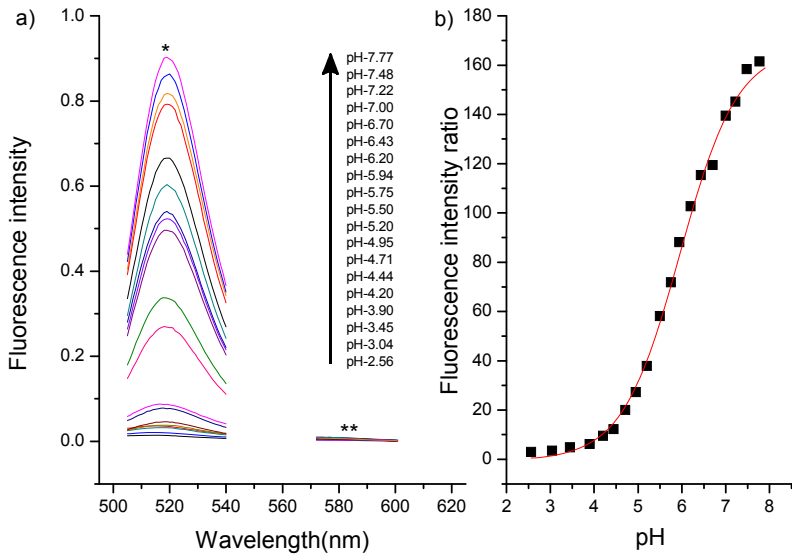

Figure 2.14. a) Fluorescence emission spectra of the pH nanosensor in buffers of different pH having sensor concentration 0.1 mg/mL. *For pH sensitive fluorophores excitation wavelength, λ_{ex} = 488 nm and **for reference fluorophore λ_{ex} = 543 nm. b) pH calibration curve made by plotting fluorescence intensity ratio (I_{OG} + I_{FA} / I_{RhB}) against pH.

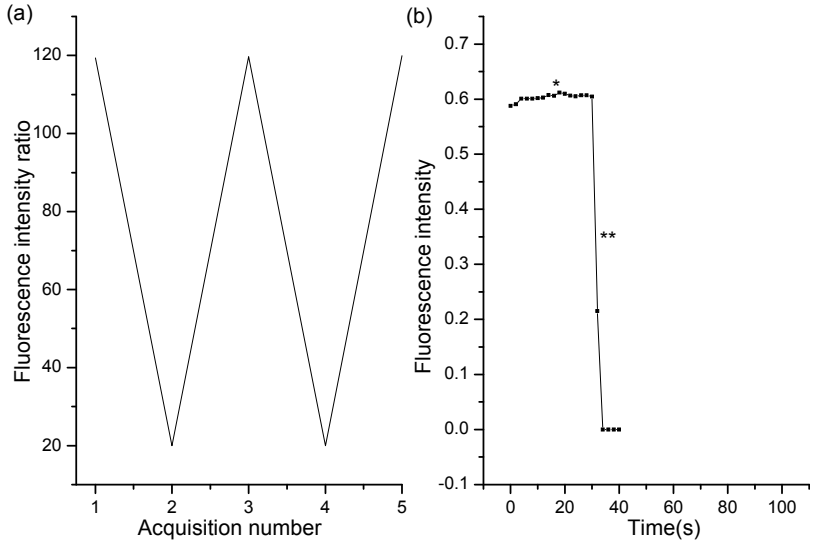

Figure 2.15. a) Reversibility of the nanosensor was tested by repeatedly changing the pH from 6.7 to 4.7 and *vice versa*. The corresponding fluorescence intensity ratio (I_{OG} + I_{FA} / I_{RhB}) was plotted against the acquisition number. The sensor concentration in each measurement was 0.1 mg/mL. b) The time for response of the pH nanosensors by fluorescence measurements. *Fluorescence intensity of the nanosensors in buffer of pH 6.5, **decrease in fluorescence intensity due to the addition of buffer of pH 2.5. The excitation wavelength (λ_{ex}) was 488 nm and emission wavelength (λ_{em}) was set to 518 nm.

2.2.4 Conclusion

Polymeric micelle based click chemistry based core cross-linked ratiometric pH nanosensors were prepared. Functional triblock copolymers are synthesized by atom transfer radical polymerization of protected functional monomers. The functional micelle resulting from the self-assembly of functional unimers is cross-linked by dendritic click reactions at the hydrophobic core. The core cross-linked core-shell-corona micelle having a radially compartmentalized corona is converted into triple fluorophore pH nanosensors by binding pH sensitive and reference fluorophores at the inner corona (shell) region. The sensor is sensitive between the pH *ca.* 4.5-7.5, reversible and quickly responsive to the pH changes in this broad pH range. The covalent cross-linking between the unimers of this nanoparticle scaffold can enhance its biomedical applications by preventing the dissociation of the sensor under infinitely diluted biological conditions even below the critical micelle concentration (CMC) of the micelles (if they were not cross-linked). The presence of excess azido functionalities on the dendritic cross-linkers of the cross-linked core provides opportunities to bind hydrophobic cargoes at the core region. The presence of excess amino groups at the hydrophilic shell region (PAEMA) of the micelle can allow the incorporation of cargoes into it. The presence of PEG corona chains may not only provide long circulation half life of the nanosensors in blood, and hence effective accumulation in the desired region, but also can protect the cargo attached to the shell and core region of the micelle nanosensors. In conclusion, an advanced pH nanosensor suitable for intracellular pH measurements has been developed. The transformation of pharmaceutical carriers into sensors may provide an opportunity to combine the pharmaceutical and sensing application together. Further studies of the micelle nanosensors *in vivo* are under progress.

Chapter 3

Photo Core Cross-linked Micelle Nanosensors Synthesis

Use of photo chemistry in covalent stabilization of block copolymer self-assembly has achieved significant research attention.[39, 68, 181-183] This strategy does not demand reagents for cross-linking at the specific micelle domain and hence additional purification steps can be avoided. The only requirement is the synthesis of well defined UV sensitive unimers. UV induced reversible cross-linking has achieved significant research attention in drug delivery. This is due to its capability to offer reversible control over encapsulation and release of drugs incorporated to pharmaceutical carriers.[184, 185] Double bonds present in molecules like cinnamic acid, thymine, and coumarin can undergo UV induced reversible [2+2] intermolecular cycloaddition and form cyclobutane rings. There are a number of reports on UV cross-linking of cinnamic acid attached block polymer micelle. Cinnamic acid attached to hydroxyl groups of the block copolymers *via* post polymer modification (esterifications)[186-188] or by poly(ethylene glycol) (PEG) is grafted onto poly(4-cinnamic acid)-*co*-poly(3,4-cinnamic acid) (PCA) by Michael addition.[189] UV Cross-linking of thymine micelle has also reported. poly(vinylbenzylthymine)-*b*-poly(styrene sulfonicacid sodium salt) diblock copolymer micelle having thymine functionality at the core is associated by hydrogen bonding and subsequent UV exposure gave photo core cross-linked micelle.[190] Reversible photo core cross-linking of coumarin containing diblock core-shell micelle are used for the preparation of nanogel,[191] photo sensitive drug and contrast agent release,[74, 192] photo induced morphological switching of polymer nanoaggregates,[193] and layer by layer film formation in acidic buffer *etc*.[194] This chapter includes UV induced micelle cross-linking as a part of our interest in making photo core stabilized core-shell-corona functional micelle nanosensor.

3.1 Irreversibly Photo Core Cross-linked Micelle Nanosensor

3.1.1 Introduction

In block selective solvents, amphiphilic triblock copolymers spontaneously self-assemble[40] to give core-shell-corona micelle spheres or cylinders, whereas amphiphilic diblock copolymers give spherical core-shell micelles.[1, 49, 57, 195] Compared to core-shell micelles, the core-shell-corona micelles are more diverse with respect to regioselective functionalization and cross-linking. For example, in biological systems, moieties conjugated to the hydrophilic outer domain (corona) of a diblock micelle can have unwanted interactions with components of its immediate surroundings, such as serum proteins. In core-shell-corona micelles, the functionalizable shell region is protected by the surrounding corona. The potential application of polymeric micelles is limited by its dissociation into unimers at concentrations below the critical micelle concentration (CMC). Cross-linking abolishes the importance of hydrophobic interactions and hence prevents micelle dissociations below its CMC. Therefore, the regioselective covalent cross-linking between the unimers of block copolymer micelles has garnered significant research attention in recent years.[152, 153, 196] Radiation-induced micelle cross-linking is thought to be practically simpler than conventional cross-linking strategies. Cross-linking of triblock micelles in water *via* conventional strategies requires transfer/accessibility of the reagent to the nanodomains, long reaction times and subsequent purification. Radiation-induced micelle cross-linking, on the other hand, demands only the presence of UV sensitive groups on the micelle. UV radiation-induced shell layer cross-linking of amphiphilic triblock copolymer micelles has been reported.[186, 197]

The recent developments in controlled radical polymerizations[17, 122, 123] can provide well-defined amphiphilic triblock copolymers. Dimensional synthetic modifications on distinct domains of triblock self-assembly in water can provide a platform for stabilized functional nanoparticle synthesis. In continuation with the interests to synthesize polymeric micelle-based nanosensors, this section utilizes the structural potential of triblock core-shell-corona micelles to synthesis photo core cross-linked ratiometric pH nanosensors.

3.1.2 Experimental: Synthesis of photo core cross-linked micelle nanosensor

Materials and measurements: 2′,7′-bis- (2-carboxyethyl)-5-(and-6) carboxyfluorescein free acid (BCECF) was purchased from Biotium. Alexa Fluor 633 carboxylic acid succinimidyl ester (Alexa 633) was obtained from Invitrogen. N-(3-Dimetyl amino propyl)-N'-ethylcarbodiimide hydrochloride (EDC·HCl) (98%), N-Hydroxysuccinimide (NHS) (98%), dialysis tube (MWCO=12kDa), tetrabutylammonium fluoride (1M THF solution) and all other solvents and chemicals were purchased from Sigma Aldrich and used as obtained. NMR spectra were recorded on a 300 MHz Varian Mercury 300 BB spectrometer; IR spectra were recorded with a Perkin Elmer Spectrum 100 FT-IR spectrometer. GPC measurements were carried out with a Viscotek refractive index detector and a PL Gel Mixed-C+D column with a flow rate of 0.5 mL/min at 25°C by THF as eluent. UV-Vis spectra were recorded with Unicam Helios Uni 4923 spectrophotometer. Fluorescence measurements were carried out using Olis Line of SLM based Spectrofluorometer.

Samples for atomic force microscopy (AFM) were prepared by placing a 5 µl drop of the nanoparticle suspension on a silicon wafer. The particles were allowed to settle for 30 minutes, before excess liquid was removed using a lens cleaning tissue. AFM imaging was performed using a PSIA XE-150 scanning force microscope using non-contact tapping mode close to the resonance frequency of the silicon cantilever (Nanoworld, pointprobe type, force constant 42 N/m and tip radius <12 nm) of around 320 kHz. All images were recorded under atmospheric conditions.

Synthesis of PEG-b-PAEMA(Teoc)-b-P(SC≡CTMS) (25): Multiple steps involved in the synthesis of PEG-*b*-PAEMA(Teoc)-*b*-P(SC≡CTMS) were explained in chapter 2 section **2.2.2**. And hence here only shows the slightly modified procedure for the synthesis of final amphiphilic triblock copolymer.

The diblock copolymer PEG-PAEMA(Teoc)-Cl (500 mg, 0.058 mmol), 5 mL anisole, 4,4′-dinonyl-2,2′-dipyridyl (48 mg, 0.116 mmol) and ESTMS (464 mg, 2.32 mmol) were added to a 25 mL schlenk flask equipped with a stirrer bar. The reaction mixture was frozen under liquid nitrogen, and CuCl (6.3 mg, 0.063 mmol) was added, and the solution was degassed by subjecting it to three freeze-pump-thaw cycles to remove the oxygen followed by stirring under argon at 130 °C for 30 h. Most of the solvent was removed under vacuum; the polymer was precipitate into cold diethyl ether and dried under vacuum, yield 0.545 g (60%). The polymer was further purified by dissolving in THF (10 mg/mL) and dialyzing (MWCO = 12 kDa) against MilliQ water. From dynamic light

scattering (DLS) of the micelle dispersion, the number-weighted average hydrodynamic diameter (D_h) was found to be 20±3 nm and zeta potential measurement showed (ξ) = -15±2 mV. The micelle solution was lyophilized to get the pure polymer. ^{1}H-NMR (300 MHz, $CDCl_3$): δ = 7.48-6.223 (m, Ar**H**), 4.17-3.72 (-NHCH$_2$C**H**$_2$O, -NHCOOC**H**$_2$CH$_2$), 3.60 (s, -C**H**$_2$C**H**$_2$O), 3.51-3.31 (-NHC**H**$_2$CH$_2$O), 2.02-0.61 (PAEMA and PES backbone, -NHCOOCH$_2$C**H**$_2$), 0.21 (s, -Si(C**H**$_3$)$_3$ of PESTMS), 0.00 (s, -Si(C**H**$_3$)$_3$ of PAEMA(Teoc)) ppm; FT-IR: υ = 3300, 2160, 2106, 1719, 1504, 1448, 1342, 1248, 1103, 962, 840 cm^{-1}. Kaiser test of the polymer was performed, and the colorless solution indicates fully protected amino groups.

Preparation of micelles (28): The triblock copolymer PEG$_{120}$-*b*-PAEMA(Teoc)$_{12}$-*b*-P(SC≡CTMS)$_{36}$ (100 mg, 0.0063 mmol) was dissolved in 12 mL of THF, followed by the addition of 1M TBAF in THF (0.182 mL, 0.63 mmol) and stirrer at room temperature for 5h. The reaction mixture was diluted by drop wise addition of 30 mL MilliQ water. The resulting opalescent micelle dispersion was transferred to a dialysis tube (MWCO = 12 kDa) and dialyzed against MilliQ water for three days; the water was replaced two times per day. The final micelle concentration was 1.82 mg/mL (D_h = 16±3 nm and (ξ) = 16±1 mV). A portion of the micelle was lyophilized for characterization. ^{1}H-NMR (300 MHz, $CDCl_3$): δ = 7.51-6.10 (m, Ar**H**), 4.25-3.44 (-COOC**H**$_2$CH$_2$NH$_2$, -C**H**$_2$C**H**$_2$O), 3.45-3.31 (-CH$_2$C**H**$_2$NH$_2$), 3.27-2.85 (br s, -C≡C-**H**), 1.90-0.71 (PAEMA and PES backbone) ppm; FT-IR: υ = 3500, 3285, 3241, 2106, 1725, 1501, 1450, 1342, 1241, 1103, 961, 840 cm^{-1}. Positive Kaiser test (blue color) indicated the presence of free amino groups.

Pyrene CMC assay[198]: 12 mg (59.3 μmol) pyrene was dissolved in 10 mL acetone. This was diluted in acetone to 29.7 μM, and 34 μL of this solution was placed in 4 mL glass vials. The acetone was allowed to evaporate in the hood over five hours, leaving 1 nmol pyrene in each vial. 2 mL micelle dispersion (concentrations of 0.05-250 μg/mL) in MilliQ water (pyrene concentration 5*10^{-7} M) was added to each of the vials. The vials were incubated for one hour (*non cross-linked micelles*) or three hours (*cross-linked micelles*) at 65 ^{0}C and then overnight (17 h) at 37 ^{0}C. The vials were then kept at room temperature, protected from light until measurement. Fluorescence was recorded on an Olis Line of SLM based Spectrofluorometer. Excitation spectra were collected at 25 ^{0}C using emission wavelength 390 nm and a 16 nm slit size. Excitation was scanned in ranges of either 325-345 nm or 310-360 nm with all slits set to 0.5 nm. Intensity ratios (I_{337}/I_{334}) were calculated from the excitation spectra and plotted as a function of the polymer concentration.

Photo core cross-linking of PEG_{120}-b-$PAEMA_{12}$-b-$P(SC{\equiv}CH)_{36}$ micelles (31): 3 mL PEG_{120}-*b*-$PAEMA_{12}$-*b*-$P(SC{\equiv}CH)_{36}$ micelles (1.82 mg/mL) were stirred in a quartz cuvette and exposed to UV radiation (3 W/cm^2) from a UV spot curing system (Omnicure S2000) having a 200 W mercury vapor short arc lamp without using a wavelength filter. The progress of the cross-linking reaction (increase in absorbance at 600 nm) was monitored by UV-Vis spectrophotometry (D_h = 19±1 nm and (ξ) = 14±2 mV).

Preparation of the photo core cross-linked micelle nanosensor (32): 3 mL photo core cross-linked PEG_{120}-*b*-$PAEMA_{12}$-*b*-$P(SC{\equiv}CH)_{36}$ micelles (1.82 mg/mL) were dialyzed (MWCO = 12 kDa) against a $NaHCO_3/Na_2CO_3$ buffer of pH 9. To this colloidal dispersion, was added activated BCECF, BCECF was activated by adding BCECF (10 µl, 0.01 mg, 0.02 µmol) to 0.5 mL of water containing EDC·HCl (0.011 mg, 0.06 µmol) and NHS (0.00345 mg, 0.03 µmol) and stirring the reaction mixture at room temperature for 2h. 102 µl of the solution (2 µl activated BCECF) was transferred into the reaction mixture along with Alexa 633 (4 µl) (1mg/mL of dry DMSO). The reaction mixture was stirred at room temperature in the absence of light for 15 h after which it was transferred to dialysis tubing of MWCO 12 kDa and dialyzed against carbonate buffer (pH 9) for three days and then against MilliQ water for another three days. Final sensor concentration was 1.76 mg/mL (D_h = 20±2 nm and (ξ) = 10±1 mV).

3.1.3 Results and Discussion

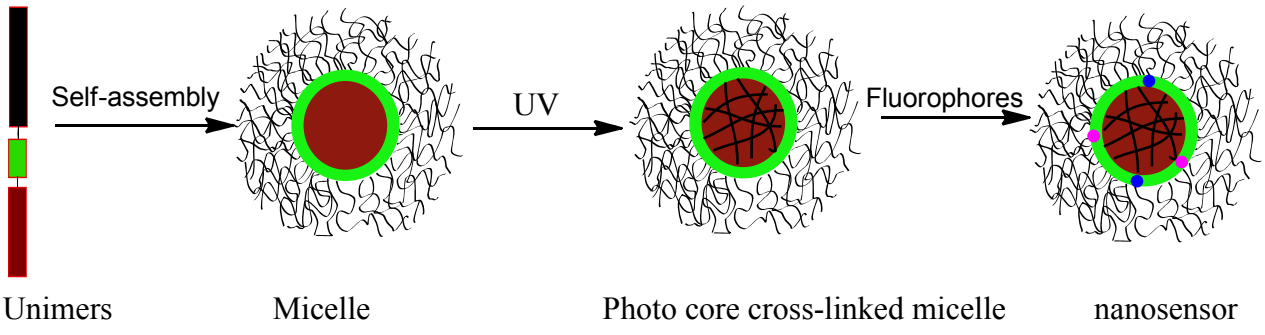

Figure 3.1. Synthesis of a photo core cross-linked micelle ratiometric pH nanosensor.

Figure 3.1 schematically illustrates the step-wise synthesis of photo core cross-linked ratiometric pH nanosensors. The amphiphilic triblock copolymer poly(ethylene glycol)$_{120}$-*b*-poly([((trimethylsilyl)ethoxy)carbonyl] aminoethyl methacrylate)$_{12}$-*b*-poly((trimethylsilylethynyl) styrene)$_{36}$ (PEG_{120}-*b*-PAEMA(Teoc)$_{12}$-*b*-$P(SC{\equiv}CTMS)_{36}$) (**25**) was synthesized from a slightly

modified ATRP procedure that have explained previously in Section 2.2. The polymers were characterized by ^{1}H-NMR and FT-IR spectroscopy. Presence of Teoc and TMS protecting groups on the polymer was confirmed by NMR (^{1}H-NMR, $CDCl_3$) peaks at δ = 0.00 ppm and 0.22 ppm respectively. FT-IR confirmed the carbonyl stretching of PAEMA(Teoc) block at *ca.* 1720 cm^{-1} and aromatic C=C stretching of PES(TMS) block at *ca.* 1500 cm^{-1}. The number-average molecular weight (M_n) calculated from ^{1}H-NMR in $CDCl_3$ was found to be lower than that measured by gel permeation chromatography (GPC) in THF with polystyrene as standard. Details of molecular weight determinations are summarized in **Table 3.1**. Simultaneous removal of Teoc and TMS protecting group from the amphiphilic triblock copolymers using tetrabutylammonium fluoride in THF followed by self-assembly of the functional triblocks in water resulted in functional core-shell-corona PEG-*b*-PAEMA-*b*-P(SC≡CH) micelles (**28**). A portion of the micelles was lyophilized for characterization. Disappearance of Teoc and TMS signal (^{1}H-NMR, $CDCl_3$) and the appearance of alkyne (-C≡CH) proton resonance at 3.06 ppm confirmed the complete de-protection. Appearance of -C≡**C-H** stretching at *ca.* 3285 cm^{-1} in FT-IR further confirmed the TMS de-protection. Teoc deprotection from the amino groups of the PAEMA(Teoc) block was further confirmed by positive Kaiser tests[159] of the lyophilized micelles. The positive zeta potential of PEG-*b*-PAEMA-*b*-P(SC≡CH) micelle (**Table 3.2**) indicated the presence of free amino groups in the shell region of the micelle and provided an additional evidence of Teoc de-protection.

Table 3.1. Molecular weights of PEG_n-*b*-$PAEMA(Teoc)_m$-*b*-$P(SC{\equiv}CTMS)_p$ (**25**).

M_n[a]	M_w[a]	M_w/M_n[a]	M_n[b]	n[c]	m[c]	p[c]
16600	20600	1.24	15750	120	12	36

[a] Determined by GPC, [b] Determined by NMR, [c] Number of repeating units of PEG block (n), PAEMA(Teoc) block (m) and P(SC≡CTMS) block (p).

The synthesis of UV core cross-linked amphiphilic triblock core-shell-corona functional micelle **31** based pH nanosensors **32** is shown in **Scheme 3.1**. The aqueous micelle dispersion **28** (1.82 mg/mL) in a quartz cuvette was exposed to UV radiation from a UV photo curing system (Omnicure S2000). The stirred sample was irradiated with irradiance level of 3 W/cm^2 (measured by the radiometer) from a high pressure mercury arc lamp (200 W), without using a wavelength filter at room temperature. The UV-induced oxidative coupling between the alkyne moieties at the micelle core was monitored by measuring the variation of absorbance of the micelle solution with UV irradiation time (**Figure 3.2**). Measurements show that the cross-linking reaction takes place rapidly during the first few minutes as indicated by the sharp initial increase in absorbance. After about five minutes, further irradiations do not increase the absorbance significantly, indicating that a saturation level of photo cross-linking has been achieved.

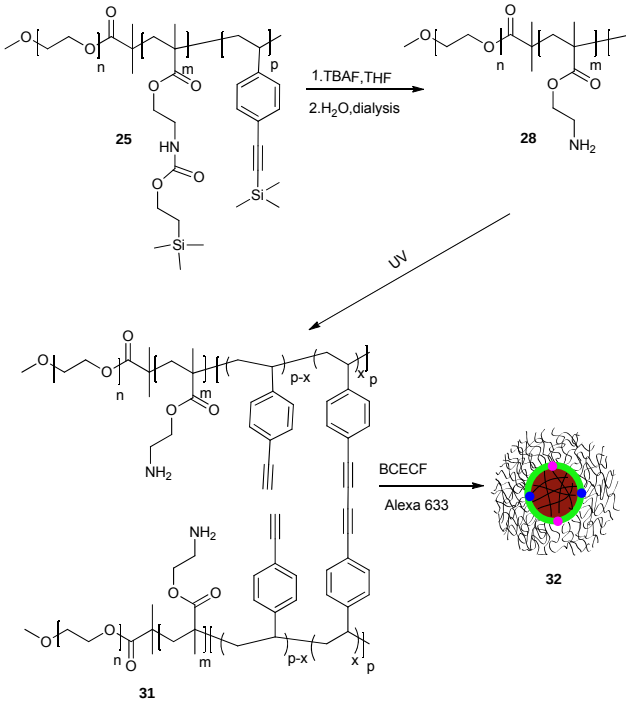

Scheme 3.1. Photo core cross-linked micelle ratiometric pH nanosensor (**32)** synthesis. TBAF = tetrabutylammonium fluoride, BCECF = 2′,7′-bis-(2-carboxyethyl)-5-(and-6) carboxyfluorescein, Alexa 633 = Alexa Fluor; x is the extent of photo core cross-linking.

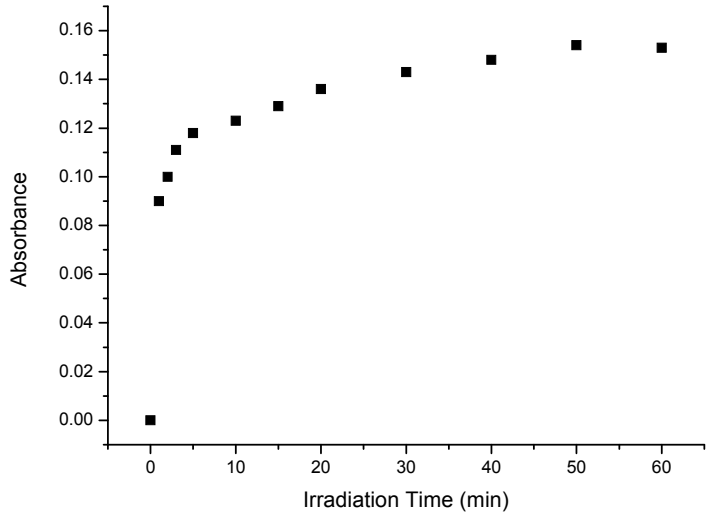

Figure 3.2. Plot of absorbance *vs* irradiation time for aqueous PEG-*b*-PAEMA-*b*-P(SC≡CH) micelle (1.82 mg/ mL) measured at 600 nm using a UV-Vis spectrophotometer, during irradiation from a UV high pressure 200 Watt mercury vapor short arc lamp with an irradiance level of 3 W/cm^2.

Table 3.2. Characterization Data for Micelles **28**, **31** and pH nanosensor **32**.

Micelle	DLS[a] D_h(nm)	AFM[b] H_{av}(nm)	Zeta(ξ)[c] (mV)
28	16±3	5±1	16±1
31	19±1	11±1	14±2
32	20±2	10±2	10±1

[a] Number-averaged hydrodynamic diameter of the polymeric micelles in MilliQ water by dynamic light scattering, [b] Average height of the micelles are calculated from the values of ca. 100 particle by tapping mode AFM, [c] Zeta potential from 10 determinations of 10 cycles each.

Photo cross-linking at the micelles core was further confirmed by FT-IR spectroscopy. During UV irradiations, the alkyne C≡C-**H** stretching absorption at 3285 cm^{-1} decreased considerably. This confirmed the consumption of the alkyne moiety present at the P(SC≡CH) core of the micelle during photo irradiation. IR spectra measured at different irradiation times showed that under a given irradiation level (3 W/cm^2), the alkyne moiety was consumed significantly within 30 minutes (**Figure 3.3**). Further increase in UV irradiation time showed only slow decrease in alkyne absorption at 3285 cm^{-1}, indicating a decreased rate of oxidative coupling between the alkyne moieties at the micelle core. As photo cross-linking progresses, time-dependent decay of the

reaction rate may be due to the decrease in UV exposure on the free alkyne moiety buried inside of the cross-linked micelle core, or may be due to conformational restriction of alkyne moiety present at the cross-linked micelle core towards the oxidative coupling.

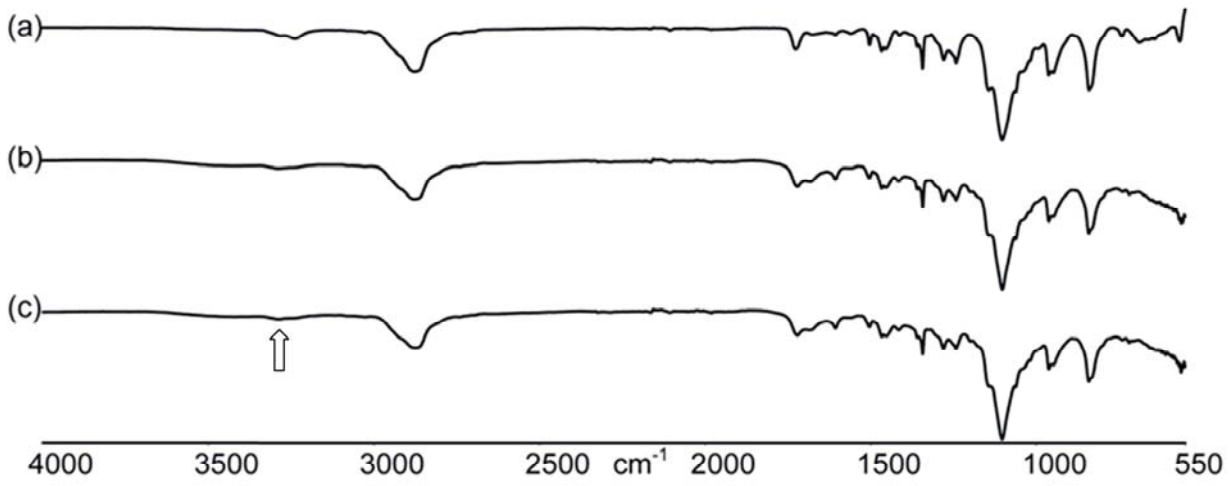

Figure 3.3. FT-IR Spectra of PEG-*b*-PAEMA-*b*-P(SC≡CH) micelle before UV irradiation (a), after 30 min of UV irradiation (b), and after 1h (c) of UV irradiation. The arrow in (c) indicates the decrease in alkyne (C-H) absorption during UV irradiations.

In order to measure the CMC values of the micelles before cross-linking and compare this with after cross-linking, the pyrene assay[199, 200] was employed. This method has previously been used on a similar system.[39] Plotting polymer concentration against the (I_{337} / I_{334}) ratio, the graphs shown in **Figure 3.4** is obtained, suggesting a CMC value around 15 mg/L. Upon examination of each obtained spectrum, however, it was found that what was observed was not a blue-shift of the pyrene spectrum. Instead, as polymer concentration increased, the initially observed pyrene spectrum was eclipsed by entirely different spectra, both in the case of non cross-linked and cross-linked micelles (**Figure 3.5**). Obtaining excitation spectra (emission 390 nm) for both micelle types at concentrations of 5 mg/L (below the observed CMC) and 250 mg/L (above the observed CMC) revealed that these micelles both exhibit significant fluorescence. This fluorescence was different between cross-linked and non-cross-linked micelles, which prompt us to ascribe it to the phenyl alkyne moieties of the PES core, which were altered during cross-linking. It may possible that this

characteristic can be used to monitor cross-linking in PES-based systems. Furthermore, it was observed that the spectra shapes for both micelle types were different at low and high concentrations. It may be possible that this may make systems with a PES-based core able to function as their own fluorescence indicators for CMC measurements, without the need for pyrene. At this point, however, conclude that, from experience, the pyrene assay seems unfit for determining the CMC of PES-based systems. In further attempts to assess the CMC, a DLS-based method inspired by Wooley *et al*.[71] was attempted, but DLS was too imprecise at low concentrations to produce reliable data. This may due to small particle size.

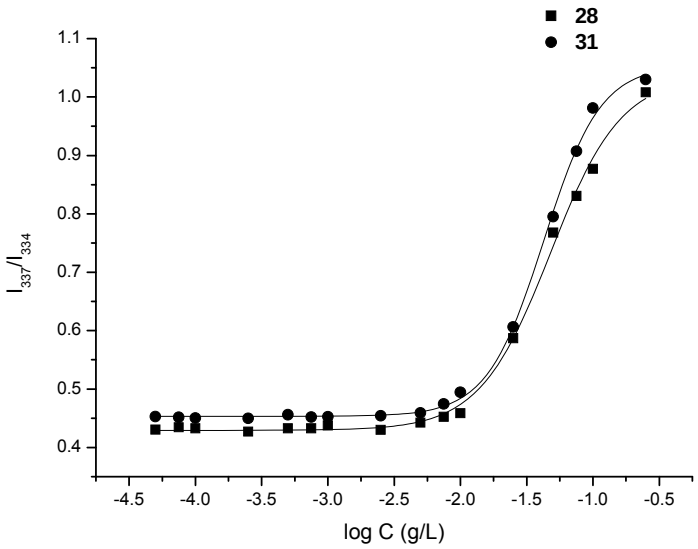

Figure 3.4. The plot of intensity ratio (I_{337} / I_{334}) of pyrene excitation spectra *vs* logarithmic concentration of cross-linked **31** (●) and non cross-linked **28** (■) PEG-*b*-PAEMA-*b*-P(SC≡CH) micelle.

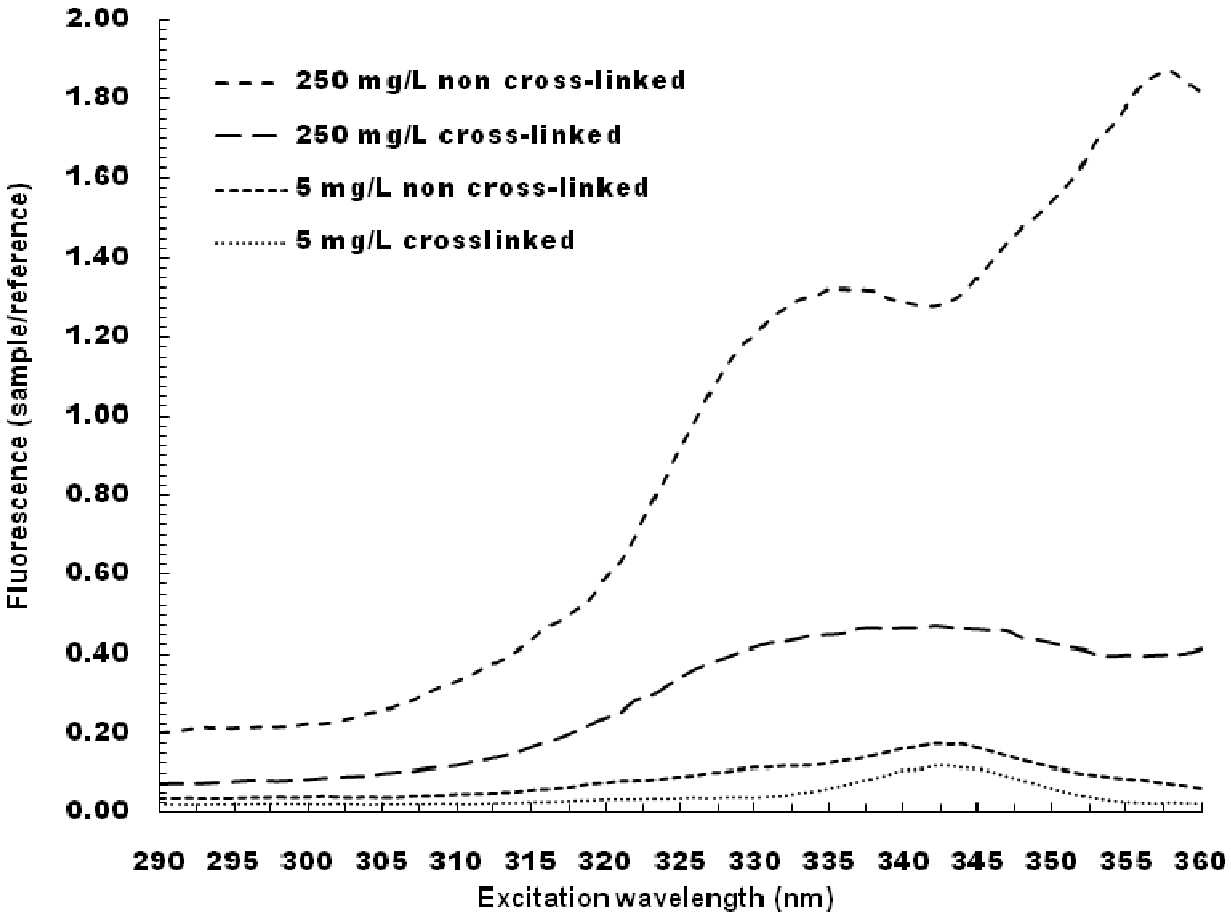

Figure 3.5. Excitation spectra (emission recorded at 390 nm) of cross-linked **31** and non-cross-linked **28** micelles at 5 and 250 mg/L. Intensity differences between 5 and 250 mg/L spectra is due to the concentration.

The UV cross-linked core-shell-corona functional micelle was converted into a ratiometric pH nanosensor by conjugating pH sensitive (BCECF) and reference (Alexa 633) fluorophores to the PAEMA shell of the micelle. pH sensitivity of the resulting pH nanosensor was measured by fluorescence measurements (**Figure 3.6a**). The fluorescence measurements confirmed the covalent attachments of fluorophores to the micelles. The nanosensor (0.176 mg/mL) was excited (λ_{ex} = 488 nm and 561 nm) in buffers of different pH, and pH dependent fluorescence intensity (I_{BCECF}), and pH independent fluorescence intensity ($I_{Alexa\ 633}$) were measured. The fluorescence intensity ratios (I_{BCECF} / $I_{Alexa\ 633}$) were plotted against corresponding pH. The resulting ratiometric pH calibration curve (**Figure 3.6b**) shows that the micelle nanosensor is sensitive between pH *ca.* 6 to 8.

The presence of the PEG corona on the nanosensor can enhance its potential for biomedical applications *via* providing long circulation of the nanosensor in blood (EPR effect),[201] and also give protection from the external surroundings to the fluorophores conjugated to the shell region. The unused functional groups at the core and shell region of this functional micelle nanosensor can provide opportunities for covalent attachments of hydrophilic and hydrophobic cargoes, and may provide capabilities to monitor the intracellular pH during drug delivery.

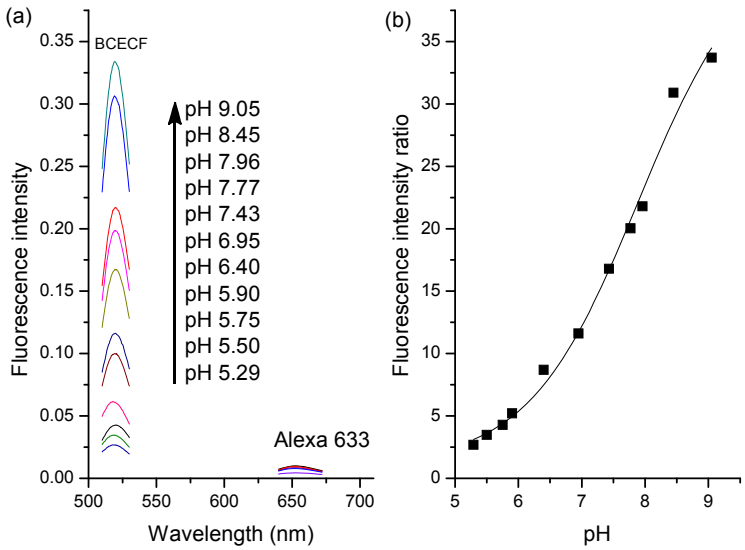

Figure 3.6. Fluorescence emission spectra (a) and pH calibration curve (b) of the pH nanosensor; fluorescence intensity (I) ratio = I_{BCECF} / $I_{Alexa\ 633}$.

DLS measurements show that the nanosensor **32** maintained the same hydrodynamic diameter (D_h) as that of the cross-linked micelles **31**. Compared to cross-linked micelles, the nanosensor shows a slight decrease in zeta potential, presumably as a result of fluorophore binding. The decrease in sensor zeta potential may thus be attributed to the presence of free carboxylic acid groups on the fluorophores attached to the PAEMA shell of the micelle (**Table 3.2**).

2D and 3D tapping mode AFM images and histograms representing the number of particles *vs* heights of the micelles; non cross-linked **28**, cross-linked **31**, and pH nanosensor **32** are given in **Figure 3.7**. 2D AFM images show the spherical morphology of the micelle nanoparticles. After UV cross-linking, the average height (H_{av}) of the particle **31** measured was found to be higher than that found before cross-linking, **28**. This indicates that, the robust micelles obtained after cross-linking were less deformed on the hydrophilic silica surfaces. The cross-linking makes the particle more

cohesive; therefore, prevents the deformation caused by association with the polar surfaces. The nanosensor **32** maintained heights (H_{av}) that were similar to that of the cross-linked micelles **31** indicating that fluorophore binding at the shell region of the cross-linked micelle was not further altered the particle surface interactions. The average heights (H_{av}) of the particles calculated from AFM measurements are also given in **Table 3.2**.

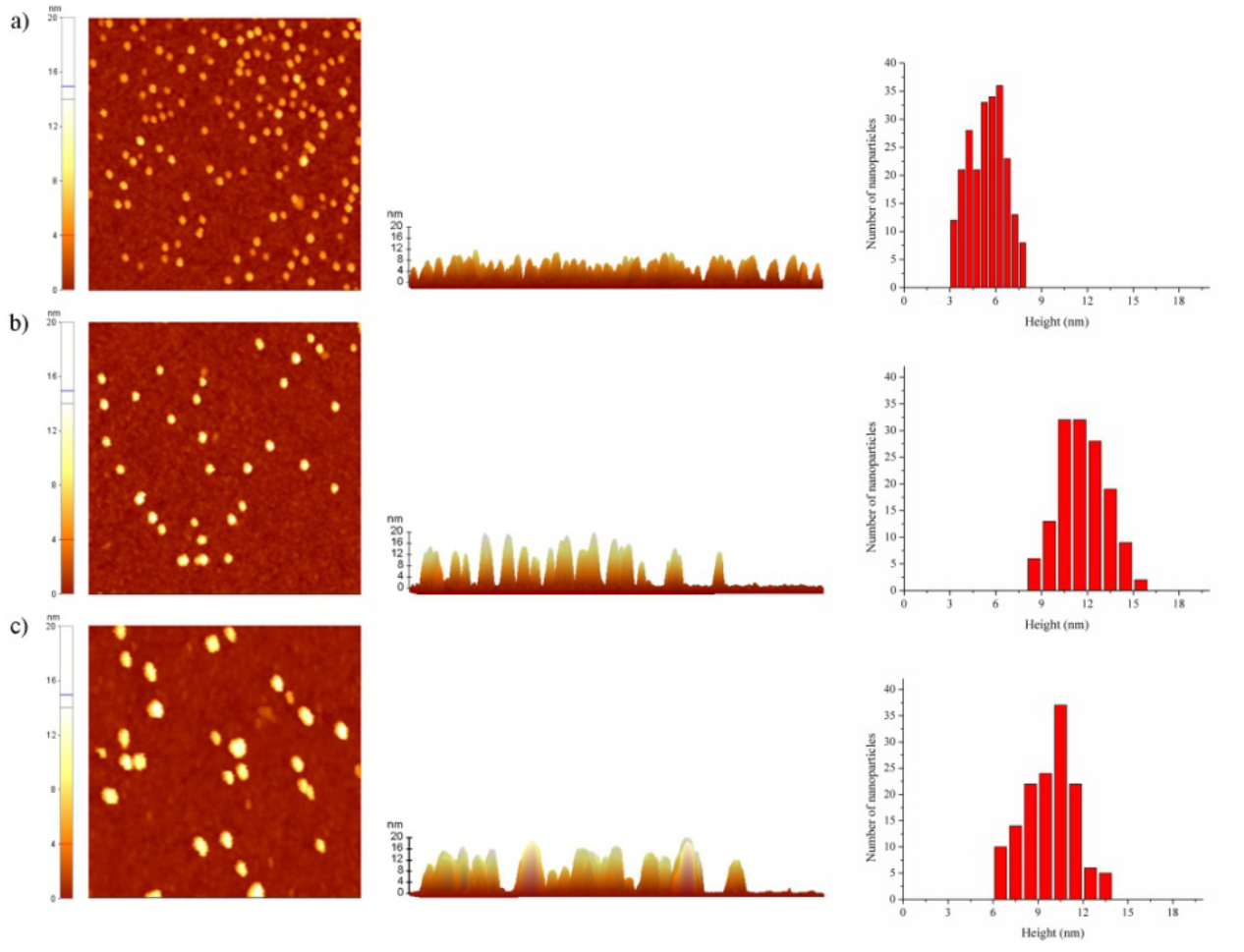

Figure 3.7. 2D, 3D AFM images and histograms of the micelle before cross-linking, **28** (a), after cross-linking **31** (b) and after converting to the pH nanosensor **32** (c). XY scan size is 1 μm x 1 μm.

3.1.4 Conclusion

A photo core stabilized ratiometric pH nanosensor is prepared by fluorophore binding to the photo-stabilized micelle. The use of UV-radiation in micelle core cross-linking is employed to reduce the difficulties in post micelle modifications, such as accessibility of reagents to the micelle core domain, long reaction time and lengthy purification procedures. Core cross-linking in micelles

nanosensors can improve their biological application by preventing sensor disintegration under infinitely diluted biological conditions (sink conditions). The fluorophores conjugated in the shell region of the micelles is well protected from the external surroundings by the PEG corona. Since the sensing molecules are less interacted by the external surroundings, the sensor may provide more accurate information about intracellular pH within the pH range 6 to 8. The presence of excess alkyne and amino functionalities at the core and shell region of the micelle may allow the covalent attachment of cargo, and hence may provide an opportunity to couple the intracellular pH with drug delivery. Intracellular pH measurements using the nanoparticle sensors are under investigation.

3.2 Reversibly Photo Core Cross-linked Micelle Nanosensor

3.2.1 Introduction

Intracellular pH plays a pivotal role in cellular processes and is highly regulated in every organelle.[97] A number of polymeric nanoparticles have been used in the designing of ratiometric fluorescence pH nanosensors for biological studies at the single cell level. These include polystyrene,[142] polyacrylamide,[97, 109, 110, 112, 113] and polysaccharide[114] particles.[99] Ratiometric measurements are more accurate as they are capable of minimizing the errors in fluorescence measurements due to probe concentration, photo bleaching, optical path length and leakage from the cells.[99] Fabrication of pH nanosensors for intracellular pH measurement should not only measure the ratio-metric fluorescent intensity changes with pH, but should also have the capability to reach effectively to the tissues of interest where the pH variations should be measured. Unfortunately, none of the particle sensors mentioned above have the capability to provide long circulations in the blood stream and reach the target. Polymeric micelles that are formed by the spontaneous self-assembly of amphiphilic block copolymers in block selective solvents have the morphological advantages to provide long circulation in blood.[144] Water exposed PEG corona chains of the block copolymer micelles are unreactive towards the blood and tissue components. The surrounding PEG corona protects the micelles from unwanted interactions with blood components, such as complement, thus preventing opsonization and prolonging circulation time. This structural advantage allows effective accumulations of micelle nanoparticle in pathological sites by enhanced permeation retention effect (EPR).[116, 202] Even with this excellent pharmacokinetics, polymeric micelles are not used for the nanosensors fabrications. The basic reasons are the difficulty in synthesis of well defined block copolymers and tendency of the self-assembled block copolymer to disintegrate into unimers under infinitely diluted biological conditions. The recent developments in radical polymerization techniques like ATRP[17] allow the synthesis of well defined functional block copolymers having, targeted composition, narrow molecular weight distribution and controlled architecture. Functional amphiphilic triblock copolymers with comparable hydrophilic to hydrophobic mass ratio in a block selective solvent can give distinct core-shell-corona functional micelles in a spherical or cylindrical form.[203] Regioselective cross-linking can enhance the applications of these functional nanoparticles by preventing its dissociation below the critical micelle concentration (CMC).[152, 153, 196]

In recent years, reversible cross-linking strategies have achieved significant research attention due to the reversible control over the drug delivery.[185] Reversible micelle cross-linking strategies have also been reported,[73, 74, 126, 184] in which light induced reversible photo cross-linking can overcome the difficult requirements such as use of cross-linking reagents, prolonged reaction time, and removal of excess reagent after reactions. Radiation induce reversible photochemical dimerizations of coumarin[204] are used for the dimensional synthetic modifications of the block copolymers self-assembly.[192-194] The cyclobutane ring resulting from the 2πS+2πS cycloaddition between the coumarin-containing unimers of the self-assembly are reversible, and provide the possibility of photo cross-linking and de-cross-linking of the micelles when illuminating the samples at two different wavelengths.

This section explains the development of reversibly photo core cross-linked functional micelle based ratiometric pH nanosensors *via* secondary dimensional synthetic modifications on a photo core cross-linked amphiphilic triblock self-assembly.

3.2.2 Experimental: Synthesis of reversibly photo core cross-linked micelle nanosensor

Materials and measurements: 2′,7′-bis-(2-carboxyethyl)-5-(and-6) carboxyfluorescein free acid (BCECF) was purchased from Biotium. Oregon Green 488 isothiocyanate (F_2FITC) and Alexa Fluor 633 carboxylic acid succinimidyl ester (Alexa 633) was obtained from Invitrogen. 2, 2'bipyridyl (bpy) (99%), PMDETA (99%), $CuCl_2$ (99.995%), trifluoroacetic acid (TFA)(99%), N-(3-Dimetyl amino propyl)-N'-ethylcarbodiimide hydrochloride (EDC·HCl) (98%), N-Hydroxysuccinimide (NHS) (98%), dialysis tube (MWCO=12kDa), and all other solvents and chemicals were purchased from Sigma Aldrich and used as obtained. CuCl (99.995%) was washed with glacial acetic acid, followed by absolute ethanol and diethylether, dried and stored under argon. Solvents used for ATRP were purified by distillation over the drying agents indicated in parentheses, stored under molecular sieves (MeOH 3 Å and DMF 4Å) and transferred under argon; MeOH ($Mg(OMe)_2$, DMF (CaH_2). Argon atmosphere (99.9999%) used in the reactions was provided by AGA Denmark. NMR spectra were recorded by using 300 MHz Varian Mercury 300 BB spectrometer. FT-IR spectra were recorded by Perkin Elmer Spectrum 100 FT-IR Spectrometer. GPC measurements were carried out with a RID10A-SHIMADZU refractive index detector and Mixed-D GPC column from Polymer Laboratories with a flow rate of 0.5 mL/min at 25°C, and

DMF with 50 mM LiCl as eluent. UV-Vis spectra were recorded on Unicam Helios Uni 4923 spectrophotometer. Fluorescence measurements were carried out by the Olis Line of SLM based Spectrofluorometer. Atomic force microscopy (AFM) images were obtained by PSIA XE-150 scanning force microscope using non-contact tapping mode close to resonance frequency of the silicon cantilever (Nanoworld, pointprobe type, force constant 42 N/m and tip radius <12 nm) of around 320kHz. All images were recorded under atmospheric conditions. Dynamic light scattering (DLS) and zeta potential measurements were carried out by Brookhaven Zeta PALS instrument.

Synthesis of the macroinitiator PEG-Br,[158] and the monomer 2-[N-(*tert*-Butoxycarbonyl)Amino]ethyl methacrylate (AEMABoc) were explained in **section 2.1.2.** The monomer 7-(2-Methacryloyloxyethoxy)-4-methylcoumarin(CMA)[205] was synthesized by the literature procedure.

Synthesis of PEG-b-PAEMA(Boc)Cl: PEG-Br (1 gram, 0.19 mmol), AEMABoc (522 mg, 2.28 mmol), 2,2'bipyridyl (62 mg, 0.40 mmol) and 5 mL MeOH were added to a 25 mL schlenk flask equipped with a magnetic stir bar. The flask was frozen in liquid nitrogen, and CuCl catalyst (21 mg, 0.21 mmol) was added. The reaction mixture was degassed with three freeze-pump-thaw cycles to remove the oxygen, and the polymerization was carried out at 40°C for 15 h under an argon atmosphere. The reaction was stopped by opening the flask to air. The reaction mixture was then passed through a silica gel column to remove the copper catalyst using MeOH as the solvent. On exposure to air, the dark brown reaction mixture turned blue, indicating the areal oxidation of the Cu(I) catalyst. After removing most of the MeOH by rotary evaporation, the polymer was precipitated into excess cold diethyl ether, isolated by filtration, and the precipitate dried under vacuum yielded 1.1 g (64%) of the diblock copolymer.

^{1}H-NMR (300 MHz, $CDCl_3$): δ = 5.50 (broad s, -N**H**), 4.0 (broad s, -OC**H**$_2$CH$_2$NH), 3.63 (s, -C**H**$_2$C**H**$_2$O), 3.37 (broad s, -OCH$_2$C**H**$_2$NH, -OC**H**$_3$), 1.82 (broad s, -C**H**$_2$ backbone), 1.43 (s, -C(C**H**$_3$)$_3$), 1.11-0.81 (m, -C(C**H**$_3$)$_2$, -C**H**$_3$ backbone) ppm; FT-IR: υ = 3387, 2892, 1716, 1520, 1466, 1391, 1361, 1342, 1279, 1241, 1150, 1112, 1060, 996, 965, 843 cm^{-1}.

Synthesis of PEG-b-PAEMA(Boc)-b-PCMA (33): PEG-*b*-PAEMA(Boc)-Cl (1g, 0.11 mmol), 7-(2-Methacryloyloxyethoxy)-4-methylcoumarin (CMA) (2.6 g, 9.02 mmol), $CuCl_2$ (12 mg, 0.088 mmol), PMDETA (0.068 mL, 0.33 mmol), and 10 mL of DMF, were added to a 25 mL schlenk flask equipped with a magnetic stir bar. The flask was frozen in liquid nitrogen, and CuCl catalyst

(11 mg, 0.11 mmol) was added. The reaction mixture was degassed with three freeze-pump-thaw cycles to remove oxygen, and the polymerization was carried out at 80°C for 24 h under an argon atmosphere. The reaction mixture was concentrated under vacuum, and the polymer was precipitated into excess of cold MeOH, filtered and dried; yield = 2 g (56%).

^{1}H-NMR (300 MHz, $CDCl_3$): δ = 7.40-5.90 (coumarin **H**), 4.38-4.04 (-OC**H**$_2$C**H**$_2$O-coumarin), 4.02-3.86 (-OC**H**$_2$CH$_2$NH), 3.58 (s, -C**H**$_2$C**H**$_2$O), 3.39-3.25 (-OCH$_2$C**H**$_2$NH), 2.22 (s, -C**H**$_3$ of coumarin), 2.04-1.55 (-C**H**$_2$ backbones of PAEMA and PCMA blocks), 1.39 (s, -C(C**H**$_3$)$_3$), 1.15-0.77 (-C**H**$_3$ backbones of PAEMA and PCMA blocks) ppm.

PEG-b-PAEMA-b-PCMA (34): PEG-*b*-PAEMA(Boc)-*b*-PCMA (500 mg, 0.016 mmol) was treated with 1:1 TFA:DCM mixture (8 mL) for 15 h at room temperature. After removing most of the solvent under rotary evaporation, the polymer was precipitated into excess cold diethyl ether, filtered and dried. The complete deprotection of *tert*-Butoxycarbonyl (Boc) was confirmed by the disappearance of Boc signal at 1.39 ppm in ^{1}H-NMR (300 MHz, $CDCl_3$).

PEG-b-PAEMA-b-PCMA micelle (35): The amphiphilic triblock copolymer (PEG-*b*-PAEMA-*b*-PCMA) (100 mg, 0.0033 mmol) was dissolved in 20 mL DMF under stirring. To the solution under stirring, was added 2 mL of MilliQ water within the time interval of 30 minutes. The stirring was continued, and additional 40 mL MilliQ water was added drop wisely. The cloudy micelle solution was transferred to a dialysis tube of MWCO 12 kDa and dialyzed against MilliQ water for three days. Final micelle concentration was 1.28 mg/mL. DLS showed a hydrodynamic diameter of (D_h) = 45±2 nm and zeta-potential (ξ) measurements showed ξ = 24±1 mV.

Photo core cross-linking of the micelle (36): 2 mL of PEG-*b*-PAEMA-*b*-PCMA aqueous micelle solution (0.03 mg/mL) in a quartz cuvette was irradiated from Omnicure UV photo curing system (S 2000) with UV intensity 2W/cm^2 (measured by the radiometer) through a standard filter (320-500 nm). The sample was irradiated at different time intervals, and the decrease in absorption of coumarin moiety (*ca.*320 nm) with time was monitored.

pH nanosensor fabrication (37): PEG-*b*-PAEMA-*b*-PCMA micelle 3.9 mL (1.28 mg/mL) under stirring was exposed to UV radiation (2W/cm^2) from the photo curing system. Progress of the photo dimerization was monitored by UV spectra (at a concentration of 0.03 mg/mL). After 55% of photo dimerization (D_h = 40±1 nm and ξ = 22±2 mV), the sample was transferred to a dialysis tube of

MWCO = 12 kDa and dialyzed against a carbonate buffer of pH 9.0. To this alkaline colloidal dispersion, was added activated BCECF (4 µl). BCECF (0.25 mg/mL) was activated with EDC·HCl and NHS in water. F_2FITC (1 µl) (1 mg/mL in dry DMSO), Alexa 633 (2 µl) (1mg/mL of dry DMSO) was also added and stirred at RT for 14 h. The reaction mixture was transferred to a dialysis tube of MWCO 12 kDa, and dialyzed against buffer of pH 9 for three days, and then against MilliQ water for another three days. The final nanosensor concentration was 1.26 mg/mL; D_h = 41±1 nm and ξ = 17±2 mV.

Photo de-core cross-linking of the micelle nanosensor (38): The core cross-linked micelle nanosensor 3 mL (0.03 mg/mL) in a quartz cuvette was exposed to UV radiation (λ < 255 nm). The cuvette was placed vertically 16 cm away from the 6 W 254 nm UVGL-58 UV lamp. The progress of de-cross-linking was monitored by UV-Vis spectroscopy; D_h = 38±3 nm and ξ = 16±1 mV.

3.2.3 Results and Discussion

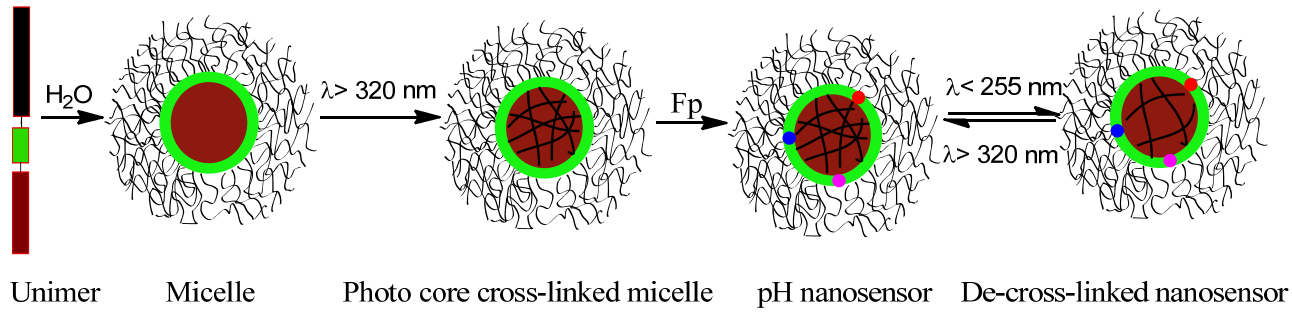

Figure 3.8. Schematic illustration of reversibly photo core cross-linked pH nanosensors fabrication, Fp = pH sensitive and reference fluorophores.

Figure 3.8 shows the synthesis of photo core cross-linked pH nanosensors. The amphiphilic triblock copolymer poly(ethylene glycol)$_{120}$-*b*-poly(2-[N-(*tert*-Butoxycarbonyl)Amino]ethyl methacrylate)$_9$-*b*-poly(coumarin methacrylate)$_{80}$ (PEG$_{120}$-*b*-PAEMA(Boc)$_9$-*b*-PCMA$_{80}$) (**33**) was synthesized by isolated macroinitiator ATRP (**Scheme 3.2**). Number-average molecular weight of the triblock measured by GPC (**Figure 3.9**) was found to be lower than that calculated by ^{1}H-NMR ($CDCl_3$) peak integration. The polydispersity index (M_w/M_n = 1.21) shows narrow molecular weight distribution. These results are summarized in **Table 3.3**. The Boc- group was removed from PEG-*b*-PAEMA(Boc)-*b*-PCMA by treatment with trifluoroacetic acid to obtain the PEG-*b*-PAEMA-*b*-PCMA (**34**). Complete deprotection of the copolymer was confirmed by the disappearance of Boc-signal at 1.39 ppm by ^{1}H-NMR ($CDCl_3$) (**Figure 3.10**).

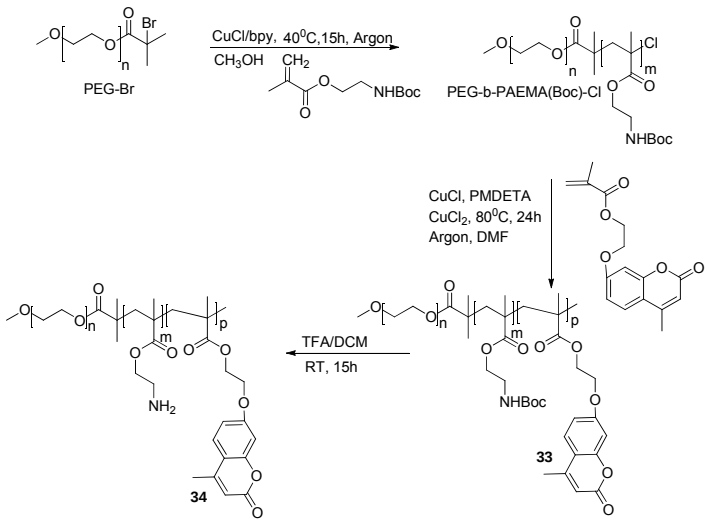

Scheme 3.2. Synthesis of PEG-*b*-PAEMA(Boc)-*b*-PCMA (**33)** by isolated macroinitiator ATRP and PEG-*b*-PAEMA-*b*-PCMA (**34**) by deprotection of **33**, bpy = 2,2'bipyridine, PMDETA = N,N,N',N',N''-pentamethyldiethylenetriamine, TFA = Trifluoroacetic acid.

Table 3.3. Molecular weights of PEG_n-*b*-$PAEMA(Boc)_m$-*b*-$PCMA_p$ (**33**).

M_n[a]	M_w[a]	M_w/M_n[a]	M_n[b]	n[c]	m[c]	p[c]
22100	26800	1.21	30390	120	9	80

[a] Determined by GPC, [b] Determined by NMR, [c] Number of repeating units of PEG block (n), PAEMA(Boc) block (m) and PCMA block (p).

The amphiphilic triblock PEG-*b*-PAEMA-*b*-PCMA core-shell-corona functional micelle **(35)** having radially compartmentalized corona was prepared by dissolving PEG-*b*-PAEMA-*b*-PCMA in DMF, followed by slow displacement of the common solvent (DMF) by a selective solvent for the hydrophilic block (water). The micelle was then kinetically trapped by complete replacement of the common solvent by the selective solvent *via* dialysis against MilliQ water. The presence of PEG corona and PCMA core may make the core-shell-corona micelle biocompatible. Dynamic light scattering measurements (DLS) show number-averaged hydrodynamic diameter (D_h) = 45±2 nm and zeta-potential (ξ) measurements show ξ = 24±1 mV (**Table 3.4**, micelle **35**).

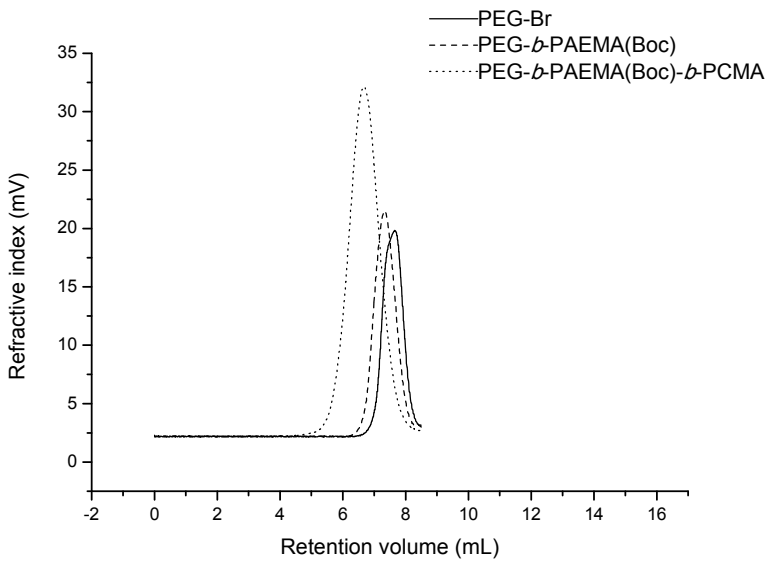

Figure 3.9. GPC spectra of macroinitiator, diblock, and triblock copolymers.

The core cross-linked PEG-*b*-PAEMA-*b*-PCMA micelle (**36**) was synthesized by UV radiation induced photo core cross-linking at the PCMA core. The PEG-*b*-PAEMA-*b*-PCMA micelle (**35)** (0.03 mg/mL) was exposed to UV radiation (2W/cm^2) (320 nm < λ < 500 nm) from a UV photo curing system, and the decrease in coumarin absorption (increase in photo dimerization) (*ca.*320 nm) with respect to irradiation time was monitored by UV-Vis spectroscopy (**Figure 3.11a**). The degree of coumarin photo dimerization (PD) at the PCMA core was also calculated from the UV-Vis spectrum. PD % = $(A_0-A_t)/A_0 \times 100$; where A_0 is the UV absorption of the coumarin core of the micelle before UV irradiation (t = 0) and after the time t, A_t (**Figure 3.11b**).

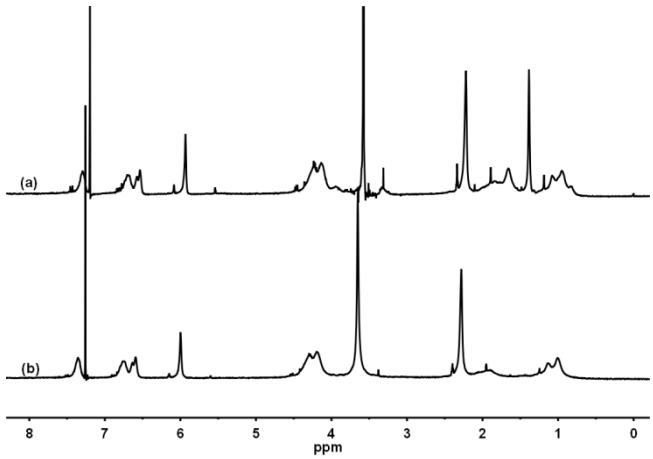

Figure 3.10. ^{1}H-NMR spectra of (a) PEG_{120}-*b*-$PAEMA(Boc)_9$-*b*-$PCMA_{80}$ (**33**) and (b) PEG_{120}-*b*-$PAEMA_9$-*b*-$PCMA_{80}$ (**34**) in $CDCl_3$.

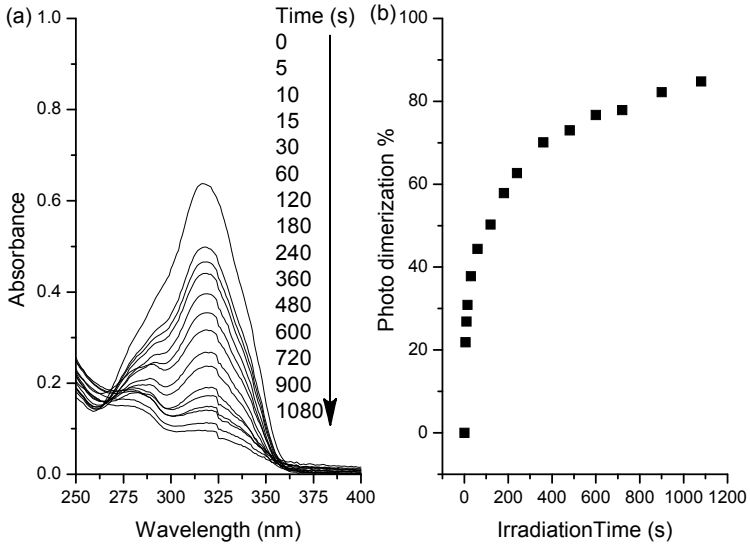

Figure 3.11. (a) Decrease in UV absorption of PEG-*b*-PAEMA-*b*-PCMA micelles (**35**) during photo irradiation (λ > 320 nm), measured by UV-Vis at different irradiation times. (b) The increase in photo dimerization degree during UV irradiation.

The micelle cross-linking by coumarin photo dimerization was further confirmed by FT-IR spectroscopy (**Figure 3.12**). Compared to the non-cross-linked micelles **35**, the FT-IR spectra of the photo core cross-linked micelles **36** show a shift in the carbonyl stretching absorption to higher energy with an increase in peak broadness. This indicates that, as the photo cross-linking increases, the number of conjugated carbonyls in the pyrone subunits of the coumarins is decreased due to the participation of the double bonds in dimerization at the micelle core. The broad absorption at 1729 cm^{-1} is due to the presence of carbonyl groups at the shell region (PAEMA), carbonyls at the PCMA

core having increased -C=O character due to flexion of conjugation and decrease in double bond character caused by extension of conjugation. The alkenes C=C stretching at 1390 cm^{-1} decrease considerably after UV irradiation, which confirm the consumption of olefinic double bond in the cyclobutane ring formation. Additionally the cross-linked micelles show an increase in absorption around 1500 cm^{-1} and a broad absorption peak at 1150 cm^{-1} and 1240 cm^{-1}. These changes are also supporting the cyclobutane ring formation at the PCMA micelle core during photo irradiation of the aqueous PEG-*b*-PAEMA-*b*-PCMA micelle solution.

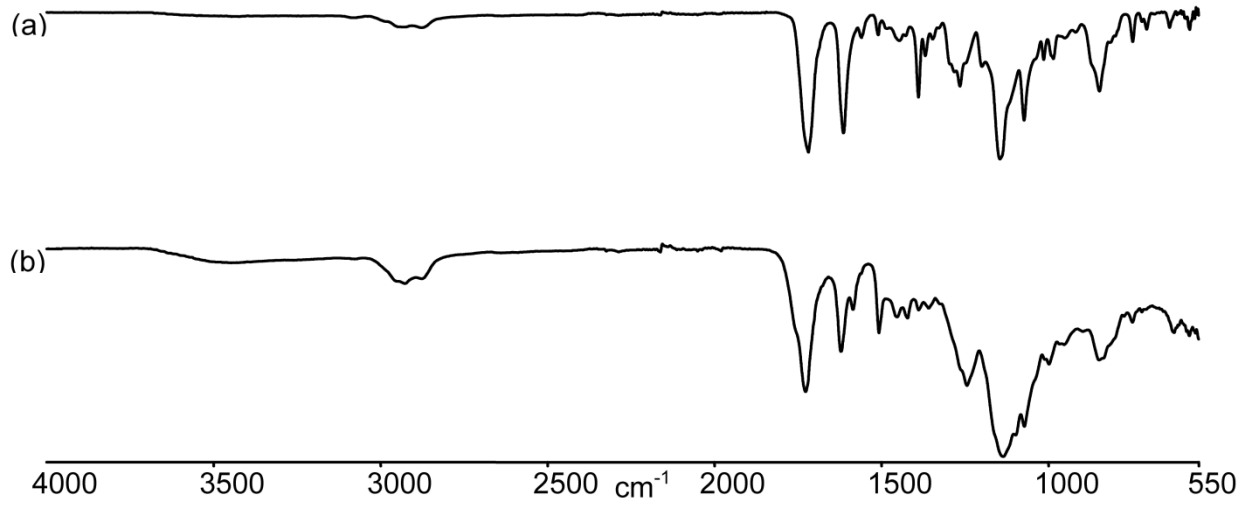

Figure 3.12. (a) FT-IR spectra of non-cross-linked micelle **35** and (b) photo core cross-linked micelle **36**.

Synthesis of the bio-compatible (expected to be) cross-linked micelle nanosensor **37** is given in Scheme **3.3**. The PEG-*b*-PAEMA-*b*-PCMA micelle **35** (1.28 mg/mL) was irradiated with $\lambda > 320$ nm using the same UV photo curing setup as explained above. After 55% of photo dimerization (determined from Figure **3.11**), DLS and zeta potential measurements show slight decrease in hydrodynamic diameter and surface charge density of the micelles (**Table 3.4**, micelle **36**). This confirms that cross-linking occurred intramicellarly within the core rather than intermicellar cross-linking between the aggregates. The exclusive intramicellar cross-linking may be attributed to the steric stabilization mechanism offered by the PEG corona.[163] The positive surface charge density further confirms the availability of free amino groups at the inner corona (shell) of the core cross-linked micelles. The photo core cross-linked micelle was then converted into a ratiometric pH nanosensor by covalently conjugating pH sensitive (F_2FITC and BCECF) and reference fluorophores (Alexa 633) at the inner corona of the micelle in an alkaline buffer (pH 9). The

resulting nanosensor was purified by dialysis; DLS and zeta potential measurements (**Table 3.4**) show that the sensor **37** maintained the same size as that of the cross-linked micelle **36** with a slightly decreased surface charge density due to the fluorophore attachments. The free carboxylate groups of the fluorophores attached to the micelle shell may be responsible for the decrease in zeta potential.

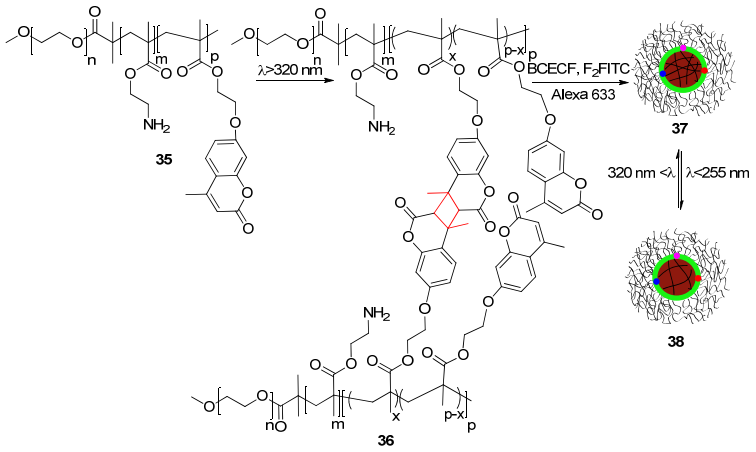

Scheme 3.3. Synthesis of core-shell-corona micelle based reversibly photo core cross-linked ratiometric pH nanosensors. BCECF = 2′,7′-bis-(2-carboxyethyl)-5-(and-6) carboxyfluorescein, F_2FITC = Oregon Green 488 isothiocyanate, Alexa 633 = Alexa Fluor; x is the % of photo dimerization.

Table 3.4. Characterization Data for Micelle **35**, **36**, **37** and **38**.

Micelle	DLS(D_h)[a] (nm)	Zeta(ξ)[b] (mV)
35	45±2	24±1
36	40±1	22±2
37	41±2	17±2
38	38±3	16±1

[a] Number-averaged hydrodynamic diameter of aqueous micelle solution measured by DLS, [b] Zeta potential from 10 determination of 10 cycles.

The pH sensitivity range of the pH nanosensor was determined by fluorescence measurements. The nanosensor (0.126 mg / mL) was excited (λ_{ex} = 490 nm for F_2FITC and BCECF; λ_{ex} = 561 nm for Alexa 633) in buffer of different pH. The pH dependent fluorescence emission spectra at 520 nm and pH independent reference spectra at 650 nm were recorded (**Figure 3.13**a). Fluorescence intensity ratio ($I_{(F2FITC)} + I_{(BCECF)} / I_{(Alexa\ 633)}$) was plotted against the pH corresponding to the

fluorescence intensities to obtain the pH calibration curves (**Figure 3.13b**). The pH calibration curve shows that the nanosensor is sensitive between the pH *ca.* 4 to 8. Intracellular pH are between 6.8 and 7.4 in the cytosol and 4.5 and 6 in the cell's acidic organelles.[206] As like the nanosensors explained in section 2.1 and 2.2, this nanosensor may also be capable of monitoring intracellular pH in the cytosol and acidic organelles of the cells.

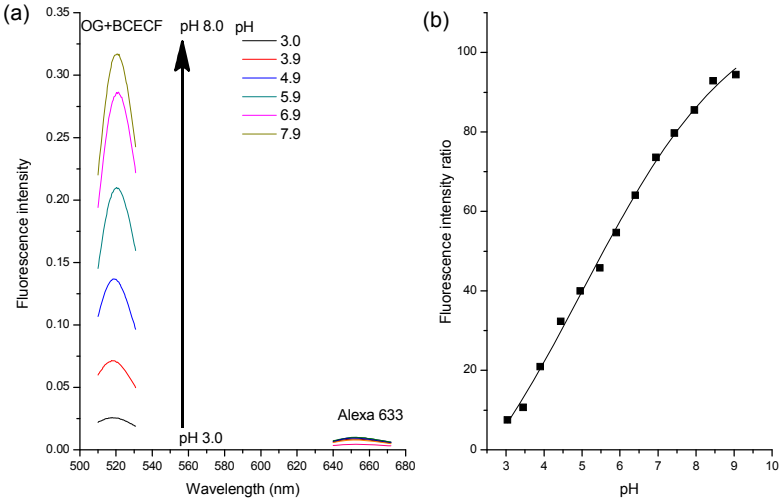

Figure 3.13. Representative fluorescence emission spectra for the pH nanosensor (a) and the pH calibration curve (b).

Photo de-cross-linking of the micelle nanosensor was also performed. pH nanosensor 3mL (0.03 mg/mL) in a quartz cuvette was exposed to UV radiation ($\lambda < 255$ nm) from a 6 W 254 nm UVGL-58 UV lamp and the increase in UV absorption (*ca.* 320 nm) as a result of cyclobutane ring scissions were monitored by UV-Vis spectroscopy (**Figure 3.14a**). The degree of photo de-dimerization was also calculated from the UV spectra (**Figure 3.14b**). The photo de-dimerization studies show that the complete sensor de-cross-linking was impossible. This indicates the presence of dynamic dimerization de-dimerization equilibrium in the PCMA core of the micelle at $\lambda < 255$ nm. DLS and zeta potential of the de-cross-linked micelle sensor **38** shows a slight decrease in number-averaged hydrodynamic diameter (D_h), whereas the surface charge density remain unaltered during photo de-dimerization (**Table 3.4**). Though the complete de-cross-linking of the nanosensor was impossible, this reversibly core cross-linked micelle nanosensor may provide a platform for the development of nanosensors that are capable of tracking intracellular pH during drug release from a de-cross-linked micelle core. Incorporation of a stimuli sensitive fully reversible

micelle cross-linking may facilitate the micelle dissociation and hence clearance of the nanosensor from the body *via* glomerular filtration; soon after its sensing applications are finished.

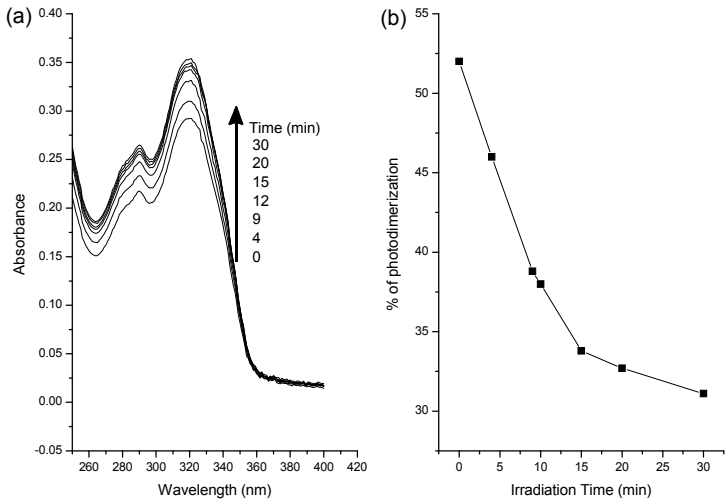

Figure 3.14. (a) Increase in UV absorption of core cross-linked micelle nanosensor (0.03 mg/mL) during exposure to UV radiation ($\lambda < 255$ nm). (b) The corresponding photo de-dimerization degree of the nanosensor.

2D and 3D AFM image of the non-cross-linked **35** and cross-linked micelle **36** shows that the spherical micelle particles were more uniform after cross-linking (**Figure 3.15**). The narrow height distribution of the cross-linked micelle particles (histogram in **Figure 3.15b**) indicates that photo core cross-linking at the coumarin core reinforces the weak hydrophobic interactions and the resulting robust micelle shows less deformed and a more uniform spherical morphology on the hydrophilic silica surface.

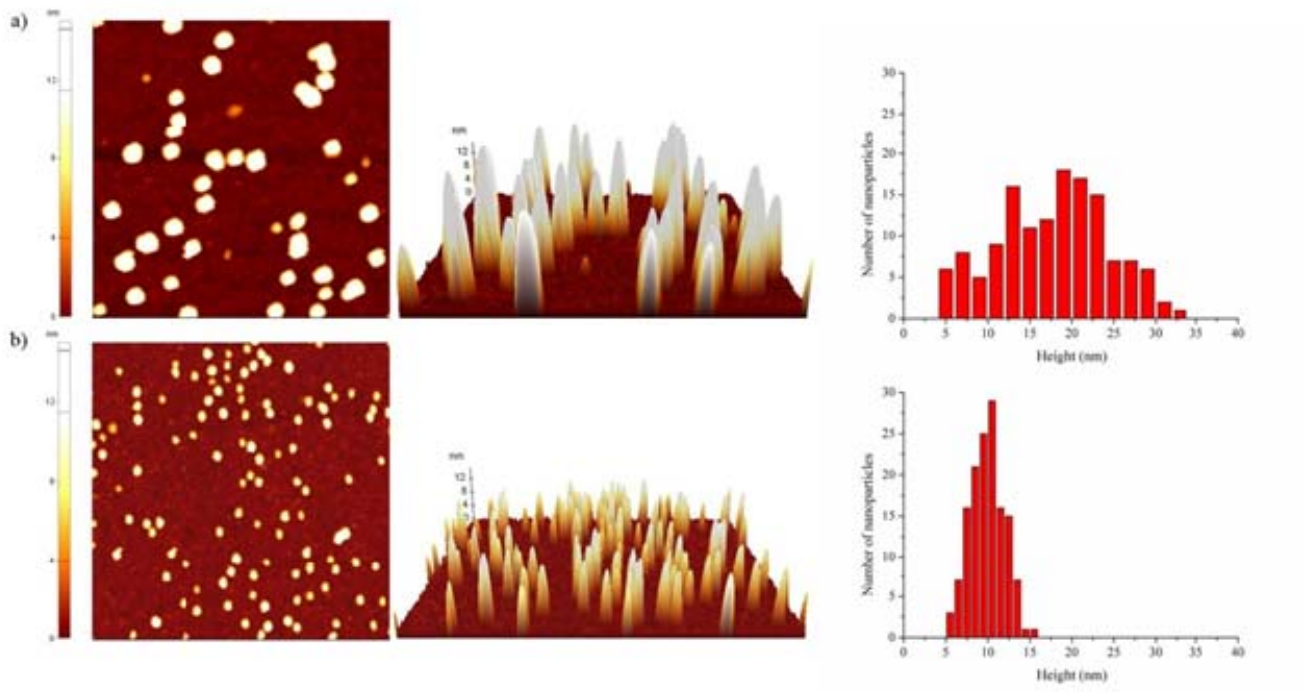

Figure 3.15. Tapping mode 2D and 3D AFM images and histogram representing height distributions (Number of nanoparticles *vs* Height) of (a) non-cross-linked micelle **35** and (b) cross-linked micelle **36**. XY scan size is 1 μm x 1 μm.

3.2.4 Conclusion

Polymeric core-shell-corona micelle based reversibly photo core cross-linked ratiometric pH nanosensors is synthesized. Wavelength dependent reversible photo dimerization of coumarin is the basis of the micelle cross-linking. Binding of pH sensitive and reference fluorophores at the shell region of the core cross-linked micelle resulted in ratiometric pH nanosensors having the pH sensitive shell protected from the external surrounding by the PEG corona. Due to the broad sensitivity range of the nanosensor (pH 4 to 8), this nanosensor may be capable of monitoring the pH in the cytosol and other intracellular organelles. The photo cross-linking may prevent the disintegration of the nanosensors in a biological environment under infinitely diluted condition; photo de-cross-linking may lead to the disintegration of nanosensors into unimers and may facilitate the excretion of the block copolymers from the body *via* renal route. The reversibly core cross-linked pH nanosensors may provide an opportunity to correlate intracellular pH with drug release from de-cross-linked micelle core.

Chapter 4

Mixed Micelle Strategy in Nanosensor Fabrications

Converting a micelle into ratiometric pH nanosensors demands more relevance to dimensional synthetic organic chemistry. The dimensional synthetic modifications are inherently inefficient and hard to quantify experimentally.[152] The yield of post micelle modification reactions can be affected by steric and conformational effects of the unimers of the self-assembly. Reactive functional-groups on the block copolymer self-assembly can be buried inside due to the various confirmations of the unimers. This can decrease the surface availability and hence over all reaction yield.[79]

Mixed micelle strategy can reduce the role of dimensional synthetic chemistry in pH nanosensors fabrications. The micelle hybridization as a result of unimers exchange between the different micelle populations is a complex process that depends upon the thermodynamic and kinetic parameters. Structure, molecular weight and composition of the unimers of the self-assembly play crucial role in this co-micellisation process. The increase in entropy as a result of mixing different unimers in mixed micelle is the driving force of this process.[207] Kinetically frozen micellisation may also affect the equilibrium between the unimers of the mixed micelle. However, reports show that micelle core having higher T_g does not kinetically hindered the unimers exchange equilibria,[208] whereas some of the micelle core having lower T_g do not shows any significant unimers exchange.[209] Review of the literature shows that the kinetic hindrance of unimers exchange is not clearly explained. The following sections examine co-micellisation of unimers having similar structure, composition and molecular weights. Hence, the possibilities of different micelle populations and unimers exchange will not affect the uniform distribution of the unimers in it self-assembly.

This chapter explains the nanosensor fabrication *via* mixed micellisation or co-micellisation of amphiphilic block copolymers having similar composition attached to different functionalities. This strategy offers the synthesis of polymeric nanoparticle having diverse functional characteristics in easy and efficient way. The strategy demands the synthesis of functionally modified amphiphilic block copolymers with well defined compositions and narrow molecular weight distributions. The

functionalized polymers can be synthesized by controlled radical polymerization especially isolated macroinitiator ATRP followed by post polymer modifications. The chapter is divided into two sections. The first section, 4.1 describes the synthesis of ratiometric targeted mixed micelle pH nanosensors; without the use of dimensional synthetic chemistry. Section 4.2 explains the synthesis of shell cross-linked ratiometric targeted mixed micelle nanosensors by combining synthetic and dimensional synthetic chemistry.

4.1 Core-shell-corona Mixed Micelle based Targeted Ratiometric Nanosensor

4.1.1 Introduction

Self-assembly[41] is an essential part of the nanotechnology. This has the capability to offer a potential strategy for making ensembles of nanostructures. One of the important requirements for this self-assembly approach is the synthesis of well defined polymer building blocks. Controlled radical polymerization[210] techniques can nowadays fulfils the well defined block copolymer synthesis. Post polymer modifications on the resulting block copolymers have the potential to provide a higher degree of functionalization. This is due to synthetic flexibility and accessibility of the reactive groups on the macromolecule than performing modifications on it self-assembly. Free energy driving spontaneous self-assembly of those well defined functionalized amphiphilic block copolymers in aqueous media can give a fascinating nanostructure, called functionalized micelle. This co micellisation of different functionalized unimers having similar composition enables functionalized nanoparticle synthesis through inexpensive bottom-up approach. Spherical core-shell mixed micelles from amphiphilic diblock copolymer self-assembly are reported.[77, 211, 212] The amphiphilic triblock copolymer self-assembly in water gives core-shell-corona micelle having compartmentalized core or radially compartmentalized corona with spherical or cylindrical morphologies.[213] Synthesis of functionalized nanoparticles from mixed triblock copolymer micelles has not been investigated yet. This section describing the preparation targeted mixed micelle pH nanosensors from functionalized amphiphilic triblock copolymer self-assembly.

4.1.2 Experimental: Preparation of targeted mixed micelle nanosensor

Materials and measurements: Details of materials and measurements and synthesis of cell penetrating peptides (**46**, **47**) are given in **appendix E**.

Synthesis of the macroinitiator Boc-NH-PEG-Br: Boc-NH-PEG-OH M_n = 4950 (1000 mg, 0.20mmol) was dissolved in 12 mL of toluene. After azeotropic distillation of 2 mL of toluene under reduced pressure to remove traces of water, TEA (0.053 mL, 0.4 mmol) was added, and the solution was cooled to room temperature. 2-bromoisobutyryl bromide (0.038 mL, 0.3 mmol) added drop wise to the above solution and the reaction mixture was stirred at 40 ^{0}C for 2 days. The solution was filtered, and most of the toluene was removed by rotary evaporation prior to

precipitation into 10 fold excess of cold ether. The crude polymer was dried under vacuum, dissolved in water at pH 8-9 and then extracted with DCM. The organic layer was collected and dried over anhydrous Na_2SO_4. The removal of the solvent under vacuum afforded the purified macroinitiator in high yield: 1 g (98%). ^{1}H-NMR (250 MHz in d^6-DMSO): δ = 3.6 (s, -C**H**$_2$C**H**$_2$O), 1.9 (s, -C(C**H**$_3$)$_2$), 1.4 (s,-COOC(C**H**$_3$)$_3$) ppm; FT-IR: υ = 2896, 1974, 1737, 1640, 1469, 1361, 1342, 1279, 1243, 1150, 1112, 1060, 1060, 961, 841 cm^{-1}; GPC: M_n = 5100, M_w = 5151, PD (M_w/M_n) = 1.01.

Synthesis of diblock copolymer Boc-NH-PEG-b-PHEMACl: Boc-NH-PEG-Br (700 mg, 0.137 mmol), HEMA (0.178mL, 1.37 mmol), 2, 2'bipyridyl (44 mg, 0.287 mmol) and 7 mL of MeOH were added to a schlenk flask equipped with a stirrer bar. The flask was frozen in liquid nitrogen, and CuCl catalyst (14.9 mg, 0.151 mmol) was added to it. The reaction mixture was degassed with three freeze-pump-thaw cycles (each 15 minute long) for removing the oxygen. The polymerization hereafter was carried out at 25 ^{0}C for 24 h under argon atmosphere. The resulting dark brown polymer solution was passed through a silica gel column for removing the copper catalyst using MeOH as solvent. After removing most of the MeOH by rotary evaporation, the polymer was precipitated into excess cold diethyl ether and isolated by filtration. The precipitate was dried under vacuum giving a good yield of 0.66 mg (77%). ^{1}H-NMR (250 MHz in d^6-DMSO): δ = 4.9 (s, -OH), 4.0-3.4 (-COOC**H**$_2$CH$_2$,-C**H**$_2$C**H**$_2$O, -COOCH$_2$C**H**$_2$), 2.0-1.5 (-C**H**$_2$ backbone of PHEMA), 1.4 (s, -COOC(C**H**$_3$)$_3$), 0.8 (-C**H**$_3$ of PHEMA) ppm; FT-IR: υ = 3452, 2887, 2741, 1974, 1731, 1645, 1469, 1359, 1344, 1281, 1243, 1148, 1114, 1060, 963, 946, 841 cm^{-1}; GPC: M_n = 6300, M_w = 7430, PD (M_w/M_n) = 1.18.

Synthesis of triblock copolymer Boc-NH-PEG-b-PHEMA-b-PMMA (39): Boc-NH-PEG-*b*-PHEMA-Cl (500 mg, 0.079 mmol), MMA (0.72 mL, 6.74 mmol), $CuCl_2$ (8.5 mg, 0.0632 mmol) PMDETA (0.057 mL, 0.27 mmol) and 3 mL of DMF were added to a 25 mL schlenk flask equipped with a stirrer bar. The solution was frozen in liquid nitrogen, and CuCl catalyst (7.8 mg, 0.079 mmol) was added. After degassing by three freeze-pump-thaw cycles (each cycle 15 minute long) for removing the oxygen, the polymerization was carried out at 35 ^{0}C for 25 h under argon atmosphere. The reaction mixture was then concentrated under vacuum, and the polymer was precipitated in petroleum ether. The crude triblock copolymer was extracted with water for removing the possible existing water soluble diblock (BocNH-PEG-*b*-PHEMA). The purified water insoluble triblock copolymer was filtered, and lyophilized gives a yield 0.7 g (61%) of the desired

polymer. ^{1}H-NMR (250 MHz in d^{6}-DMSO): δ = 4.8 (s, -OH), 3.9-3.4 (-COOC**H**$_2$CH$_2$, -C**H**$_2$C**H**$_2$O, -COOC**H**$_3$, -COOCH$_2$C**H**$_2$), 2.0-1.5 (-C**H**$_2$ backbone of PHEMA and PMMA), 1.4 (s,-COOC(C**H**$_3$)$_3$), 1.1-0.5 (-C**H**$_3$ of PHEMA and PMMA) ppm; FT-IR: υ = 3439, 2952, 1967, 1733, 1634, 1488, 1451, 1352, 1277, 1247, 1195, 1150, 1107, 1060, 961, 912, 841 cm^{-1}; GPC: M_n = 14400, M_w = 19900, PD (M_w/M_n) = 1.38, M_n (from ^{1}H-NMR) = 12810.

Synthesis of the macroinitiator PEG-Br: Synthesis explained in **section 2.1.2**

Synthesis of diblock copolymer PEG-b-PHEMACl: PEG-Br (1 gram, 0.1869 mmol), HEMA (0.226 mL, 1.86 mmol), 2,2'bipyridyl (61 mg, 0.39 mmol) and 5 mL dry MeOH were added to 25 mL Schlenk flask equipped with a stirrer bar. The solution was frozen in liquid nitrogen, and CuCl catalyst (20 mg, 0.205 mmol) was added. The reaction mixture was degassed with three freeze-pump-thaw cycles (each 15 minute long) for removing the oxygen. The polymerization was hereafter carried out at 25 ^{0}C for 24 h under argon atmosphere. The resulting dark brown reaction mixture was passed through a silica gel column using MeOH as solvent to remove the copper. After removing the MeOH by rotary evaporation, the polymer precipitated into excess cold diethyl ether and isolated by filtration. The precipitate was dried under vacuum giving a good yield of 1 g (82%) of the diblock copolymer. ^{1}H-NMR (250 MHz in ^{6}d-DMSO): δ = 4.9 (s, -OH), 3.9-3.4 (-COOC**H**$_2$CH$_2$-, -C**H**$_2$C**H**$_2$O-, -COOCH$_2$C**H**$_2$), 2.1-1.5 (-C**H**$_2$- backbone of PHEMA), 0.8 (-C**H**$_3$ of PHEMA) ppm; FT-IR: υ = 3405, 2892, 2741, 1731, 1469, 1359, 1344, 1279, 1244, 1153, 1112, 1060, 964, 843 cm^{-1}; GPC: M_n = 6560, M_w = 8350, PD (M_w/M_n) = 1.27.

Synthesis of triblock copolymer PEG-b-PHEMA-b-PMMA (40): PEG-*b*-PHEMA-Cl (500 mg, 0.076 mmol), MMA (0.647 mL, 6.46 mmol), $CuCl_2$ (7.7 mg, 0.057 mmol), PMDETA (0.052 mL, 0.25 mmol), and 2 mL DMF were added to 25 mL schlenk flask containing a stirrer bar. The solution was frozen in liquid nitrogen, and CuCl catalyst (7 mg, 0.076 mmol) was added. After degas using three freeze-pump-thaw cycles (each cycle 15 minute long) to remove oxygen, the polymerization was carried out at 35 ^{0}C for 25 h under argon atmosphere. The mixture was then concentrated under vacuum, and the polymer was precipitated in petroleum ether. The crude triblock polymer was extracted with water for removing the possible existing water soluble diblock copolymer (PEG-*b*-PHEMA). The purified water insoluble triblock copolymer was filtered and lyophilized giving 0.7 g (63%) of the desired compound. ^{1}H-NMR (250 MHz in d^{6}-DMSO): δ = 4.9 (s, -OH), 4.0-3.4 (-COOC**H**$_2$CH$_2$, -C**H**$_2$C**H**$_2$O, -COOC**H**$_3$, -COOCH$_2$C**H**$_2$), 2.1-1.6 (-C**H**$_2$ backbone

of PHEMA and PMMA), 1.1-0.5 (-C**H**$_3$ backbone of PHEMA and PMMA) ppm; FT-IR: υ = 3422, 2888, 1731, 1469, 1361, 1342, 1279, 1243, 1148, 1109, 1060, 965, 841 cm^{-1}; GPC: M_n = 14500, M_w = 19500, PD (M_w/M_n) = 1.34, M_n (from ^{1}H-NMR) = 13000.

Conjugation of Rhodamine to PEG-b-PHEMA-b-PMMA(42): To an ice cold solution of PEG-*b*-PHEMA-*b*-PMMA (500 mg, 0.034 mmol) and Rhodamine B (17.9 mg, 0.0374 mmol) in 5 mL DCM, was added EDC.HCl (8 mg, 0.040 mmol), and DMAP (0.207 mg, 0.0017 mmol) which was stirred at 0 ^{0}C for 30 minutes. The reaction mixture was slowly warmed to room temperature and stir for another 20 h. After removing most of the solvent by rotary evaporation, the crude product was precipitated into excess of cold diethyl ether. The Rhodamine bounded polymer was further purified by dissolving it in DMF and using dialysis (MWCO = 2kDa) against MilliQ water for three days. After three days of continuous dialysis, solid RhB conjugated triblock copolymer was isolated by lyophilization. The binding of Rhodamine B to the polymer was confirmed by GPC analysis (Figure in **appendix E**) also by fluorescence spectroscopy.

Conjugation of Fluorescein to PEG-b-PHEMA-b-PMMA(43): PEG-*b*-PHEMA-*b*-PMMA (100 mg, 6.8 μmol) and Fluorescein-5-carbonyl azide diacetate (3.63 mg, 13.6 μmol) were dissolved in 4ml of DMF in a 10 mL round-bottom flask. The solution was stirred at 80 ^{0}C for 4h, followed by two drops of hydroxyl amine aqueous solution (50% wt/V), and 2mL of ethanol were added and mixed well to hydrolyze the acetate groups. The yellow colored solution was then cooled to room temperature and transferred into dialysis tubing of (MWCO = 2kDa) and dialyzed against carbonate buffer of pH 9.2 for three days and then against MilliQ water for another three days. The micelle solution was then lyophilized to get the pure product. The binding of Fluorescein to the polymer was confirmed by GPC analysis (Figure in **appendix E**), also by fluorescence spectroscopy.

Conjugation of Oregon Green to PEG-b-PHEMA-b-PMMA (44): The triblock copolymer PEG-*b*-PHEMA-*b*-PMMA (0.5 g, 0.034 mmol) was dissolved in 15 mL dry pyridine and the solution was cooled to 0 ^{0}C. MsCl (0.130 mL, 1.7 mmol) in dry DCM (5mL) was added drop wise over several minutes. The resulting solution was warm to room temperature and stir over night. After filtration of the solid precipitate, the filtrate was washed with saturated $NaHCO_3$ solution, extracted with DCM and dried over anhydrous Na_2SO_4. After removing most of the DCM by rotary evaporation, the mixture was precipitated into excess of cold diethyl ether and the yellow yellow mesylated polymer was isolated. The mesylated polymer (200 mg, 0.013mmol) was dissolved in 3 mL DMF,

and NaN_3 (45 mg, 0.689 mmol) was added. The solution was stirred at 90 ^{0}C for 5h under argon atmosphere, then at room temperature for another 20 h. After removing most of the DMF under vacuum, the polymer was precipitated into an excess of cold diethyl ether followed by drying under vacuum giving PEG-*b*-PAzEMA-*b*-PMMA polymer. This triblock copolymer was further purified by dissolving it in DMF and using dialysis against MilliQ water for three days. The pure product was then recovered by lyophilization giving a yield of 0.136 g (72%). ^{1}H-NMR (250 MHz in d^6-DMSO): δ = 4.1-3.4 (-C**H**$_2$CH$_2$N$_3$, -C**H**$_2$C**H**$_2$O, -COOC**H**$_3$, -CH$_2$C**H**$_2$N$_3$), 2.0-1.6 (-C**H**$_2$ backbone of PHEMA and PMMA), 1.0-0.6 (-C**H**$_3$ of PHEMA and PMMA) ppm; FT-IR: υ = 2952, 2896, 2107, 1729, 1486, 1451, 1385, 1350, 1275, 1243, 1191, 1148, 1109, 987, 963, 841, 748 cm^{-1}.

PEG-*b*-PAzEMA-*b*-PMMA (**41**) (15 mg, 1.0 μmol) was dissolved in 3 mL DMF by stirring over night. The solution under stirring, was added 0.3 mL of MilliQ water with in the interval of 30 minutes, followed by 6 mL more MilliQ water drop wise. The cloudy micelle solution was transferred into a dialysis tube (MWCO = 12 kDa) and dialyzed against MilliQ water for three days. The micelle solution was transferred into a 25 mL round-bottom flask, was added 5 mL *tert*-butanol, $CuSO_45H_2O$ (0.075 mg, 0.3 μmol), freshly prepared sodium ascorbate solution (0.594 mg (as 5% aqueous solution)), and Oregon Green488 alkyne 6-isomer (0.449 mg, 1.0 μmmol) (in 0.2 mL of DMF). The solution was stirred for 48 h at room temperature. The crude reaction mixture was then transferred into the dialysis tubing of MWCO 2kDa and dialysis against carbonate buffer (pH-9.2) for three days and then against MilliQ water for another three days. The micelle solution was then lyophilized to obtain the solid Oregon Green conjugated polymer. Binding of Oregon Green was confirmed by GPC analysis (Figure in **appendix E**) also by fluorescence spectroscopy.

Conjugation of targeting peptide to NH_2-PEG-b-PHEMA-b-PMMA(45)

Deprotection of Boc-NH-PEG-b-PHEMA-b-PMMA: The triblock copolymer Boc-NH-PEG-*b*-PHEMA-*b*-PMMA (300 mg, 0.020 mmol) was dissolved in 3 mL of DCM and 3 mL trifluoroacetic acid was added drop wise to the solution. The reaction mixture was stirred for 10 h at room temperature. The solvent was removed under reduced pressure, and the polymer was precipitated into excess of cold diethyl ether, dried under vacum. The complete deprotection of Boc- was confirmed by NMR spectroscopy (disappearance of peak at δ 1.4 (s, 9H) also by a positive Ninhydrin test.

Binding of maleimide group to NH_2-PEG-b-PHEMA-b-PMMA: NH_2-PEG-*b*-PHEMA-*b*-PMMA (120 mg, 0.0083 mmol) was dissolved in 2 mL of THF containing 50µl TEA. 3-maleimido-propionicacid-N-hydroxysuccinimide ester (2.2 mg, 0.0083 mmol) was added, and the reaction mixture was stirred at room temperature for 3h. Most of the solvent was removed by rotary evaporation; the crude product was precipitated into excess cold diethyl ether and dried under vacuum. The absence of free amino group was confirmed by a negative Ninhydrin test. (Instead of 3-maleimido-propionicacid-N-hydroxysuccinimide ester, water soluble sulfo-GMBS (N-gamma-Maleimidobutyryl-oxysulfosuccinimide ester) was also used for the peptide conjugation. The change in linker does not alter the yield of peptide conjugations.

Binding of peptide to the polymer: Polymer bearing the maleimide group (25 mg, 0.0017 mmol) was dissolved in 5 mL of DMF. The polymer solution under stirring was added 0.5 mL of MilliQ water within a time interval of 30 minutes, followed by drop wise addition of another 10 mL of MilliQ water. The cloudy micelle solution was transferred into a dialysis tube (MWCO = 12kDa) and dialysis against buffer of pH 6.75 for 6h. The micelle solution in buffer of pH 6.75, was transferred into a round-bottom flask. The peptide (RhB-Pro-Ahx-Cys-$(Arg)_8$-NH_2 (**46**) (3.4 mg, 0.0017 mmol) was added, and the mixture was stirred at room temperature for 7h. The peptide conjugated polymer was dialyzed against MilliQ water for five days to remove un-reacted peptides. The concentration of peptide attached to the polymer was then determined from Rhodamine B calibration curve and was found to be $7*10^{-7}$ M, 1.4 mg; yield (41%). The micelle solution was then lyophilized to obtain the solid peptide conjugated polymer. The RhB free peptide (Ac-(Cys)-Ahx-$(Arg)_8CONH_2$) (**47**) was conjugated to the polymer using exactly same procedure.

Targeted mixed micelle nanosensor for the pH range 6 to 8 having reference fluorophores on the targeting ligands: The amphiphilic triblock copolymer PEG-*b*-PHEMA-*b*-PMMA bounded to Fluorescein (3.99 mg, 0.27 µmol), RhB attached targeting peptide (RhB-Pro-Ahx-Cys-$(Arg)_8$-NH_2) (0.23 mg, 0.015 µmol), along with free PEG-*b*-PHEMA-*b*-PMMA (5.71 mg, 0.39 µmol) in the ratio (7 : 0.4 : 10) (total 10 mg) were dissolved in 2 mL DMF by overnight stirring. The polymer solution under stirring, 0.2 mL of MilliQ water within the interval of 30 minutes was added followed by 4 mL more of MilliQ water drop wise. The cloudy micelle solution was then transferred into a dialysis tube (MWCO = 12 kDa), and dialysis against MilliQ water for 5 days. DLS measurement

showed hydrodynamic diameter (intensity average) (D_h) 49±1 nm and zeta potential measurement showed (ξ) -6±2 mV respectively.

Targeted mixed micelle nanosensor for the pH range 6 to 8 having (2%/weight) targeting peptides: Targeted ratiometric pH nanosensors sensitive between the pH 6 to 8 was synthesized as follows. The amphiphilic triblock copolymer PEG-*b*-PHEMA-*b*-PMMA bounded to Fluorescein (3.99 mg, 0.27 μmol), Rhodamine B (0571 mg, 0.0039 μmol), and the targeting peptide (Ac-(Cys)-Ahx-$(Arg)_8CONH_2$) (0.22 mg, 0.015 μmol), along with free PEG-*b*-PHEMA-*b*-PMMA (5.71 mg, 0.39 μmol) in the ratio (7 : 0.1 : 0.4 : 10) (total 10 mg) were dissolved in 2 mL DMF by overnight stirring. The stirring was continued, 0.2 mL of MilliQ water within the interval of 30 minutes was added, followed by 4 mL more of MilliQ water drop wise. The cloudy micelle solution was then transferred into a dialysis tube (MWCO = 12 kDa), and dialysis against MilliQ water for 5 days. DLS measurement showed hydrodynamic diameter (D_h) 50±1 nm and zeta potential measurement showed (ξ) -5±2 mV respectively.

Targeted mixed micelle nanosensor for the pH range 4 to 8 having (1%/weight) targeting peptides: The amphiphilic triblock copolymer PEG-*b*-PHEMA-*b*-PMMA conjugated to Fluorescein (3.44 mg, 0.23 μmol), Oregon Green (1.48 mg, 0.10 μmol), Rhodamine B (0.0492 mg, 0.0033 μmol), and targeting peptide (Ac-(Cys)-Ahx-$(Arg)_8CONH_2$) (0.098 mg, 0.0067 μmol), along with free PEG-*b*-PHEMA-*b*-PMMA (4.92 mg, 0.33 μmol) in the ratio (7 : 3 : 0.1 : 0.2 : 10) (total 10 mg) were dissolved in 2 mL of DMF by overnight stirring. Stirring was continued, and 0.2 mL of MilliQ water within the interval of 30 minutes was added to the above solution. Additionally 4 mL more of MilliQ water was added drop wise, and the cloudy micelle solution was transferred into a dialysis tube (MWCO = 12 kDa) and dialyzed against MilliQ water for 5 days. DLS measurement showed hydrodynamic diameter (D_h) 51±3 nm and zeta potential measurement showed (ξ) = -7±3 mV respectively.

4.1.3 Results and Discussion

Targeted ratiometric mixed micelle pH nanosensor fabrication is schematically given in **Figure 4.1**. The amphiphilic triblock copolymers, Boc-NH-poly(ethylene glycol)-*b*-poly(hydroxyethyl methacrylate)-*b*-poly(methyl methacrylate) (Boc-NH-PEG-*b*-PHEMA-*b*-PMMA) (**39**) (M_n = 14400), poly(ethylene glycol)-*b*-poly(hydroxyethyl methacrylate)-*b*-poly(methyl methacrylate) (PEG-*b*-PHEMA-*b*-PMMA) (**40**) (M_n = 14500) were synthesized by isolated macroinitiator atom

transfer radical polymerization techniques (ATRP) (**Scheme.4.1**). Compared to PEG-*b*-PHEMA-*b*-PMMA, ^{1}H-NMR (250 MHz in d^{6}-DMSO) spectra of Boc-NH-PEG-*b*-PHEMA-*b*-PMMA showed an additional Boc group signal at δ 1.38 ppm (s, 9H) (**Figure 4.2**). The apparent molecular weight (M_n) calculated for both the polymers from ^{1}H-NMR was lower than that measured by GPC (**Table 4.1**).

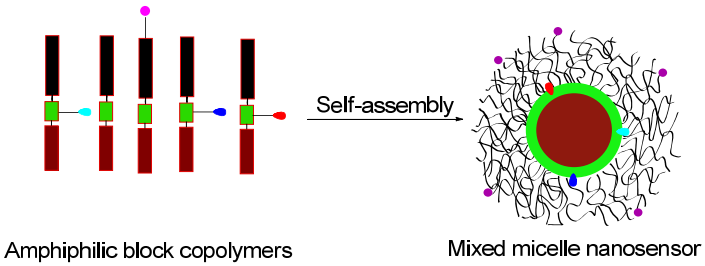

Figure 4.1. Schematic representation of mixed micelle nanosensor preparation.

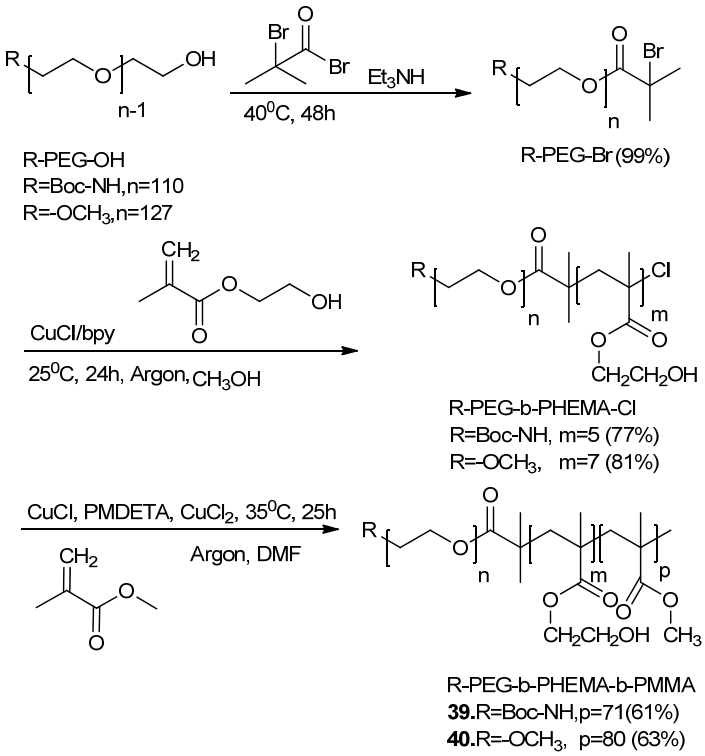

Scheme 4.1. Synthesis of R-PEG-*b*-PHEMA-*b*-PMMA. bpy = 2,2'bipyridyl, PMDETA = N,N,N',N'',N' pentamethyl-diethylenetriamine, (Yield of each steps are given in parenthesis).

Table 4.1. Molecular weights of Boc-NH-PEG_{110}-*b*-$PHEMA_5$-*b*-$PMMA_{71}$ (**39**) and PEG_{127}-*b*-$PHEMA_7$-*b*-$PMMA_{80}$ (**40**).

polymer	M_n[a]	M_w[b]	M_n[b]	M_w/M_n[b]
39	12810	19900	14400	1.38
40	13000	19500	14500	1.34

[a] by ^{1}H-NMR, [b] by GPC measurements, DMF with 50mM LiCl solution was used as eluent.

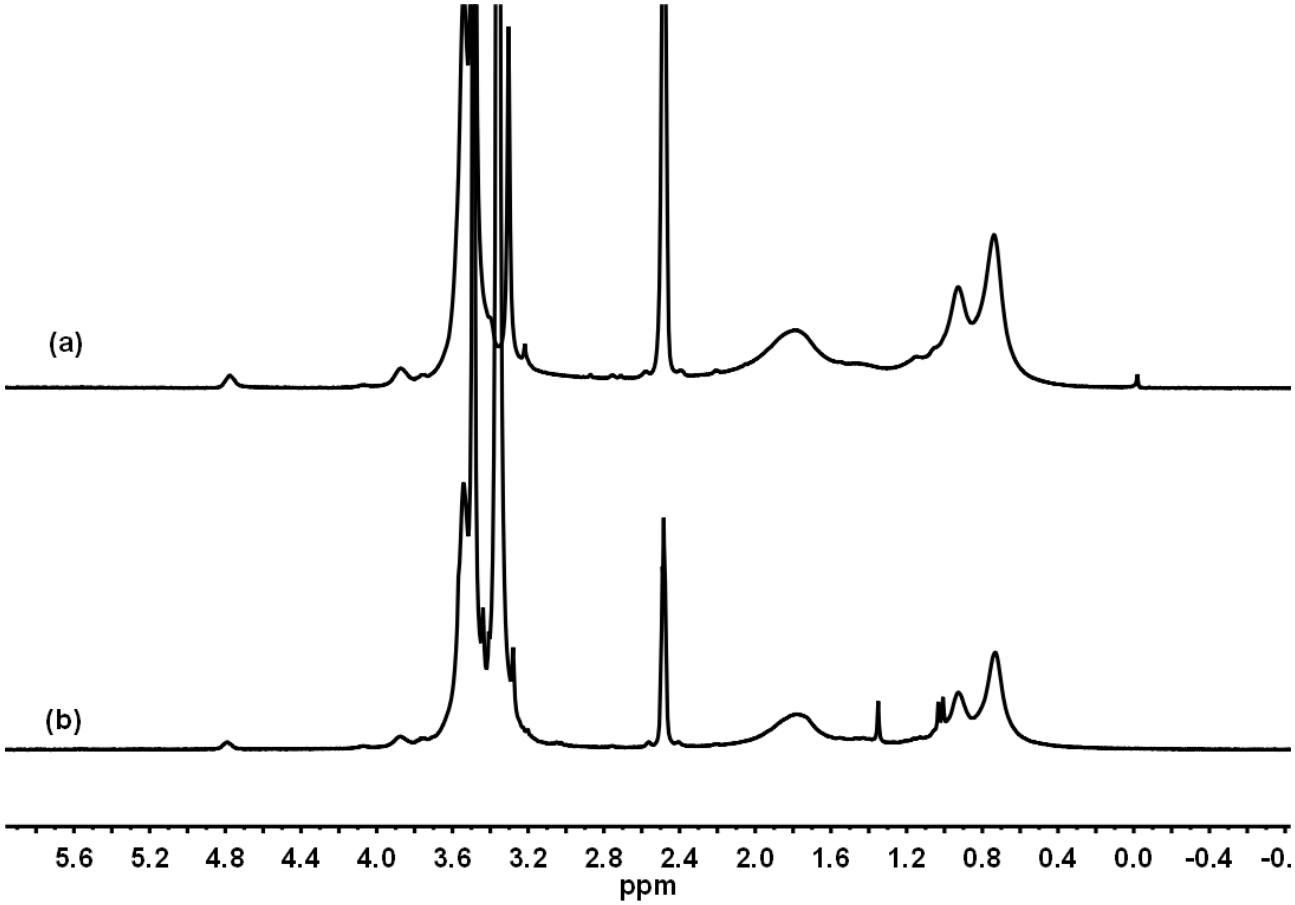

Figure 4.2. (a) ^{1}H-NMR spectra of PEG_{127}-*b*-$PHEMA_7$-*b*-$PMMA_{80}$ (**40**) and (b) Boc-NH-PEG_{110}-*b*-$PHEMA_5$-*b*-$PMMA_{71}$ (**39**) in d^6-DMSO.

Interfacial alcoholic groups (PHEMA) of the triblock copolymer PEG-*b*-PHEMA-*b*-PMMA were converted into azido group by nucleophilic substitution at the activated (mesylated) alcohol bearing carbon by azide ion.[214] The formation of poly(ethylene glycol)-*b*-poly(2-azidoethyl methacrylate)-

b-poly(methyl methacrylate) (PEG-*b*-PAzEMA-*b*-PMMA) (**41**) was confirmed by the disappearance of –OH peak from δ 4.9 ppm by ^{1}H-NMR (250 MHz in ^{6}d-DMSO) and appearance of azide peak at 2107cm^{-1} by FT-IR spectroscopy. pH sensitive fluorophore Fluorescein and pH insensitive Rhodamine B were introduced to the PHEMA block of the amphiphilic triblock copolymers by esterification **42**[215] and Curtius rearrangement **43**[216] respectively. The pH sensitive Oregon Green fluorophore was conjugated to PAzEMA block of the triblock **41** by click reactions **44**[80, 81] (**Scheme 4.2**). Cell penetrating peptides were introduced to the maleimide containing triblock copolymers **45** *via* thiol maleimide addition reaction. Rhodamine B contain peptide **46** was used to quantify the peptide binding. Rhodamine B free peptide **47** was conjugated to the maleimide containing polymer under otherwise identical conditions (**Scheme 4.3**).

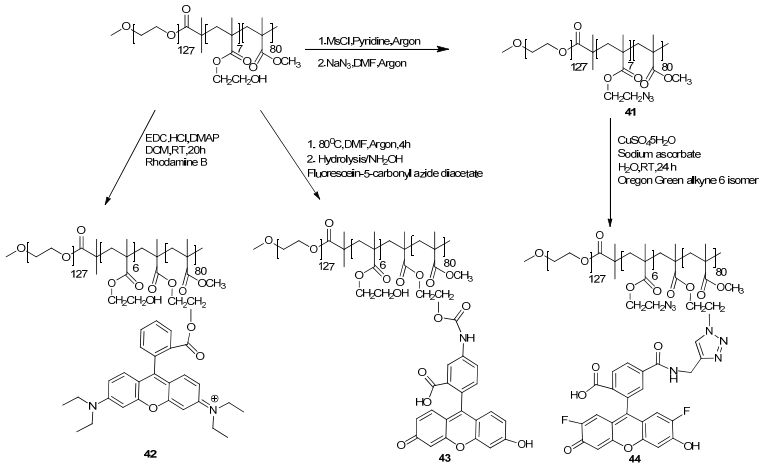

Scheme 4.2. Conjugation of pH sensitive and reference fluorophores to PEG-*b*-PHEMA-*b*-PMMA.

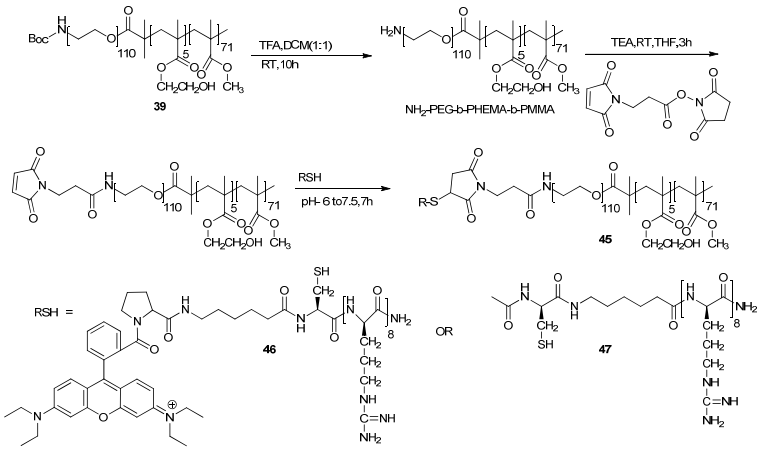

Scheme 4.3. Conjugation of targeting peptides to NH_2-PEG-*b*-PHEMA-*b*-PMMA.

Amphiphilic triblock copolymer **43** and targeting peptides **46** conjugated to the triblock **45,** along with free PEG-*b*-PHEMA-*b*-PMMA (**40**) in desired ratios were dissolved together in a common solvent (DMF) for all the blocks. The common solvent was slowly displaced by selective solvent for the hydrophilic blocks (water). The resulting octaarginine targeted polymeric mixed micelle pH nanosensor was then kinetically trapped by complete displacement of the DMF by water *via* dialysis against MilliQ water. The peptide **46** can not only act as a targeting ligand, but also provide a source for reference dye. In this sensor formulation, the pH sensitive fluorescein fluorophores are well protected from the external surrounding by PEG corona. The reference fluorophore on PEG corona may be easily affected by the external surroundings especially during its circulation in the blood stream. In order to have effective ratiometric intracellular pH monitoring, the reference and pH sensitive fluorophores should be under identical environments. Instead of using triblock copolymer having targeting peptide **46**; the mixed micelle prepared from the peptide **47** conjugated triblock copolymers **45** along with pH sensitive and reference fluorophores bounded PEG-*b*-PHEMA-*b*-PMMA (**43, 42**), and free PEG-*b*-PHEMA-*b*-PMMA (**40**) was provided ratiometric octaarginine targeted dual fluorophore labelled targeted nanosensors. This resulted dual labelled nanosensors having pH sensitive and reference fluorophores at the core coronal interface of the micelle. Dynamic light scattering (DLS) and zeta potential measurements show the sensor of a given polymer composition having intensity average hydrodynamic diameter (D_h) 50±1 nm and surface charge density -5±2 mV respectively. pH calibration curve was constructed using fluorescence spectroscopy. pH nanosensor in buffer of different pH was excited (λ_{ex} for Fluorescein = 490 nm, and for Rhodamine B = 543 nm). Fluorescence emission spectra of the nanosensors as a function of pH were plotted (**Figure 4.3a)**. pH calibration curve of the nanosensor was made by plotting fluorescence intensity (I) ratio (I_{FA} / I_{RhB}) against the corresponding pH (**Figure 4.3b)**. The pH calibration curve shows that the sensor is sensitive between the pH 5.75 to 7.75. Fluorescence measurement also confirms the quick response and reversibility of the nanosensor towards the change in pH within the pH range 5.75 to 7.75 (**Figure 4.4a, 4.4b**).

pH sensitivity range of the mixed micelle nanosensor was expanded by additionally incorporating Oregon Green conjugated unimers **44** into the above stated mixed micelle formulation. pH calibration curve of the resulting triply labelled targeted ratiometric mixed micelle sensor was constructed by plotting fluorescence intensity ratio (I_{OG} + I_{FA}) / I_{RhB}) against pH. The pH calibration

curve shows the broader sensitivity range (4.3 to 7.8) of the nanosensor (**Figure 4.3c, 4.3d**). Time for responses and reversibility of the nanosensors were also tested by fluorescence measurement, which indicate that the sensors are quickly responsive and reversible between the pH range 4.3 to 7.8 (**Figure 4.4c, 4.4d**). (Additional information regarding the fluorescence measurements can be found in **appendix E**).

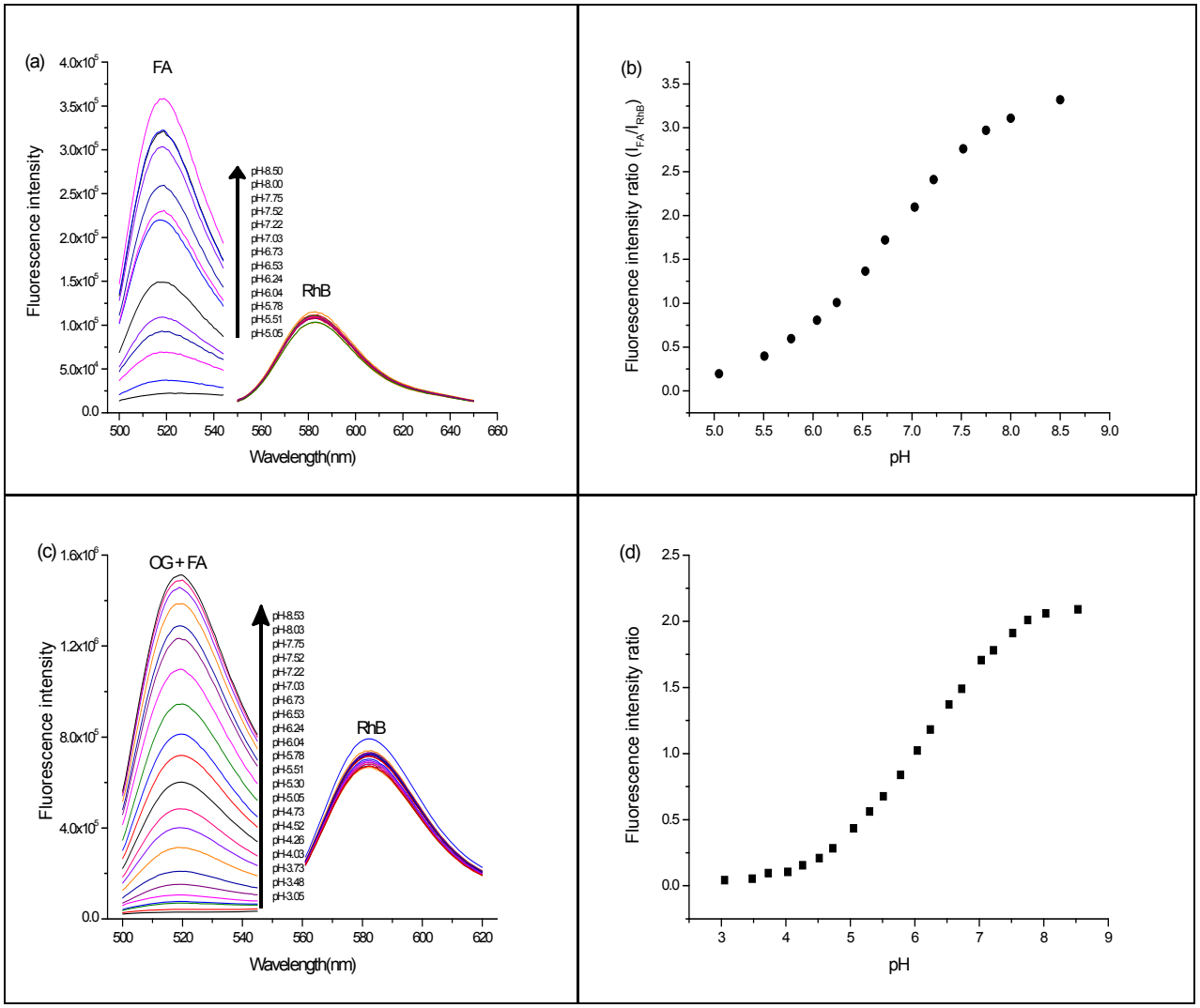

Figure 4.3. Fluorescence emission spectra (a, c) and pH calibration curves (b, d) of dual and triply labelled mixed micelle nanosensors respectively. OG = Oregon Green, FA = Fluorescein, RhB = Rhodamine B.

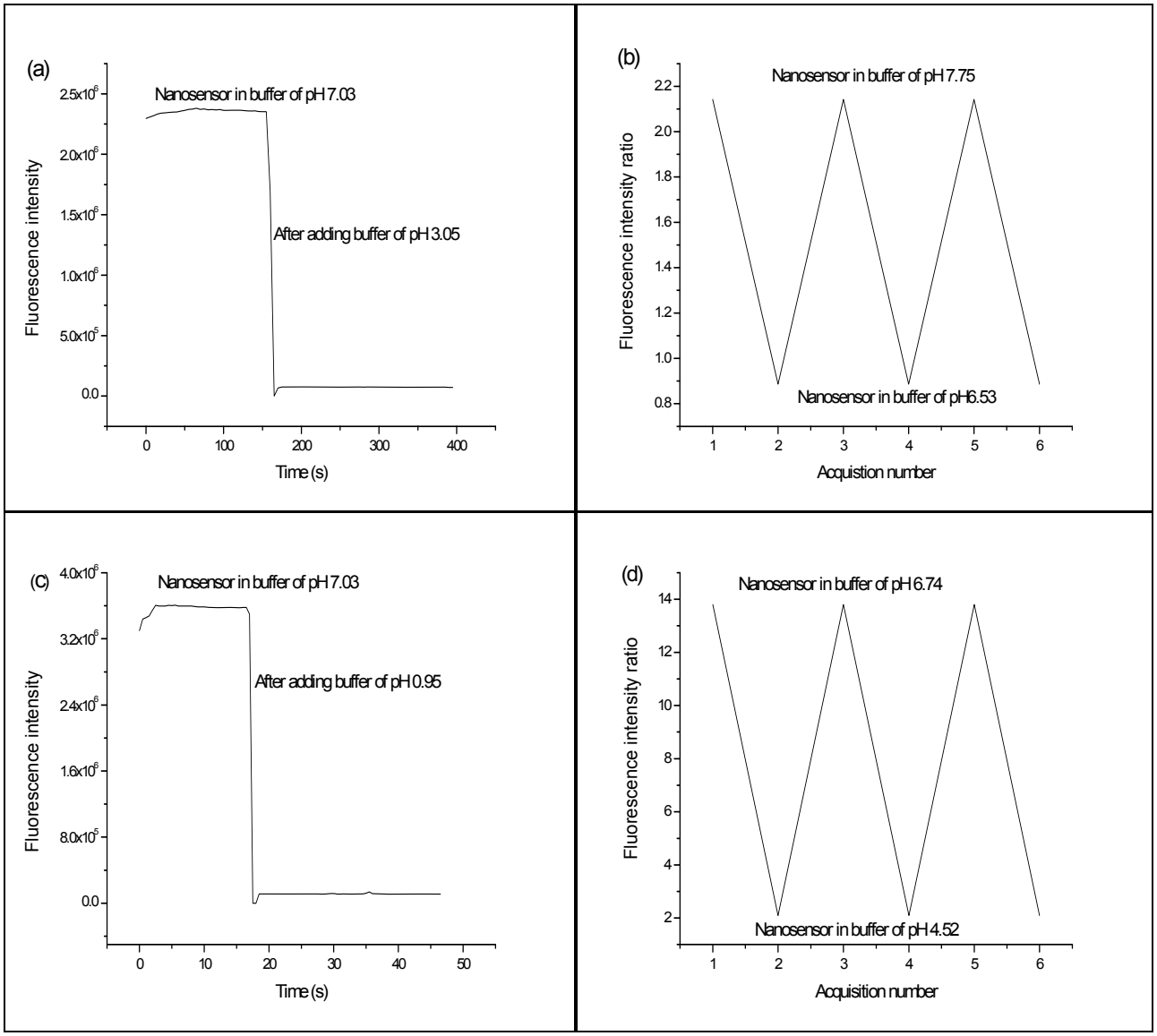

Figure 4.4. Response time (a) and reversibility (b) of the nanosensors sensitive between the pH 5.75 to 7.75 and that of sensor sensitive between the pH 4.3 to 7.8 (c, d) respectively.

Nanosensor having broad pH sensitivity range (4.3 to 7.8) was characterized by DLS, Zeta potential and cryo-TEM measurements. DLS measurement showed that the sensor having hydrodynamic diameter was around 50 nm, and zeta potential measurement showed the negative (-7±2 mV) surface charge density of the micelle nanosensor under given block copolymers composition. Cryo-TEM of the nanosensor shows "spherical" assemblies with high molecular density (**Figure. 4.5**). The PEG layer is not visualized well in the cryo-TEM, and it is the core of the micelle figure shows as a dense structure. It is fascinating that the interface area between the assembly and the water

phase is not minimized indicating that the surface tension is relatively low. Based on this, it can be hypothesize that the structures are highly flexible.

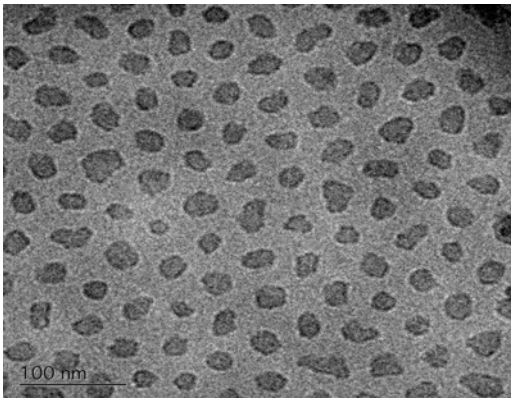

Figure 4.5. Cryo-TEM image of the pH nanosensor.

4.1.4 Conclusion

Amphiphilic triblock core-shell-corona micelle based ratiometric octaarginine peptide targeted pH nanosensors are fabricated. Different functional characteristics on nanosensors are bringing together by mixed or co-micellisation of functionalized unimers. This strategy gives attention to post polymer modifications rather than post micelle modifications, and hence avoids the role of dimensional synthetic modifications on polymeric micelles. The ability to tune the overall composition of nanosensor by simply altering the ratio of functionalized unimers in the self-assembly provides versatility in pH nanosensor fabrications. Interestingly, this co-micellisation strategy combined unimers having both hydrophilic (PEG-*b*-*PHEMA*-*b*-PMMA) and hydrophobic (PEG-*b*-*PAzEMA*-*b*-PMMA) intermediate blocks. So, the resulting triblock self-assembly is neither a core-shell-corona micelle with compartmentalized core nor a micelle with radially compartmentalized corona. This is the first example of hybrid core-shell-corona micelle known today. The cryo-TEM image shows uniform distribution of the nanoparticle, since same amphiphilic triblock are used for the different post polymer modifications, possibilities of different micelle populations of it self-assembly can be ignored. Even though the synthetic flexibility can make mixed micelle strategy as more demanding in nanosensor fabrications, the tendency for dissociation of unimers attached to different functionalities under dilute conditions may be more than a micelle composed of single unimers. If covalent cross-linking between the functionalized unimers of the mixed micelle scaffolds can be achieved, then this mixed micelle strategy can provide the best strategy in pH nanosensor fabrications due to synthetic flexibility.

4.2 c(RGDfK) Targeted Shell Cross-linked Mixed Core-shell-corona Micelle Nanosensor

4.2.1 Introduction

Intracellular pH control the metabolic activities of the enzymes,[217] ion channel conductivity,[218] cell cycle and cell divisions,[219] of several cell types. Intracellular pH measurements can also provide information about pH dependant drug release from engineered pharmaceutical carriers.[220, 221] In recent years, number of polymeric nanoparticle based ratiometric sensor systems have been developed for the pH probing of microscopic environments. This include polystyrene,[142] polyacrylamide,[97, 109, 110, 112, 113] polysaccharide[114] based particles. The nanoparticles are converted into pH nanosensors by post functional modifications. The main limitation of these post particle modification strategies is the uncertainty in predicting exact concentrations of fluorophores and degree of bioconjugation on the resulting nanosensors. Atom transfer radical polymerization technique (ATRP)[17] can provide an ease and efficient way of synthesizing amphiphilic triblock copolymers with well defined compositions and narrow molecular weight distributions. Post polymer modifications, co-micellisation[78, 207] followed by covalent stabilization of the resulting functionalized micelle can provide a platform for the synthesis of advanced polymeric nanomaterials in an easy and inexpensive procedure. It is also would like to mention that the cyclic RGD peptides can mimic the cell adhesion proteins and bind to the heterodimeric cell surface receptors, integrins.[222] This section describes the first synthesis of polymeric mixed micelle based c(RGDfK) targeted and shell cross-linked ratiometric pH nanosensors.

4.2.2 Experimental: Targeted shell cross-linked mixed micelle nanosensor synthesis

Materials and measurements: Details of materials and measurements are given in **appendix F**.

Synthesis of Amphiphilic triblock copolymers: Synthetic details of BocNH-PEG-*b*-PHEMA-*b*-PMMA (**39**), PEG-*b*-PHEMA-*b*-PMMA (**40**), and PEG-*b*-PAzEMA-*b*-PMMA (**41**) are given in the experimental **section 4.1.2**. ^{1}H-NMR spectra of **39**, **40**, **41**, **48** and FT-IR spectra of **50** and that of $CuSO_4.5H_2O$/Sodium ascorbate click shell cross-linking are given in **appendix F**.

Synthesis of NH_2-PEG-b-PAzEMA-b-PMMA(49): The triblock copolymer Boc-NH-PEG-*b*-PHEMA-*b*-PMMA (200 mg, 0.013 mmol) (**48**) was dissolved in 3mL dry pyridine and the solution was cooled to 0 ^{0}C. MsCl (0.049 mL, 0.65 mmol) in dry DCM (1mL) was added drop wise over several minutes to the above solution. The resulting solution was warm to room temperature and stir over night. After filtration of the solid precipitate, the filtrate was washed with saturated $NaHCO_3$, extracted with DCM and dried over anhydrous Na_2SO_4. After removing most of DCM by rotary evaporation, the yellowish mesylated polymer was precipitated into excess of diethyl ether and dry under vacuum. The mesylated polymer (200 mg, 0.0132 mmol) was dissolved in 3ml DMF, followed by NaN_3 (45 mg, 0.689 mmol) was added. The solution was stirred at 90 ^{0}C for 5 hours under argon atmosphere, and then at room temperature for another 20 h. After removing most of the DMF under vacuum, the polymer was precipitated into excess of cold diethyl ether, filtered and dried under vacuum gives Boc-NH-PEG-*b*-PAzEMA-*b*-PMMA polymer. The copolymer was further purified by dissolved in DMF, subsequently dialyzed against MilliQ water for 3 days and recovered by lyophilization. Isolated yield 0.13 g (70%). ^{1}H-NMR (250 MHz in d^6-DMSO): δ = 4.1-3.4 (-C**H**$_2$CH$_2$N$_3$, -C**H**$_2$C**H**$_2$O, -COOC**H**$_3$, -CH$_2$C**H**$_2$N$_3$), 2.0-1.6 (-C**H**$_2$- backbone of PHEMA and PMMA), 1.36 (s, -COOC(C**H**$_3$)$_3$), 1.0-0.6 (-C**H**$_3$ of PHEMA and PMMA) ppm; FT-IR: υ = 3439, 2952, 2896, 2107, 1731, 1486, 1449, 1389, 1348, 1273, 1243, 1193, 1148, 1109, 987, 961, 843, 750 cm^{-1}.

NH_2-PEG-*b*-PAzEMA-*b*-PMMA: The amphiphilic triblock copolymer Boc-NH-PEG-*b*-PAzEMA-*b*-PMMA (100 mg, 0.0069 mmol) was dissolved in 1 mL of DCM, followed by TFA (1 mL TFA in 1 mL DCM) was added and stirred at room temperature for 12 h. The solvent was removed under vacuum, and the polymer was precipitated from excess of cold diethyl ether and dried. The complete deprotection was confirmed by the disappearance of Boc- group signal at δ (1.36 ppm) ^{1}H-NMR (250 MHz in d^6-DMSO).

c(RGDfK) peptide (50) conjugated NH_2-PEG-b-PAzEMA-b-PMMA (51): c(RGDfK) peptide synthesis is described in **appendix F**. The c(RGDfK) peptide (10 mg, 0.016 mmol) was dissolved in 1 mL dry DMF followed by anhydrous triethylamine (0.022 mL, 0.16 mmol) and disuccinimidylcarbonate (4 mg, 0.016 mmol) were added and stirred at room temperature under Argon for 8h. After 8h, NH_2-PEG-*b*-PAzEMA-*b*-PMMA (200 mg, 0.016 mmol) was added and stirred at room temperature for 24 h. Most of the solvent was removed under vacuum, and the product was precipitated from excess of cold diethyl ether. The qualitative Kaiser test was

performed, and colorless solution indicated the absence of free amino groups. FT-IR: υ = 3277, 2105, 1721, 1670, 1639, 1535 cm^{-1}.

Binding of pH sensitive and reference fluorophores to PEG-b-PAzEMA-b-PMMA-

Preparation of PEG-b-PAzEMA-b-PMMA micelle: The amphiphilic triblock copolymer PEG-*b*-PAzEMA-*b*-PMMA (500 mg, 0.034 mmol) was dissolved in 50 mL DMF by stirring overnight. This clear solution under stirring, 5 mL of MilliQ water was added drop wise within the time interval of 30 minute, followed by 100 mL more MilliQ water was added drop wise. The cloudy micelle solution was then transferred into dialysis tube of molecular weight cut off (MWCO) 12 kDa and dialysis against MilliQ water for 3 days. Final micelle concentration was 2.5 mg/mL. Hydrodynamic diameter (D_h) = 33 ± 2 nm and zeta potential (ξ) = -13 ± 2 mV.

Conjugation of Rhodamine B-alkyne to PEG-b-PAzEMA-b-PMMA (52): To the PEG-*b*-PAzEMA-*b*-PMMA micelle (40 mL, 100 mg, 0.0068 mmol), was added 10 mL *tert*-butanol and $CuSO_4.5H_2O$ (2.54 mg, 0.010 mmol). The mixture was allowed to stir at RT for 15 min, followed by freshly prepared aqueous solution of sodium ascorbate (4.0 mg in 1 mL MilliQ water, 0.020 mmol), and Rhodamine B-alkynes (dissolved in 0.2mL of MilliQ water) (4.27 mg, 0.0068 mmol) was also added. The reaction mixture allowed to stirrer at room temperature for 3 days, transferred into dialysis tube of MWCO 12 kDa and dialysis against carbonate buffer (pH = 9) for 3 days and then against MilliQ water for another 3 days. The solution was lyophilized to get the solid Rhodamine B bounded amphiphilic triblock.

Conjugation of Fluorescein-alkyne to PEG-b-PAzEMA-b-PMMA (53): PEG-*b*-PAzEMA-*b*-PMMA micelle (40 mL, 100 mg, 0.0068 mmol), 10 mL *tert*-butanol and $CuSO_4.5H_2O$ (2.54 mg, 0.010 mmol) were allowed to stir at RT for 15 min. Freshly prepared aqueous solution of sodium ascorbate (4.0 mg in 1 mL MilliQ water, 0.020 mmol), and Fluorescein-alkynes (dissolved in 0.2mL of MeOH) (2.91 mg, 0.0068 mmol) were added, and the reaction mixture was stirred at room temperature for 3 days. The reaction mixture was transferred into dialysis tube of MWCO 12 kDa and dialysis against carbonate buffer (pH = 9) for 3 days and then against MilliQ water for another 3 days. The solution was lyophilized to get the solid Fluorescein bounded triblock copolymer.

Conjugation of Oregon Green-alkynes to PEG-b-PAzEMA-b-PMMA (44): To the PEG-*b*-PAzEMA-*b*-PMMA micelle (40 mL, 100 mg, 0.0068 mmol), was added 10 mL *tert*-butanol and

$CuSO_4.5H_2O$ (2.54 mg, 0.010 mmol). The mixture was allowed to stir at RT for 15 min, followed by freshly prepared aqueous solution of sodium ascorbate (4.0 mg in 1 mL MilliQ water, 0.020 mmol), and Oregon Green488 alkyne 6-isomer (dissolved in 0.2 mL of DMF) (3.05 mg, 0.0068 mmol) was also added. The reaction mixture was stirred at room temperature for 3days, transferred into dialysis tube of MWCO 12 kDa and dialysis against carbonate buffer (pH = 9) for 3 days and then against MilliQ water for another 3 days. The solution was lyophilized to get the solid Oregon Green bounded polymer.

Synthesis of dendritic click cross-linker ((Alkyne)$_4$-[G-1])) (55): The dendritic alcohol $(HO)_4$-[G-1] was synthesized by a procedure described in the literature[179]. A solution of $(HO)_4$-[G-1] (500 mg, 0.73 mmol) in anhydrous DMF (5 mL), was stirred at 0 °C with propargyl bromide (80 wt.% in Xylene) (3 mL, 33 mmol). Portions of finely ground KOH (2490 mg, 44.5 mmol) were added over a period of 30 min. The reaction mixture was warmed to room temperature and stir for 24 h under argon atmosphere. The course of the reaction was monitored by TLC (10% MeOH in DCM $R_{f(product)}$ = 0.80). After completion of the reaction, mixture was concentrated to dryness and the residue partitioned between DCM (100 mL) and brine (20 mL). The organic layer was washed with water, dried over anhydrous Na_2SO_4, and the solvent was removed under reduce pressure to give the crude product, which was further purified by Column chromatography. The column was first run with the solvent system 1:1 Ethylacetate : Hexane to remove traces of impurity, then changed to 1:1 MeOH : Ethylacetate, yield 450 mg (84%). ^{1}H-NMR (300 MHz in $CDCl_3$): δ = 7.8 (s, 2H, triazole), 6.95 (s, 4H, Ar**H**), 6.94 (s, 2H, Ar**H**), 5.20 (s, 4H, triazole-C**H**$_2$O), 4.59 (s, 8H, -C**H**$_2$OCH$_2$C≡CH), 4.54 (t, 4H, -CH$_2$OCH$_2$C**H**$_2$-triazole), 4.1 (d, J = 2Hz, 8H, -C**H**$_2$C≡CH), 3.84 (t, 4H, -CH$_2$OC**H**$_2$CH$_2$-triazole), 3.54 (s, 4H, -C**H**$_2$OCH$_2$CH$_2$-triazole), 2.45 (t, J = 2Hz, 4H, -CH$_2$C≡C**H**) ppm; FT-IR: υ = 3282, 3138, 2111, 1600, 1459, 1352, 1290, 1078, 842, 641 cm^{-1}.

Synthesis of shell cross-linked micelle using CuBr(PPh$_3$)$_3$/DIPEA catalyst (56): The PEG-*b*-PAzEMA-*b*-PMMA micelle solution in MilliQ water was dialyzed (MWCO = 12 kDa) against THF : buffered water (1:4) for 3 days. The solution was transferred into 100 mL round-bottom flask equipped with a stirrer bar. To the stirred solution of PEG-*b*-PAzEMA-*b*-PMMA micelle in 1:4 THF : buffered water (100 mg, 0.0069 mmol, 0.048 mmol of azide), was added $CuBr(PPh_3)_3$ (prepared by the literature procedure)[178] (13 mg, 0.014 mmol), DIPEA (0.025mL, 0.144 mmol), Cu wire (to prevent the oxidation of the catalyst) (*ca.* 100 mg), and the dendritic cross-linker (Alkyl)$_4$-[G-1] (in 0.5 mL of THF) (18 mg, 0.024 mmol). The reaction mixture was allowed to stirrer at RT

for 3 days. The reaction mixture was transferred to dialysis tube (MWCO = 12 kDa) and dialyzed against MilliQ water, and THF (5 : 1) for 4 days then against MilliQ water for another 4 days. D_h (DLS) = 31±1 nm, Zeta potential = -12±2 mV. FT-IR: υ = 3268, 1726, 1596, 1443, 1237, 1145, 983, 838, 747 cm^{-1}.

Synthesis of shell cross-linked micelle using $CuSO_4.5H_2O$/Sodium ascorbate catalyst: To the stirred aqueous solution of PEG-*b*-PAzEMA-*b*-PMMA micelle (100 mg (40 mL), 0.0069 mmol, 0.048 mmol of azide), was added 10 mL of *tert*-butanol, $CuSO_4.5H_2O$ (3.6 mg, 0.014 mmol), sodium ascorbate (28 mg, 0.144 mmol) (5%wt aqueous solution) and the dendritic cross-linker $(Alkyl)_4$-[G-1] (in 0.5 mL of THF) (18 mg, 0.024 mmol). The reaction mixture was stirred at room temperature for 3 days. The reaction mixture was transferred into dialysis tube (MWCO = 12 kDa) and dialysis against MilliQ water and THF (5 : 1) for 4 days and then against MilliQ water for another 4 days. D_h (DLS) = 33±2 nm, Zeta potential = -11±1 mV. FT-IR: υ = 3270, 2107, 1728, 1599, 1447, 1239, 1148, 988, 839, 748 cm^{-1}.

Fabrication of shell cross-linked targeted ratiometric pH nanosensors: The amphiphilic triblock copolymer PEG-*b*-PAzEMA-*b*-PMMA conjugated to Fluorescein (**53**) (3.43 mg, 0.23 µmol), Oregon Green (**44**) (1.47 mg, 0.10 µmol), Rhodamine B (**52**) (0.049 mg, 0.0033 µmol), cRGDfK peptide (**51**) (0.098 mg, 0.0067 µmol), and free PEG-*b*-PAzEMA-*b*-PMMA (**41**) (4.9 mg, 0.33 µmol) in the ratio 7 : 3 : 0.1 : 0.2 : 10 (total 10 mg) were dissolved in 2 mL of DMF by stirring overnight. To the polymer solution under stirring, 0.2 mL of MilliQ water was added within the time interval of 30 minute followed by 4 mL more water added drop wise. The cloudy micelle solution was then transferred into dialysis tube of MWCO (12 kDa) and dialysis against MilliQ water for 3 days (D_h = 39±2 nm, Zeta potential = -19±2 mV) and then against buffered water: THF (4:1) for another 3 days.

The micelle solution (10 mg, 0.68 µmol, 4.8 µmol of azide) was transferred into a 25 mL round-bottom flask equipped with a stirrer bar, was added $CuBr(PPh_3)_3$ (1.36 mg, 1.4 µmol), DIPEA (2.5 µL, 14.4 µmol), Cu wire (*ca.* 2 mg), and the dendritic benzylether cross-linker $(Alkyl)_4$-[G-1] (in 100 µL of THF) (1.76 mg, 2.4 µmol). The reaction mixture was allowed to stirrer at RT for 3 days, transfer to dialysis tube (MWCO 12 kDa), and dialyze against MilliQ water : THF (5 : 1) for 4 days and then against MilliQ water for another 4 days. Final sensor concentration was = 1.25 mg/mL. D_h = 38±1 nm, Zeta potential = -17±1 mV.

4.2.3 Results and Discussion

Fabrication of shell cross-linked targeted and ratiometric pH nanosensors by the mixed micelle approach is schematically illustrating in **Figure 4.6**. The amphiphilic triblock copolymers Boc-NH-poly(ethylene glycol)-*b*-poly(hydroxyethyl methacrylate)-*b*-poly(methyl methacrylate) (Boc-NH-PEG-*b*-PHEMA-*b*-PMMA) (**39**) and poly(ethylene glycol)-*b*-poly(hydroxyethyl methacrylate)-*b*-poly(methyl methacrylate) (PEG-*b*-PHEMA-*b*-PMMA) (**40**) were synthesized by isolated macroinitiator atom transfer radical polymerization techniques. Post polymer modifications of **39**, **40** were achieved by mesylation of the PHEMA hydroxyl groups followed by nucleophilic substitution by sodium azide. This resulted in Boc-NH-poly(ethylene glycol)-*b*-poly(2-azidoethyl methacrylate)-*b*-poly(methyl methacrylate) (Boc-NH-PEG-*b*-PAzEMA-*b*-PMMA) (**48**) and poly(ethylene glycol)-*b*-poly(2-azidoethyl methacrylate)-*b*-poly(methyl methacrylate) (PEG-*b*-PAzEMA-*b*-PMMA) (**41**) (**Scheme 4.4a**). Disappearance of the –OH protons (^{1}H-NMR (d^6-DMSO) δ = 4.70 ppm) confirmed the complete conversion and the presence of *tert*-Butoxycarbony (Boc) group on Boc-NH-PEG-*b*-PAzEMA-*b*-PMMA at δ = 1.36 ppm confirmed the stability of the protecting group under the reaction conditions. FT-IR further confirmed the presence of azido groups on the polymers (υ = 2110 cm^{-1}). The Boc group from Boc-NH-PEG-*b*-PAzEMA-*b*-PMMA was removed by treatment with TFA/DCM (**Scheme 4.4b**). The complete deprotection was confirmed by the disappearance of Boc- signal at 1.36 ppm in ^{1}H-NMR (d^6-DMSO).

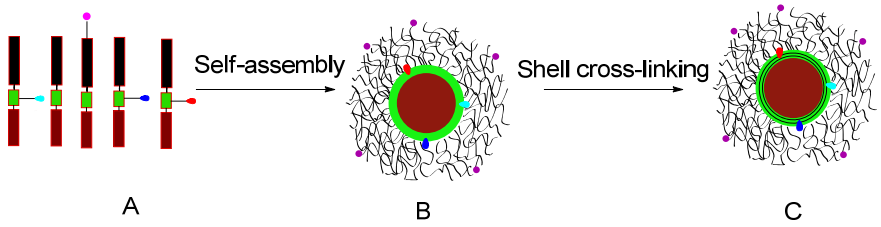

Figure 4.6. Fabrication of shell cross-linked targeted ratiometric pH nanosensors (**C**) from targeted ratiometric mixed micelle pH nanosensors (**B**) formed by the spontaneous self-assembly of amphiphilic functionalized triblock copolymers (**A**).

The targeting cyclic RGD peptide, c(RGDfK) (**50**) was coupled to the chain end of the polymer **49** by using *N,N'*-Disuccinimidyl carbonate linker (**Scheme 4.4c**). The peptide conjugated polymer **51** was confirmed by FT-IR spectroscopy (amide N-H stretch at 3277 cm^{-1} and amide -C=O stretch at 1670 cm^{-1}), in addition to a Kaiser test,[159] which indicated the absence of free amino groups on the polymer.

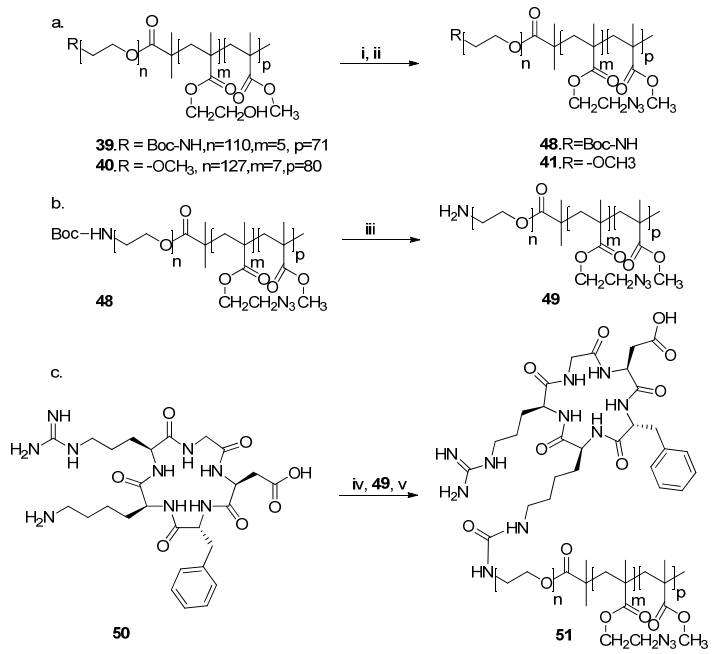

Scheme 4.4. Post functional modifications of the amphiphilic triblocks, at the side chain (a) and chain ends (b, c). i) CH_3SO_2Cl, Py, Argon atm, RT, overnight; ii) NaN_3, DMF, Argon atm, 90 ^{0}C (5h) to RT (20 h); iii) TFA, CH_2Cl_2, RT, 12 h; iv) N,N'-Disuccinimidyl carbonate, TEA, DMF (dry), Argon atm, RT, 8h; v) RT, 24 h.

pH sensitive (Fluorescein and Oregon Green alkyne) and pH insensitive reference fluorophore (Rhodamine B alkyne) were attached separately to PEG-*b*-PAzEMA-*b*-PMMA (**53, 44, 52**) by CuAAC reaction (**Scheme 4.5**). The catalysts and un-reacted fluorophores were removed by extensive dialysis against carbonate buffer and MilliQ water, followed by fluorescence measurements confirmed the covalent attachment of fluorophores to the amphiphilic triblocks. The fluorophores conjugated triblock copolymers were isolated by lyophilization.

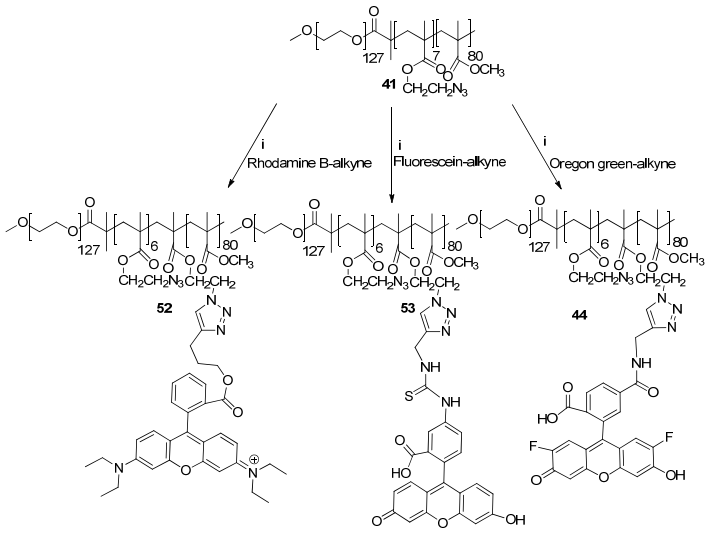

Scheme 4.5. Conjugation of fluorophores to the amphiphilic triblock copolymer **41** by click reactions. i) $CuSO_4.5H_2O$, Sodium ascorbate, H_2O : *tert*-butanol (4:1), RT, 72 h.

Effectiveness of dendritic shell cross-linking of PEG-*b*-PAzEMA-*b*-PMMA (**41**) micelle was investigated by click reaction. The dendritic alkyne benzyl ether cross-linker, $(Alkyne)_4$-[G-1] (**55**) was synthesized from dendritic alcohol $(OH)_4$-[G-1][179] (**54**) and propargyl bromide by Williamson ether synthesis (**Scheme 4.6**). The dendritic click shell cross-linking at the hydrophobic shell region of the micelles was performed by two different catalytic systems under otherwise identical conditions; $CuBr(PPh_3)_3$ / DIPEA in 1 : 4 (THF : Buffered H_2O) (**Scheme 4.7**) and $CuSO_4.5H_2O$ / sodium ascorbate in 1 : 4 (*tert*-butanol : H_2O). After three days of reaction, subsequent dialysis and lyophilization, FT-IR spectra of the shell cross-linked micelle **56** obtained by the $CuBr(PPh_3)_3$ / DIPEA approach showed complete disappearances of N≡N asymmetric stretching absorption of azide at 2100 cm^{-1} and the appearance of -C≡**C-H** and aromatic C=C stretching at 3270 cm^{-1} and 1593 cm^{-1} respectively. This indicate complete participation of the azide groups in the triazole ring formation, and the absorption at 3270 cm^{-1} and 1593 cm^{-1} confirms the presence of excess alkyne groups on the dendritic *benzyl* ether cross-linker of the cross-linked micelle (**Figure 4.7**). Dynamic light scattering (DLS) and zeta potential measurements revealed that the cross-linking reaction did not affect the hydrodynamic diameter (D_h) and the zeta potential (ξ) of the nanoparticles. (**Table 4.2, micelle 41&56**) thus indicating that the shell cross-linking of the well defined core-shell-corona micelle occurred intramicellarly even at high block copolymer concentrations (2.5 mg/mL). The dendritic shell cross-linking reaction using $CuSO_4.5H_2O$ / sodium ascorbate in 1 : 4 *tert*-butanol : H_2O system was also effective, but the presence of azide peak at 2100cm^{-1} (**Figure 4.8**)

indicated partialness. These optimization studies show that click reaction at the hydrophobic shell region of the PEG-*b*-PAzEMA-*b*-PMMA micelle gave better results under more hydrophobic conditions.

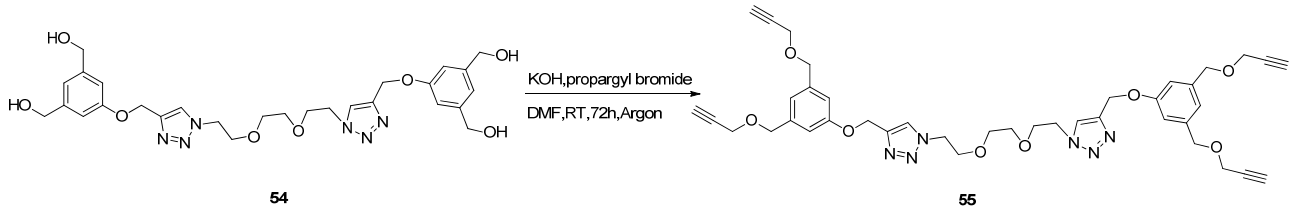

Scheme 4.6. Synthesis of dendritic alkyne benzyl ether cross-linker from dendritic benzyl alcohol.

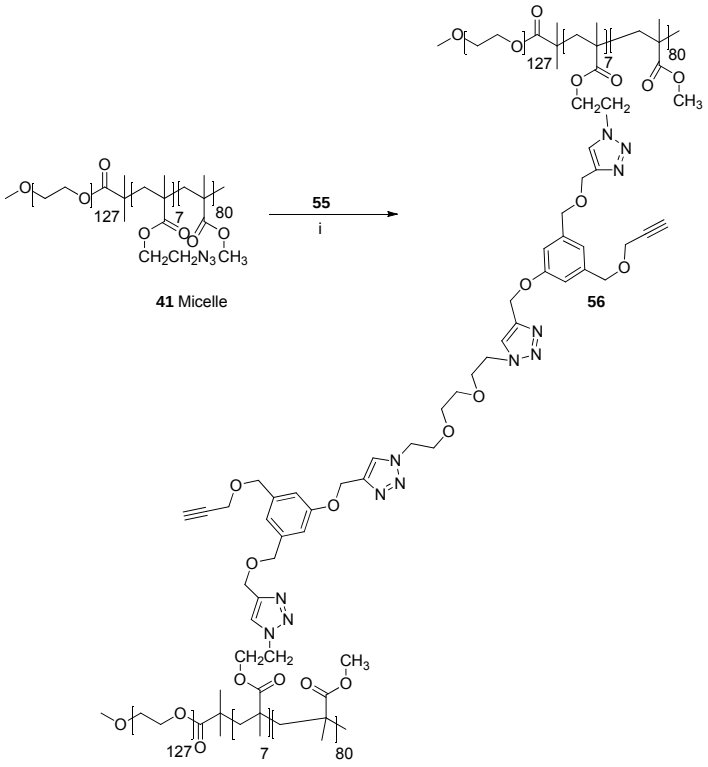

Scheme 4.7. Synthesis of dendritic click shell cross-linked core-shell-corona-micelle **56** using dendritic alkyne cross-linker, **55**. The minimum cross-linking possibility of the linker is shown in the scheme. i) $CuBr(PPh_3)_3$, DIPEA, Cu wire, THF : Buffered water (1 : 4), RT, 72h.

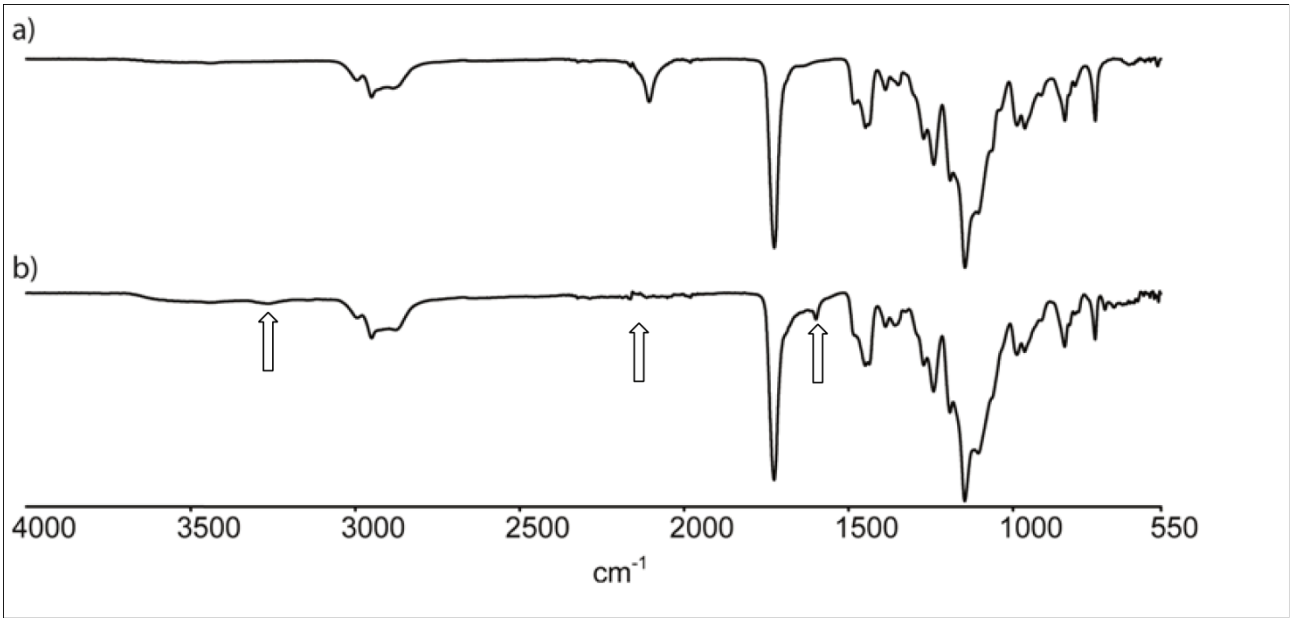

Figure 4.7. FT-IR spectra of PEG-*b*-PAzEMA-*b*-PMMA (**41**) micelle; (a) before cross-linking and (b) after cross-linking, **56**. Arrows in (b) indicates the presence of alkyne (C-H) and aromatic C=C stretching, and the absence of azide stretching absorptions, y-axis is % of transmittance (arbitrary units).

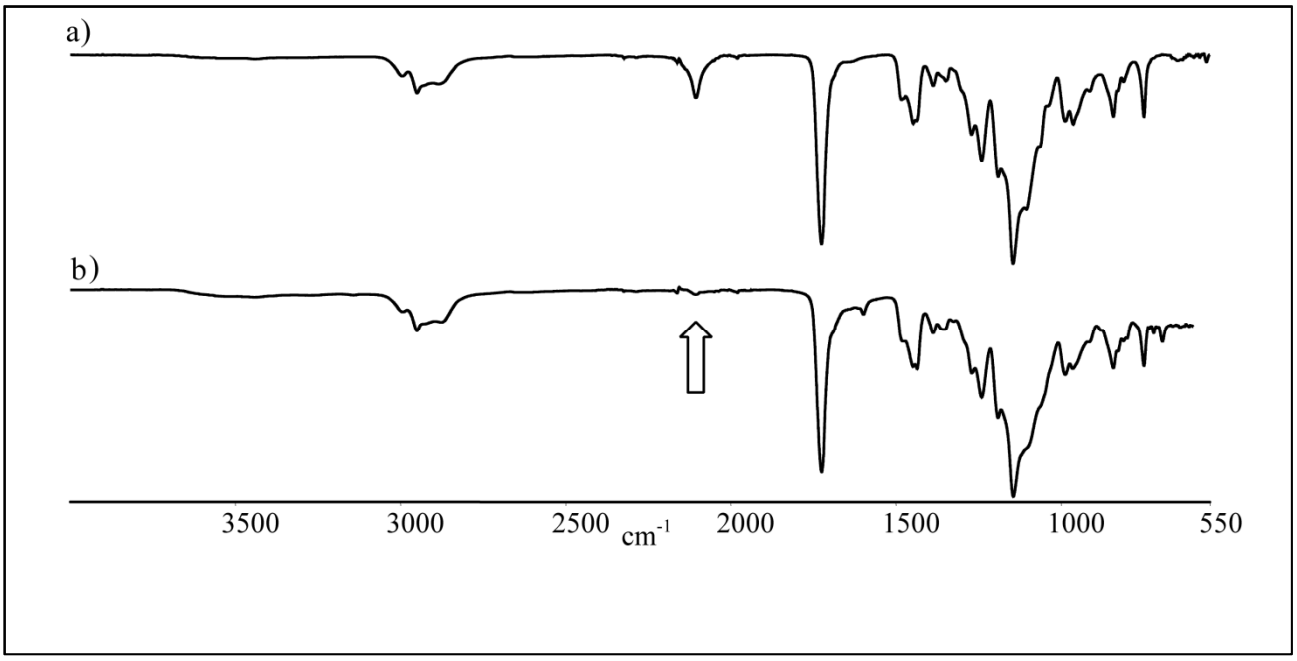

Figure 4.8. FT-IR spectra of PEG-*b*-PAzEMA-*b*-PMMA micelle (a) before cross-linking and (b) after cross-linking using $CuSO_4.5H_2O$ / Sodium ascorbate. Arrow in (b) indicates the presence of azide stretching at 2100 cm^{-1} due to the incomplete shell cross-linking, y-axis is % of transmittance (arbitrary units).

Table 4.2. Characterization Data for the Micelle **B**, **C**, **41** and **56**.

Micelle	DLS(D_h)[a] (nm)	Zeta(ξ)[b] (mV)	H_{av}[c] (nm)
B	39±2	-19±2	15±4
C	38±1	-17±1	20±10
41[d]	33±2	-13±2	---------
56	31±1	-12±2	---------

*[a] Number-averaged hydrodynamic diameters of aqueous micelle solutions by DLS. [b] ζ-potential from 10 determinations of 10 cycles. [c] Average heights of the micelles measured by tapping mode AFM and calculated from values of ca 100 particles. [d] Micelle of **41**.*

The targeted ratiometric and cross-linked pH nanosensor (**C**) was prepared by a two step procedure. The amphiphilic triblock copolymers attached to c(RGDfK) peptide (**51**), pH sensitive and reference fluorophores (**53**, **44**, **and 52**) and the PEG-*b*-PAzEMA-*b*-PMMA (**41**) were dissolved in DMF in the desired ratio (degree of functionalization). Displacement of DMF by a selective solvent (water) resulted in non cross-linked but targeted ratiometric mixed micelle nanosensors (**B**). The targeted mixed micelle nanosensor was then cross-linked by dendritic benzyl ether cross-linker using $CuBr(PPh_3)_3$/DIPEA catalyst under the above stated optimized reaction condition. After removing the catalyst and excessive reagents by extensive dialysis, the DLS and ζ-potential measurements showed that before and after cross-linking, the hydrodynamic diameter and zeta potential of the nanosensors are almost same. This confirms the exclusive intramicellar cross-linking at the shell region of the nanosensors (**Table 4.2. micelle B&C**).

Nanosensors dispersion in MilliQ water was added to buffer of different pH for the construction of ratiometric *in vitro* pH calibration curve by fluorescence spectroscopy (**Figure 4.9**). The presence of pH sensitive Oregon Green and Fluorescein; and insensitive reference fluorophore, Rhodamine B at the shell region of the shell cross-linked core-shell-corona micelle were confirmed by the pH calibration curve. The pH calibration curve shows that the nanosensors are sensitive between the pH *ca.*4.5 to 7.5, and confirm the broad pH sensitivity range of the triply labelled robust micelle sensor.

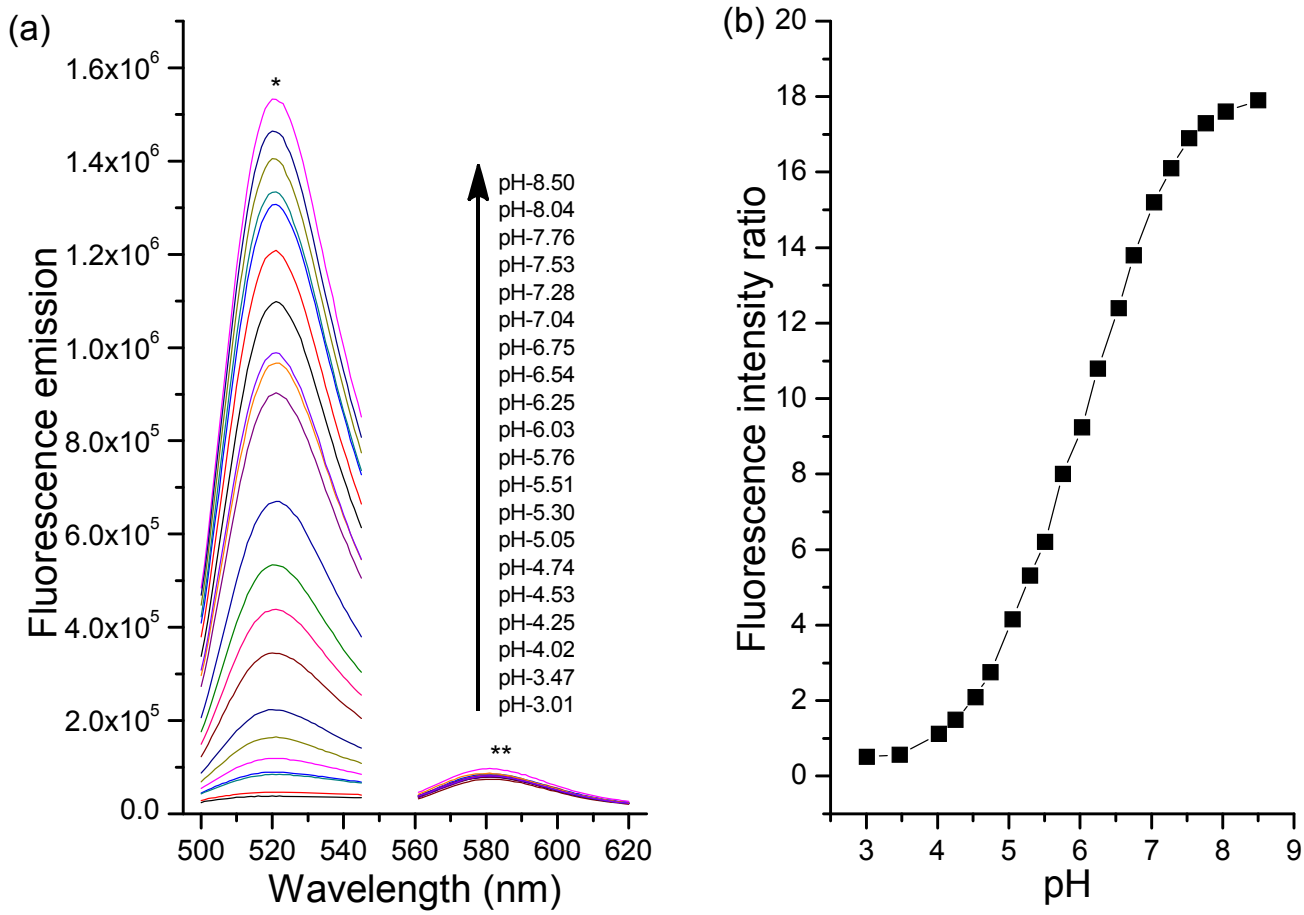

Figure 4.9. (a) Fluorescence emission spectra of the nanosensor. *Fluorescence intensity of pH sensitive fluorophores (excitation wavelength λ_{ex}= 488 nm) and **reference fluorophore (λ_{ex}= 543 nm), in buffer of different pH having sensor concentration 0.125 mg/mL. (b) pH calibration curve of the nanosensor. Curve made by plotting fluorescence intensity ratios (I_{FA} + I_{OG} / I_{RhB}) of the pH sensitive (I_{FA} + I_{OG}) and reference (I_{RhB}) fluorophores against the corresponding pH. FA = Fluorescein, OG = Oregon Green, RhB = Rhodamine B.

The morphology of the cross-linked nanosensor (**C**) was analyzed by atomic force microscopy (AFM) and transmission electron microscopy (TEM) as shown in **Figure 4.10**. Both techniques showed spherical nanosensors, and TEM confirmed the 30 nm size range of the nanosensor. The hydrodynamic diameter measured from DLS was slightly larger than diameter measured by TEM, indicating shrinking of the sensor during air dried sample preparation for TEM imaging. The average height of the sensor (H_{av}) calculated from AFM measurements show that, after cross-linking the height of the nanosensor does not change considerably (**Table 4.2 B**, **C**). This indicates that the shell cross-linking of the core-shell-corona micelle nanosensor does not significantly alter its interaction with the hydrophilic silica surface.

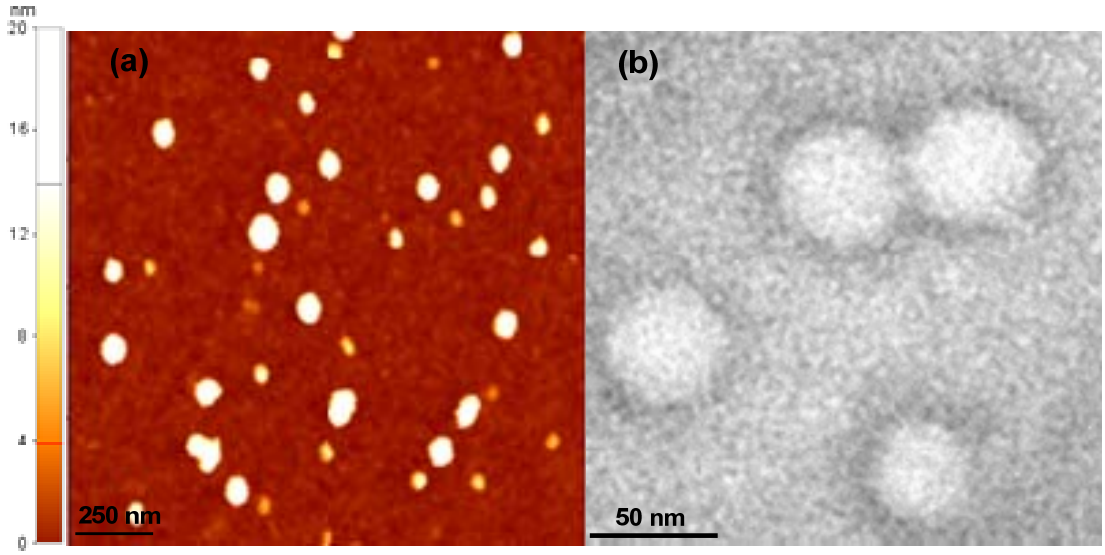

Figure 4.10. AFM (a) and TEM image (b) of the pH nanosensor (**C**).

Effect of dilution on micelle stability was studied by DLS measurements (**Figure 4.11**). In a given block copolymer concentration (1.2 mg/mL), the non-cross-linked micelle sensor (**B**) and non-cross-linked micelle of **41** was not detectable after certain dilution. At the same time, the cross-linked micelle **56** and the nanosensor (**C**) were maintained their structural integrity throughout the experiments. Dissociation of mixed micelle nanosensor (**B**) was faster, and occurred at a concentration below *ca.* 20 mg/ L, whereas, the non cross-linked micelle showed much lower CMC (*ca.* 10 (mg/L)). This indicates the importance of covalent shell cross-linking between the unimers of these nanoparticle scaffolds during the mixed micelle nanosensor fabrications.

The self-assembly of amphiphilic functionalized unimers followed by covalent cross-linking at the shell region of the resulting core-shell-corona micelle provides an advanced micelle nanosensor. Mixed micellisation provide control over sensor compositions. The covalent stabilization can prevent nanosensor dissociation below the critical micelle concentration (CMC) and thus enhances its applications in infinitely diluted biological conditions. Due to compatibility and orthogonality towards a wide range of functionalities, a dendritic click reaction is used for the covalent cross-linking at the shell domain. The presence of un-reactive PEG corona on the core-shell-corona micelle nanosensors can provide long circulating half life's for the sensors in blood by preventing the sensor recognition by the phagocytic cells and certain proteins (opsonization). The pH sensitive and reference fluorophores at the shell region are protected from the external surroundings by the PEG corona. The PEG corona also offers repulsive interaction between the micelle nanosensors,

thus providing exclusive intramicellar cross-linking of the nanosensors even at high block copolymer concentrations (1.25 mg/mL). The cell surface adhesion proteins $\alpha_v\beta_3$ integrins are responsible for tumor-induced angiogenesis. The binding of $\alpha_v\beta_3$ with the cyclic RGD peptide (c(RGDfK)) reduces the rate of angiogenesis.[223] Thus, the nanosensors with surface functionalized c(RGDfK) may provide an opportunity to monitor the intracellular pH during tumor regressions.

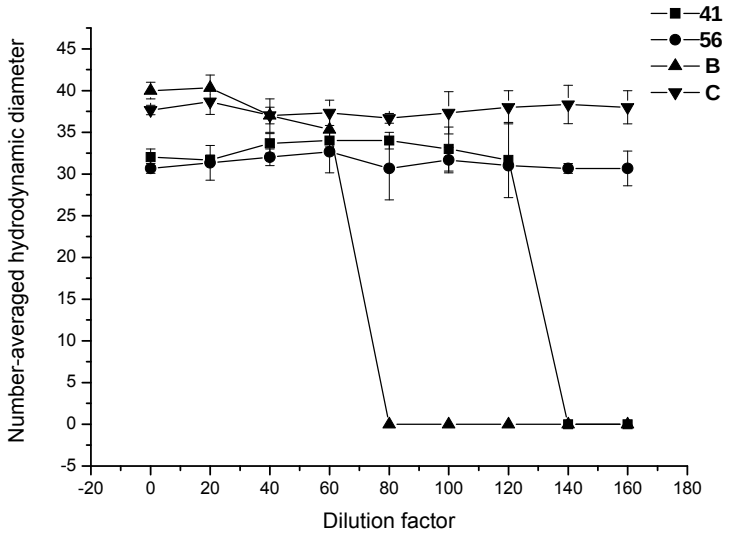

Figure 4.11. Number-averaged hydrodynamic diameter (D_h) of the micelles measured by DLS as a function of dilution; for non-cross-linked mixed micelle sensor (**B**) (▲), micelle of **41** (■), cross-liked mixed micelle sensor (**C**) (▼) and cross-linked micelle **56** (●).

4.2.4 Conclusion

With the help of synthetic and dimensional synthetic organic chemistry and the principle of self-assembly, a ratiometric shell cross-linked and c(RGDfK) targeted mixed micelle nanosensor for intracellular pH measurement is fabricated. The ratiometric fluorescence measurements eliminate the errors in fluorescence intensity due to excitation source fluctuations, fluorophore concentrations and environmental factors. The mixed micelle strategy allows the tuning of the exact amount of fluorophores and targeting ligands present in the nanosensors. The covalent dendritic shell cross-linking makes the nanosensor more robust and hence can prevent the sensor disintegration under diluted conditions. Thus, a new strategy for nanosensor synthesis is developed, which reduced the uncertainty in functional modification of nanoparticles during nanosensors fabrications. Further investigations of these nanosensors in a biological setting may provide information about intracellular pH during tumor regressions.

Chapter 5

Summary and Outlook

5.1 Summary

This Ph.D thesis investigated the synthetic flexibility and structural potentials of polymeric micelle nanoparticles in nanosensor fabrications primarily for ratiometric fluorescence based intracellular pH monitoring. ATRP was used for the synthesis of well defined functional unimers (amphiphilic triblock copolymers). Incorporation of protection and deprotection chemistry made the well defined functional block copolymer synthesis easier, *via* preventing the functional monomers interaction with the ATRP catalyst systems during the chain growth. The self-assembly of the resulting amphiphilic functional triblocks in hydrophilic block selective solvent (water) afforded the core-shell-corona functional micelles. Distinct core-shell-corona domains on the functional micelle provided opportunities for regioselective functionalization and cross-linking. Presence of PEG corona (in all the micelles used in this thesis) could implement long circulation time in blood. This may be allows effective accumulation of these nanoparticles in desired tumor tissues *via* EPR effect. The PEG corona not only protected the functionalities introduced to the shell region of the micelle, but also stabilized (cross-linked) the micelle under high block copolymer concentration *via* steric stabilization mechanism. This stabilization could prevent the micelle dissociations under infinitely diluted biological conditions and hence enhance its potentials in biological applications.

The first strategy used for the nanosensor invention was based on post micelle modifications. The functional core-shell-corona micelle prepared from the self-assembly of functional unimers were modified with the help of dimensional synthetic chemistry. The micelles were cross-linked by either amidation shell cross-linking (PEG-*b*-PAEMA-*b*-PS micelle) or dendritic-click core cross-linking (PEG-*b*-PAEMA-*b*-PES micelle) reactions. The click chemistry based core cross-linking strategy was superior over the amidation with respect to its functional group insensitivity and excellent reaction yield. The core cross-linking provided an entirely free shell region for functionalization, but in shell cross-linking, a portion of the free amino groups present in the shell region was used in the amide bond formation. Amidation shell cross-linking was synthetically much easier to perform in pure water within short reaction time, whereas the click core cross-linking demanded prolonged

reaction time. The dendritic click core cross-linking also demanded availability of click reactive functional groups at the micelle core, synthesis of dendritic cross-linking agents, mixture of organic and aqueous reaction media, the accessibility of the reagents at the hydrophobic swollen nanodomains, removal of water insoluble excess reagents *etc*. The shell and core cross-linked core-shell-corona functional micelle were then converted into ratiometric pH nanosensor *via* covalent attachments of pH sensitive and reference fluorophores at the shell region. Since dimensional synthetic chemistry was inherently inefficient and hard to quantify, there was no precise knowledge about the degree of cross-linking and amount of pH sensitive and reference molecules conjugated to the shell region of the micelle. As a result, numbers of dimensional synthetic modifications and fluorescence optimization studies were carried out to have nanosensor for desired pH sensitivity range.

UV radiation induced core cross-linking of a core-shell-corona micelle did not require the transfer of reagent to the hydrophobic nanodomains. Synthesis of amphiphilic triblock copolymers having UV sensitive groups at the core forming block, followed by their self-assembly in water afforded photo sensitive core-shell-corona micelles. UV exposure on this aqueous micelle solution was given non-reversibly and reversibly photo core cross-linked micelle. The degree of micelle cross-linking was controlled by the duration of UV exposure to the micelle solution. Photo cross-linking *via* UV induced oxidative coupling between the alkyne groups at the poly ethynylstyrene (P(SC≡CH)) core of the PEG-*b*-PAEMA-*b*-P(SC≡CH) micelle, followed by conjugation of pH sensitive and reference fluorophores at the PAEMA shell provided photo core cross-linked micelle based nanosensors. Replacement of (P(SC≡CH)) block by poly (coumarin methacrylate) (PCMA) provided a reversibly photo core cross-linked micelle nanosensor. Wavelength dependant photo dimerization of coumarin ($\lambda > 320$ nm) at the micelle core (PCMA) was used to prepare the photo core cross-linked PEG-*b*-PAEMA-*b*-PCMA micelle nanosensor. Illuminating the cross-linked micelle sensor at higher energy ($\lambda < 255$ nm) afforded a de-cross-linked micelle sensor. This reversible strategy may provide an opportunity to combine sensing and drug delivery application together in the same particle. However, complete micelle de-cross-linking was not practically possible, and applications of this reversible strategy *in vivo* may be limited by the low UV penetration depth in tissues.

The mixed micelle nanosensor fabrication strategy was given well defined pH nanosensors with respect to fluorophores concentration and degree of surface functionalization on the polymeric micelles. Here, post polymer modifications gained more significance than the post micelle

modifications. Co-micellisation of the amphiphilic triblock copolymers, PEG-*b*-PHEMA-*b*-PMMA and NH_2-PEG-*b*-PHEMA-*b*-PMMA having similar composition but attached to different functionalities such as fluorophores and targeting ligand implemented mixed micelle sensors. Since synthetic improvement on unimers was more easily and precisely controllable than it self-assembly, co-micellisation of functionalized unimers provided better control over the nanosensor composition. The role of dimensional synthetic chemistry can be reduced but cannot be entirely ignored in the fabrication of covalently stabilized mixed micelle nanosensors. A dendritic click shell cross-linking on mixed micelle prepared from functionalized PEG-*b*-PAzEMA-*b*-PMMA and NH_2-PEG-*b*-PAzEMA-*b*-PMMA was used for the synthesis of stabilized mixed micelle nanosensors. The nanosensor synthesized by post micelle modification may be capable of monitoring intracellular pH *via* accumulation in the pathological sites by passive targeting (EPR effects). Micelle nanosensors having active targeting capabilities were prepared by the mixed micelle method.

Thus, the dissertation explained the synthesis of some stabilized advanced functional core-shell-corona micelle nanomaterials by combining ATRP with click reaction, amidation reaction, light induced oxidative coupling reactions, photo dimerization *etc*. This amphiphilic triblock copolymer micelles having compartmentalized core or radially compartmentalized corona provided more regioselective functionalization and cross-linking, than extensively reported synthetically and morphologically basic diblock core-shell spherical micelle. These synthetic advantages will extend the applications and demands of these advanced functional nanomaterials especially in the biomedical field.

5.2 Future work

As described, this thesis has only showed the application of core-shell-corona functional micelles in ratiometric pH nanosensor fabrications. Simply changing the fluorophores attached to the shell region of the micelle was providing nanosensors with different pH sensitivity range. Conjugation of molecules that are sensitive to different analyte concentration in cells may provide a broad range of application to the micelle nanosensors in biology. Since surface functionalization chemistry on the micelle surface was relatively easy, attaching different targeting ligands on the micelle surface may allow accurate design of nanosensors for specific tissues. Site-specific micelle sensors may exhibit more effective intracellular sensing capabilities than a non targeted micelle sensor. Since polymeric micelles are well known pharmaceutical carriers, by combining the sensing and pharmaceutical

applications together may provide further information about the pH sensitive drug delivery. Fabrication of a reversibly cross-linked micelle sensor was explained in the thesis. The reversible strategy may provide opportunities for the development of micelle sensors, which may be capable of monitoring intracellular pH during drug delivery from a de-cross-linked micelle. It would be fascinating to use reversible photo cross-linking strategy to investigate the UV induced morphological switching and its impact on drug encapsulation efficiency of amphiphilic triblock self-assembly. Since cross-linked polymeric micelles are large entities, its clearance from the body by glomerular filtration will be rather difficult. So it will be significant to develop bio degradable, hydrolysable cross-linking agents and fully reversible micelle cross-linking strategies. The synthetic strategies described in this project can be used for nanogel preparation from a thermosensitive cross-linked block copolymer micelle (below its LCST), or for the preparation of pH sensitive micelles, those micelles may find applications in thermosensitive and pH sensitive drug release. The structural potential of triblocks may also be useful in making nanocages from it self-assembly. Core or shell cross-linked diblock core-shell micelles were used for the fabrications of carbon nanospheres. Our newly developed core-shell-corona micelle may provide core and shell cross-linking in the same micelle. Carbon nanospheres prepared from these advanced functional materials may provide more precise control over the size and shape.

Chapter 6

Bibliography

[1] L. Zhang, A. Eisenberg, *Science* **1995**, *268*, 1728.
[2] M. Hillmyer, *Current Opinion in Solid State and Materials Science* **1999**, *4*, 559.
[3] M. Szwarc, *Nature* **1956**, *178*, 1168.
[4] S. Aoshima, S. Kanaoka, *Chemical Reviews* **2009**, *109*, 5245.
[5] G. Odian, *Principles of polymerization*, Wiley, New York,N.Y., **1991**.
[6] T. Otsu, M. Yoshida, T. Tazaki, *Die Makromolekulare Chemie, Rapid Communications* **1982**, *3*, 133.
[7] M. K. Georges, R. P. N. Veregin, P. M. Kazmaier, G. K. Hamer, *Macromolecules* **1993**, *26*, 2987.
[8] C. J. Hawker, *Accounts of Chemical Research* **1997**, *30*, 373.
[9] D. Benoit, V. Chaplinski, R. Braslau, C. J. Hawker, *Journal of the American Chemical Society* **1999**, *121*, 3904.
[10] C. J. Hawker, A. W. Bosman, E. Harth, *Chemical Reviews* **2001**, *101*, 3661.
[11] J. Chiefari, Y. K. Chong, F. Ercole, J. Krstina, J. Jeffery, T. P. T. Le, R. T. A. Mayadunne, G. F. Meijs, C. L. Moad, G. Moad, E. Rizzardo, S. H. Thang, *Macromolecules* **1998**, *31*, 5559.
[12] G. Moad, E. Rizzardo, S. H. Thang, *Polymer* **2008**, *49*, 1079.
[13] M. R. Wood, D. J. Duncalf, S. P. Rannard, S. B. Perrier, *Organic Letters* **2006**, *8*, 553.
[14] M. S. Kharasch, E. V. Jensen, W. H. Urry, *Science* **1945**, *102*, 128.
[15] J.-S. Wang, K. Matyjaszewski, *Journal of the American Chemical Society* **1995**, *117*, 5614.
[16] M. Kato, M. Kamigaito, M. Sawamoto, T. Higashimura, *Macromolecules* **1995**, *28*, 1721.
[17] K. Matyjaszewski, N. V. Tsarevsky, *Nat Chem* **2009**, *1*, 276.
[18] H. Fischer, *Chemical Reviews* **2001**, *101*, 3581.
[19] T. Pintauer, K. Matyjaszewski, *Chemical Society Reviews* **2008**, *37*, 1087.
[20] W. Jakubowski, K. Min, K. Matyjaszewski, *Macromolecules* **2006**, *39*, 39.
[21] L. Mueller, W. Jakubowski, W. Tang, K. Matyjaszewski, *Macromolecules* **2007**, *40*, 6464.
[22] K. Matyjaszewski, S. M. Jo, H.-J. Paik, D. A. Shipp, *Macromolecules* **1999**, *32*, 6431.
[23] S. T. Nguyen, L. K. Johnson, R. H. Grubbs, J. W. Ziller, *Journal of the American Chemical Society* **1992**, *114*, 3974.
[24] K. A. Davis, K. Matyjaszewski, *Macromolecules* **2000**, *33*, 4039.
[25] K. Matyjaszewski, J. Xia, *Chemical Reviews* **2001**, *101*, 2921.
[26] M. Kamigaito, T. Ando, M. Sawamoto, *Chemical Reviews* **2001**, *101*, 3689.
[27] Y. Nakagawa, P. J. Miller, K. Matyjaszewski, *Polymer* **1998**, *39*, 5163.
[28] A. Muhlebach, S. G. Gaynor, K. Matyjaszewski, *Macromolecules* **1998**, *31*, 6046.
[29] X. Zhang, K. Matyjaszewski, *Macromolecules* **1999**, *32*, 1763.
[30] K. Matyjaszewski, D. A. Shipp, G. P. McMurtry, S. G. Gaynor, T. Pakula, *Journal of Polymer Science Part A: Polymer Chemistry* **2000**, *38*, 2023.
[31] Y. Mori, S. Nagaoka, H. Takiuchi, T. Kikuchi, N. Noguchi, H. Tanzawa, Y. Noishiki, *ASAIO Journal* **1982**, *28*, 459&463.
[32] K. Jankova, X. Chen, J. Kops, W. Batsberg, *Macromolecules* **1998**, *31*, 538.
[33] K. Jankova, J. H. Truelsen, X. Chen, J. Kops, W. Batsberg, *Polymer Bulletin* **1999**, *42*, 153.
[34] X. Wang, L. Liu, Y. Luo, H. Zhao, *Langmuir* **2008**, *25*, 744.
[35] Q. Zhao, J. Qian, Q. An, Z. Zhu, P. Zhang, Y. Bai, *Journal of Membrane Science* **2008**, *311*, 284.
[36] K. H. Kim, J. Kim, W. H. Jo, *Polymer* **2005**, *46*, 2836.
[37] K. A. Davis, B. Charleux, K. Matyjaszewski, *Journal of Polymer Science Part A: Polymer Chemistry* **2000**, *38*, 2274.

[38] M.-H. Dufresne, J.-C. Leroux, *Pharmaceutical Research* **2004**, *21*, 160.
[39] B. J. Kim, J. Y. Chang, *Macromolecules* **2005**, *39*, 90.
[40] N. Kossovsky, D. Millett, A. Gelman, E. Sponsler, H. Hnatyszyn, *Biotechnology (N Y)* **1993**, *11*, 1534.
[41] G. M. Whitesides, B. Grzybowski, *Science* **2002**, *295*, 2418.
[42] J. H. van Esch, *Nature* **2010**, *466*, 193.
[43] C. Tanford, *Journal of Molecular Biology* **1972**, *67*, 59.
[44] F. Evans, H. Wennerstrom, *The colloidal domain / Where physics, chemistry, biology and technology meet*, Wiley, New York,NY, **1999**.
[45] J. C. Brackman, J. B. F. N. Engberts, *Chemical Society Reviews* **1993**, *22*, 85.
[46] J. N. Israelachvili, D. J. Mitchell, B. W. Ninham, *Journal of the Chemical Society, Faraday Transactions 2: Molecular and Chemical Physics* **1976**, *72*, 1525.
[47] D. M. Vriezema, M. Comellas Aragones, J. A. A. W. Elemans, J. J. L. M. Cornelissen, A. E. Rowan, R. J. M. Nolte, *Chemical Reviews* **2005**, *105*, 1445.
[48] K. L. Wooley, *Journal of Polymer Science Part a-Polymer Chemistry* **2000**, *38*, 1397.
[49] S. E. Webber, *The Journal of Physical Chemistry B* **1998**, *102*, 2618.
[50] P. Alexandridis, B. Lindman, *Amphiphilic block copolymers : self-assembly and applications*, Elsevier, Amsterdam, Oxford, **2000**.
[51] V. P. Torchilin, *Cellular and Molecular Life Sciences* **2004**, *61*, 2549.
[52] R. Haag, F. Kratz, *Angewandte Chemie International Edition* **2006**, *45*, 1198.
[53] M. E. Davis, Z. Chen, D. M. Shin, *Nat Rev Drug Discov* **2008**, *7*, 771.
[54] C. Oerlemans, W. Bult, M. Bos, G. Storm, J. Nijsen, W. Hennink, *Pharmaceutical Research* **2010**, *27*, 2569.
[55] U. Breiner, U. Krappe, T. Jakob, V. Abetz, R. Stadler, *Polymer Bulletin* **1998**, *40*, 219.
[56] U. Breiner, U. Krappe, V. Abetz, R. Stadler, *Macromolecular Chemistry and Physics* **1997**, *198*, 1051.
[57] G.-E. Yu, A. Eisenberg, *Macromolecules* **1998**, *31*, 5546.
[58] J. Kriz, B. Masar, J. Plestil, Z. Tuzar, H. Pospisil, D. Doskocilova, *Macromolecules* **1998**, *31*, 41.
[59] R. Erhardt, A. Boker, H. Zettl, H. K. Kaya, W. Pyckhout-Hintzen, G. Krausch, V. Abetz, A. H. E. Muller, *Macromolecules* **2001**, *34*, 1069.
[60] M. Yokoyama, *Critical Reviews in Therapeutic Drug Carrier Systems* **1992**, *9*, 213.
[61] F. M. Winnik, A. R. Davidson, G. K. Hamer, H. Kitano, *Macromolecules* **1992**, *25*, 1876.
[62] Z. Gao, A. Eisenberg, *Macromolecules* **1993**, *26*, 7353.
[63] H. Huang, E. E. Remsen, T. Kowalewski, K. L. Wooley, *Journal of the American Chemical Society* **1999**, *121*, 3805.
[64] Q. Zhang, E. E. Remsen, K. L. Wooley, *Journal of the American Chemical Society* **2000**, *122*, 3642.
[65] J. L. Turner, K. L. Wooley, *Nano Letters* **2004**, *4*, 683.
[66] S. Sugihara, S. P. Armes, A. L. Lewis, *Angewandte Chemie International Edition* **2010**, *49*, 3500.
[67] I. Astafieva, X. F. Zhong, A. Eisenberg, *Macromolecules* **1993**, *26*, 7339.
[68] K. Prochazka, M. K. Baloch, Z. Tuzar, *Makromolekulare Chemie-Macromolecular Chemistry and Physics* **1979**, *180*, 2521.
[69] K. B. Thurmond, T. Kowalewski, K. L. Wooley, *Journal of the American Chemical Society* **1996**, *118*, 7239.
[70] H. Huang, T. Kowalewski, E. E. Remsen, R. Gertzmann, K. L. Wooley, *Journal of the American Chemical Society* **1997**, *119*, 11653.
[71] M. J. Joralemon, R. K. O'Reilly, C. J. Hawker, K. L. Wooley, *Journal of the American Chemical Society* **2005**, *127*, 16892.
[72] V. Butun, X. S. Wang, M. V. de Paz Banez, K. L. Robinson, N. C. Billingham, S. P. Armes, Z. Tuzar, *Macromolecules* **1999**, *33*, 1.
[73] Y. Li, B. S. Lokitz, S. P. Armes, C. L. McCormick, *Macromolecules* **2006**, *39*, 2726.
[74] J. Jiang, B. Qi, M. Lepage, Y. Zhao, *Macromolecules* **2007**, *40*, 790.

[75] K. Yasugi, T. Nakamura, Y. Nagasaki, M. Kato, K. Kataoka, *Macromolecules* **1999**, *32*, 8024.
[76] M. J. Joralemon, K. S. Murthy, E. E. Remsen, M. L. Becker, K. L. Wooley, *Biomacromolecules* **2004**, *5*, 903.
[77] K. Qi, Q. Ma, E. E. Remsen, C. G. Clark, K. L. Wooley, *Journal of the American Chemical Society* **2004**, *126*, 6599.
[78] M. J. Joralemon, N. L. Smith, D. Holowka, B. Baird, K. L. Wooley, *Bioconjugate Chemistry* **2005**, *16*, 1246.
[79] A. L. Martin, B. Li, E. R. Gillies, *Journal of the American Chemical Society* **2008**, *131*, 734.
[80] H. C. Kolb, M. G. Finn, K. B. Sharpless, *Angewandte Chemie International Edition* **2001**, *40*, 2004.
[81] C. W. Tornoe, C. Christensen, M. Meldal, *The Journal of Organic Chemistry* **2002**, *67*, 3057.
[82] V. V. Rostovtsev, L. G. Green, V. V. Fokin, K. B. Sharpless, *Angewandte Chemie-International Edition* **2002**, *41*, 2596.
[83] J. A. Prescher, C. R. Bertozzi, *Nat Chem Biol* **2005**, *1*, 13.
[84] P. Scheiner, J. H. Schomaker, S. Deming, W. J. Libbey, G. P. Nowack, *Journal of the American Chemical Society* **1965**, *87*, 306.
[85] Z. P. Demko, K. B. Sharpless, *The Journal of Organic Chemistry* **2001**, *66*, 7945.
[86] Z. Li, T. S. Seo, J. Ju, *Tetrahedron Letters* **2004**, *45*, 3143.
[87] N. J. Agard, J. A. Prescher, C. R. Bertozzi, *Journal of the American Chemical Society* **2004**, *126*, 15046.
[88] J. Liu, Q. Zhang, E. E. Remsen, K. L. Wooley, *Biomacromolecules* **2001**, *2*, 362.
[89] D. Pan, J. L. Turner, K. L. Wooley, *Chemical Communications* **2003**, *19*, 2400.
[90] R. Rossin, D. Pan, K. Qi, J. L. Turner, X. Sun, K. L. Wooley, M. J. Welch, *Journal of Nuclear Medicine* **2005**, *46*, 1210.
[91] J. L. Turner, M. L. Becker, X. Li, J.-S. A. Taylor, K. L. Wooley, *Soft Matter* **2005**, *1*, 69.
[92] R. K. O'Reilly, M. J. Joralemon, K. L. Wooley, C. J. Hawker, *Chemistry of Materials* **2005**, *17*, 5976.
[93] R. K. O'Reilly, M. J. Joralemon, C. J. Hawker, K. L. Wooley, *Chemistry – A European Journal* **2006**, *12*, 6776.
[94] C. J. Hawker, R. K. O'Reilly, M. J. Joralemon, K. L. Wooley, *New Journal of Chemistry* **2007**, *31*, 718.
[95] D. L. Taylor, A. S. Waggoner, F. Lanni, R. F. Murphy, R. R. Birge, *Applications of fluorescence in the biomedical sciences*, **1986**.
[96] D. Pinkel, *Analytical Chemistry* **1982**, *54*, 503A.
[97] R. V. Benjaminsen, H. Sun, J. R. Henriksen, N. M. Christensen, K. Almdal, T. L. Andresen, *ACS Nano* **2011**, *5*, 5864.
[98] O. Salata, *Journal of Nanobiotechnology* **2004**, *2*, 3.
[99] J. Han, K. Burgess, *Chemical Reviews* **2009**, *110*, 2709.
[100] V. Ntziachristos, C. Bremer, R. Weissleder, *European Radiology* **2003**, *13*, 195.
[101] K. Sasaki, Z. Y. Shi, R. Kopelman, H. Masuhara, *Chemistry Letters* **1996**, *25*, 141.
[102] H. A. Clark, S. L. R. Barker, M. Brasuel, M. T. Miller, E. Monson, S. Parus, Z.-Y. Shi, A. Song, B. Thorsrud, R. Kopelman, A. Ade, W. Meixner, B. Athey, M. Hoyer, D. Hill, R. Lightle, M. A. Philbert, *Sensors and Actuators B: Chemical* **1998**, *51*, 12.
[103] W. Tan, Z. Shi, S. Smith, D. Birnbaum, R. Kopelman, *Science* **1992**, *258*, 778.
[104] S. W. Ashley, D. I. Soybel, C. D. Moore, L. Y. Cheung, *Surgery* **1987**, *102*, 371.
[105] S. W. Ashley, D. I. Soybel, L. Y. Cheung, *American Journal of Physiology* **1986**, *250*, G625.
[106] J. Ji, N. Rosenzweig, C. Griffin, Z. Rosenzweig, *Analytical Chemistry* **2000**, *72*, 3497.
[107] K. P. McNamara, N. Rosenzweig, Z. Rosenzweig, *Microchimica Acta* **1999**, *131*, 57.
[108] K. P. McNamara, T. Nguyen, G. Dumitrascu, J. Ji, N. Rosenzweig, Z. Rosenzweig, *Analytical Chemistry* **2001**, *73*, 3240.
[109] K. Almdal, H. Sun, A. K. Poulsen, L. Arleth, I. Jakobsen, H. Gu, A. M. Scharff-Poulsen, *Polymers for Advanced Technologies* **2006**, *17*, 790.

[110] H. Sun, A. M. Scharff-Poulsen, H. Gu, K. Almdal, *Chemistry of Materials* **2006**, *18*, 3381.
[111] H. Sun, T. L. Andresen, R. V. Benjaminsen, K. Almdal, *Journal of Biomedical Nanotechnology* **2009**, *5*, 676.
[112] H. Sun, K. Almdal, T. L. Andresen, *Chemical Communications* **2011**, *47*, 5268.
[113] V. M. Chauhan, G. R. Burnett, J. W. Aylott, *Analyst* **2011**, *136*, 1799.
[114] A. Schulz, S. Hornig, T. Liebert, E. Birckner, T. Heinze, G. J. Mohr, *Organic & Biomolecular Chemistry* **2009**, *7*, 1884.
[115] L. F. Zhang, A. Eisenberg, *Science* **1995**, *268*, 1728.
[116] A. L. Klibanov, K. Maruyama, V. P. Torchilin, L. Huang, *Febs Letters* **1990**, *268*, 235.
[117] T. N. Palmer, V. J. Caride, M. A. Caldecourt, J. Twickler, V. Abdullah, *Biochim Biophys Acta* **1984**, *797*, 363.
[118] H. Maeda, J. Wu, T. Sawa, Y. Matsumura, K. Hori, *Journal of Controlled Release* **2000**, *65*, 271.
[119] V. P. Torchilin, *Journal of Liposome Research* **1996**, *6*, 99.
[120] R. Gref, A. Domb, P. Quellec, T. Blunk, R. H. Muller, J. M. Verbavatz, R. Langer, *Advanced Drug Delivery Reviews* **1995**, *16*, 215.
[121] S. A. Hagan, A. G. A. Coombes, M. C. Garnett, S. E. Dunn, M. C. Davies, L. Illum, S. S. Davis, S. E. Harding, S. Purkiss, P. R. Gellert, *Langmuir* **1996**, *12*, 2153.
[122] V. Sciannamea, R. Jerome, C. Detrembleur, *Chemical Reviews* **2008**, *108*, 1104.
[123] C. Boyer, V. Bulmus, T. P. Davis, V. Ladmiral, J. Liu, S. B. Perrier, *Chemical Reviews* **2009**, *109*, 5402.
[124] X. Jiang, S. Luo, S. P. Armes, W. Shi, S. Liu, *Macromolecules* **2006**, *39*, 5987.
[125] J. Kim, J. Youk, *Macromolecular Research* **2009**, *17*, 926.
[126] X. Xu, J. D. Flores, C. L. McCormick, *Macromolecules* **2011**, *44*, 1327.
[127] X. Xu, A. E. Smith, C. L. McCormick, *Australian Journal of Chemistry* **2009**, *62*, 1520.
[128] Y. Li, B. S. Lokitz, C. L. McCormick, *Macromolecules* **2005**, *39*, 81.
[129] S. Liu, S. P. Armes, *Journal of the American Chemical Society* **2001**, *123*, 9910.
[130] M. V. de Paz Banez, K. L. Robinson, V. Butun, S. P. Armes, *Polymer* **2001**, *42*, 29.
[131] G. Jiang, *Journal of Applied Polymer Science* **2009**, *114*, 3472.
[132] D.-Z. Liu, J.-H. Hsieh, X.-C. Fan, J.-D. Yang, T.-W. Chung, *Carbohydrate Polymers* **2007**, *68*, 544.
[133] S. Liu, Y. Ma, S. P. Armes, C. Perruchot, J. F. Watts, *Langmuir* **2002**, *18*, 7780.
[134] J. V. M. Weaver, Y. Tang, S. Liu, P. D. Iddon, R. Grigg, N. C. Billingham, S. P. Armes, R. Hunter, S. P. Rannard, *Angewandte Chemie International Edition* **2004**, *43*, 1389.
[135] X. Jiang, G. Zhang, R. Narain, S. Liu, *Langmuir* **2009**, *25*, 2046.
[136] B. S. Sumerlin, A. B. Lowe, D. B. Thomas, A. J. Convertine, M. S. Donovan, C. L. McCormick, *Journal of Polymer Science Part A: Polymer Chemistry* **2004**, *42*, 1724.
[137] F. Henselwood, G. Liu, *Macromolecules* **1997**, *30*, 488.
[138] A. Asokan, M. J. Cho, *Journal of Pharmaceutical Sciences* **2002**, *91*, 903.
[139] H. A. Clark, R. Kopelman, R. Tjalkens, M. A. Philbert, *Analytical Chemistry* **1999**, *71*, 4837.
[140] J. Lu, Z. Rosenzweig, *Fresenius' Journal of Analytical Chemistry* **2000**, *366*, 569.
[141] J. Peng, X. He, K. Wang, W. Tan, Y. Wang, Y. Liu, *Analytical and Bioanalytical Chemistry* **2007**, *388*, 645.
[142] E. Allard, C. Larpent, *Journal of Polymer Science Part A: Polymer Chemistry* **2008**, *46*, 6206.
[143] S. M. Moghimi, A. C. Hunter, J. C. Murray, *Pharmacological Reviews* **2001**, *53*, 283.
[144] V.P Torchilin, *Journal of Controlled Release* **2001**, *73*, 137.
[145] L. Zhang, K. Yu, A. Eisenberg, *Science* **1996**, *272*, 1777.
[146] A. A. Gabizon, *Advanced Drug Delivery Reviews* **1995**, *16*, 285.
[147] N. Nasongkla, X. Shuai, H. Ai, B. D. Weinberg, J. Pink, D. A. Boothman, J. Gao, *Angewandte Chemie International Edition* **2004**, *116*, 6483.
[148] M. Oishi, Y. Nagasaki, K. Itaka, N. Nishiyama, K. Kataoka, *Journal of the American Chemical Society* **2005**, *127*, 1624.
[149] X.-B. Xiong, A. Mahmud, H. Uludacs, A. Lavasanifar, *Biomacromolecules* **2007**, *8*, 874.

[150] H. S. Yoo, T. G. Park, *Journal of Controlled Release* **2004**, *96*, 273.
[151] G. Sun, H. Cui, L. Y. Lin, N. S. Lee, C. Yang, W. L. Neumann, J. N. Freskos, J. J. Shieh, R. B. Dorshow, K. L. Wooley, *Journal of the American Chemical Society* **2011**, *133*, 8534.
[152] R. K. O'Reilly, C. J. Hawker, K. L. Wooley, *Chemical Society Reviews* **2006**, *35*, 1068.
[153] E. S. Read, S. P. Armes, *Chemical Communications* **2007**, *29*, 3021.
[154] H. Fan, E. W. Leve, C. Scullin, J. Gabaldon, D. Tallant, S. Bunge, T. Boyle, M. C. Wilson, C. J. Brinker, *Nano Letters* **2005**, *5*, 645.
[155] D. Maysinger, O. Berezovska, R. Savic, P. L. Soo, A. Eisenberg, *Biochimica et Biophysica Acta (BBA) - Molecular Cell Research* **2001**, *1539*, 205.
[156] L. Luo, J. Tam, D. Maysinger, A. Eisenberg, *Bioconjugate Chemistry* **2002**, *13*, 1259.
[157] R. Savic, L. Luo, A. Eisenberg, D. Maysinger, *Science* **2003**, *300*, 615.
[158] S. Liu, J. V. M. Weaver, Y. Tang, N. C. Billingham, S. P. Armes, K. Tribe, *Macromolecules* **2002**, *35*, 6121.
[159] E. Kaiser, R. L. Colescott, C. D. Bossinger, P. I. Cook, *Analytical biochemistry* **1970**, *34*, 595.
[160] L. Stryer, R. P. Haugland, *Proceedings of the National Academy of Sciences of the United States of America* **1967**, *58*, 719.
[161] R. F. Chen, J. R. Knutson, *Analytical biochemistry* **1988**, *172*, 61.
[162] V. Andrisano, M. Bartolini, C. Bertucci, V. Cavrini, B. Luppi, T. Cerchiara, *Journal of Pharmaceutical and Biomedical Analysis* **2003**, *32*, 983.
[163] D. H. Napper, *Journal of Colloid and Interface Science* **1977**, *58*, 390.
[164] C. J. Hawker, K. L. Wooley, *Science* **2005**, *309*, 1200.
[165] M. Meldal, *Macromolecular Rapid Communications* **2008**, *29*, 1016.
[166] R. Fu, G.-D. Fu, *Polymer Chemistry* **2011**, *2*, 465.
[167] J. N. Israelachvili, S. Marcelja, R. G. Horn, *Quarterly Reviews of Biophysics* **1980**, *13*, 121.
[168] D. W. P. M. Lowik, J. C. M. van Hest, *Chemical Society Reviews* **2004**, *33*, 234.
[169] J. H. Fuhrhop, J. Koning, C. Royal Society of, Rsc, *Membranes and molecular assemblies / The synkinetic approach*, Cambridge, **1994**.
[170] W. T. S. Huck, K. Velonia, J. J. L. M. Cornelissen, M. C. Feiters, A. E. Rowan, R. J. M. Nolte, *Nanoscale Assembly* (Ed.: D. J. Lockwood), Springer US, **2005**, pp. 119.
[171] S. Liu, S. P. Armes, *Current Opinion in Colloid & Interface Science* **2001**, *6*, 249.
[172] R. S. Tu, M. Tirrell, *Advanced Drug Delivery Reviews* **2004**, *56*, 1537.
[173] R. K. O'Reilly, M. J. Joralemon, C. J. Hawker, K. L. Wooley, *New Journal of Chemistry* **2007**, *31*, 718.
[174] M. L. Adams, A. Lavasanifar, G. S. Kwon, *Journal of Pharmaceutical Sciences* **2003**, *92*, 1343.
[175] V. P. Torchilin, V. S. Trubetskoy, *Advanced Drug Delivery Reviews* **1995**, *16*, 141.
[176] J. Srivastava, D. L. Barber, M. P. Jacobson, *Physiology* **2007**, *22*, 30.
[177] T. L. Andresen, S. S. Jensen, K. Jørgensen, *Progress in Lipid Research* **2005**, *44*, 68.
[178] R. Gujadhur, D. Venkataraman, *Synthetic Communications* **2001**, *31*, 2865.
[179] M. J. Joralemon, R. K. O'Reilly, J. B. Matson, A. K. Nugent, C. J. Hawker, K. L. Wooley, *Macromolecules* **2005**, *38*, 5436.
[180] S. Takahashi, Y. Kuroyama, K. Sonogashira, N. Hagihara, *Synthesis-Stuttgart* **1980**, pp. 627.
[181] J. S. Kim, J. H. Youk, *Polymer* **2009**, *50*, 2204.
[182] D. J. Wilson, G. Riess, *European Polymer Journal* **1988**, *24*, 617.
[183] S. PiogeÌ , A. Nesterenko, G. Brotons, S. Pascual, L. Fontaine, C. D. Gaillard, E. Nicol, *Macromolecules* **2011**, *44*, 594.
[184] H.-I. Lee, W. Wu, J. K. Oh, L. Mueller, G. Sherwood, L. Peteanu, T. Kowalewski, K. Matyjaszewski, *Angewandte Chemie International Edition* **2007**, *46*, 2453.
[185] N. K. Mal, M. Fujiwara, Y. Tanaka, *Nature* **2003**, *421*, 350.
[186] J. S. Kim, H. J. Jeon, M. S. Park, Y. C. You, J. H. Youk, *European Polymer Journal* **2009**, *45*, 1918.
[187] M. Jamroz-Piegza, W. Walach, A. Dworak, B. Trzebicka, *Journal of Colloid and Interface Science* **2008**, *325*, 141.

[188] S.-I. Yusa, M. Sugahara, T. Endo, Y. Morishima, *Langmuir* **2009**, *25*, 5258.
[189] D. Shi, M. Matsusaki, M. Akashi, *Bioconjugate Chemistry* **2009**, *20*, 1917.
[190] K. Saito, L. R. Ingalls, J. Lee, J. C. Warner, *Chemical Communications* **2007**, *24*, 2503.
[191] J. He, X. Tong, Y. Zhao, *Macromolecules* **2009**, *42*, 4845.
[192] M. Lepage, L. Tremblay, J. Jiang, J. Babin, B. Qi, Y. Zhao, *Physics in Medicine and Biology* **2007**, *52*, 1923
[193] J. Jiang, Q. Shu, X. Chen, Y. Yang, C. Yi, X. Song, X. Liu, M. Chen, *Langmuir* **2010**, *26*, 14247.
[194] Y. Zhao, J. Bertrand, X. Tong, Y. Zhao, *Langmuir* **2009**, *25*, 13151.
[195] J. Kriz, B. Masar, J. Plestil, Z. Tuzar, H. Pospisil, D. Doskocilova, *Macromolecules* **1998**, *31*, 41.
[196] C. F. van Nostrum, *Soft Matter* **2011**, *7*, 3246.
[197] J. S. Kim, H. J. Jeon, J. J. Park, M. S. Park, J. H. Youk, *Journal of Polymer Science Part a-Polymer Chemistry* **2009**, *47*, 4963.
[198] M. Wilhelm, C. L. Zhao, Y. Wang, R. Xu, M. A. Winnik, J. L. Mura, G. Riess, M. D. Croucher, *Macromolecules* **1991**, *24*, 1033.
[199] Y.-C. Wang, Y. Li, T.-M. Sun, M.-H. Xiong, J. Wu, Y.-Y. Yang, J. Wang, *Macromolecular Rapid Communications* **2010**, *31*, 1201.
[200] X. Hu, X. Chen, J. Wei, S. Liu, X. Jing, *Macromolecular Bioscience* **2009**, *9*, 456.
[201] M. Hiroshi, *Advances in Enzyme Regulation* **2001**, *41*, 189.
[202] D. D. Lasic, *Nature* **1996**, *380*, 561.
[203] L. Lei, J.-F. Gohy, N. Willet, J.-X. Zhang, S. Varshney, R. Jerome, *Macromolecules* **2004**, *37*, 1089.
[204] S. R. Trenor, A. R. Shultz, B. J. Love, T. E. Long, *Chemical Reviews* **2004**, *104*, 3059.
[205] M. Obi, S. Y. Morino, K. Ichimura, *Chemistry of Materials* **1999**, *11*, 656.
[206] J. Llopis, J. M. McCaffery, A. Miyawaki, M. G. Farquhar, R. Y. Tsien, *Proceedings of the National Academy of Sciences* **1998**, *95*, 6803.
[207] S. E. Webber, P. Munk, Z. Tuzar, N. S. A. Division, *Solvents and self-organization of polymers / Proceedings of the NATO Advanced Study Institute, Antalya 1995*, Kluwer, Dordrecht, **1996**.
[208] T. Rager, W. H. Meyer, G. Wegner, *Macromolecular Chemistry and Physics* **1999**, *200*, 1672.
[209] K. Schilen, A. Yekta, S. Ni, M. A. Winnik, *Macromolecules* **1998**, *31*, 210.
[210] W. A. Braunecker, K. Matyjaszewski, *Progress in Polymer Science* **2007**, *32*, 93.
[211] P. Matejicek, J. Humpolickova, K. Prochazka, Z. Tuzar, M. Spirkova, M. Hof, S. E. Webber, *The Journal of Physical Chemistry B* **2003**, *107*, 8232.
[212] O. Terreau, L. Luo, A. Eisenberg, *Langmuir* **2003**, *19*, 5601.
[213] J.-F. Gohy, V. Abetz*, Vol. 190*, Springer Berlin / Heidelberg, **2005**, pp. 65.
[214] E. F. V. Scriven, K. Turnbull, *Chemical Reviews* **1988**, *88*, 297.
[215] M. Mikolajczyk, P. Kielbasinski, *Tetrahedron* **1981**, *37*, 233.
[216] P. A. S. Smith, *Organic Reactions* **1946**, *3*, 337.
[217] M. Ui, *Biochimica et Biophysica Acta (BBA) - General Subjects* **1966**, *124*, 310.
[218] W. Moody, *Annual Review of Neuroscience* **1984**, *7*, 257.
[219] R. J. Gillies, D. W. Deamer, *Journal of Cellular Physiology* **1979**, *100*, 23.
[220] C. Y. Wang, L. Huang, *Biochemistry* **1989**, *28*, 9508.
[221] V. Torchilin, *European Journal of Pharmaceutics and Biopharmaceutics* **2009**, *71*, 431.
[222] M. D. Pierschbacher, E. Ruoslahti, *Nature* **1984**, *309*, 30.
[223] P. Brooks, R. Clark, D. Cheresh, *Science* **1994**, *264*, 569.

Appendices

Appendix A

Pramod Kumar EK, Nynne M. Christensen, Rikke Vicki Benjaminsen, Jonas Rosager Henriksen**,** Kristoffer Almdal, Thomas L. Andresen. ‘‘Intermediary Layer Cross-linked Core-Shell-Corona Micelle based Ratiometric Nanosensors for Intracellular pH Measurements in HeLa Cells’’. *ACS Nano* **2012** (Submitted), supporting information.

Intermediary Layer Cross-linked Core-Shell-Corona Micelle based Ratiometric Nanosensors for Intracellular pH Measurements in HeLa Cells

*Pramod Kumar EK, Nynne M. Christensen, Rikke Vicki Benjaminsen, Jonas Rosager Henriksen, Kristoffer Almdal, Thomas L. Andresen**

DTU Nanotech, Department of Micro-and Nanotechnology, Technical University of Denmark

AUTHOR EMAIL ADDRESS: thomas.andresen@nanotech.dtu.dk.

RECEIVED DATE (to be automatically inserted after your manuscript is accepted if required according to the journal that you are submitting your paper to)

*Dr. T.L.Andresen
DTU Nanotech, Department of Micro-and Nanotechnology
Technical University of Denmark, Building 423
2800 Lyngby, Denmark.

Amphiphilic triblock copolymer poly (ethylene glycol)-*b*-poly(2-[N-(*tert*-Butoxycarbonyl)Amino]ethyl methacrylate)-*b*-poly(styrene) (PEG-*b*-PAEMA(Boc)-*b*-PS) is synthesized by isolated macrointiator atom transfer radical polymerization. De-protection of *tert*-Butyloxycarbonyl (Boc) group followed by self-assembly in water gives PEG-b-PAEMA-b-PS core-shell-corona micelle. PAEMA shell of the micelle is cross-linked by amidation reaction using 3, 6, 9-trioxaundecandioic acid cross-linker. The shell cross-linked micelle is triply labelled with pH sensitive and reference fluorophores, and the resulting pH nanosensor is used for constructing *in vitro* pH calibration curve. The calibration curve shows broad pH sensitivity range of the pH nanosensor in aqueous buffer solutions. Uptake experiments of the nanosensor by HeLa cells show that the sensor is capable of monitoring the pH distributions in cellular compartments of the HeLa cells.

KEYWORDS: amphiphilic triblock copolymers, intermediary layer cross-linked micelle, core-shell-corona micelle, pH nanosensor, ratiometric pH measurements, intracellular pH.

INTRODUCTION

Intracellular pH measurements give information about the pH gradients maintained by the intracellular organelles (which varies from 4 to 8 among varies organelles). Exploitation of this intracellular pH gradient[1] allows the developments of pH sensitive drug release or drug/drug carrier partitions in the desired cellular compartments. There are a number of nanosensors developed for pH measurement[2-11] but in order to have effective intracellular pH monitoring the sensors have to overcome effective sequestration from the blood by macrophages of the mononuclear phagocyte system (MPS)[12] located in the liver and spleen. This MPS system prevents long-circulation and efficient accumulation of above mentioned particle sensors in relevant cells. Even though the well-known pharmaceutical carrier, polymeric micelles can overcome the sequestration by macrophages,[13] polymeric micelles in nanosensor fabrications has not been investigated yet. Difficulties in synthesizing well defined functional unimers and the instability of their self-assembly under infinitely diluted biological conditions are the two main reasons for excluding polymeric micelles from nanosensor fabrications.

Controlled radical polymerization, especially the redox-active transition metal complex catalyzed atom transfer radical polymerization (ATRP)[14] can nowadays fulfill the well defined polymer pre-requests for designing advanced functional materials with precise control over the composition and the molecular architecture. Nanoscale phase separations of amphiphilic block copolymers having definite hydrophilic to hydrophobic blocks mass ratios in block selective solvents gives verities of morphologies such as l micelles, lamellae, tube, rode *etc*.[15, 16] In biology, the micellar morphology provides a set of unbeatable advantages over the other morphologies. They have a long circulating half life in the blood, which provide its gradual accumulation in the required area via enhanced permeability and retention effect (EPR),[17-19] the surface functionalization chemistry is easy and hence provide a platform for efficient biological targeting. In recent years, block copolymer micelles have attracted increasing research

attention due to its numerous biological applications such as imaging labelling, sensing and drug delivery.[20-25] Often these diverse spectrums of applications require robust and stabilized structures, which can be achieved *via* covalent cross-linking between the functional unimers of these nanoparticle scaffolds.[26, 27] Fluorescent labelled micelles for sensing applications are divided into two main classes. Fluorescent dyes or quantum dot encapsulated micelles[28, 29] and micelles with chemically conjugated fluorescent dyes.[30, 31] The chemical conjugation can overcome problems like cytotoxicity and leakage into cellular environments.

RESULTS AND DISCUSSION

Synthesis and characterization of shell cross-linked micelle nanosensor (SCMN). Fabrication of a ratiometric nanosensor for intracellular pH measurement is schematically represented in Figure 1. The sensor is based on an intermediary layer cross-linked polymeric micelle and can be synthesized as follows. The amphiphilic triblock copolymer, poly (ethylene glycol)$_{127}$-*b*-poly(2-[N-(tert-Butoxycarbonyl)Amino]ethyl methacrylate)$_{12}$-*b*-poly(styrene)$_{28}$ (PEG$_{127}$-*b*-PAEMA(Boc)$_{12}$-*b*-PS$_{28}$) (**1**) was synthesized by isolated macroinitiator atom transfer radical polymerization (Scheme 1). The triblock copolymer was characterized by NMR and IR spectroscopy. From ^{1}H NMR data, the number-average degree of polymerization (DP_n); and from GPC analysis, polydispersity index (Mw/Mn) of the amphiphilic triblock copolymers was calculated. The results are summarized in Table 1. The Boc groups from PEG-*b*-PAEMA(Boc)-*b*-PS were de-protected by TFA in DCM, and the complete de-protection was confirmed by the disappearance of Boc group signal at δ 1.4 ppm (s, -C(C**H**$_3$)$_3$) ^{1}H-NMR (250 MHz in ^{6}d DMSO).

Stepwise synthesis of shell cross-linked micelle nanosensor (SCMN) is given in Scheme 2. First, the nanoscale phase separation of PEG-*b*-PAEMA-*b*-PS (**2**) in water was achieved by dissolving the triblock copolymer in DMF and the common solvent for the triblock was then slowly removed by dialysis against selective solvent for the hydrophilic blocks (water). Stabilization of the resulting

entropy driving self-assembly, PEG-*b*-PAEMA-*b*-PS micelle (**3**), was achieved by covalent cross-linking between the unimers through amidation reactions. Water soluble 3,6,9-trioxaundecandioic acid was used as a cross-linking agent. The diacid cross-linker was first converted into o-Acylisourea by treatment with 1-[3-(dimethylamino)propyl]-3-ethylcarbodiimide methiodide (EDC.MeI). This active ester was then reacted with the free amino groups present at the intermediate layer (PAEMA shell) of the polymer micelle. Stoichiometrically 60 % of the amino groups were used for the cross-linking reactions. The cross-linked micelles were first dialyzed against MilliQ water to remove the urea by-products and then against carbonate buffer of pH 9.6. The cross-linked micelle, **4** in basic buffer was converted into ratiometric pH nanosensor, **5** by treatment with suitable ratios of pH sensitive Fluoresceine isothiocyanate (FITC), and Oregon Green isothiocyanate (F_2FITC); and pH insensitive reference fluorophore-Rhodamine B isothiocyanate (RhBITC). Some of the free amino groups present at the intermediate layer of the cross-linked micelle were nucleophilically attacked on the central elctrophilic carbon atoms of the pH sensitive and reference isothiocyanates. The un-reacted free dyes from the isothiourea product were removed by dialysis against carbonate buffer, followed by dialysis against MilliQ water, gave the pH nanosensor dispersion in MilliQ water. The concentration of fluorophores on the sensor was adjusted to get maximum fluorescence intensities with minimum distance dependent excited state interactions (Förster resonance energy transfer, FRET)[32] between the pH sensitive and reference fluorophores and to have minimum self quenching.[33] The amount of dye attached can be quantified from first derivative UV-Visible measurements as reported.[34]

The morphology and homogeneity of the micelles was investigated by atomic force microscopy (AFM) under ambient conditions (Figure 2). The figure indicates the shape of the particles is homogeneous and shows round flat particles with a round shape. The spherical morphology can be seen very clearly in the phase image (Figure 2b), which depicts the phase shift of the cantilever oscillation and visualizes differences in material properties of the sample. AFM image also confirms exclusive intramicellar shell cross-linking in the sensor and absence of intermicellar cross-linking or aggregation.

Characterizations of the shell cross-linked core-shell-corona micelles by ^{1}H NMR was not possible; in D_2O the hydrophobic core of the lyophilized micelle was invisible, and the particles were completely invisible in ^{6}d-DMSO. IR spectra of the lyophilized micelle after cross-linking shows additional overlapped amide I and II bands appear at *ca.* 1640-1550 cm^{-1}. This confirms the amide bond formation at the shell region of the micelle (Figure S3 supporting information).

The inner shell stabilization did not affect the outer coronal mobility considerably. Hence was not entropically impaired the stabilizing capability of the hydrophilic micelle domains. As a result, the exclusive intramicellar cross-linking occurred. The intramicellar cross-linking was confirmed by dynamic light scattering (DLS) and zeta potential (ξ) measurements. DLS and ξ-potential measurement showed decreases in hydrodynamic diameter (D_h) and ξ-potential after micelle cross-linking. DLS and ξ measurements ensured that the cross-linking made more robust nanostructure with a decrease in surface charge density. The decrease in charge density also confirmed the participation of amino groups of the shell domain in amidation cross-linking. The concentration of fluorophores in the nanosensor was extremely small, so that the binding of fluorophores to the cross-linked micelle did not show any significant change in hydrodynamic diameter and ξ-potential (Table.2).

The critical micelle concentrations (CMC) of the micelles are especially valuable when it is designed for biological applications. In infinitely diluted biological conditions, below its CMC values, the nanosensors can be dissociated into unimers. The micelle stabilization by covalent cross-linking throughout a domain can provide reinforcement to the weak hydrophobic interactions and hence prevent its dissociation below CMC. The sensitivity towards the microenvironment polarity of the hydrophobic probe pyrene was used to measure the CMC value of the micelles before and after cross-linking. A blue shift of the (0,0) absorption band from 340 nm to 334 with a decrease in peak intensity ratio I_{340} / I_{334}

(Figure 3a) indicated that the pyrene was moving from nonpolar to polar environment. Comparing the decrease in intensity ratio I_{340} / I_{334} of the micelles before and after cross-linking showed that, before cross-linking the decay was faster than after cross-linking. This demonstrates the presence of a hydrophobic environment in cross-linked micelle even below the CMC of the non cross-linked micelle (10 mgL^{-1}) (Figure 3b).

The pH sensitive Oregon Green (OG), Fluorescein (FA) and insensitive reference dye-Rhodamine B (RhB) presented at the shell region of the shell cross-linked micelle dispersion in aqueous buffer of different pH, was excited at (λex) 488 nm 543 nm respectively (Figure 4a). Fluorescence intensity ratios (I_{OG} + I_{FA}) / I_{RhB} were plotted against the pH corresponding to the fluorescence intensities to get the pH calibration curve. The pH calibration curve confirmed the covalent conjugation of pH sensitive and reference fluorophore at the shell region of the shell cross-linked micelle. The calibration curves (Figure 4b) show that the sensor is sensitive between the pH *ca.* 4 to 7.5. Time for response and reversibility of the pH nanosensor was also tested (Figure 5a and 5b). This shows the nanosensors are quickly responding (with in micro seconds) towards the change in pH and are reversible between any two pH within the pH range 4 to 7.5.

The sensors can be easily tuned by changing the fluorophores, which can reconfigure its Π electron system during protonation. Binding of pH sensitive Fluorescein along with Rhodamine B to the cross-linked micelles can give ratiometric nanosensors for the pH range *ca.* 6 to 8. Incorporation of Oregon green expands the sensitivity from pH 4 to 7.5. Ratiometric measurements minimize the errors due to excitation source fluctuations and sensor concentrations. The PEG corona of the core-shell-corona micelle sensors will enhances the biological advantages such as circulation half life of the nanosensors in blood. PEG corona is provided exclusive intramicellar shell cross-linking via steric stabilization mechanism.[35] The functionalities introduced in the shell region can also be protected by the PEG

corona. If protected from the light, the SCMN was appeared to be clear and remain stable for several months.

HeLa cell uptake of nanosensor. The inertness of the sensor was tested by calibrating in the presents of proteins (serum) comparing it to calibration done in buffers alone (Figure 6a). The sensor showed not to be effected by proteins. When compared to cell lysate there was a small difference between the lysed cells and the pure buffer curve but it was not significant when looking at the pH distribution as calculated using the two different calibration curves. We also calibrated the sensor *in-situ* by using an ionophore, nigericin, to equilibrate the internal pH to that of the external buffer solution.[8] However, analysis of the pH distribution at each pH value showed a broad pH distribution within the cells indicating that the ionophore was not able to adjust the internal pH completely with that of the external pH. Ionophores does hold potential for frauds and should be used with caution, the affected transporter may not be the only relevant one during a calibration.[36, 37] Thus the nigericin calibration curve was not used further.

The sensor is spontaneously taken up by the HeLa cells into small compartments probably through endocytosis due to the cationic surface chemistry of the sensor. Cellular uptake was seen after 4 hours where two tops are visible in the pH distributions (Figure 6b), one at pH 5.4 and one at pH 3.8. Illustrating an uptake route that gets acidified suggesting uptake trough endosomes to lysosome. After 24 hours, structures mainly in the cytosol around the nucleus are labelled (see Figure S4 in supporting information) with a mean pH distribution of pH 3.8 suggesting the sensor were residence in the lysosomes at this time point (Figure 6b). From the pH distribution, it is clear that the sensor is well suited to measure in the endosome-lysosome pathway as only 2% of the ratios obtained from the images fall outside the sensor's range.

CONCLUSION

We have demonstrated the first synthesis characterization and applications of shell cross-linked core-shell-corona micelle based ratiometric pH nanosensors (SCMN) for intracellular measurements. ATRP

and principle of self-assembly were used to prepare polymeric micelles having well defined core-shell-corona morphology. The reinforcement of the weak hydrophobic interactions between the unimers of the micelle was provided by covalent cross-linking using amidation reaction. The stabilized micelles were converted to ratiometric pH nanosensors by fluorophores conjugation at the shell region. *In vitro* and *in-situ* pH calibration curves for the nanosensors were constructed by fluorescence measurement. The cell uptake experiments of the nanosensors were performed, and the pH distributions in HeLa cells were monitored. This showed that the sensor was able to pass the cell membrane and respond to pH changes within a cellular environment. The uses of triple fluorophore labelled sensor enable ratiometric pH measurement within the whole endocytic pathway.

EXPERIMENTAL METHODS

Shell cross-linked micelle nanosensor (SCMN) 5 fabrication. The de-protected amphiphilic triblock copolymer PEG-*b*-PAEMA-*b*-PS (100 mg, 0.0088 mmol) was dissolved in 10 mL DMF by stirring overnight. To the polymeric solution under stirring, 2 mL of MilliQ water was added drop wise within 30 minutes followed by 20 mL more MilliQ water added drop wise. The cloudy micelle solution was transferred into dialysis tube of molecular weight cut off (MWCO = 12 kDa) and dialysis against MilliQ water for 5 days. Hydrodynamic diameter (D_h) and zeta potentials (ξ) were found to be 29 ± 2 nm and 29 ± 1 mV respectively. The final block copolymer concentration after dialysis was 2 mg/mL. To the micelle solution 25 mL (50 mg, 0.0044 mmol, 0.053 mmol of amine), 3,6,9-trioxaundecandioic acid (3.6 mg, 0.016 mmol) and 1-[3-(dimethylamino)propyl]-3-ethylcarbodiimide methiodide (9.5 mg, 0.032 mmol) was added and stirred at room temperature for 10 h. The reaction mixture was then dialyzed against MilliQ water for 3 days (D_h = 24 ± 1 nm and ξ = 18 ± 2), then against carbonate buffer (pH = 9.8) for another 3 days. To the basic amphiphilic colloidal dispersion, RhBITC (0.014 mg, 0.0264 μmol), FITC (0.026 mg, 0.066 μmol) and F_2FITC (0.028 mg, 0.066 μmol) were added and stirred in the absence of light at room temperature for 12 hrs. The reaction mixture was transferred into dialysis tube (MWCO = 12 kDa); and dialysis was conducted against carbonate buffer for 3 days, then against MilliQ

water for another 5 days (D_h = 25±2 nm and ξ = 16±2 mV). The final nanosensor concentration was 1.9 mg of polymers/mL of water.

pH calibration curve from spectrofluorometer. The pH calibration curve was constructed by fluorescence measurements. 50 µl of the pH nanosensor was added to 1 mL of buffer solutions having different pH, and the nanosensor solutions were excited at 490 and 543 nm respectively. Fluorescence emission spectra of the nanosensors at different pH were plotted. From the fluorescence emission spectra of Fluorescein (FA), Oregon Green (OG) and Rhodamine (RhB), fluorescence intensity (I) ratios I_{Org} + I_{FA} / I_{RhB} were calculated. This fluorescence intensity ratio was then plotted against corresponding pH to obtain the ratiometric pH calibration curves.

***In vitro* and *in situ* calibration of polymeric micelle nanosensor from microscope.** *In vitro* calibration curves were generated from fluorescence images of nanosensor at 12.5 or 25 mg/mL in 60 mM buffers (20 mM HEPES / 20 mM MES / 20 mM Acetate / 100 mM NaCl) from pH 2.1 to 7.6. The influence of proteins on the sensors behaviour was tested by mixing media (without phenol red plus 10% serum) 1:2 with 120 mM buffer solutions, measure pH, and finally mixing with sensors in a ration of 3:1 for a final concentration of 60 mM buffer and 12.5 mg/ml nanosensor. For calibration in buffers with artificial cytoplasm, 10^6 HeLa cells per ml milliQ water were lysed and mixed with buffer as for media. The microscope was focused in a plane within the solution and, with the same settings (e.g. laser power, gain and resolution) as was employed for the imaging of corresponding cells with internalized nanosensor, images were taken with sequential excitation at 488 nm and 561 nm. Each pH solution was imaged in triplicates and calibration curves are presented with mean ± SD. The calibration data was used to find the best fit sigmoid curve, and determine the pKa values and the R values from the formula:

$$10^{pKa_1+pKa_2}\cdot x^2+\left(10^{pKa_1}+10^{pKa_2}-\frac{R_1}{R-R_0}\cdot 10^{pKa_2}-\frac{R_2}{R-R_0}\cdot 10^{pKa_1}\right)\cdot x+1-\frac{R_1+R_2}{R-R_0}=0$$

Where $x = 10^{-pH}$.

Acknowledgement. The authors would like to thank Kræftens Bekæmpelse and the Danish Research Council for Technology and Production (Grant 274-07-0172) for financial.

Supporting Information Avilable: Synthesis of PEG-*b*-PAEMA-*b*-PS, ^{1}H NMR and FT-IR spectra of the polymers and micelles, details of cell uptake experiments and AFM measurement. This material is available free of charge via the internet at http://pubs.acs.org.

TOC graphic

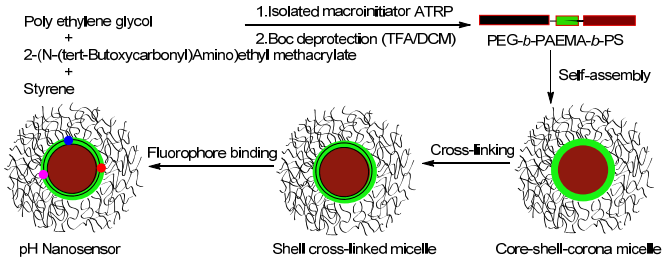

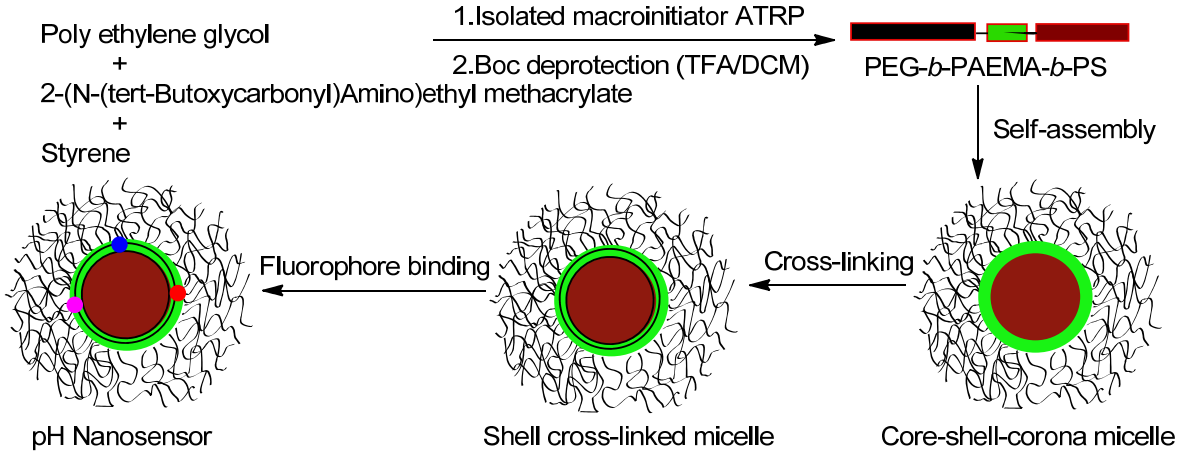

Figure 1. Schematic representation of shell cross-linked core-shell-corona micelle nanosensor.

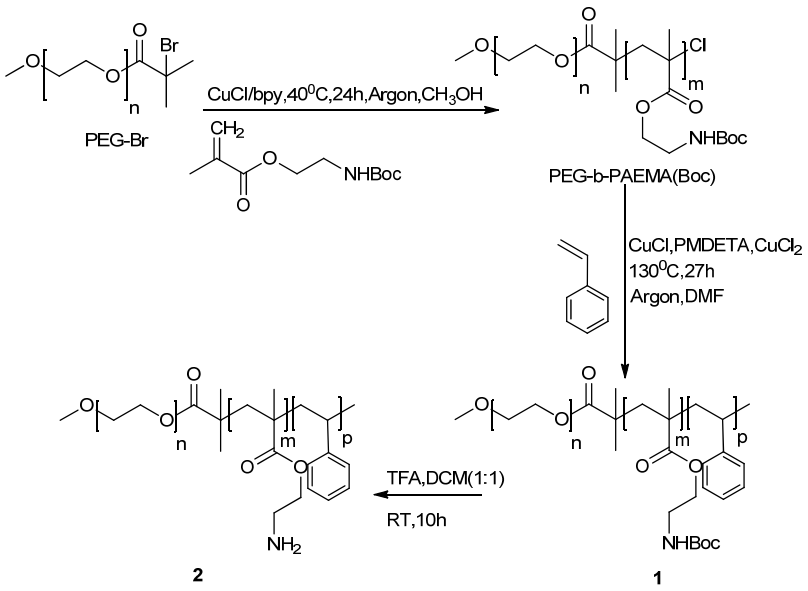

Scheme 1. Synthesis of PEG-*b*-PAEMA(Boc)-*b*-PS (**1)** by ATRP and PEG-*b*-PAEMA-*b*-PS (**2**) by de-protection of **1**. bpy = 2,2'bipyridyl, PMDETA = N,N,N',N'',N'-Pentamethyldiethylenetriamine.

Table 1. Molecular weights of amphiphilic triblock copolymer, PEG-*b*-PAEMA(Boc)-*b*-PS (1)

M_n[a]	M_w[a]	M_w/M_n[a]	M_n[b]	n[c]	m [c]	p [c]
9280	11800	1.27	11250	127	12	28

[a] Determined by GPC, [b] Determined by NMR, [c] Number of repeating units of PEG block(n), PAEMA(Boc) block (m) and PS block(p)

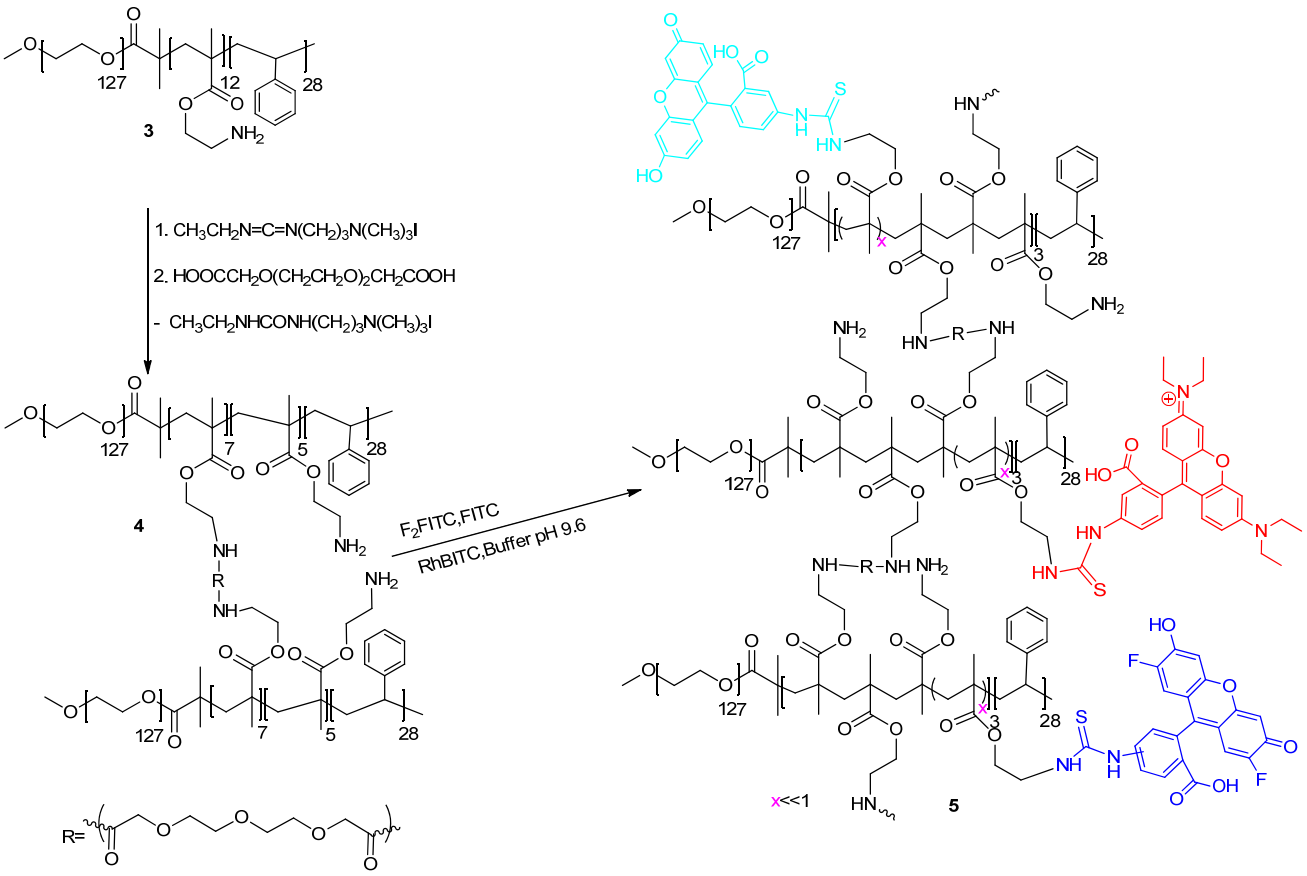

Scheme 2. Synthesis of shell cross-linked ratiometric micelle nanosensor

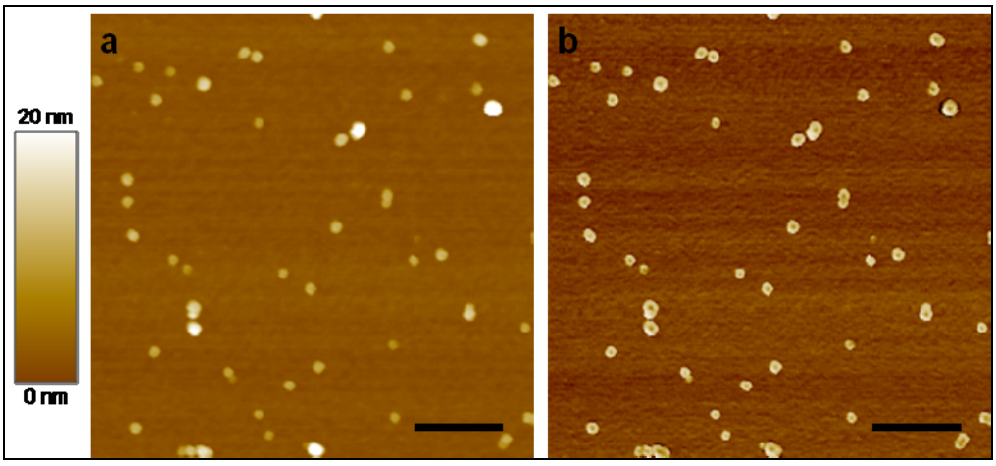

Figure 2. AFM images of cross-linked micelles. **a** Topographic image and **b** phase image. Scale bar 1 μm

Table 2. DLS and Zeta potential measurements of Nanoparticles at 25^{0}C in MilliQ water

Particles	DLS(D_h)[a] (nm)	Zeta(ξ)[b] (mV)
3	29±2	29±1
4	24±1	18±2
5	25±2	16±2

[a]Number-averaged hydrodynamic diameters of nanoparticles by dynamic light scattering. [b]Zeta potential from 10 determinations, each having 10 cycles

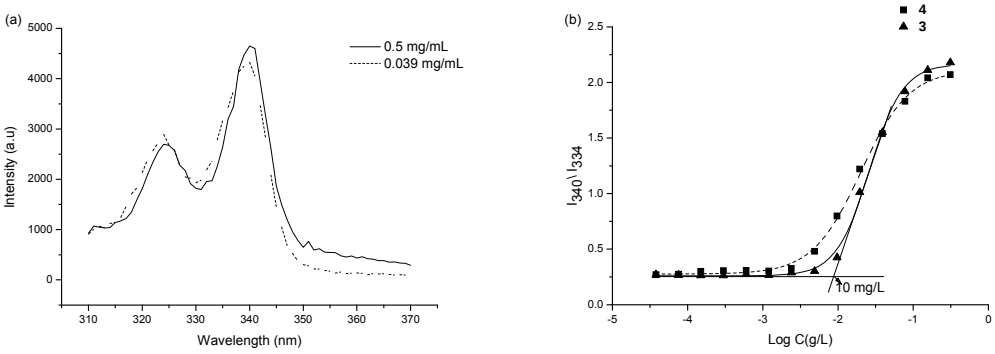

Figure 3. (a) Excitation spectra monitored at λ_{em} = 390 nm, representative spectra for the blue shift of (0,0) absorption band of pyrene with the decrease in block copolymer concentration (micelle concentration); (b) Plot of intensity ratio I_{340} / I_{334} (from pyrene excitation spectra) *vs* PEG-*b*-PAEMA-*b*-PS concentration of cross-linked (**4**) (■) and non-cross-linked (**3**) (▲) micelle, for each measurement [pyrene] = 6×10^{-7}M.

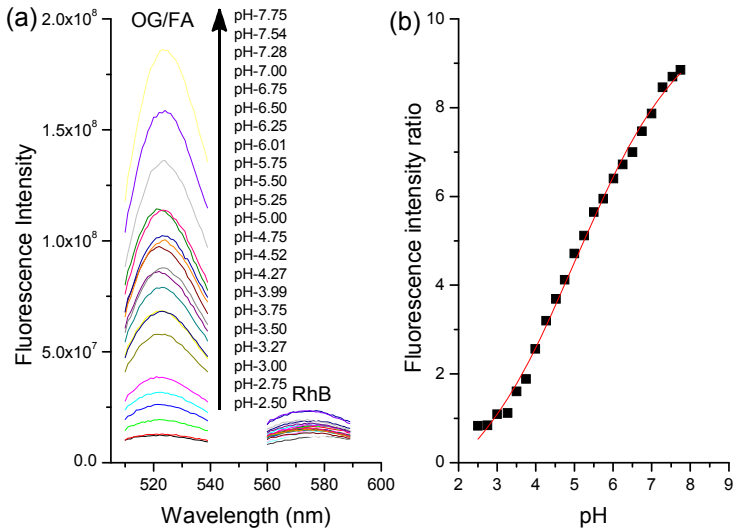

Figure 4. (a) Fluorescence emission curve for the pH nanosensor. b) pH calibration curve of the nanosensor made by plotting fluorescence intensity ratio (I_{OG} + I_{FA} / I_{RhB}) against pH. OG = Oregon Green, FA = Fluorescein, RhB = Rhodamine B.

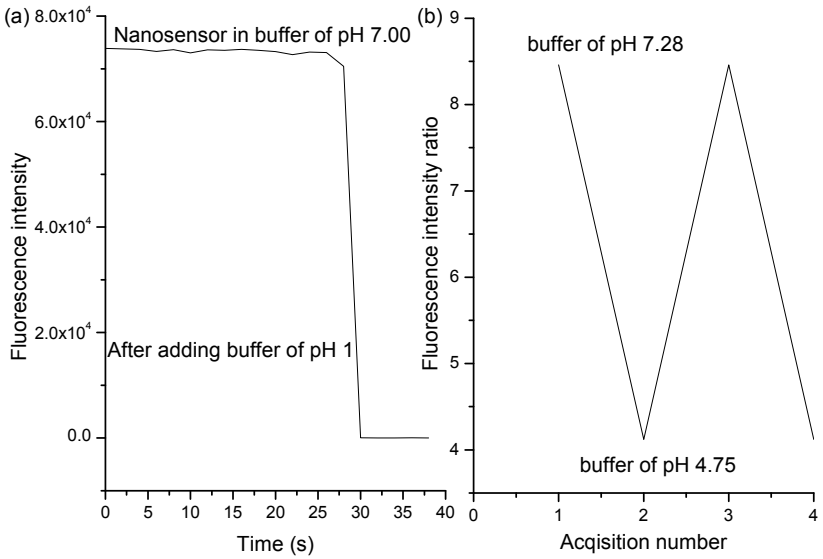

Figure 5. (a) Time for response of the nanosensor towards the change in pH. (b) Reversibility of the nanosensor, tested by repeatedly measuring the fluorescence intensity ratio (I_{OG} + I_{FA} / I_{RhB}) between two different pH.

a) 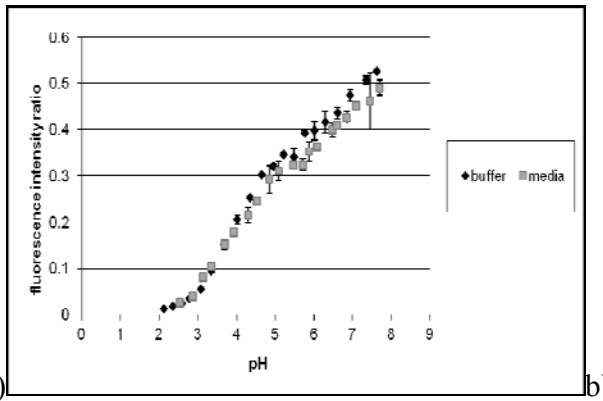

b) 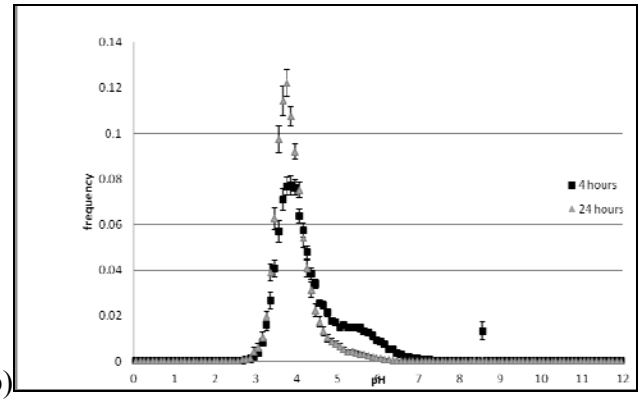

Figure 6. a) pH calibration curves in buffer and serum done with microscope settings, b) pH distributions in HeLa cells with nanosensors uptake after 4 or 24 hours. Values falling outside the sensor range is marked at pH 1.5 and pH 8.6 for lower and higher than sensor range respectively. At 4 hours less than 2% falls higher than the sensors range. No values fall below sensor range and at 24 hours all values lie within the sensors range.

REFERENCES AND NOTES

1. Asokan, A.; Cho, M. J., Exploitation of intracellular pH gradients in the cellular delivery of macromolecules. *Journal of Pharmaceutical Sciences* **2002**, *91*, 903-913.
2. Clark, H. A.; Kopelman, R.; Tjalkens, R.; Philbert, M. A., Optical Nanosensors for Chemical Analysis inside Single Living Cells. 2. Sensors for pH and Calcium and the Intracellular Application of PEBBLE Sensors. *Analytical Chemistry* **1999**, *71*, 4837-4843.
3. Ji, J.; Rosenzweig, N.; Griffin, C.; Rosenzweig, Z., Synthesis and application of submicrometer fluorescence sensing particles for lysosomal pH measurements in murine macrophages. *Analytical Chemistry* **2000**, *72*, 3497-3503.
4. Lu, J.; Rosenzweig, Z., Nanoscale fluorescent sensors for intracellular analysis. *Fresenius' Journal of Analytical Chemistry* **2000**, *366*, 569-575.
5. McNamara, K. P.; Nguyen, T.; Dumitrascu, G.; Ji, J.; Rosenzweig, N.; Rosenzweig, Z., Synthesis, Characterization, and Application of Fluorescence Sensing Lipobeads for Intracellular pH Measurements. *Analytical Chemistry* **2001**, *73*, 3240-3246.
6. Peng, J.; He, X.; Wang, K.; Tan, W.; Wang, Y.; Liu, Y., Noninvasive monitoring of intracellular pH change induced by drug stimulation using silica nanoparticle sensors. *Analytical and Bioanalytical Chemistry* **2007**, *388*, 645-654.
7. Sun, H.; Scharff-Poulsen, A. M.; Gu, H.; Almdal, K., Synthesis and Characterization of Ratiometric, pH Sensing Nanoparticles with Covalently Attached Fluorescent Dyes. *Chemistry of Materials* **2006**, *18*, 3381-3384.
8. Benjaminsen, R. V.; Sun, H.; Henriksen, J. R.; Christensen, N. M.; Almdal, K.; Andresen, T. L., Evaluating Nanoparticle Sensor Design for Intracellular pH Measurements. *ACS Nano* **2011**, *5*, 5864-5873.
9. Chauhan, V. M.; Burnett, G. R.; Aylott, J. W., Dual-fluorophore ratiometric pH nanosensor with tuneable pKa and extended dynamic range. *Analyst* **2011**, *136*, 1799-1801.

10. Schulz, A.; Hornig, S.; Liebert, T.; Birckner, E.; Heinze, T.; Mohr, G. J., Evaluation of fluorescent polysaccharide nanoparticles for pH-sensing. *Organic & Biomolecular Chemistry* **2009**, *7*, 1884-1889.
11. Allard, E.; Larpent, C., Core-shell type dually fluorescent polymer nanoparticles for ratiometric pH-sensing. *Journal of Polymer Science Part A: Polymer Chemistry* **2008**, *46*, 6206-6213.
12. Moghimi, S. M.; Hunter, A. C.; Murray, J. C., Long-Circulating and Target-Specific Nanoparticles: Theory to Practice. *Pharmacological Reviews* **2001**, *53*, 283-318.
13. Vladimir P, T., Structure and design of polymeric surfactant-based drug delivery systems. *Journal of Controlled Release* **2001**, *73*, 137-172.
14. Matyjaszewski, K.; Tsarevsky, N. V., Nanostructured functional materials prepared by atom transfer radical polymerization. *Nat Chem* **2009**, *1*, 276-288.
15. Zhang, L.; Eisenberg, A., Multiple Morphologies of "Crew-Cut" Aggregates of Polystyrene-b-poly(acrylic acid) Block Copolymers. *Science* **1995**, *268*, 1728-1731.
16. Zhang, L.; Yu, K.; Eisenberg, A., Ion-Induced Morphological Changes in "Crew-Cut" Aggregates of Amphiphilic Block Copolymers. *Science* **1996**, *272*, 1777-1779.
17. Gabizon, A. A., Liposome circulation time and tumor targeting: implications for cancer chemotherapy. *Advanced Drug Delivery Reviews* **1995**, *16*, 285-294.
18. Maeda, H.; Wu, J.; Sawa, T.; Matsumura, Y.; Hori, K., Tumor vascular permeability and the EPR effect in macromolecular therapeutics: a review. *Journal of Controlled Release* **2000**, *65*, 271-284.
19. Palmer, T. N.; Caride, V. J.; Caldecourt, M. A.; Twickler, J.; Abdullah, V., The mechanism of liposome accumulation in infarction. *Biochimica et Biophysica Acta (BBA) - General Subjects* **1984**, *797*, 363-368.
20. Nasongkla, N.; Shuai, X.; Ai, H.; Weinberg, B. D.; Pink, J.; Boothman, D. A.; Gao, J., cRGD-Functionalized Polymer Micelles for Targeted Doxorubicin Delivery. *Angewandte Chemie* **2004**, *116*, 6483-6487.
21. Oishi, M.; Nagasaki, Y.; Itaka, K.; Nishiyama, N.; Kataoka, K., Lactosylated Poly(ethylene glycol)-siRNA Conjugate through Acid-Labile β-Thiopropionate Linkage to Construct pH-Sensitive Polyion Complex Micelles Achieving Enhanced Gene Silencing in Hepatoma Cells. *Journal of the American Chemical Society* **2005**, *127*, 1624-1625.
22. Qi, K.; Ma, Q.; Remsen, E. E.; Clark, C. G.; Wooley, K. L., Determination of the Bioavailability of Biotin Conjugated onto Shell Cross-Linked (SCK) Nanoparticles. *Journal of the American Chemical Society* **2004**, *126*, 6599-6607.
23. Xiong, X.-B.; Mahmud, A.; Uludag, H.; Lavasanifar, A., Conjugation of Arginine-Glycine-Aspartic Acid Peptides to Poly(ethylene oxide)-b-poly(ε-caprolactone) Micelles for Enhanced Intracellular Drug Delivery to Metastatic Tumor Cells. *Biomacromolecules* **2007,** *8* (3), 874-884.
24. Yoo, H. S.; Park, T. G., Folate receptor targeted biodegradable polymeric doxorubicin micelles. *Journal of Controlled Release* **2004**, *96*, 273-283.
25. Sun, G.; Cui, H.; Lin, L. Y.; Lee, N. S.; Yang, C.; Neumann, W. L.; Freskos, J. N.; Shieh, J. J.; Dorshow, R. B.; Wooley, K. L., Multicompartment Polymer Nanostructures with Ratiometric Dual-Emission pH-Sensitivity. *Journal of the American Chemical Society* **2011**, *133*, 8534-8543.
26. O'Reilly, R. K.; Hawker, C. J.; Wooley, K. L., Cross-linked block copolymer micelles: functional nanostructures of great potential and versatility. *Chemical Society Reviews* **2006,** *35*, 1068-1083.
27. Read, E. S.; Armes, S. P., Recent advances in shell cross-linked micelles. *Chemical Communications* **2007**, 29, 3021-3035.
28. Fan, H.; Leve, E. W.; Scullin, C.; Gabaldon, J.; Tallant, D.; Bunge, S.; Boyle, T.; Wilson, M. C.; Brinker, C. J., Surfactant-Assisted Synthesis of Water-Soluble and Biocompatible Semiconductor Quantum Dot Micelles. *Nano Letters* **2005**, *5*, 645-648.
29. Maysinger, D.; Berezovska, O.; Savic, R.; Lim Soo, P.; Eisenberg, A., Block copolymers modify the internalization of micelle-incorporated probes into neural cells. *Biochimica et Biophysica Acta (BBA) - Molecular Cell Research* **2001**, *1539*, 205-217.

30. Luo, L.; Tam, J.; Maysinger, D.; Eisenberg, A., Cellular Internalization of Poly(ethylene oxide)-b-poly(ε-caprolactone) Diblock Copolymer Micelles. *Bioconjugate Chemistry* **2002**, *13*, 1259-1265.
31. Savic, R.; Luo, L.; Eisenberg, A.; Maysinger, D., Micellar Nanocontainers Distribute to Defined Cytoplasmic Organelles. *Science* **2003**, *300*, 615-618.
32. Stryer, L.; Haugland, R. P., Energy Transfer - a Spectroscopic Ruler. *Proceedings of the National Academy of Sciences of the United States of America* **1967**, *58*, 719-726.
33. Chen, R. F.; Knutson, J. R., Mechanism of fluorescence concentration quenching of carboxyfluorescein in liposomes: Energy transfer to nonfluorescent dimers. *Analytical biochemistry* **1988**, *172*, 61-77.
34. Andrisano, V.; Bartolini, M.; Bertucci, C.; Cavrini, V.; Luppi, B.; Cerchiara, T., Analytical methods for the determination of folic acid in a polymeric micellar carrier. *Journal of Pharmaceutical and Biomedical Analysis* **2003**, *32*, 983-989.
35. D.H, Napper., Steric stabilization. *Journal of Colloid and Interface Science* **1977**, *58*, 390-407.
36. Boyarsky, G.; Hanssen, C.; Clyne, L. A., Inadequacy of high K+/nigericin for calibrating BCECF. I. Estimating steady-state intracellular pH. *American Journal of Physiology - Cell Physiology* **1996**, *271*, C1131-C1145.
37. Boyarsky, G.; Hanssen, C.; Clyne, L. A., Inadequacy of high K+/nigericin for calibrating BCECF. II. Intracellular pH dependence of the correction. *American Journal of Physiology - Cell Physiology* **1996**, *271*, C1146-C1156.

Intermediary Layer Cross-linked Core-Shell-Corona Micelle based Ratio-metric Nanosensors for Intracellular pH Measurements

*Pramod Kumar EK, Nynne M. Christensen, Rikke Vicki Benjaminsen, Jonas Rosager Henriksen, Kristoffer Almdal, Thomas L. Andresen**

DTU Nanotech, Department of Micro-and Nanotechnology, Technical University of Denmark

*thomas.andresen@nanotech.dtu.dk.

Contents

1. Additional experimental information

Materials: Styrene (99.5%) obtained from Fluka and radical inhibitors was removed by passing through a column filled with basic alumina. 2-Aminoethyl methacrylate hydrochloride (AEMA.HCl) (90%), Bis(*tert*-butyl) dicarbonate (99%), triethylamine (TEA) (99.5%), 2-bromo-isobutyryl-bromide (98%), CuCl (99.995%), 2,2'bipyridyl (bpy) (99%), PMDETA (99%), $CuCl_2$ (99.995%), trifluoroacetic acid (TFA) (99%), dialysis tubing (MWCO = 12 kDa), N-(3-Dimetylaminopropyl)-N'-ethylcarbodiimide methiodide (EDC.MeI), Rhodamine B isothiocyanate (RhBITC) and Fluorescein 5(6)-isothiocyanate (FITC) (90%) were purchased from Sigma Aldrich and used as obtained. 3,6,9-Trioxaundecandioic acid (TUDA) was purchased from iris biotech GMBH, Oregon Green 488 isothiocyanate (F_2FITC) was purchased from Invitrogen, and CH_3O-PEG-OH (poly (ethylene glycol) monomethylether (M_n = 5000) was from Fluka. Solvents used for atom transfer polymerization (ATRP) were purified by distillation over the drying agents indicated in parentheses, stored under molecular sieves (MeOH 3Å and DMF 4Å) and transferred under argon; MeOH ($Mg(OMe)_2$), and DMF (CaH_2). Other solvents and commercially available chemicals were used as obtained. Water used was collected from Millipore; aqueous buffer solutions were prepared from the reported procedures.

Instrumentation details: ^{1}H-nmr spectra were recorded on a Bruker 250 MHz in solvents as indicated, chemical shifts (δ) were given in ppm relative to TMS. The residual solvent signals were used as a reference, and the chemical shifts converted into TMS scale ($CDCl_3$: δ_H = 7.24 ppm, ^{6}d-DMSO: δ_H = 2.50 ppm, D_2O: δ_H = 4.79 ppm). Infrared spectra's were recorded by Perkin Elmer FT-IR Spectrometer (KBr pellets method), and the wave numbers of recorded IR signals were quoted in cm^{-1}. The number-average molecular weight (M_n) weight average molecular weight (M_w) and polydispersity (M_w/M_n) of block copolymers were determined by GPC analysis based on poly styrene calibration standards. Measurements were carried out by using Mixed-D GPC column from Polymer Laboratories (7.4 × 300 mm) and RID10A-SHIMADZU refractive index detector. DMF with 50mM LiCl solution was used as eluent (0.5 mL / min.) at 25 ^{0}C. Hydrodynamic diameters (D_h) and size distributions of the amphiphilic colloidal dispersion in MilliQ water at 25 ^{0}C were determined by Brookhaven ZETA PALS instrument. Calculation of the particle size distribution and distribution averages were performed with the ISDA software package (from Brookhaven) through CONTIN particle size distribution analysis routines. All determinations were made in triplicate and duration of 2 minutes each. Zeta potential measurements were carried out by using Brookhaven ZETA PALS analyzer. The measurements were made in MilliQ water at 25 ^{0}C, and the zeta potential (ξ) was calculated using Smoluchowski equation. Electrophoretic mobility (μ) = $\boldsymbol{\xi \epsilon/\eta}$, where η and ϵ are the absolute viscosity and dielectric constant of the medium respectively. Mean value of ξ was chosen from 10 determinations of 10 data accumulations. Fluorescence measurements were carried out by

using EDINBURGH F-900 fluorometer. PSIA XE-150 scanning force microscope was used for AFM measurements. Argon atmosphere (99.9999 %) used in the reactions was provided by AGA Denmark

Synthesis of $PEG_{5000}Br$: The macroinitiator was synthesized by using a slightly modified procedure from that reported in the literature.[1] CH_3O-PEG-OH, M_n = 5000 (5 gram, 1 mmol) was dissolved in 60 mL of toluene. After azeotropic distillation of 10 mL of toluene under reduced pressure to remove traces of water, TEA (0.278 mL, 2 mmol) was added, and the solution was cooled to room temperature. 2-bromoisobutyryl bromide (0.185 mL, 1.5 mmol) was added drop wise to the mixture, and the reaction mixture was stirred at 40 ^{0}C for 2 days under a calcium chloride guard tube. The solution was filtered, and most of the toluene was removed by rotary evaporation prior to precipitation into 10 fold excess of cold ether. The crude polymer was dried under vacuum, dissolved in water at pH 8-9 and then extracted with DCM. The organic layers were collected and dried over anhydrous sodium sulfate. The removal of the solvent under reduced pressure afforded the purified macroinitiator in a yield of 5.1 g (99 %). ^{1}H-NMR (250 MHz, $CDCl_3$): δ = 3.63 (s, -C**H**$_2$C**H**$_2$O-), 1.91 (s, -C(C**H**$_3$)$_2$); FT-IR (cm^{-1}): 2887, 1737, 1466, 1359, 1342, 1279, 1241, 1148, 1107, 1060, 963, 841.

Synthesis of 2-[N-(tert-Butoxycarbonyl)Amino]ethyl methacrylate (AEMA(Boc)): AEMA(Boc) was synthesized by a slightly modified procedure than reported.[2] AEMA HCl (2.5 g, 15.15 mmol) was dissolved in 40 mL of dry DCM and cooled to 0 ^{0}C in an ice water bath. Anhydrous triethylamine (4.2 mL, 30.3 mmol) was added drop wise to the ice cold solution and stirred for 20 minutes. Bis(*tert*-butyl) dicarbonate (5.22 mL, 22.725 mmol) dissolved in 10 mL of dry DCM was slowly added to the reaction mixture, warmed to room temperature and stirred for 24 h under argon atmosphere. The organic layer was washed with water (2 × 25 mL), 1M HCl (2 × 25 mL), saturated aqueous sodium bicarbonate (2 × 25 mL) and with saturated brine solution (2 × 20 mL). The organic layer was dried over anhydrous sodium sulphate; this was followed by removal of the solvent under reduced pressure gave crystalline solid 3.3 g (95%). ^{1}H-NMR (250 MHz, $CDCl_3$): δ = 6.11 (1H, Vinylic **H**), 5.58 (1H, Vinylic **H)**, 4.76 (broad (br), 1H, -N**H**), 4.20 (2H, -COOC**H**$_2$CH$_2$), 3.42 (2H, -COOCH$_2$C**H**$_2$), 1.94 (s, 3H, -C**H**$_3$), 1.44 (s, 9H, -C(C**H**$_3$)$_3$); FT-IR (cm^{-1}): 3386, 2981, 1692, 1633, 1521, 1453, 1423, 1388, 1364, 1323, 1158, 1107, 1042, 998, 957, 915, 880, 853, 818, 777, 756, 653, 597.

PEG_{127}-b-$P(AEMA(Boc))_{12}Cl$: PEG-Br (2 gram, 0.36 mmol) AEMABoc (852 mg, 5 mmol), 2,2'bipyridyl (122 mg, 0.76 mmol) and 10 mL dry MeOH were added to 25 mL schlenk flask equipped with a stirrer bar. The flask was frozen in liquid nitrogen, and CuCl catalyst (40 mg, 0.40 mmol) was added. The reaction mixture was degassed with 3 freeze-pump-thaw cycles (each 15 minute long) to remove the oxygen, and the polymerization was carried out at 40 ^{0}C for 24 h under argon atmosphere. The dark brown reaction solution was passed through a silica gel column to remove the copper catalyst using MeOH as solvent. On exposure to air, the solution turned

to blue, which indicated the areal oxidation of the Cu(I) catalyst. After the removal of most of the MeOH by rotary evaporation, the polymer precipitated into excess cold diethyl ether. It was then isolated by filtration, and the precipitate was dried under vacuum to yield 1.86 g (62%) of the diblock copolymer. ^{1}H-NMR (250 MHz, $CDCl_3$): δ = 5.50 (br s, -N**H**), 4.0 (br s, -OC**H**$_2$CH$_2$NH), 3.63 (s, -C**H**$_2$C**H**$_2$O), 3.37 (br m, -OCH$_2$C**H**$_2$NH, -OC**H**$_3$), 1.82 (br, -C**H**$_2$ backbone), 1.43 (s, -C(C**H**$_3$)$_3$), 1.11-0.81 (m, -C(C**H**$_3$)$_2$, -C**H**$_3$ backbone); FT-IR (cm^{-1}): 3387, 2892, 1716, 1520, 1466, 1391, 1361, 1342, 1279, 1241, 1150, 1112, 1060, 996, 965, 843; M_n (NMR) = 8340; M_n (GPC) = 5600, M_w = 6460, PD (M_w/M_n) = 1.15.

Synthesis of PEG$_{127}$-b-P(AEMA(Boc))$_{12}$-b-PS$_{28}$ (1): PEG-*b*-PAEMA(Boc)-Cl (1 g, 0.12 mmol), Styrene (0.48 mL, 4.2 mmol), $CuCl_2$ (13 mg, 0.096 mmol), PMDETA (0.087 mL, 0.42 mmol) and 3 mL of DMF were taken in 25 mL schlenk flask equipped with a stirrer bar. The flask was frozen in liquid nitrogen, and CuCl catalyst (12 mg, 0.12 mmol) was added to it. After being degassed with 3 freeze-pump-thaw cycles (each cycle 15 minute long) to remove the oxygen, the polymerization was carried out at 130 ^{0}C for 27 h under argon atmosphere. The reaction mixture was concentrated under vacuum, and the polymer was precipitated into cold diethyl ether. The precipitate was dried under vacum yielded 0.74 mg (55%) of the triblock copolymer. ^{1}H-NMR (250 MHz, ^{6}d-DMSO): δ = 7.3-6.5 (m, Ar**H**), 3.80 (br, -OC**H**$_2$CH$_2$NH), 3.50 (s, -C**H**$_2$C**H**$_2$O), 3.20 (br s, -OCH$_2$C**H**$_2$NH), 2.00-1.50 (br, C**H**$_2$ and -C**H** backbone), 1.40 (s, -C(C**H**$_3$)$_3$), 1.20-0.70 (m, -C**H**$_3$ backbone); FT-IR (cm^{-1}): 3370, 3025, 2887, 1716, 1602, 1518, 1496, 1466, 1451, 1391, 1361, 1342, 1279, 1243, 1146, 1105, 961, 841; M_n (NMR) = 11250; M_n (GPC) = 9280, M_w = 11800, PD (M_w/M_n) = 1.27.

PEG-b-PAEMA-b-PS (2): The triblock copolymer, PEG-*b*-PAEMA(Boc)-*b*-PS (1g, 0.088 mmol) was dissolved in 4 mL of DCM, followed by 4 mL TFA was added drop wise, and stirred at room temperature for 10 hours. After evaporating most of the solvent under reduced pressure; the polymer was precipitated into excess of cold diethyl ether, and dried under vacuum. The complete de-protection of amino group was confirmed by the disappearance of Boc group signal at δ 1.40 (s, -C(C**H**$_3$)$_3$) ^{1}H-NMR (250 MHz in ^{6}d-DMSO), and qualitatively by conducting Kaiser test.[3]

3. Cell uptake experiments

a. Cell culture.

HeLa cell lines were originally obtained from the American Type Culture Collection (ATCC) and maintained in Dulbecco's Modified Eagle's Medium (DMEM) supplemented with 10% fetal bovine serum (FBS) (Sigma-Aldrich) and 100 UI/ml penicillin and streptomycin (Lonza). Cell cultures were incubated in a 5% CO_2 humidified incubator at 37°C.

b. Cell uptake

HeLa cells were seeded in 8 well slides with cover glass bottom (company)for 24 h. Cells were incubated with 50 µg/ml nanosensor for 24 h, washed three times with ice-cold phosphate buffered saline (PBS) supplemented with heparin (20 units/ml), washed once with PBS and kept in growth medium without phenol-red for observation by confocal microscopy. The microscope was equipped with an incubator box and CO_2 supply to ensure optimal growth conditions during microscopy. Cells were imaged sequentially (by line) with excitation at 488 nm and 561 nm along with a DIC image.

4. AFM measurements

Atomic Force Microscopy (AFM) images of the micelles were obtained using a PSIA XE 150 microscope (Park Systems, Suwon, Korea) in tapping mode. Measurements were performed under ambient conditions in air using standard silicon tips (NCHR-POINTPROBE, Nanoworld) with a typical resonance frequency of 330 kHz and a nominal spring constant of 42 N/m. Scan speed was adapted to the scan size and set between 0.5 and 1 Hz. The image resolution was 256 x 256 pixels. The average height of the respective particles was determined by the mean value of the nanoparticle regions of at least 4 images.

For the measurements silicon wafers coated with an amino-silane monolayer were used as substrate. Before use the silicon surface was cleaned in 2-propanol and rinsed successive in vast amount of 2-propanol, water/ethanol (1/1) mixture and Milli-Q water. The solutions of the micelles were diluted to a typical concentration of around 0.0032 mg/ml. A drop (5 µl) was deposited on the dry wafer and allowed to dry freely in air.

5. Important spectra

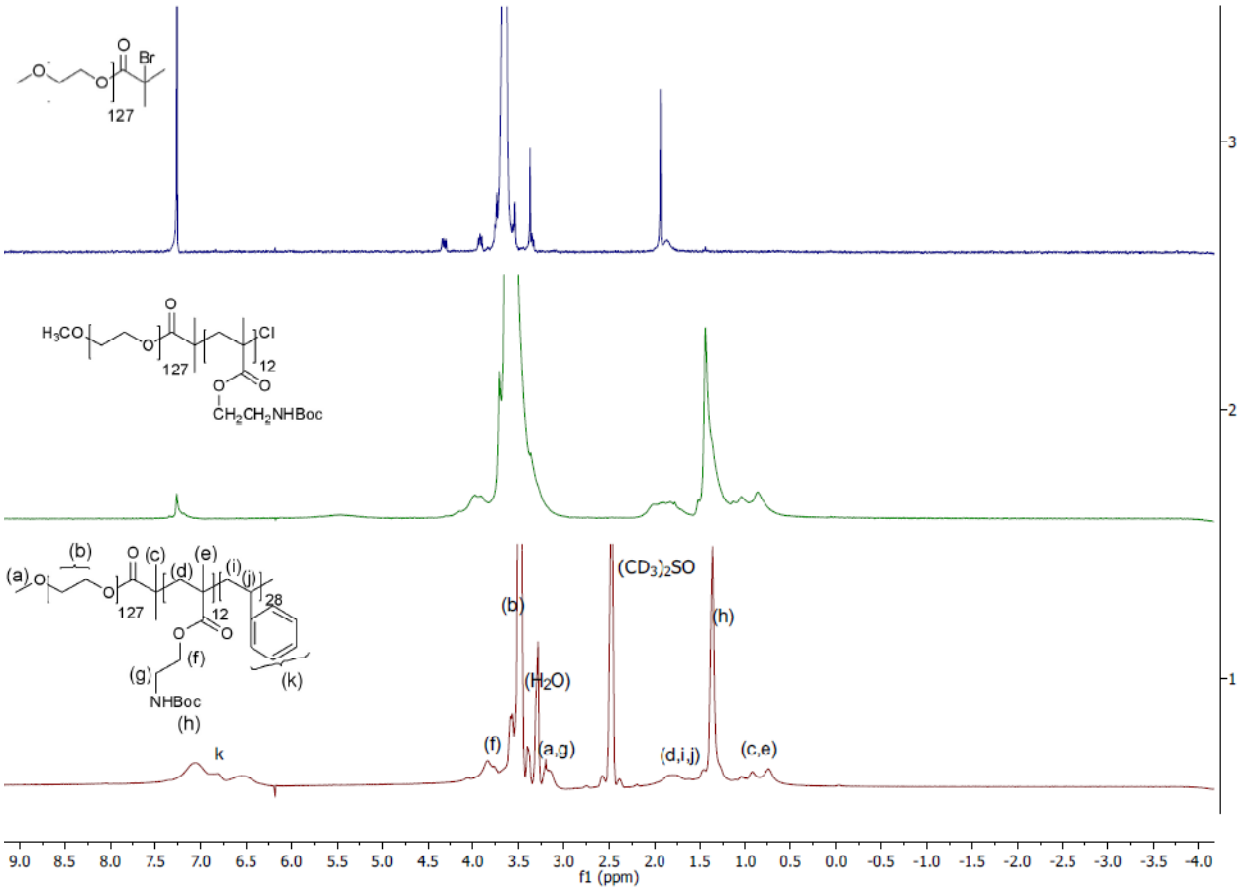

Figure S1. ^{1}H-NMR spectra of the polymers; PEG-Br and PEG-*b*-PAEMA(Boc) in $CDCl_3$ and PEG-*b*-PAEMA(Boc)-*b*-PS in ^{6}d-DMSO.

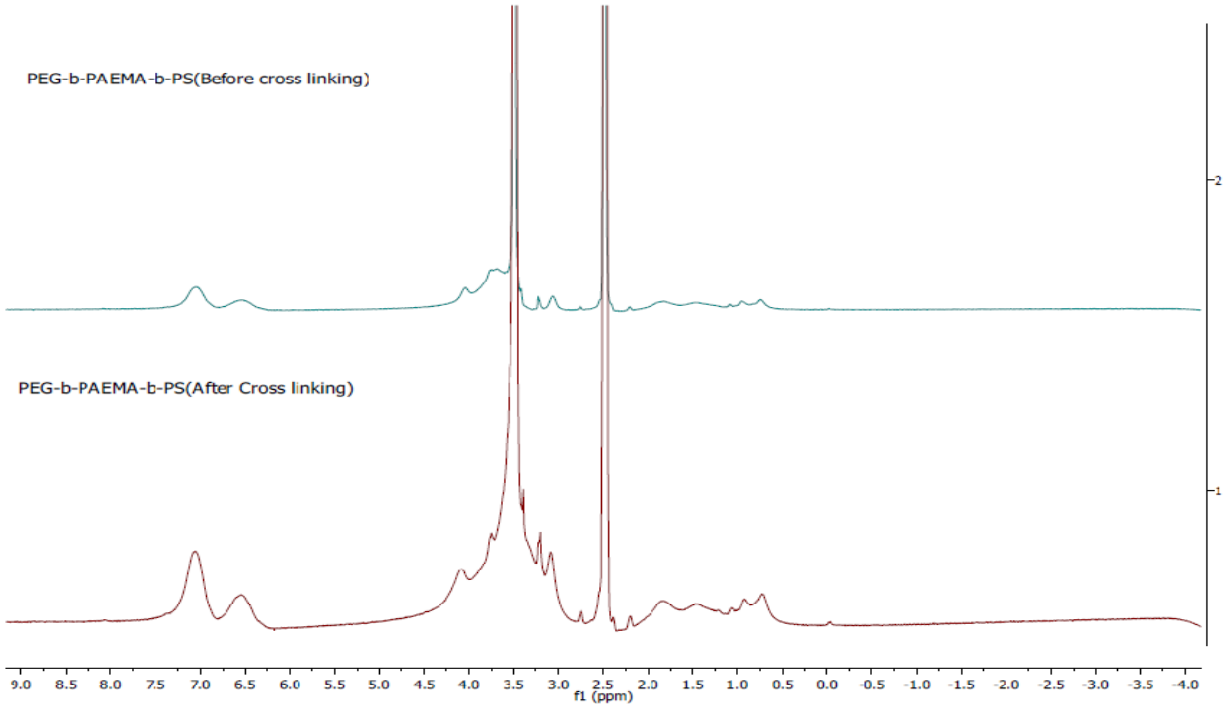

Figure S2. ^{1}H-NMR Spectra of the lyophilized micelle in ^{6}d-DMSO, before cross-linking, **3** and after cross-linking, **4**.

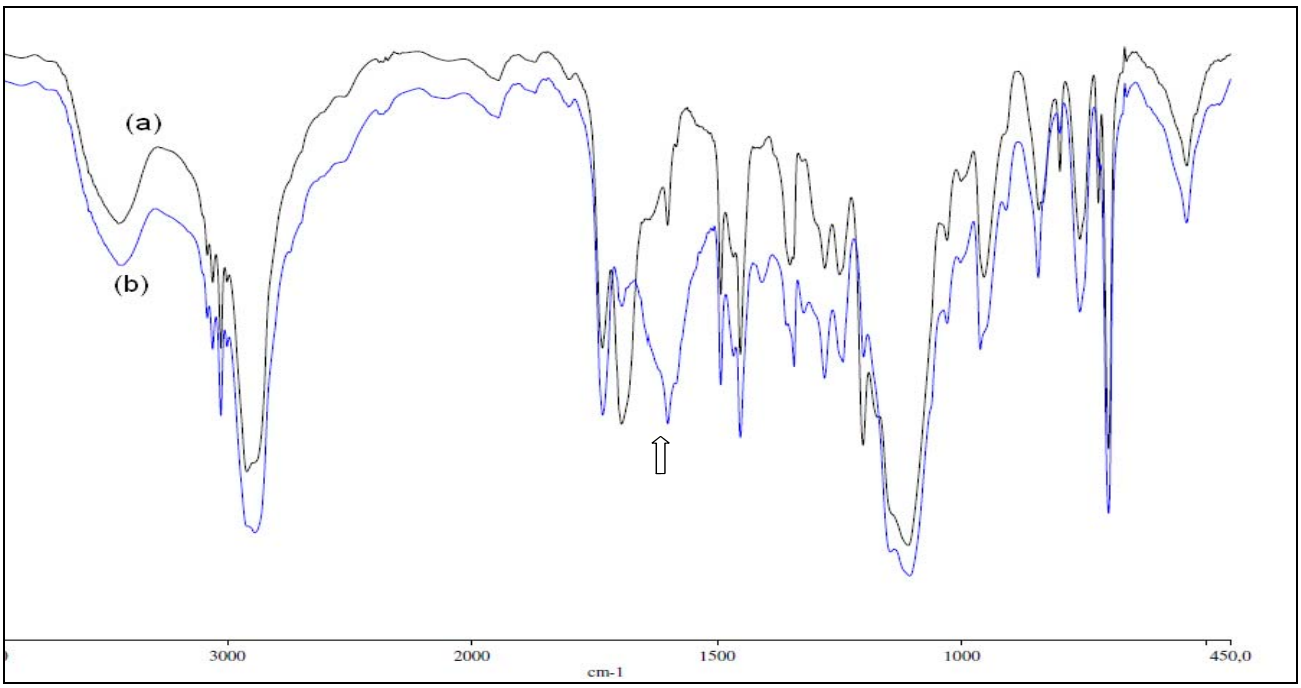

Figure S3. (a) FT-IR spectra of PEG-*b*-PAEMA-*b*-PS micelle (**3)** and (b) cross-linked micelle, **4**, arrow in (b) indicates the overlapped amide I and II bands after cross-linking.

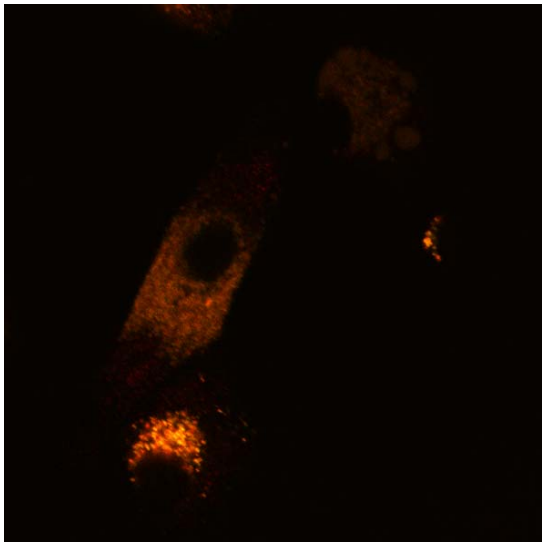

Figure S4. Fluorescence microscopic image of nanosensor (SCMN) uptake by HeLa cells.

6. References

1. Liu, S.; Weaver, J. V. M.; Tang, Y.; Billingham, N. C.; Armes, S. P.; Tribe, K., Synthesis of Shell Cross-Linked Micelles with pH-Responsive Cores Using ABC Triblock Copolymers. *Macromolecules* **2002,** *35* (16), 6121-6131.
2. Dufresne, M.-H.; Leroux, J.-C., Study of the Micellization Behavior of Different Order Amino Block Copolymers with Heparin. *Pharmaceutical Research* **2004,** *21* (1), 160-169.
3. Kaiser, E.; Colescott, R. L.; Bossinger, C. D.; Cook, P. I., Color test for detection of free terminal amino groups in the solid-phase synthesis of peptides. *Analytical biochemistry* **1970,** *34* (2), 595-8.

Appendix B

Pramod Kumar EK, Lise N. Feldborg, Kristoffer Almdal and Thomas L. Andresen. ‘‘Synthesis of core cross-linked polymeric core-shell-corona functional micelle based triple fluorophore nanosensors for broad range ratiometric pH measurements’’. *Adv. Funct. Mater*. **2012** (Submitted).

Submitted to ADVANCED FUNCTIONAL MATERIALS

DOI: 10.1002/adfm.((please insert DOI)

Synthesis of core cross-linked polymeric core-shell-corona functional micelle based triple fluorophore nanosensors for broad range ratiometric pH measurements

By Pramod Kumar EK, Lise N. Feldborg, Kristoffer Almdal and Thomas L. Andresen*

[*] Dr. T. L. Andresen
DTU Nanotech, Department of Micro-and Nanotechnology
Technical University of Denmark, Building 423
2800 Lyngby, Denmark
E-mail: Thomas.andresen@nanotech.dtu.dk.

Keywords: amphiphilic triblock copolymers, functional micelle, dendritic click core cross-linking, polymeric micelle nanosensors, pH nanosensors.

We describe the conversion of core cross-linked amphiphilic triblock core-shell-corona functional polymeric micelles into nanosensors for fluorescence based ratiometric pH monitoring. This is achieved via atom transfer radical polymerization (ATRP), principle of self-assembly and post micelle modifications. The amphiphilic triblock copolymer poly(ethylene oxide)$_{120}$-b-poly((((trimethylsilyl)ethoxy)carbonyl) aminoethyl methacrylate)$_8$-b-poly((trimethylsilylethynyl) styrene)$_{26}$ (PEG_{120}-b-PAEMA(Teoc)$_8$-b-PES(TMS)$_{26}$ is synthesized by ATRP. Removal of protecting groups followed by self-assembly in water results in poly(ethylene oxide)$_{120}$-b-poly(2-aminoethyl methacrylate)$_8$-b-poly(4-ethynylstyrene)$_{26}$ (PEG_{120}-b-$PAEMA_8$-b-PES_{26}) functional micelles. Dendritic core cross-linking of the micelles is performed by copper catalyzed azide-alkyne Huisgen 1,3-dipolar cycloaddition (CuAAC) known as the click reaction. The robust micelles are then converted into ratiometric pH nanosensors by binding pH sensitive and reference fluorophores to the PAEMA shell. Fluorescence measurements show that the sensor is sensitive, reversible and quickly responsive between the pH of 4.5 to 7.5.

1. Introduction

The combination of controlled radical polymerization and click chemistry is nowadays extensively used for the preparation of polymeric nanomaterials. [1-3] Recent achievements in giving living characteristics to the radical polymerization [4-9] have been able to provide simple and efficient ways of synthesizing amphiphilic block copolymers with well defined composition as well as a narrow molecular weight distribution. By controlling the block copolymer composition (packing parameters) [10, 11] and conditions for assembly in solution, a wide range of morphologies [12-14] can be achieved by the spontaneous self-assembly of amphiphilic block copolymers. The amphiphilic diblock copolymers in block selective solvents give polymeric micelles having a spherical core-shell morphology [15] whereas the amphiphilic linear triblock (ABC) copolymers give core-shell-corona spheres or cylinders.[16, 17] Many of the potential biomedical applications of these well known pharmaceutical carriers [18, 19] require stabilization by covalent cross-linking; enabling the resulting robust nano morphology to maintain its structural integrity under various conditions.[20-22] Copper(I) catalysed Huisgen 1,3-dipolar cycloadditions between azides and alkynes to yield triazoles are extensively used for functional modifications and cross-linking of diblock copolymer micelles due to its orthogonality and compatibility with other functional groups.[23, 24] As a result of the risks of intermicellar cross-linking or aggregation, the click cross-linking at the core [25] or shell region [26] of the diblock micelles are reported under very dilute conditions. In the case of triblock copolymer micelles, the presence of polyethylene glycol (PEG) coronal chains on a well defined core-shell-corona micelle will not only ensure primarily shell [27, 28] intramicellar cross-linking at high block copolymer concentration due to steric stabilization mechanisms,[29] but will also protect the functionalities introduced at the shell or core regions from the external surroundings. The protective PEG corona of this well known pharmaceutical carriers [30] could also provide prolonged

circulation in blood and hence improve the effective accumulation in desired regions by the enhanced permeation and retention effect (EPR).[31, 32]

Compared to the diblock core-shell micelle, even with the potential to provide diversity in applications, regioselective functionalization and stabilization, the three layer core-shell-corona-micelles are not investigated considerably. This is due to its structural complexity and synthetic difficulties in unimers synthesis. Synthesis of functional core-shell-corona micelles required the synthesis of functional triblock copolymers. The functional block copolymers (unimers) can be synthesized by controlled radical polymerization, in which transition metal catalyzed ATRP provide an easy and efficient way.[33] ATRP in functional block copolymer synthesis is associated with protection and de-protection chemistry. The two main reasons for incorporation of protection chemistry in block copolymer synthesis is the sensitivity of the functional monomer towards the transition metal catalyst as well as the stability of the monomer under ATRP conditions.[34] Selection of monomer protecting groups for the synthesis of block copolymers having more than one functional block is a critical issue as the protecting groups should be stable throughout the ATRP process and should be cleaved easily and simultaneously under mild conditions. In addition to this, functional modification and covalent cross-linking at the hydrophobic core domains of the amphiphilic triblock copolymer self assembly require accessibility of reactants and catalysts into this domain. Hence the reagents should transverse the corona, shell and core-shell interface of the micelle and should be soluble in the hydrophobic core domain. [21]

Intracellular pH measurements provide information about the pH dependant cellular process [35] and pH sensitive drug delivery. [36] As a consequence of this number of nanoparticle especially polymeric nanoparticle based nanosensors for ratiometric pH measurements are developed. [37-41] It

is interesting but not surprising that even with the excellent pharmaceutical advantages[42] of polymeric micelle, are not utilized in pH nanosensor fabrication due to synthetic difficulties and structural instability under infinitely diluted biological conditions. In continuation with our interest to synthesize polymeric nanosensors for intracellular pH measurements, [40, 43] we will in this paper elucidate the first synthesis of click core cross-linked core-shell-corona functional polymeric micelles into ratiometric pH nanosensors by ATRP, self-assembly and dimensional synthetic organic chemistry.

2. Results and Discussion

Schematic representation of the polymeric micelle based core cross-linked ratiometric pH nanosensor fabrication is shown in Figure 1. The amphiphilic triblock copolymer poly(ethylene oxide)$_{120}$-b-poly((((trimethylsilyl)ethoxy)carbonyl) aminoethyl methacrylate)$_8$-b-poly((trimethylsilylethynyl) styrene)$_{26}$ (PEG$_{120}$-b-PAEMA(Teoc)$_8$-b-PES(TMS)$_{26}$ (**1**) was synthesized by isolated macrointiator atom transfer radical polymerization (ATRP) (Scheme 1a). The presence of Teoc and TMS protecting groups on the polymer were confirmed by NMR (^{1}H NMR, $CDCl_3$), δ = 0.00 ppm and 0.22 ppm respectively (Figure 2a). FTIR spectroscopy confirmed the carbonyl and aromatic (C=C) stretching of PAEMA(Teoc) and PES(TMS) blocks *ca.* 1700 cm^{-1} and 1500 cm^{-1} respectively. The number-average molecular weight (M_n) of the polymers measured by gel permeation chromatography (GPC) in THF with polystyrene as standard was higher than that calculated from ^{1}H-NMR spectroscopy. The GPC analysis and ^{1}H NMR spectroscopic results are summarized in Table 1.

The silyl protecting groups of the amphiphilic triblock copolymers were removed by the treatment with 1M tetrabutylammonium fluoride (TBAF) in THF. The common solvent (THF) was slowly

displaced by a selective solvent (water) and the micelles were kinetically trapped by dialysis against MilliQ water. A portion of the micelles was lyophilized for characterization. The complete de-protection of TMS and Teoc groups was confirmed by the disappearance of nuclear magnetic resonance of the $-SiC(CH_3)_3$ at δ 0.22 ppm and 0.00 ppm respectively (Figure 2b). Appearance of alkyne (-C≡CH) proton resonance at 3.06 ppm in NMR and -C≡**C-H** stretching at *ca.* 3250 cm^{-1} in FTIR further confirms the TMS de-protection. Positive Kaiser test [44] for the lyophilized micelle (appearance of blue colour) and the increase in zeta potential of the micelle solution due to Teoc de-protection of the amino groups further confirmed the presence of free amino groups at the shell region of the micelle (Table 2, micelle 1 & 4).

Synthesis of the click core cross-linked pH nanosensors is shown in Scheme 2. The poly(4-ethynyl styrene) (PES) core of the de-protected PEG_{120}-b-$PAEMA_8$-b-PES_{26} micelle (**4**) was swollen by dialyzing against 4:1 buffered water:THF. The swollen solvent filled core enhances the solubility of the hydrophobic dendritic azide benzyl ether cross linker (**3**) in the hydrophobic nanodomain. The dendritic cross-linker was synthesized via nucleophilic substitution of benzyl mesylate of the dendritic benzyl alcohol (**2**) by sodium azide (Scheme 1b). The click reaction was performed between the click readied hydrophobic core and the dendritic cross-linker using $CuBr(PPh_3)_3$/DIPEA as a catalyst at high block copolymer concentrations (2.5 mg/mL). The click core cross-linked micelle (**5**) was purified by dialysis. DLS measurements of the cross-linked micelles in MilliQ water showed no significant change in the hydrodynamic diameter of the micelle after cross-linking. This confirm intramicellar core cross-linking of the more confined core-shell-corona micelle at high block copolymer concentration (Table 2, micelle 5). IR spectra of the lyophilized PEG_{120}-b-$PAEMA_8$-b-PES_{26} micelle before and after core cross-linking show the disappearance of -C≡C-**H** stretching absorption at *ca.* 3250 cm^{-1} and the appearance of a strong -

N≡N asymmetric stretching absorption from the azide at *ca.* 2100 cm^{-1} after cross-linking. This confirms the consumption of alkyne functionality at the core domain and the presence of excess azide groups on the cross-linker of the core cross-linked micelle (Figure 3). Characterization of the cross-linked micelle by NMR was unsuccessful due to solubility problems in deuterated solvents.

The core cross-linked micelle was converted into a ratiometric pH nanosensor (**6**) by binding pH sensitive (Fluorescein and Oregon green) and reference (Rhodamine B) fluorophores at the shell region of the micelle. In an alkaline buffer few of the free amino groups present at the PAEMA shell of the core cross-linked micelle were nucleophilically attacked at the central elctrophilic carbon atoms of the pH sensitive and reference fluorophore-isothiocyanates. The un-reacted free dyes from the thiourea product were removed by extensive dialysis against a carbonate buffer followed by dialysis against MilliQ water. DLS measurements show that the nanosensor (**6**) in MilliQ water have approximately same hydrodynamic diameter as that of the cross-linked micelle (**5**), however, the zeta potential measurements show a slight decrease in surface charge density as a result of fluorophore binding (Table 2, micelle 6).

2D and 3D Atomic force microscopic (AFM) images of micelle **4**, **5** and **6** absorbed on a hydrophilic silica surface are shown in Figure 4. Compared to the non-cross linked micelle (**4**), the robust cross-linked micelle (**5**) and nanosensor (**6**) shows significant increase in average height (H_{av}) calculated by AFM measurements (Table 2). The significant increase in nanoparticle heights (H_{av}) during core cross-linking indicates that the extent of interaction between the spherical nanoparticles and the silica substrate changes considerably after cross-linking. Core cross-linking using the hydrophobic benzyl ether cross-linker enhances the hydrophobicity of the polystyrene core via covalent reinforcement to the hydrophobic interactions at the core domain. The resulting

hydrophobic core of the robust micelle strongly repels the hydrophilic silica surface (less flattening on the surface) and as a result of this hydrophobic hydrophilic repulsion, the nanoparticle height increases. The fluorophores binding to the core cross-linked micelles do not show further significant increase in the height of the resulting nanosensors .Thus the AFM studies revels the effect of core cross linking on the core-shell-corona micelle-surface interactions.

DLS measurements of aqueous micelle solutions at different temperature were performed to confirm the solution stability of this block copolymer self-assembly. By heating the micelle solutions from 25^0C to 70^0C, thermodynamically favoured micelle dissociation of non-cross-linked micelle (**4**) occurred ca. 65^0C, and there after no self-assembled structures were detectable. But the cross-linked micelle (**5**) and nanosensor (**6**), were maintained their structural integrity through out the experiments, and provides an additional evidence for the covalent cross-linking between the unimers of this nanoparticle scaffolds (Figure 5).

A pH calibration curve for the nanosensors was constructed by fluorescence measurements. The pH sensitive Oregon green and Fluorescein (OG and FA) and reference fluorophores Rhodamine B (RhB) of the nanosensors were excited in buffer of different pH. The fluorescence intensity ratio ($(I_{OG} + I_{FA})/I_{RhB}$) was then plotted against the corresponding pH. This calibration curve confirms the covalent attachment of pH sensitive and reference fluorophores to the PAEMA shell of core cross-linked core-shell-corona micelle, and demonstrate that the resulting pH nanosensor is sensitive between the pH 4.5 to 7.5 (Figure 6). Reversibility and time of response for the nanosensor were also measured by fluorescence spectroscopy (Figure 7). The measurements show that the sensors are quickly responding (with in micro seconds) towards the change in pH and are reversible between any two pH with in the broad pH sensitivity range.

3. Conclusions

Polymeric micelle based click core cross-linked ratiometric pH nanosensors were prepared. Functional triblock copolymers were synthesized by atom transfer radical polymerization of protected functional monomers. The functional micelle resulting from the self-assembly of functional unimers was cross-linked by dendritic click reactions at the hydrophobic core. The core cross-linked core-shell-corona micelle having a radially compartmentalized corona was converted into triple fluorophore pH nanosensors by binding pH sensitive and reference fluorophores at the inner corona (shell) region. The sensor was sensitive between the pH ca. 4.5-7.5, and reversible and quickly responsive between this broad pH range. The ratiometric fluorescence intensity measurements could eliminate the errors in pH measurements due to source fluctuation and fluorophore concentrations. The covalent cross-linking between the unimers of this nanoparticle scaffold could enhance its biomedical applications by preventing the dissociation of the sensor under infinitely diluted biological conditions even below the critical micelle concentration (CMC) of the micelles. The presence of excess azido functionalities on the dendritic cross-linkers of the cross-linked core provides opportunities to bind hydrophobic cargoes at the core region. The presence of excess amino groups at the hydrophilic shell region (PAEMA) of the micelle could allow the incorporation of cargoes into it. The presence of PEG corona chains not only provides long circulation half life of the nanosensors in blood and hence effective accumulation in the desired region, but also could protect the cargo attached to the shell and core region of the micelle nanosensors. In conclusion an advanced pH nanosensors suitable for intracellular pH measurements has been developed. The transformation of pharmaceutical carriers into sensors may be capable of

providing information about pH sensitive drug release. Further studies of the micelle nanosensors in vivo are under progress.

4. Experimental

Materials and measurements: poly (ethylene glycol) monomethylether (Mn = 5000), 2-Bromo-isobutyryl-bromide (98 %), dichlorobis(triphenylphosphine)palladium(II) (98 %), copper(I) iodide (98%), (Trimethylsilyl)acetylene (98 %), 4-Bromostyrene (98 %), 2-Aminoethyl methacrylate hydrochloride (AEMA HCl) (90 %), 1-[2-(Trimethylsilyl)ethoxycarbonyloxy] pyrrolidin-2,5-dione, 2,2'-bipyridyl (bpy) (99 %), anisol (anhydrous) (99.7 %), 4,4′-Dinonyl-2,2′-dipyridyl (dNbpy) (97%), N,N-Diisopropylethylamine (DIPEA) (99.5 %), Dialysis tubing (MWCO = 12kDa), Tetrabutylammonium fluoride (1M THF solution), Methanesulfonyl chloride (MsCl) (99.7 %) and Sodium azide were purchased from Sigma Aldrich and used as obtained. CuCl (99.995 %) was washed with glacial acetic acid, followed by absolute ethanol and diethylether, dried and stored under argon. Triethylamine (TEA) was distilled from calcium hydride and stored under molecular sieves (4 Å), methanol used for ATRP was purified by distillation over the drying agent $Mg(OMe)_2$, stored over molecular sieves (3 Å) and was transferred under argon, $CuBr(PPh_3)_3$ and Dendritic alcohol $(OH)_4$-[G-1] (**2**) were synthesized by literature procedures [45, 46]. Argon atmosphere (99.9999 %) used in the reactions was provided by AGA Denmark. All other solvents and chemicals were purchased from Sigma Aldrich and used as obtained. NMR spectra were recorded by using a 300 MHz Varian Mercury 300 BB spectrometer, IR spectra were recorded by Perkin Elmer Spectrum 100 FT-IR Spectrometer, GPC measurements were carried out with a Viscotek refractive index detector and PL Gel Mixed-C+D column with a flow rate of 0.5 mL/min at 25^0C using THF as eluent. Fluorescence measurements were carried out by the Olis Line of SLM based Spectrofluorimeter. Samples for atomic force microscopy (AFM) were prepared by placing a 5 µl

drop of the nanoparticle suspension on a silicon wafer. The particles were allowed to settle for 30 minutes, before excess liquid were removed using the corner of a lens-cleaning tissue. AFM images were obtained by PSIA XE-150 scanning force microscope using non-contact tapping mode close to resonance frequency of the silicon cantilever (Nanoworld, pointprobe type, force constant 42 N/m and tip radius <12 nm) of around 320 kHz. All images were recorded under atmospheric conditions. Dynamic light scattering (DLS) and zeta potential measurements were carried out by Brookhaven Zeta PALS instrument.

Synthesis of 2-(((2-(trimethylsilyl)ethoxy)carbonyl)amino)ethyl methacrylate(AEMA-Teoc): 2-Aminoethylmethacrylate hydrochloride (AEMA HCl) (590 mg, 3.56 mmol) was dissolved in 15 mL of dry DCM. Anhydrous triethylamine (1.080 mL, 10.68 mmol) and 1-[2-(Trimethylsilyl)ethoxycarbonyloxy]pyrrolidin-2,5-dione (1015 mg, 3.916 mmol,) were added and stirred at room temperature under argon atmosphere for 7 h. The progress of the reaction was monitored by TLC (Ethylacetate : Hexane (1:1) $R_{f(product)}$ = 0.56). The reaction mixture was diluted with 50 mL of DCM, then washed with 5 % HCl (2 × 20 mL) followed by saturated sodium bicarbonate (2 × 20 mL) and brine (2 × 20 mL). The organic layer was dried over anhydrous sodium sulfate, filtered, and removal of solvent under reduced pressure gave a pale pink crystalline solid. Isolated yield: 0.8 g (82 %). ^{1}H NMR (300 MHz, $CDCl_3$): δ = 6.08 (d, 1 H; vinylic), 5.55 (d, 1 H; vinylic), 4.84 (br s, 1 H; -N**H**), 4.20 (t, 2 H; -NHCH$_2$C**H**$_2$O), 4.12 (t, 2 H; -NHCOOC**H**$_2$CH$_2$), 3.44 (m, 2 H; -NHC**H**$_2$CH$_2$O), 1.91 (s, 3 H; -C**H**$_3$), 0.97 (t , 2 H; -NHCOOCH$_2$C**H**$_2$), 0.001 (s, 9 H; -Si(C**H**$_3$)$_3$); FT-IR: υ = 3344, 1701, 1636, 1524, 1453, 1246, 1158, 1042, 833 cm^{-1}.

Synthesis of 4-(Trimethylsilylethynyl) styrene (ESTMS): The monomer was synthesized by modifying the previously reported reaction [47]. To a solution of 4-Bromostyrene (2.357 mL, 18

mmol) in 165 mL of TEA, small amounts of hydroquinone (to prevent polymerization), (Trimethylsilyl)acetylene (3.415 mmol, 24 mmol), Bis(triphenylphosphine)palladium(II) dichloride (0.252 g, 0.36 mmol), and copper(I) iodide (33 mg, 0.18 mmol) were added and the reaction mixture stirred for 6 h at 55 °C under argon atmosphere. The progress of the reaction was monitored by TLC ($R_{f(product)}$ = 0.28 in hexane). The reaction mixture was filtered and solvent was evaporated under vacuum .The residue was washed with water, extracted with hexane and dried over anhydrous sodium sulfate. After filtration and evaporation, a pale yellow liquid product was isolated by column chromatography on silica gel using hexane as eluent; yield: 1.810 g (50 %). ^{1}H NMR (300 MHz, $CDCl_3$,) δ = 7.45 (d, 2H; o-Ar**H**), 7.33 (d, 2H; m-Ar**H**), 6.69 (dd, J = 11.2, 17.6 Hz, 1H; CH_2=C**H**), 5.79 (d, J = 17.6 Hz, 1H; trans C**H**$_2$=CH)), 5.29 (d, J = 11.2 Hz, 1H; cis C**H**$_2$=CH), 0.22 (s, 9 H; -Si(C**H**$_3$)$_3$); FT-IR: υ = 3085, 2958, 2896, 2155, 1627, 1503, 1400, 1249, 1113, 1013, 986, 910, 856, 833 cm^{-1}.

Synthesis of PEG_{5000}-Br: The macrointiator was synthesized by a procedure reported in literature [48]*:* CH_3O-PEG-OH, Mn = 5000 (5 gram, 1 mmol) was dissolved in 60 mL of toluene. After azeotropic distillation of 10 mL of toluene under reduced pressure to remove traces of water, TEA (0.278 mL, 2 mmol) was added and the solution was cooled to room temperature. 2-bromoisobutyryl bromide (0.185 mL, 1.5 mmol) was added dropwise and the reaction mixture was stirred at 40 ^{0}C for 2 days under a calcium chloride guard tube. The solution was filtered and most of the toluene was removed by rotary evaporation prior to precipitation into 10 fold excess of cold ether. The crude polymer was dried under vacuum, dissolved in water at pH 8-9 and then extracted with DCM. The organic layers were collected and dried over anhydrous sodium sulfate. The removal of the solvent under reduced pressure afforded the purified macroinitiator in a yield of 99

%. ^{1}H NMR (300 MHz, $CDCl_3$): δ = 3.63 (s, -C**H**$_2$C**H**$_2$O-), 1.91 (s, -C(C**H**$_3$)$_2$); FT-IR: υ = 2887, 1737, 1466, 1359, 1342, 1279, 1241, 1148, 1107, 1060, 963, 841 cm^{-1}.

Synthesis of diblock copolymer (PEG-b-PAEMA(Teoc)-Cl): PEG-Br (1 gram, 0.189 mmol), AEMA-Teoc (516 mg , 1.89 mmol), 2,2'-bipyridyl (59 mg, 0.378 mmol) and 5 mL of dry methanol were added to a 25 mL schlenk flask equipped with a stirrer bar. The flask was frozen in liquid nitrogen and CuCl (21 mg, 0.20 mmol) catalyst was added. The reaction mixture was then degassed with three freeze-pump-thaw cycles (each 15 minute long) to remove the oxygen and the polymerization was carried out at 40 ^{0}C for 18 h under argon atmosphere. The resulting polymer was passed through a silica gel column to remove the copper catalyst using methanol as eluent. Most of the methanol was removed by rotary evaporation and the polymer was precipitated into excess cold diethyl ether, isolated by filtration, and the precipitate dried under vacuum; yield 0.9 g (63 %). ^{1}H NMR (300 MHz, $CDCl_3$): δ = 4.11-3.72 (-NHCH$_2$C**H**$_2$O, -NHCOOC**H**$_2$CH$_2$), 3.60 (s, -C**H**$_2$C**H**$_2$O), 3.41-3.30 (-NHC**H**$_2$CH$_2$O), 2.00-1.73 (-C**H**$_2$ of the polymer backbone), 1.33-0.82 (-C**H**$_3$ of the polymer backbone, -NHCOOCH$_2$C**H**$_2$), 0.001 (s, -Si(C**H**$_3$)$_3$); FT-IR: υ = 3341, 1718, 1642, 1529, 1464, 1341, 1240, 1104, 960, 839 cm^{-1}.

*Synthesis of triblock copolymer (PEG-b-PAEMA(Teoc)-b-P(ESTMS))(**1**):* The diblock copolymer PEG-PAEMA(Teoc)-Cl (500 mg, 0.067 mmol), 5 mL anisole, 4,4′-Dinonyl-2,2′-dipyridyl (55 mg, 0.134 mmol) and ESTMS (402 mg, 2.01 mmol) were added to a 25 mL schlenk flask equipped with a stirrer bar. The reaction mixture was frozen under liquid nitrogen, CuCl (7.2 mg, 0.073 mmol) was added and degassed with three freeze-pump thaw cycles and stirred under argon at 130 ^{0}C for 30 h. After removing most of the solvent under vacuum, the polymer was precipitated into excess cold diethyl ether and dried under vacuum; yield 0.5 g (58 %). The polymer was further purified by

dissolving in THF (10 mg/mL) and dialyzed (MWCO = 12 kDa) against MilliQ water. From dynamic light scattering (DLS) of the micelle dispersion, number average hydrodynamic diameter (D_h) was found to be 23±3 nm and zeta potential measurement showed (ξ) = -16±2 mV. The micelle solution was lyophilized to get the pure polymer. ^{1}H NMR (300 MHz, $CDCl_3$): δ = 7.47-6.22 (m, Ar**H**), 4.18-3.72 (-NHCH$_2$C**H**$_2$O, -NHCOOC**H**$_2$CH$_2$), 3.60 (s, -C**H**$_2$C**H**$_2$O), 3.50-3.31 (-NHC**H**$_2$CH$_2$O), 2.04-0.60 (PAEMA and PES backbone, -NHCOOCH$_2$C**H**$_2$), 0.22 (s, -Si(C**H**$_3$)$_3$ of PESTMS), 0.00 (s, -Si(C**H**$_3$)$_3$ of PAEMA(Teoc)); FT-IR: υ = 3300, 2160, 2106, 1719, 1504, 1448, 1342, 1248, 1103, 962, 840 cm^{-1}. Kaiser test of the polymer was performed, the colourless solution indicate completely protected amino groups.

PEG$_{120}$-b-PAEMA$_8$-b-PES$_{26}$ *micelle* ***(4):*** The triblock copolymer PEG-b-PAEMA(Teoc)-b-P(ESTMS) (150 mg, 0.011 mmol) was dissolved in 9 mL of THF, followed by addition of 1M TBAF in THF (0.318 mL, 1.1 mmol) and stirred at room temperature for 5 h. The reaction mixture was diluted drop wise with 40 mL MilliQ water. The resulting cloudy micelle solution was transferred to a dialysis tube (MWCO = 12 kDa) and dialyzed against MilliQ water for three days. The final micelle concentration was 2.5 mg/mL (D_h = 20±1 nm and (ξ) = 11±2 mV). A portion of the micelle was lyophilized for characterization. ^{1}H NMR (300 MHz, $CDCl_3$): δ = 7.50-6.10 (m, Ar**H**), 4.25-3.45 (-COOC**H**$_2$CH$_2$NH$_2$, -C**H**$_2$C**H**$_2$O), 3.45-3.31 (-CH$_2$C**H**$_2$NH$_2$), 3.27-2.85 (br s, -C≡C-**H**), 1.90-0.70 (PAEMA and PES backbone); FT-IR: υ = 3500, 3289, 3241, 2106, 1725, 1501, 1450, 1342, 1241, 1103, 961, 840 cm^{-1}. Positive Kaiser test (blue colour) indicates the presence of free amino groups.

*Synthesis of dendritic cross linker ((N$_3$)$_4$-[G-1]) (**3**):* The dendritic alcohol (HO)$_4$-[G-1] (**2**) (500 mg, 0.73 mmol) and triethylamine (0.610 mL, 4.35 mmol) were dissolved in 5 mL of DMF and

allowed to stir for 15 min at room temperature. The mixture was then cooled to 0 ^{0}C, Methanesulfonyl chloride (0.340 mL, 4.35 mmol) was added dropwise, warmed to room temperature and stirred for 12 h under argon. Then NaN_3 (570 mg, 8.75 mmol) was added and the reaction mixture was allowed to stir at 90 ^{0}C for another 18 h under argon. The progress of the reaction was monitored by TLC (10 % MeOH in DCM, $R_{f(product)}$ = 0.56). The reaction mixture was poured into brine and extracted with DCM (3×20 mL) and washed with saturated sodium bicarbonate (2×20 mL). The combined organic layers were dried over anhydrous sodium sulfate, filtered, concentrated via rotary evaporation and the residue dried under vacuum ; yield 0.45 g (90 %). ^{1}H NMR (300 MHz, $CDCl_3$): δ = 7.78 (s, 2H; 2-triazole **H**), 6.93 (s, 4 H; Ar**H**), 6.92 (s, 2 H; Ar**H**), 5.24 (s, 4 H; traizole-C**H**$_2$O), 4.53 (t, J = 5 Hz, 4 H; triazole-C**H**$_2$CH$_2$OCH$_2$), 4.34 (s, 8 H; -C**H**$_2$N$_3$), 3.85 (t, J = 5 Hz, 4 H; triazole-CH$_2$C**H**$_2$OCH$_2$), 3.56 (s, 4 H; triazole-CH$_2$CH$_2$OC**H**$_2$); FT-IR: υ = 3150-2850, 2090, 1597, 1453, 1293, 1116, 1048, 839 cm^{-1}.

*Synthesis of cross-linked micelle (**5**):* 30 mL (75 mg, (2.5 mg/mL) of the PEG_{120}-b-$PAEMA_8$-b-PES_{26} micelle solution was transferred into dialysis tube (MWCO = 12 kDa) and dialyzed against 4:1 buffered water: THF for three days. The micelle solution (75 mg, 0.153 mmol of alkyne equivalent) was transferred into 100 mL round bottom flask, added $CuBr(PPh_3)_3$ (42.78 mg, 0.046 mmol), DIPEA (80 μL, 0.46 mmol), Cu wire (to prevent oxidation of the catalyst) (ca. 100 mg), and the cross-linker $(N_3)_4$-[G-1] (in 2.5 mL of THF) (52.6 mg, 0.077 mmol). The reaction mixture was stirred for 3 days at room temperature and then transferred to a dialysis tube of (MWCO = 12 kDa) and dialyzed against MilliQ water and THF (4:1) for 4 days and then against MilliQ water for another 4 days. The final concentration of the micelle was 2 mg/mL (D_h = 22±2 nm and zeta potential (ξ) = 10±2 mV). A portion of the micelle was lyophilized for characterization. ^{1}H NMR:

Solubility of the cross-linked micelles in deuterated solvents was very low. FT-IR: υ = 3460, 3138, 2872, 2099, 1721, 1600, 1453, 1346, 1290, 1101, 948, 833 cm^{-1}.

*Preparation of pH nanosensors (**6**):* The cross-linked PEG_{120}-b-$PAEMA_8$-b-PES_{26} micelle solution (15 mL, 30 mg, 0.0023 mmol) in MilliQ water was dialysed against carbonate buffer (pH = 9) for three days, transferred into 100 mL round bottom flask, FITC (0.020 mg, 0.0525 µmol), Oregon Green ITC (0.022 mg, 0.0525 µmol) and RhBITC (0.01 mg, 0.021 µmol) were added and stirred at room temperature for 12 h in the absence of light. The reaction mixture was then transferred to dialysis tubing (MWCO = 12 kDa), dialysis against carbonate buffer (pH = 9) for three days and then against MilliQ water for another three days (D_h = 23±1 nm, ξ = 7±3 mV).The sensor solution was covered with aluminium foil to protect from the light, if protected from the light the sensor was capable to maintain same sensitivity for several weeks.

Acknowledgements: The authors would like to thank Kræftens Bekæmpelse and the Danish Research Council for Technology and Production (Grant 274-07-0172) for financial.

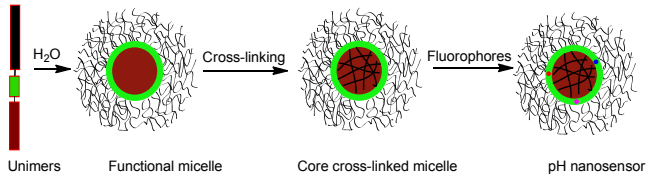

Figure 1. Core cross-linked ratiometric pH nanosensors synthesized from self-assembly of functional amphiphilic triblock copolymers (unimers).

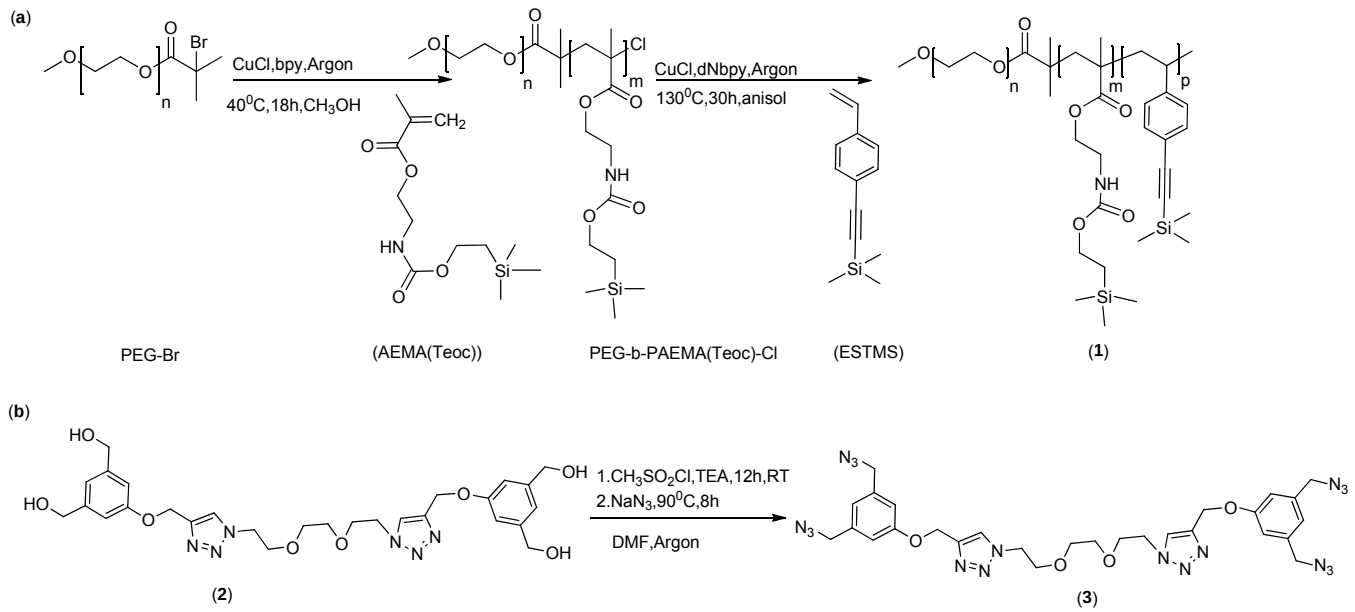

Scheme 1. a) Synthesis of amphiphilic triblock copolymer PEG-b-PAEMA(Teoc)-b-PES(TMS). b) Synthesis of dendritic azide cross-linker. bpy = 2,2'bipyridine, dNbpy = 4,4′-Dinonyl-2,2′-dipyridyl, TEA = triethylamine, DMF = N,N-Dimethylformamide.

Table 1. Molecular weight of PEG$_n$-b-PAEMA(Teoc)$_m$-b-PES(TMS)$_p$ (1)

M_n[a]	M_w[a]	M_w/M_n[a]	M_n[b]	n[c]	m [c]	p [c]
13700	16850	1.23	12670	120	8	26

[a] Determined by GPC, [b] determined by NMR, [c] number of repeating units of PEG block (n), PAEMA(Teoc) block (m) and PES(TMS) block (p).

Table 2. Characterization data for micelles 1, 4 and 5 and pH nanosensor 6

Micelle	DLS(D_h)[a] (nm)	AFM[b] H_{av}(nm)	Zeta(ξ)[c] (mV)
1[d]	23±3	…….	-16±2
4	20±1	05±1	+11±2
5	22±2	13±3	+10±2
6	23±1	14±3	+7±3

[a] Number averaged hydrodynamic diameter of the polymeric micelles in MilliQ water by dynamic light scattering, [b] average height of the micelles were calculated from the values for *ca.* 100 particle by tapping mode AFM, [c] zeta potential from 10 determination of 10 cycles and [d] micelle of (**1**).

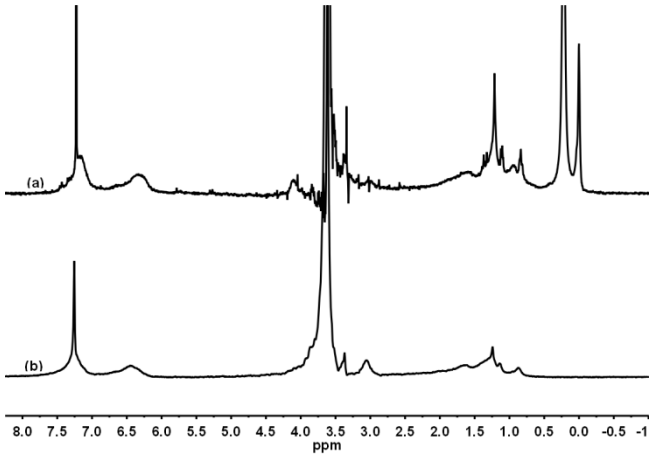

Figure 2. ^{1}H NMR spectra of a) PEG_{120}-b-$PAEMA(Teoc)_8$-b-$PES(TMS)_{26}$ (**1**) and b) lyophilized PEG_{120}-b-$PAEMA_8$-b-PES_{26} (**4**), in $CDCl_3$ without containing tetramethylsilane as an internal standard.

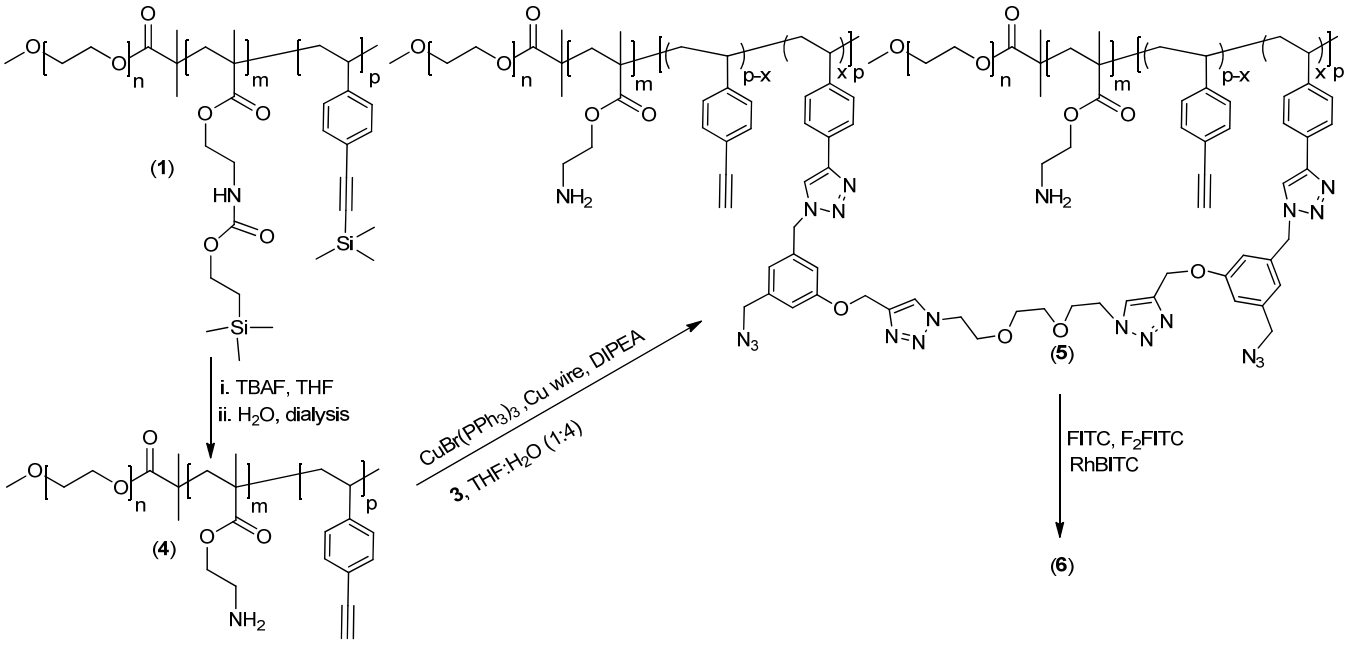

Scheme 2. Synthesis of click core cross-liked ratiometric pH nanosensors. The cross-linking reaction was performed by dendritic azide cross-linker (0.5 equiv) (**3**), the minimum click core cross-linking potential of a single cross-linker molecule is shown in the scheme. TBAF = Tetrabutylammonium fluoride, DIPEA = N,N-Disopropylethylamine, FITC = Fluorescein isothiocyanate, F_2FITC = Oregon Green 488 isothiocynate, RhBITC = Rhodamine B isothiocyanate; at 100% cross-linking, p = x.

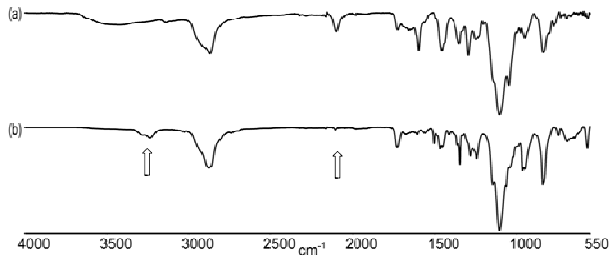

.

Figure 3. FTIR spectra of PEG_{120}-b-$PAEMA_8$-b-PES_{26} micelle, (a) after cross-linking (**5**) and (b) before cross-linking (**4**). The arrows in (b) indicate the presence of acetylenic groups and absence of azide groups; y-axis is % of transmittance in arbitrary units.

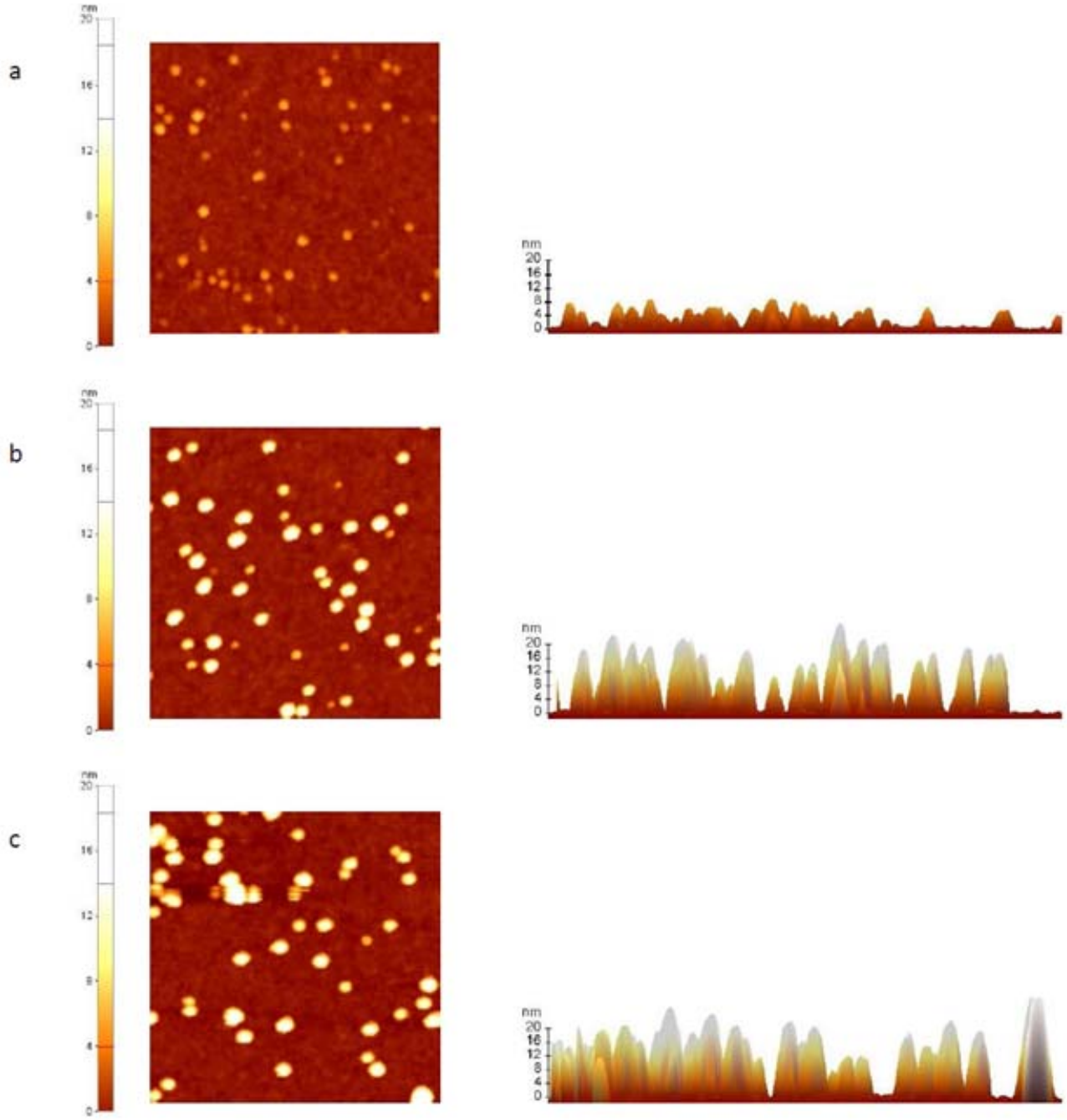

Figure 4. Representative tapping-mode 2D and 3D AFM images of nanoparticles; a) non-cross-linked micelle **4**, b) cross-linked micelle **5,** and c) pH nanosensors **6**. xy scan size 1 μm × 1 μm.

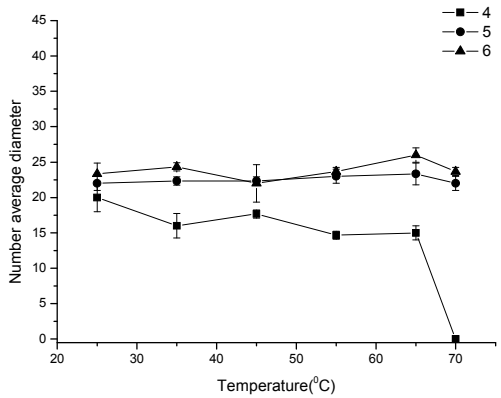

Figure 5. Variation of number average hydrodynamic diameter (D_h) with temperature determined from DLS measurements; non-cross-linked micelle (■) (**4**), cross-linked micelle (●) (**5**), and cross-linked nanosensor (▲) (**6**)

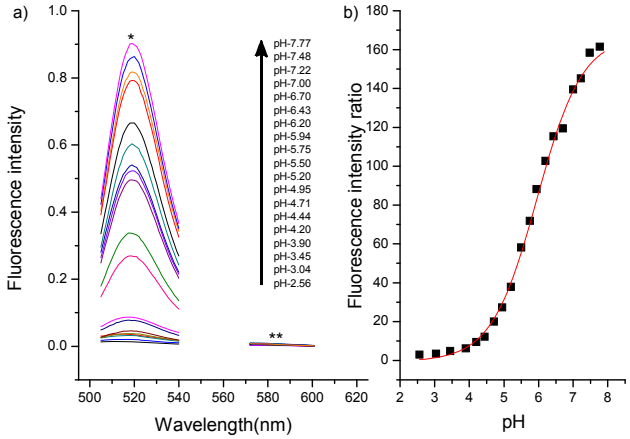

Figure 6. a) Fluorescence emission spectra of the pH nanosensor in buffers of different pH having sensor concentration 0.1 mg/mL. *For pH sensitive fluorophores excitation wavelength, λ_{ex} = 488 nm and **for reference fluorophore λ_{ex} = 543 nm. b) pH calibration curve made by plotting fluorescence intensity ratio ($I_{OG} + I_{FA} / I_{RhB}$) against pH

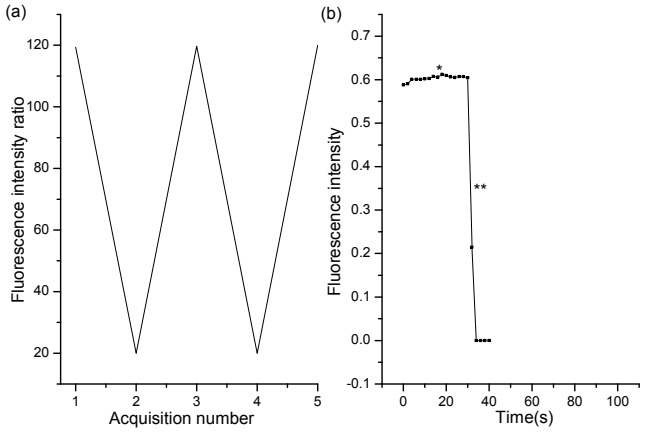

Figure 7. a) Reversibility of the nanosensors was tested by repeatedly changing the pH from 6.7 to 4.7 and vice versa. The corresponding fluorescence intensity ratio (I_{OG} + I_{FA} / I_{RhB}) was plotted against the acquisition number. The sensor concentration in each measurement was 0.1 mg/mL. b) The time for response of the pH nanosensors by fluorescence measurements. *Fluorescence intensity of the nanosensors in buffer of pH 6.5, **decrease in fluorescence intensity due to the addition of buffer of pH 2.5. The excitation wavelength (λ_{ex}) was 488 nm and emission wavelength (λ_{em}) was set to 518 nm.

The table of contents entry should be fifty to sixty words long, written in the present tense, and refer to the chosen figure.

A ratiometric pH nanosensor is fabricated from core cross-linked core-shell-corona micelle. The pH sensitive and reference fluorophores are attached to the radialy compartmentalized inner corona of the core cross-linked micelle. A measurement shows the sensitivity, reversibility and quick response nature of the nanosensors towards the change in pH within the range 4.5 to 7.5.

Keyword: amphiphilic triblock copolymers, functional micelle, dendritic click core cross-linking, polymeric micelle nanosensors, pH nanosensors

Pramod Kumar EK, Lise N. Feldborg, Kristoffer Almdal and Thomas L. Andresen*

Title: **Synthesis of core cross-linked polymeric core-shell-corona functional micelle based triple fluorophore nanosensors for broad range ratiometric pH measurements**

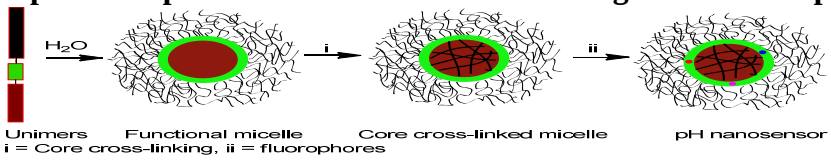

Reference

[1] C. J. Hawker, K. L. Wooley, *Science* **2005**, *309*, 1200.
[2] M. Meldal, *Macromolecular Rapid Communications* **2008**, *29*, 1016.
[3] R. Fu, G.-D. Fu, *Polymer Chemistry* **2011**, *2*, 465.
[4] T. Otsu, M. Yoshida, T. Tazaki, *Die Makromolekulare Chemie, Rapid Communications* **1982**, *3*, 133.
[5] M. K. Georges, R. P. N. Veregin, P. M. Kazmaier, G. K. Hamer, *Macromolecules* **1993**, *26*, 2987.
[6] D. Benoit, V. Chaplinski, R. Braslau, C. J. Hawker, *Journal of the American Chemical Society* **1999**, *121*, 3904.
[7] J. Chiefari, Y. K. Chong, F. Ercole, J. Krstina, J. Jeffery, T. P. T. Le, R. T. A. Mayadunne, G. F. Meijs, C. L. Moad, G. Moad, E. Rizzardo, S. H. Thang, *Macromolecules* **1998**, *31*, 5559.
[8] J.-S. Wang, K. Matyjaszewski, *Journal of the American Chemical Society* **1995**, *117*, 5614.
[9] M. Kato, M. Kamigaito, M. Sawamoto, T. Higashimura, *Macromolecules* **1995**, *28*, 1721.
[10] J. N. Israelachvili, D. J. Mitchell, B. W. Ninham, *Journal of the Chemical Society, Faraday Transactions 2: Molecular and Chemical Physics* **1976**, *72*, 1525.
[11] J. N. Israelachvili, S. Marĉelja, R. G. Horn, *Quarterly Reviews of Biophysics* **1980**, *13*, 121.
[12] D. W. P. M. Lowik, J. C. M. van Hest, *Chemical Society Reviews* **2004**, *33*, 234.
[13] J. H. Fuhrhop, J. Koning, C. Royal Society of, Rsc, *Membranes and molecular assemblies / The synkinetic approach*, Cambridge, **1994**.
[14] W. T. S. Huck, K. Velonia, J. J. L. M. Cornelissen, M. C. Feiters, A. E. Rowan, R. J. M. Nolte, in *Nanoscale Assembly* (Ed.: D. J. Lockwood), Springer US, **2005**, pp. 119.
[15] S. E. Webber, *The Journal of Physical Chemistry B* **1998**, *102*, 2618.
[16] J. Kriz, B. Masar, J. Plestil, Z. Tuzar, H. Pospisil, D. Doskocilova, *Macromolecules* **1998**, *31*, 41.
[17] G.-e. Yu, A. Eisenberg, *Macromolecules* **1998**, *31*, 5546.
[18] S. Liu, S. P. Armes, *Current Opinion in Colloid & Interface Science* **2001**, *6*, 249.
[19] R. S. Tu, M. Tirrell, *Advanced Drug Delivery Reviews* **2004**, *56*, 1537.
[20] E. S. Read, S. P. Armes, *Chemical Communications* **2007**, 3021.
[21] R. K. O'Reilly, C. J. Hawker, K. L. Wooley, *Chemical Society Reviews* **2006**, *35*, 1068.
[22] K. L. Wooley, *Journal of Polymer Science Part A: Polymer Chemistry* **2000**, *38*, 1397.
[23] R. K. O'Reilly, M. J. Joralemon, K. L. Wooley, C. J. Hawker, *Chemistry of Materials* **2005**, *17*, 5976.
[24] R. K. O'Reilly, M. J. Joralemon, C. J. Hawker, K. L. Wooley, *Chemistry – A European Journal* **2006**, *12*, 6776.
[25] R. K. O'Reilly, M. J. Joralemon, C. J. Hawker, K. L. Wooley, *New Journal of Chemistry* **2007**, *31*, 718.
[26] M. J. Joralemon, R. K. O'Reilly, C. J. Hawker, K. L. Wooley, *Journal of the American Chemical Society* **2005**, *127*, 16892.
[27] V. Bütün, X. S. Wang, M. V. de Paz Banez, K. L. Robinson, N. C. Billingham, S. P. Armes, Z. Tuzar, *Macromolecules* **1999**, *33*, 1.
[28] S. Liu, S. P. Armes, *Journal of the American Chemical Society* **2001**, *123*, 9910.
[29] D. H. Napper, *Journal of Colloid and Interface Science* **1977**, *58*, 390.

[30] M. L. Adams, A. Lavasanifar, G. S. Kwon, *Journal of Pharmaceutical Sciences* **2003**, *92*, 1343.
[31] A. L. Klibanov, K. Maruyama, V. P. Torchilin, L. Huang, *Febs Letters* **1990**, *268*, 235.
[32] V. P. Torchilin, V. S. Trubetskoy, *Advanced Drug Delivery Reviews* **1995**, *16*, 141.
[33] K. Matyjaszewski, N. V. Tsarevsky, *Nat Chem* **2009**, *1*, 276.
[34] K. Matyjaszewski, J. Xia, *Chemical Reviews* **2001**, *101*, 2921.
[35] J. Srivastava, D. L. Barber, M. P. Jacobson, *Physiology* **2007**, *22*, 30.
[36] T. L. Andresen, S. S. Jensen, K. Jørgensen, *Progress in Lipid Research* **2005**, *44*, 68.
[37] E. Allard, C. Larpent, *Journal of Polymer Science Part A: Polymer Chemistry* **2008**, *46*, 6206.
[38] H. Sun, A. M. Scharff-Poulsen, H. Gu, K. Almdal, *Chemistry of Materials* **2006**, *18*, 3381.
[39] V. M. Chauhan, G. R. Burnett, J. W. Aylott, *Analyst* **2011**, *136*, 1799.
[40] R. V. Benjaminsen, H. Sun, J. R. Henriksen, N. M. Christensen, K. Almdal, T. L. Andresen, *ACS Nano* **2011**, *5*, 5864.
[41] A. Schulz, S. Hornig, T. Liebert, E. Birckner, T. Heinze, G. J. Mohr, *Organic & Biomolecular Chemistry* **2009**, *7*, 1884.
[42] T. Vladimir P, *Journal of Controlled Release* **2001**, *73*, 137.
[43] H. Sun, K. Almdal, T. L. Andresen, *Chemical Communications* **2011**, *47*, 5268.
[44] E. Kaiser, R. L. Colescott, C. D. Bossinger, P. I. Cook, *Analytical biochemistry* **1970**, *34*, 595.
[45] R. Gujadhur, D. Venkataraman, *Synthetic Communications* **2001**, *31*, 2865.
[46] M. J. Joralemon, R. K. O'Reilly, J. B. Matson, A. K. Nugent, C. J. Hawker, K. L. Wooley, *Macromolecules* **2005**, *38*, 5436.
[47] S. Takahashi, Y. Kuroyama, K. Sonogashira, N. Hagihara, *Synthesis-Stuttgart* **1980**, 627.
[48] S. Liu, J. V. M. Weaver, Y. Tang, N. C. Billingham, S. P. Armes, K. Tribe, *Macromolecules* **2002**, *35*, 6121.

Appendix C

Pramod Kumar EK, Andreas I. Jensen, Lise N. Feldborg, and Thomas L. Andresen. ‘‘Photo Core Cross-linked Core-shell-corona Functional Micelle based Ratiometric pH Nanosensor Fabrications’’. *J. Photochem. Photobiol., A* **2012** (Submitted).

Photo Core Cross-linked Core-shell-corona Functional Micelle based Ratiometric pH Nanosensor Fabrications

Pramod Kumar EK[a], Andreas I. Jensen[a], Lise N. Feldborg[a], and Thomas L. Andresen[a,] *

[a] DTU Nanotech, Department of Micro-and Nanotechnology, Technical University of Denmark, Building 423, 2800 Lyngby, Denmark

*Corresponding author. Tel.: +4545258168; fax: +45887762; E-mail: thomas.andresen@nanotech.dtu.dk.

Keywords: ATRP, Core-shell-corona micelle, Functional micelle, Photo core cross-linking, pH nanosensor, Ratiometric pH measurement

Abstract

A ratiometric fluorescence pH nanosensor based on photo core cross-linked polymeric micelles was developed. The functional amphiphilic triblock copolymer poly(ethylene oxide)$_{120}$-*b*-poly((((trimethylsilyl)ethoxy)carbonyl) aminoethyl methacrylate)$_{12}$-*b*-poly((trimethylsilylethynyl) styrene)$_{36}$ (PEG$_{120}$-*b*-PAEMA(Teoc)$_{12}$-*b*-P(SC≡CTMS)$_{36}$) was synthesized by isolated macroinitiator atom transfer radical polymerization. The removal of the protecting groups was followed by self-assembly in water resulting in core-shell-corona functional micelles. The micelles were stabilized by UV-induced photo core cross-linking. The core cross-linked micelle was then converted to a ratiometric pH-nanosensor by the covalent attachments of a pH-sensitive fluorophore (BCECF) and reference (Alexa 633) at the PAEMA shell of the micelle. Fluorescence measurements show that the micelle nanosensor is sensitive between pH 6 to 8.

1. Introduction

In block selective solvents, amphiphilic triblock copolymers spontaneously self-assemble[1] to give core-shell-corona micelle spheres or cylinders, whereas amphiphilic diblock copolymers give spherical core-shell micelles.[2-5] Compared to core-shell micelles, the core-shell-corona micelles are more diverse with respect to regioselective functionalization and cross-linking. For example, in biological systems, moieties conjugated to the hydrophilic outer domain (corona) of a diblock micelle can have unwanted interactions with components of its immediate surroundings, such as serum proteins. In core-shell-corona micelles, the functionalizable shell region is protected by the surrounding corona. The potential application of polymeric micelles is limited by its dissociation into unimers at concentrations below the critical micelle concentration (CMC). Cross-linking abolishes the importance of hydrophobic interactions and hence prevents micelle dissociations below its CMC. Therefore, the regioselective covalent cross-linking between the unimers of block copolymer micelles has garnered significant research attention in recent years[6-8]. Radiation-induced micelle cross-linking is thought to be practically simpler than conventional cross-linking strategies, since the

cross-linking of triblock micelles in water via conventional strategies requires transfer/accessibility of the reagent to the specific nanodomains, long reaction times and subsequent purification steps[26]. Radiation-induced micelle cross-linking on the other hand, demands only the presence of UV sensitive groups on the micelle. UV radiation-induced shell layer cross-linking of amphiphilic triblock copolymer micelles has been reported[9, 10].

Intracellular pH measurements may provide opportunities to develop pH sensitive drug delivery system which can precisely deliver drugs at the intracellular compartment.[11] In contrast to pH sensitive amphiphilic block polymer micelles in anticancer drug delivery,[12-14] polymeric micelles in pH nanosensor fabrications has not been investigated yet. This is primarily due to the difficulty in synthesis of well defined functional micelles. The recent developments in controlled radical polymerizations[15-17] can provide well-defined functional amphiphilic triblock copolymers. Dimensional synthetic modification on specific domains of it self-assembly can provide a platform for stabilized functional nanoparticle synthesis. In continuation with our interest to investigate the excellent engineerability of amphiphilic triblock copolymer self-assemblies in pH nanosensor fabrications,[26, 27, 28] we are now utilizing the structural potential of triblock core-shell-corona micelles to synthesis photo core cross-linked ratiometric pH nanosensors.

2. Material and methods

2.1 Materials and measurements: 2′,7′-bis- (2-carboxyethyl)-5-(and-6) carboxyfluorescein free acid (BCECF) was purchased from Biotium. Alexa Fluor 633 carboxylic acid succinimidyl ester (Alexa 633) was obtained from Invitrogen. N-(3-Dimetyl amino propyl)-N'-ethylcarbodiimide hydrochloride (EDC·HCl) (98%), N-hydroxysuccinimide (NHS) (98%), dialysis tubing (MWCO=12kDa), tetrabutylammonium fluoride (1M THF solution) and all other solvents and chemicals were purchased from Sigma Aldrich and used as obtained. NMR spectra were recorded on a 300 MHz Varian Mercury 300 BB spectrometer; IR spectra were recorded on a Perkin Elmer Spectrum 100 FT-IR spectrometer. GPC measurements were carried out with a Viscotek refractive index detector and a PL Gel Mixed-C+D column with a flow rate of 0.5 mL/min at 25°C using THF as eluent. UV-vis spectra were recorded on Unicam Helios Uni 4923 spectrophotometer. Fluorescence measurements were carried out on an Olis SLM 8000 fluorometer.

Samples for atomic force microscopy (AFM) were prepared by placing a 5 µl drop of the nanoparticle suspension on a silicon wafer. The particles were allowed to settle for 30 minutes, before excess liquid was removed using a lens cleaning tissue. AFM imaging was performed using a PSIA XE-150 scanning force microscope using non-contact tapping mode close to the resonance frequency of the silicon cantilever (Nanoworld, pointprobe type, force constant 42 N/m and tip radius <12 nm) of around 320 kHz. All images were recorded under atmospheric conditions.

2.2 Synthesis of PEG_{120}-b-PAEMA(Teoc)$_{12}$-b-P(SC≡CTMS)$_{36}$: Multiple steps involved in the synthesis of PEG_{120}-*b*-PAEMA(Teoc)-*b*-P(SC≡CTMS) are explained in our previous paper [26]. And hence here we only show the slightly modified procedure for the synthesis of final amphiphilic triblock copolymer.

The diblock copolymer PEG-PAEMA(Teoc)-Cl (500 mg, 0.058 mmol), 5 mL anisole, 4,4′-dinonyl-2,2′-dipyridyl (48 mg, 0.116 mmol) and ESTMS (464 mg, 2.32 mmol) were added to a 25 mL schlenk flask equipped with a stirrer bar. The reaction mixture was frozen under liquid nitrogen. CuCl (6.3 mg, 0.063 mmol) was added and the solution was degassed by subjecting it to three freeze-pump-thaw cycles to remove the oxygen followed by stirring under argon at 130 °C for 30 h. After removing most of the solvent under vacuum, the polymer was precipitated into cold diethyl ether and dried under vacuum, yielding 0.545 g (60%). The polymer was further purified by dissolving in THF (10 mg/mL) and dialyzing (MWCO = 12 kDa) against MilliQ water. From dynamic light scattering (DLS) of the micelle dispersion the number-averaged hydrodynamic diameter (D_h) was found to be 20±3 nm and zeta potential measurement showed (ξ) = -15±2 mV. The micelle solution was lyophilized to get the pure polymer. ^{1}H NMR (300 MHz, $CDCl_3$): δ = 7.48-6.223 (m, Ar**H**), 4.17-3.72 (-NHCH_2C**H**$_2$O, -NHCOOC**H**$_2$CH_2), 3.60 (s, -C**H**$_2$C**H**$_2$O), 3.51-3.31 (-NHC**H**$_2$CH_2O), 2.02-0.61 (PAEMA and PES backbone, -NHCOOCH_2C**H**$_2$), 0.21 (s, -Si(C**H**$_3$)$_3$ of PESTMS), 0.00 (s, -Si(C**H**$_3$)$_3$ of PAEMA(Teoc)); FT-IR: υ = 3300, 2160, 2106, 1719, 1504, 1448, 1342, 1248, 1103, 962, 840 cm^{-1}. Kaiser test of the polymer was performed, the colourless solution indicate completely protected amino groups.

2.3 Preparation of micelles: The triblock copolymer PEG_{120}-*b*-PAEMA(Teoc)$_{12}$-*b*-P(ESTMS)$_{36}$ (100 mg, 0.0063 mmol) was dissolved in 12 mL of THF, followed by addition of 1M TBAF in THF (0.182 mL, 0.63 mmol) and stirred at room temperature for 5h. The reaction mixture was diluted by drop wise addition of 30 mL MilliQ water. The resulting opalescent micelle dispersion was transferred to a dialysis tube (MWCO = 12 kDa) and dialyzed against MilliQ water for three days, the water was replaced two times per day. The final micelle concentration was 1.82 mg/mL (D_h = 16±3 nm and (ξ) = 16±1 mV). A portion of the micelle was lyophilized for characterization. ^{1}H NMR (300 MHz, $CDCl_3$): δ = 7.51-6.10 (m, Ar**H**), 4.25-3.44 (-COOC**H**$_2$CH_2NH_2, -C**H**$_2$C**H**$_2$O), 3.45-3.31 (-CH_2C**H**$_2$NH_2), 3.27-2.85 (br s, -C≡C-**H**), 1.90-0.71 (PAEMA and PES backbone); FT-IR: υ = 3500, 3285, 3241, 2106, 1725, 1501, 1450, 1342, 1241, 1103, 961, 840 cm^{-1}. Positive Kaiser test (blue colour) indicates the presence of free amino groups.

2.4 Photo core cross-linking of PEG_{120}-b-$PAEMA_{12}$-b-P(SC≡CH)$_{36}$ micelles: 3 mL PEG_{120}-*b*-$PAEMA_{12}$-*b*-P(SC≡CH)$_{36}$ micelles (1.82 mg/mL) was stirred in a quartz cuvette and exposed to UV radiation (3 W/cm^2) from a UV spot curing system (Omnicure S2000) having a 200 W mercury vapour short arc lamp without using a wavelength filter. The progress of the cross-linking reaction (increase in absorbance at 600 nm) was monitored by UV-vis spectrophotometry (D_h = 19±1 nm and (ξ) = 14±2 mV).

2.5 Pyrene CMC assay [18]: 12 mg (59.3 µmol) pyrene was dissolved in 10 mL acetone. This was diluted in acetone to 29.7 µM and 34 µL of this solution was placed in 4 mL glass vials. The acetone was allowed to evaporate in the hood over five hours, leaving 1 nmol pyrene in each vial. To each vial was added 2 mL micelle dispersion in concentrations of 0.05-250 µg/mL in Milli-Q water (pyrene concentration 5×10^{-7} M). The vials were incubated for one hour (*non cross-linked micelles*) or three hours (*cross-linked micelles*) at 65 ^{0}C and then overnight (17 h) at 37 ^{0}C. The vials were then kept at room temperature, protected from light until measurement. Fluorescence was recorded on an Olis SLM 8000 fluorometer. Excitation spectra were collected at 25 ^{0}C using emission wavelength 390 nm and a 16 nm slit size. Excitation was scanned in ranges of either 325-345 nm or 310-360 nm with all slits set to 0.5 nm. Intensity ratios (I_{337}/I_{334}) were calculated from the excitation spectra and plotted as a function of the polymer concentration.

2.6 Preparation of the photo core cross-linked micelle nanosensor: 3 mL photo core cross-linked PEG_{120}-*b*-$PAEMA_{12}$-*b*-$P(SC{\equiv}CH)_{36}$ micelles (1.82 mg/mL) was dialyzed against a $NaHCO_3/Na_2CO_3$ buffer of pH 9. To this colloidal dispersion, was added activated BCECF. BCECF was activated by adding BCECF (10 µl, 0.01 mg, 0.02 µmol) to 0.5 mL of water containing EDC·HCl (0.011 mg, 0.06 µmol) and NHS (0.00345 mg, 0.03 µmol) and stirring the reaction mixture at room temperature for 2h. 102 µl of the solution (2 µl activated BCECF) was transferred into the reaction mixture along with Alexa 633 (4 µl) (1mg/mL of dry DMSO). The reaction mixture was stirred at room temperature in the absence of light for 15 h after which it was transferred to dialysis tubing of MWCO 12 kDa and dialyzed against carbonate buffer (pH 9) for three days and then against MilliQ water for another three days. Final sensor concentration was 1.76 mg/mL (D_h = 20±2 nm and (ξ) = 10±1 mV).

3. Results and discussion

Figure 1 illustrates the step-wise preparation of photo core cross-linked ratiometric pH nanosensors. The amphiphilic triblock copolymer poly(ethylene oxide)$_{120}$-*b*-poly((((trimethylsilyl)ethoxy)carbonyl) aminoethyl methacrylate)$_{12}$-*b*-poly((trimethylsilylethynyl) styrene)$_{36}$ (PEG_{120}-*b*-PAEMA(Teoc)$_{12}$-*b*-P(SC≡CTMS)$_{36}$) (**1**) was synthesized by a slightly modified ATRP procedure that we have reported previously.[26] The polymers were characterized by ^{1}H-NMR and FT-IR spectroscopy. Presence of Teoc and TMS protecting groups on the polymers was confirmed by NMR (^{1}H-NMR, $CDCl_3$) peaks at δ = 0.00 ppm and 0.22 ppm respectively. FT-IR confirmed the carbonyl stretching of PAEMA(Teoc) block at ca. 1720 cm^{-1} and aromatic C=C stretching of PES(TMS) block at ca. 1500 cm^{-1}. The number-average molecular weight (Mn) calculated from NMR was found to be lower than that measured by gel permeation chromatography (GPC) in THF with polystyrene as standard. Details of molecular weight determinations are summarized in Table 1. Simultaneous removal of Teoc and TMS protecting group from the amphiphilic triblock copolymers using tetrabutylammonium fluoride in THF followed by self-assembly of the resulting functional triblocks in water

resulted in functional core-shell-corona PEG-*b*-PAEMA-*b*-P(SC≡CH) micelles (**2**). A portion of the micelles was lyophilized for characterization. Disappearance of Teoc and TMS signal (^{1}H-NMR, $CDCl_3$) and the appearance of alkyne (-C≡CH) proton resonance at 3.06 ppm confirms the complete deprotection. Appearance of -C≡**C-H** stretching at *ca.* 3285 cm^{-1} in FT-IR further confirms the TMS deprotection. Teoc deprotection from the amino groups of the PAEMA(Teoc) block were further confirmed by positive Kaiser tests[19] of the lyophilized micelles. The positive zeta potential of PEG-*b*-PAEMA-*b*-P(SC≡CH) micelle (Table 2) indicate the presence of free amino groups in the shell region of the micelle, and provides additional evidence of Teoc deprotection.

The synthesis of UV core cross-linked amphiphilic triblock core-shell-corona functional micelle **3** based pH nanosensors **4** is shown in Scheme 1. The aqueous micelle dispersion **2** (1.82 mg/mL) in a quartz cuvette was exposed to UV radiation from a UV photo curing system (Omnicure S2000). The stirred sample was irradiated with irradiance level of 3 W/cm^2 (measured by the radiometer) from a high pressure mercury arc lamp (200 W), without using a wavelength filter at room temperature. The UV-induced oxidative coupling between the alkyne moity at the micelle core was monitored by measuring the variation of absorbance of the micelle solution with UV irradiation time (Figure 2). Measurements show that the cross-linking reaction takes place rapidly during the first few minutes as indicated by the sharp initial increase in absorbance. After about five minutes, further irradiation does not increase the absorbance significantly, indicating that a saturation level of photo cross-linking has been achieved.

Photo cross-linking at the micelles core was further confirmed by FT-IR spectroscopy. During UV irradiations the alkyne C≡C-**H** stretching absorption at 3285 cm^{-1} decreases considerably. This confirms the consumption of the alkyne moiety present at the P(SC≡CH) core of the micelle during photo irradiation. IR spectra measured at different irradiation times show that under a given irradiation level (3 W/cm^2), the alkyne moiety was consumed significantly within 30 minutes (Figure 3). Further increase in UV irradiation time shows only slow decrease in alkyne absorption at 3285 cm^{-1}, indicating a decreased rate of oxidative coupling between the alkyne moieties at the micelle core. This observation is in agreement with the UV absorption results shown above (Figure 2). As photo cross-linking progresses, time-dependent decay of the reaction rate may be due to the decrease in UV exposure on the free alkyne moiety buried inside of the cross-linked micelle core. This may also due to conformational restriction of alkyne moiety present at the cross-linked micelle core towards the oxidative coupling.

In order to measure the CMC values of the micelles before cross-linking and compare this with after cross-linking, the pyrene assay[20, 21] was employed. This method has previously been used on a similar system [22] . Plotting polymer concentration against the (I_{337}/I_{334}) ratio, the graphs shown in Figure 4 were obtained, suggesting a CMC value around 15 mg/L. Upon examination of each obtained spectrum however, it was found that what was observed was not a blue-shift of the pyrene spectrum. Instead, as polymer concentration

increased, the initially observed pyrene spectrum was eclipsed by entirely different spectra, both in the case of non cross-linked and cross-linked micelles (Figure 5). Obtaining excitation spectra (emission 390 nm) for both micelle types at concentrations of 5 mg/L (below our observed CMC) and 250 mg/L (above our observed CMC) revealed that these micelles both exhibit significant fluorescence. This fluorescence is different between cross-linked and non-cross-linked micelles, which prompt us to ascribe it to the phenyl alkyne moieties of the PES core, which are altered during cross-linking. It is possible that this characteristic can be used to monitor cross-linking in PES-based systems. Furthermore, it is observed that the spectra shapes for both micelle types are different at low and high concentrations. It is possible that this may make systems with a PES-based core able to function as their own fluorescence indicators for CMC measurements, without the need for pyrene. At this point however, we conclude that in our experience, the pyrene assay seems unfit for determining the CMC of PES-based systems.

In further attempts to assess the CMC, a DLS-based method inspired by Wooley et al [23]was attempted but we found that in our hands, DLS was too imprecise at low concentrations to produce reliable data. In addition it was contemplated using the fluorescence correlation spectroscopy (FCS) [24]technique, but as neither cross-linked nor non cross-linked micelles showed fluorescence when excited at 405 or 470 nm, this technique was abandoned.

The UV cross-linked core-shell-corona functional micelle was converted into a ratiometric pH nanosensor by conjugating pH sensitive (BCECF) and reference (Alexa 633) fluorophores to the PAEMA shell of the micelle. pH sensitivity of the resulting pH nanosensor was measured by fluorescence measurements (Figure 6a). The fluorescence measurements confirm the covalent attachments of fluorophores to the micelles. The nanosensor (0.176 mg/mL) was excited (λ_{ex} = 488 nm and 561 nm) in buffers of different pH and pH dependent fluorescence intensity (I_{BCECF}) and pH independent fluorescence intensity ($I_{Alexa\ 633}$) were measured. The fluorescence intensity ratio (I_{BCECF} / $I_{Alexa\ 633}$) was plotted against corresponding pH. The resulting ratiometric pH calibration curve (Figure 6b) shows that the micelle nanosensor is sensitive between pH *ca.* 6 to 8.

The presence of the PEG corona on the nanosensor could enhance its potential for biomedical applications via providing long circulation of the nanosensor in blood (EPR effect)[25] and give protection from the external surroundings to the fluorophores conjugated to the shell region. The unused functional groups at the core and shell region of this functional micelle nanosensor could provide opportunities for covalent attachments of hydrophilic and hydrophobic cargoes. This may provide capabilities to combine sensing and drug delivery applications together in the same particle.

DLS measurements show that the nanosensor **4** maintains the same hydrodynamic diameter (Dh) as that of the cross-linked micelles **3**. Compared to cross-linked micelles, the nanosensor shows a slight decrease in

zeta potential, presumably as a result of fluorophore binding. The decrease in sensor zeta potential may thus be attributed to the presence of free carboxylic acid groups on the fluorophores attached to the PAEMA shell of the micelle (Table 2).

2D and 3D tapping mode AFM images and histograms representing number of particles *versus* heights of the non cross-linked micelle **2**, cross-linked micelle **3** and pH nanosensor **4** are given in Figure 7. 2D AFM images show the spherical morphology of the micelle nanoparticles. After UV cross-linking, the average height (H_{av}) of the particle **3** measured was found to be higher than that found before cross-linking, **2**. It indicates that the robust micelles obtained after cross-linking were less deformed on the hydrophilic silica surfaces. The cross-linking makes the particle more cohesive and therefore prevents the deformation caused by association with the polar surfaces. The nanosensor **4** maintained heights (H_{av}) that are similar to that of the cross-linked micelles indicating that fluorophore binding at the shell region of the cross-linked micelle do not further alter the particle surface interactions. The average heights (H_{av}) of the particles calculated from AFM measurements are also given in Table 2. The histograms given in Figure 7 show the distribution of the micelle particles heights before and after UV irradiations.

4. Conclusions

A photo core stabilized ratiometric pH nanosensor was prepared by fluorophore binding to the photo-stabilized micelle. The use of UV-radiation in micelle core cross-linking was employed to reduce the difficulties in post micelle modifications, such as accessibility of reagents to the micelle core domain, long reaction time and lengthy purification procedures. Core cross-linking in micelles nanosensors can improve their biological application by preventing sensor disintegration under infinitely diluted biological conditions (sink conditions). The fluorophores conjugated in the shell region of the micelles are well protected from the external surroundings by the PEG corona. Since the sensing molecules are less interacted by the external surroundings, the sensor may provide more accurate information about intracellular pH within the pH range *ca.* 6 to 8. The presence of excess alkyne and amino functionalities at the core and shell region of the micelle may allow the covalent attachment of cargo and hence may provide an opportunity to monitor the intracellular pH during drug delivery. Intracellular pH measurements using the nanoparticle sensors are under investigation.

Acknowledgements: The authors would like to thank Kræftens Bekæmpelse and the Danish Research Council for Technology and Production (Grant 274-07-0172) for financial.

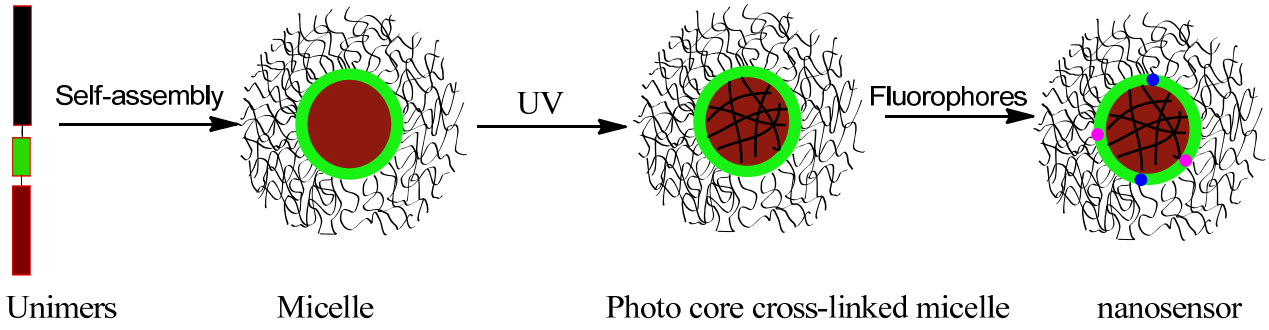

Figure 1. Preparation of a photo core cross-linked micelle pH nanosensor.

Table 1. Molecular weight of PEG_n-*b*-$PAEMA(Teoc)_m$-*b*-$P(SC{\equiv}CTMS)_p$ (1)

M_n[a]	M_w[a]	M_w/M_n[a]	M_n[b]	n[c]	m[c]	p[c]
16600	20600	1.24	15750	120	12	36

[a] Determined by GPC, [b] determined by NMR, [c] Number of repeating units of PEG block (n), PAEMA(Teoc) block (m) and P(SC≡CTMS) block (p).

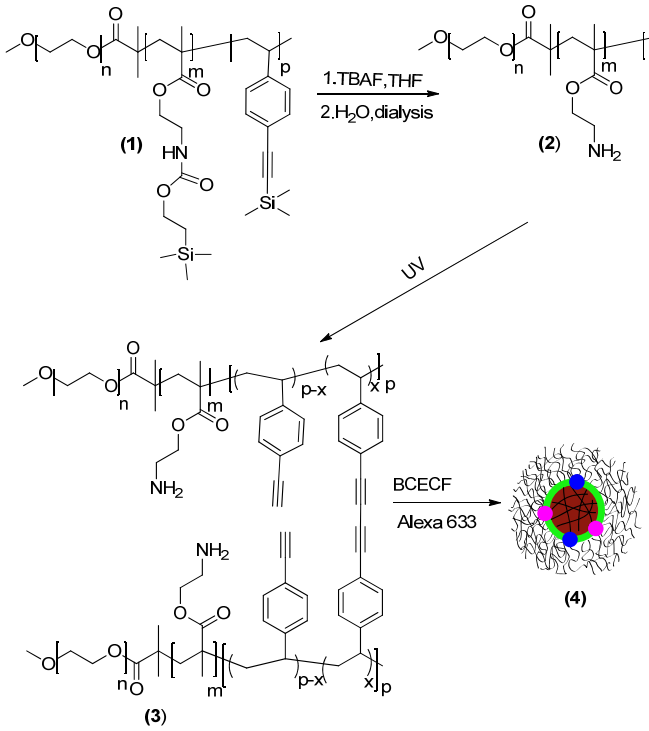

Scheme 1. Photo core cross-linked ratiometric pH nanosensor synthesis. TBAF = tetrabutylammonium fluoride, BCECF = 2′,7′-bis- (2-carboxyethyl) -5-(and-6) carboxyfluorescein, Alexa 633 = Alexa Fluor; x is the extent of photo cross-linking.

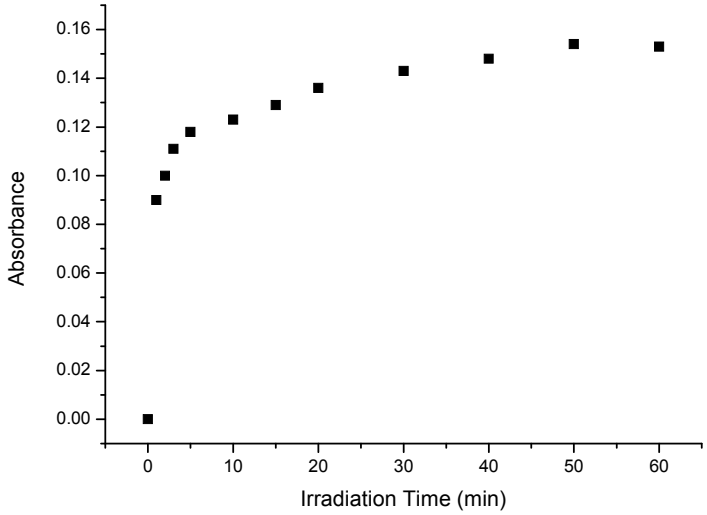

Figure 2. Plot of absorbance versus irradiation time for aqueous PEG-*b*-PAEMA-*b*-P(SC≡CH) (1.82 mg/ mL) measured at 600 nm using a UV-vis spectrophotometer during irradiation with a UV high pressure 200 Watt mercury vapor short arc lamp with an irradiance level of 3 W/cm^2.

Table 2. Characterization data for micelles 2, 3 and pH nanosensor 4

Micelle	DLS(D_h)[a] (nm)	AFM[b] H_{av}(nm)	Zeta(ξ)[c] (mV)
2	16±3	5±1	+16±1
3	19±1	11±1	14±2
4	20±2	10±2	10±1

[a] Number averaged hydrodynamic diameter of the polymeric micelles in MilliQ water by dynamic light scattering, [b] average height of the micelles were calculated from the values for *ca.* 100 particle by tapping mode AFM, [c] zeta potential from 10 determinations of 10 cycles each.

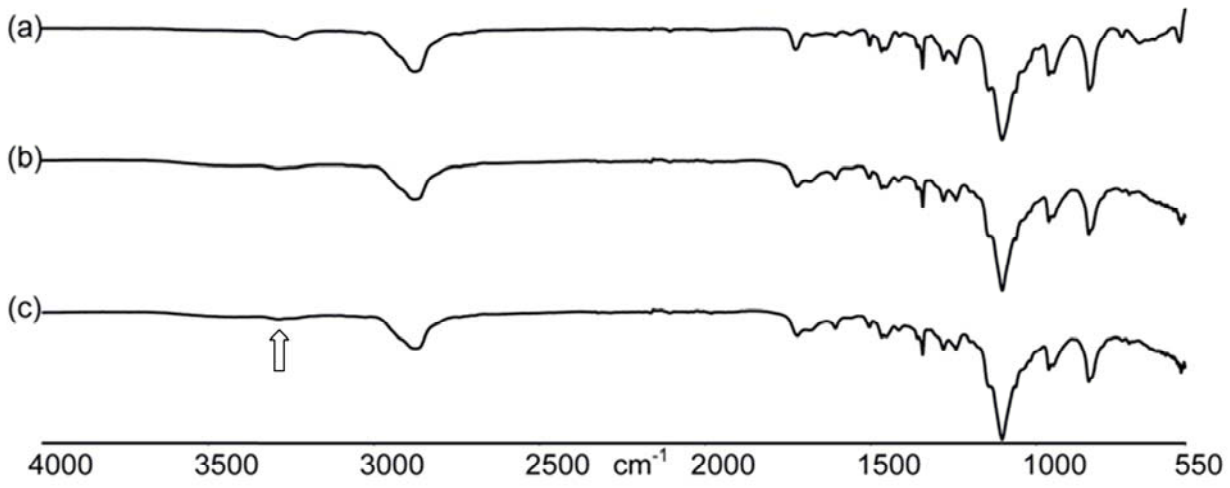

Figure 3. FT-IR Spectra of PEG-*b*-PAEMA-*b*-P(SC≡CH) micelle before UV irradiation (a), after 30 min (b) and 1h (c) of UV irradiation. The arrow in (c) indicates the decrease in alkyne (C-H) stretching during UV irradiations.

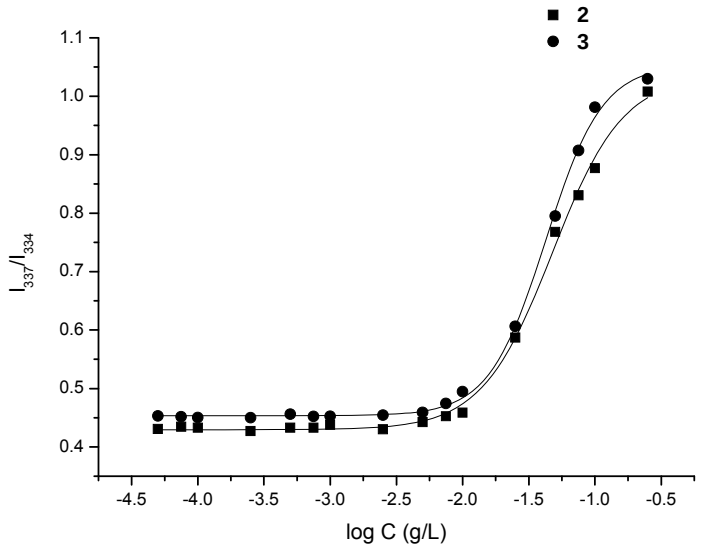

Figure 4. The plot of intensity ratio (I_{337}/I_{334}) of pyrene excitation spectra *vs* logarithmic concentration of cross-linked micelle **3** (●) and non cross-linked micelle **2** (■).

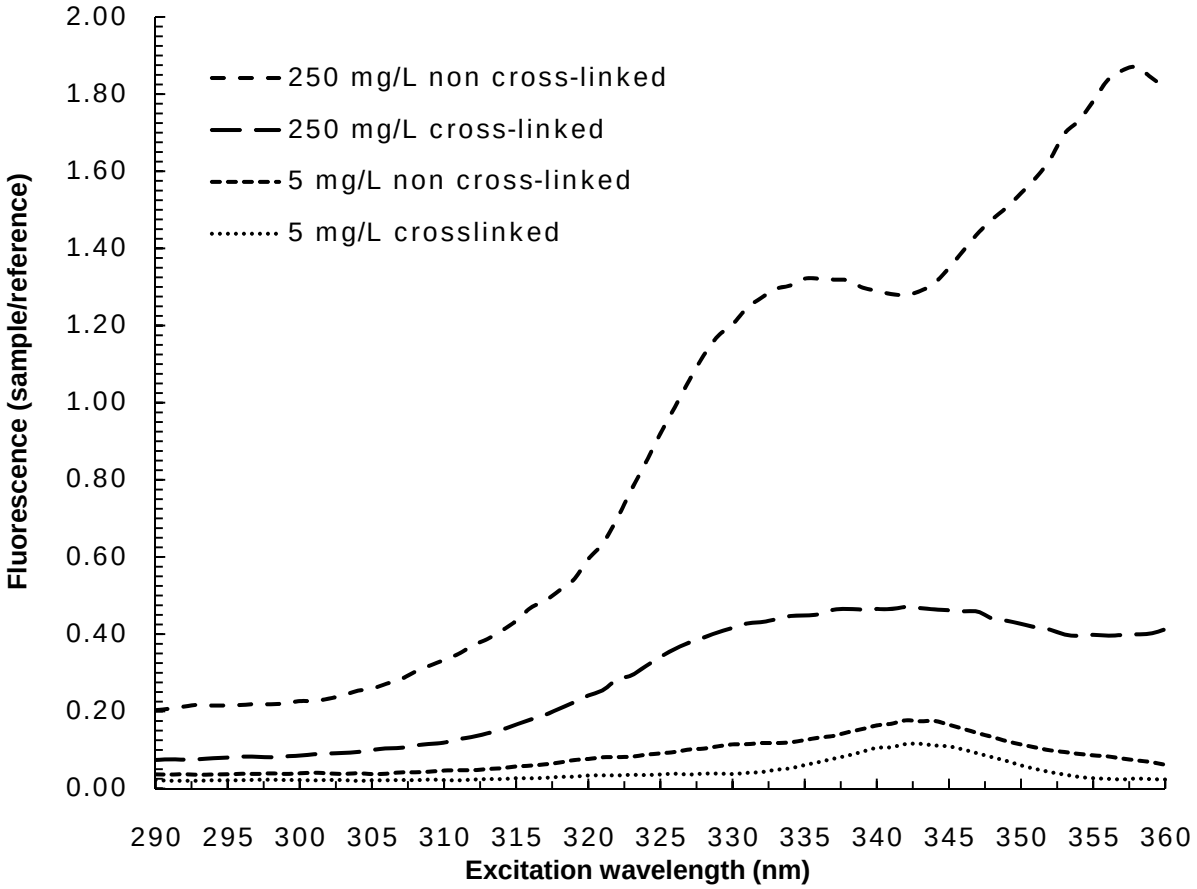

Figure 5. Excitation spectra (emission recorded at 390 nm) of cross-linked and non-cross-linked micelles at 5 and 250 mg/L. Intensity differences between 5 and 250 mg/L spectra are due to the concentration.

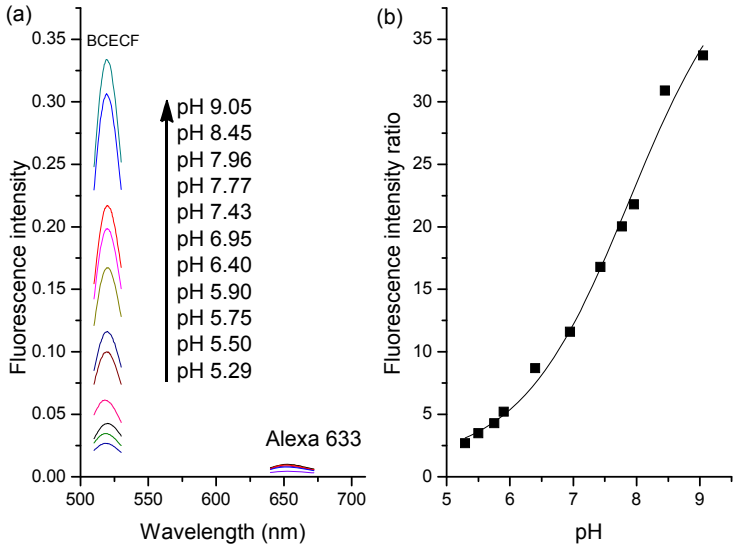

Figure 6. Fluorescence emission curve (a) and pH calibration curve (b) of the pH nanosensor; fluorescence intensity (I) ratio = I_{BCECF} / $I_{Alexa\ 633}$.

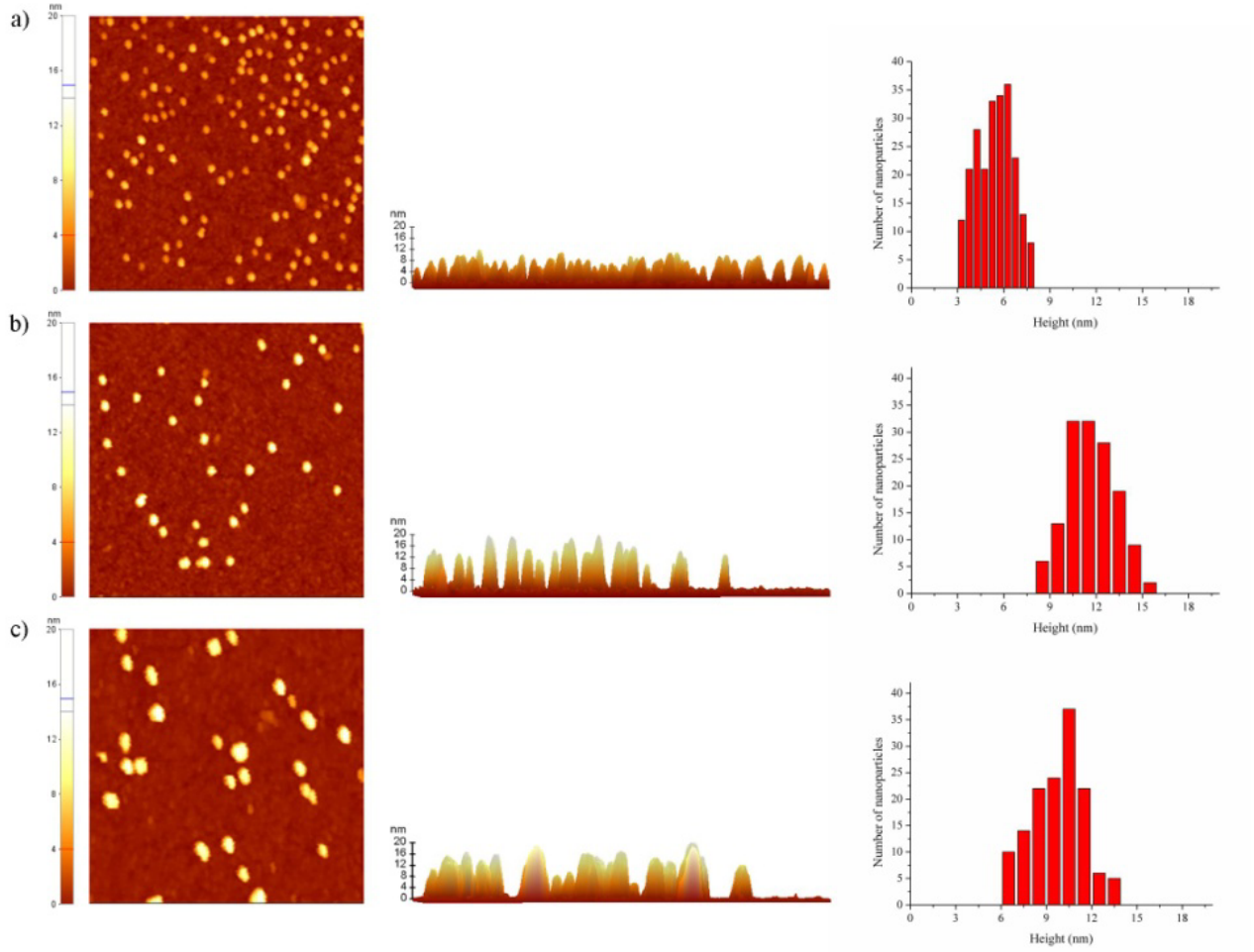

Figure 7. 2D, 3D AFM images and histograms of the micelle before cross-linking (**2**) (a), after cross-linking (**3**) (b) and after conversion to the pH nanosensor (**4**) (c).

References

[1] N. Kossovsky, D. Millett, A. Gelman, E. Sponsler, H.J. Hnatyszyn, Nat Biotech 11 (1993) 1534-1536.
[2] J. Kriz, B. Masar, J. Plestil, Z. Tuzar, H. Pospisil, D. Doskocilova, Macromolecules 31 (1998) 41-51.
[3] G.-E. Yu, A. Eisenberg, Macromolecules 31 (1998) 5546-5549.
[4] L. Zhang, A. Eisenberg, Science 268 (1995) 1728-1731.
[5] S.E. Webber, The Journal of Physical Chemistry B 102 (1998) 2618-2626.
[6] E.S. Read, S.P. Armes, Chemical Communications 29 (2007) 3021-3035.
[7] R.K. O'Reilly, C.J. Hawker, K.L. Wooley, Chemical Society Reviews 35 (2006) 1068-1083.
[8] C.F. van Nostrum, Soft Matter 7 (2011) 3246-3259.
[9] J.S. Kim, H.J. Jeon, M.S. Park, Y.C. You, J.H. Youk, European Polymer Journal 45 (2009) 1918-1923.

[10] J.S. Kim, H.J. Jeon, J.J. Park, M.S. Park, J.H. Youk, Journal of Polymer Science Part A-Polymer Chemistry 47 (2009) 4963-4970.
[11] R.V. Benjaminsen, H. Sun, J.R. Henriksen, N.M. Christensen, K. Almdal, T.L. Andresen, ACS Nano 5 (2011) 5864-5873.
[12] E.S. Lee, K. Na, Y.H. Bae, Nano Letters 5 (2005) 325-329.
[13] E.R. Gillies, T.B. Jonsson, J.M.J. Frachet, Journal of the American Chemical Society 126 (2004) 11936-11943.
[14] Y. Bae, S. Fukushima, A. Harada, K. Kataoka, Angewandte Chemie International Edition 42 (2003) 4640-4643.
[15] K. Matyjaszewski, N.V. Tsarevsky, Nat Chem 1 (2009) 276-288.
[16] C. Boyer, V. Bulmus, T.P. Davis, V. Ladmiral, J. Liu, S.B. Perrier, Chemical Reviews 109 (2009) 5402-5436.
[17] V. Sciannamea, R. Jerome, C. Detrembleur, Chemical Reviews 108 (2008) 1104-1126.
[18] M. Wilhelm, C.L. Zhao, Y. Wang, R. Xu, M.A. Winnik, J.L. Mura, G. Riess, M.D. Croucher, Macromolecules 24 (1991) 1033-1040.
[19] E. Kaiser, R.L. Colescott, C.D. Bossinger, P.I. Cook, Analytical biochemistry 34 (1970) 595-598.
[20] Y.-C. Wang, Y. Li, T.-M. Sun, M.-H. Xiong, J. Wu, Y.-Y. Yang, J. Wang, Macromolecular Rapid Communications 31 (2010) 1201-1206.
[21] X. Hu, X. Chen, J. Wei, S. Liu, X. Jing, Macromolecular Bioscience 9 (2009) 456-463.
[22] B.J. Kim, J.Y. Chang, Macromolecules 39 (2005) 90-94.
[23] M.J. Joralemon, R.K. O'Reilly, C.J. Hawker, K.L. Wooley, Journal of the American Chemical Society 127 (2005) 16892-16899.
[24] O. Krichevsky, G. Bonnet, Reports on Progress in Physics 65 (2002) 251-297.
[25] M. Hiroshi, Advances in Enzyme Regulation 41 (2001) 189-207.
[26] E.K. Pramod Kumar, N.F. Lise, K. Almdal, T.L. Andresen, Advanced functional materials (submitted) (2012).
[27] E.K. Pramod Kumar, K. Almdal, T.L. Andresen, Chemcomm (submitted) (2012).
[28] E.K. Pramod Kumar, N.M. Christensen, R.V. Benjaminsen, J.R Henriksen**,** K. Almdal, T.L**.** Andresen. ACS Nano (submitted) (2012).

Appendix D

Pramod Kumar EK, Lise N. Feldborg, Kristoffer Almdal and Thomas L. Andresen. ‘‘Synthesis of Reversibly Photo Core Cross-Linked Core-Shell-Corona Micelle based triply labelled Ratio-metric pH Nanosensors’’. *Soft Matter* **2012** (Submitted).

Soft Matter

Dynamic Article Links ►

Cite this: DOI: 10.1039/c0xx00000x

www.rsc.org/softmatter

PAPER

Synthesis of Reversibly Photo Core Cross-Linked Core-Shell-Corona Micelle based triply labelled Ratio-metric pH Nanosensors.

Pramod Kumar EK[a], Lise N. Feldborg[a], Kristoffer Almdal[a], Thomas L. Andresen*[a]

Received (in XXX, XXX) Xth XXXXXXXXX 20XX, Accepted Xth XXXXXXXXX 20XX
DOI: 10.1039/b000000x

The Amphiphilic triblock copolymers poly (ethylene-glycol)-*b*-poly(2-[N-(tert-Butoxycarbonyl)Amino]ethyl methacrylate)-*b*-poly(coumarin methacrylate) (PEG-*b*-PAEMA(Boc)-*b*-PCMA) is synthesized by isolated macroinitiator atom transfer radical polymerization (ATRP). Deprotection of the Boc- group followed by self-assembly in water gives PEG-*b*-PAEMA-*b*-PCMA micelles. Photo core cross-linking at the coumarin core of the micelles are performed by UV irradiation ($320\ nm < \lambda < 500\ nm$) and the progress of the cross-linking was monitored by UV spectroscopy. The photo core cross-linked core-shell-corona micelle was converted into ratiometric pH nanosensors by binding pH sensitive F_2FITC and BCECF and pH-insensitive reference fluorophore Alexa 633 at the PAEMA shell. Fluorescence measurements show that these pH nanosensors are sensitive between the pH *ca.* 4-8.0. Photo de-cross-linking by illuminating the nanosensor at $\lambda < 255\ nm$ shows partial de-cross-linking possibilities of the nanosensor.

.

Introduction

Intracellular pH play an important role in cellular processes and is highly regulated in every organelle.[1] A number of polymeric nanoparticles have been used in the designing of ratiometric fluorescence pH nanosensors for biological studies at the single cell level. These include, polystyrene,[2] polyacrylamide,[1, 3-6], and polysaccharide,[7] particles *etc*.[8] Ratiometric measurements are more accurate as they are capable of minimizing the errors in fluorescence measurements due to probe concentration, photo bleaching, optical path length and leakage from the cells.[8] Development of pH nanosensors for intracellular pH measurement should not only be capable of measuring the ratio-metric fluorescent intensity changes with pH, but should also have the capability to reaches effectively the tissues of interest where the pH variations should be measured. Unfortunately none of the particle sensors mentioned above display long circulation in the blood stream and reaches the target. Polymeric micelles that are formed by the spontaneous self-assembly of amphiphilic block copolymers in block selective solvents have the morphological advantages of providing long circulation in blood.[9] Water exposed PEG corona chains of the block copolymer micelles are unreactive towards the blood and tissue components. This structural advantage allows them to stay rather long in the blood without being opsonized by the phagocytic cells and hence provide effective accumulations in pathological sites by enhanced permeation retention effect (EPR).[10, 11] Even with this excellent pharmaceutical advantage, polymeric micelles were not used for the nanosensors fabrications. The basic reasons for this is the difficulty in synthesizing well defined block copolymers and the tendency of the self-assembled block copolymer to disintegrate into unimers under infinitely diluted biological conditions. The recent developments in radical polymerization techniques like ATRP[12] allow the synthesis of well defined functional block copolymers having narrow molecular weight distribution and controlled architecture. The structural potential of the amphiphilic triblock self-assembly in a block selective solvent (water) is dependent on the mass ratio of hydrophilic to hydrophobic blocks. Functional amphiphilic triblock copolymers with comparable hydrophilic to hydrophobic ratio in a block selective solvent can be gave well defined core-shell-corona functional micelles in a spherical or cylindrical form.[13] Regioselective functionalization and cross-linking could enhance the applications of these functional nanoparticles by preventing its dissociation below the critical micelle concentration (CMC).[14-16]

In recent years reversible cross-linking strategies have achieved significant research attention due to the reversible control over the drug delivery.[17] Reversible micelle cross-linking strategies have also been reported,[18-21] in which light induced reversible photo cross-linking could overcome the difficult requirements such as use of cross-linking reagents, prolonged reaction time, and removal of excess reagent after reactions. Radiation induced

reversible photochemical dimerizations of coumarin [22] was used for the dimensional synthetic modifications of the block copolymer micelles. [23-25] The cyclobutane ring resulting from the 2πS+2πS cycloaddition between the coumarin containing unimers of the self-assembly are reversible and hence provide possibilities of photo cross-linking and de-cross-linking of the micelles by illuminating the samples at two different wavelengths.

In this paper we are explain the development of reversibly photo core cross-linked functional micelle based ratiometric pH nanosensors *via* subsequent dimensional synthetic modifications on a photo core cross-linked amphiphilic triblock copolymer self-assembly.

Experimental

Materials and measurements:

2′,7′-bis-(2-carboxyethyl)-5-(and-6) carboxyfluorescein free acid (BCECF) was purchased from Biotium. Oregon Green 488 isothiocyanate (F_2FITC) and Alexa Fluor 633 carboxylic acid succinimidyl ester (Alexa 633) were obtained from Invitrogen. 2,2'bipyridyl (bpy) (99%), PMDETA (99%), $CuCl_2$ (99.995%), trifluoroacetic acid (TFA)(99%), N-(3-Dimetyl amino propyl)-N'-ethylcarbodiimide hydrochloride (EDC·HCl) (98%), N-Hydroxysuccinimide (NHS) (98%), dialysis tubing (MWCO=12kDa), and all other solvents and chemicals were purchased from Sigma Aldrich and used as obtained. CuCl (99.995%) was washed with glacial acetic acid, followed by absolute ethanol and diethylether, dried and stored under argon. Solvents used for ATRP were purified by distillation over the drying agents indicated in parentheses, stored under molecular sieves and were transferred under argon, MeOH ($Mg(OMe)_2$, DMF (CaH_2). Argon atmosphere (99.9999%) used in the reactions was provided by AGA Denmark. NMR spectra were recorded by using 300 MHz Varian Mercury 300 BB spectrometer, IR spectra were recorded by Perkin Elmer Spectrum 100 FT-IR Spectrometer. GPC measurements were carried out with a RID10A-SHIMADZU refractive index detector and Mixed-D GPC column from Polymer Laboratories with a flow rate of 0.5 mL/min at 25 ^{0}C using DMF with 50 mM LiCl as eluent. UV-Vis spectra were recorded on Unicam Helios Uni 4923 spectrophotometer. Fluorescence measurements were carried out by the Olis Line of SLM based Spectrofluorimeter. Atomic force microscopy (AFM) images were obtained by PSIA XE-150 scanning force microscope using non-contact tapping mode close to resonance frequency of the silicon cantilever (Nanoworld, pointprobe type, force constant 42 N/m and tip radius <12 nm) of around 320kHz. All images were recorded under atmospheric conditions. Dynamic light scattering (DLS) and zeta potential measurements were carried out by Brookhaven Zeta PALS instrument.

Synthesis of PEG-*b*-PAEMA-*b*-PCMA (2)

The macroinitiator PEG-Br[26] and the monomers 2-[N-(tert-Butoxycarbonyl)Amino]ethyl methacrylate(AEMABoc)[27] and 7-(2-Methacryloyloxyethoxy)-4-methylcoumarin(CMA)[28] were synthesized by the reported procedures.

PEG-b-PAEMA(Boc)Cl: PEG-Br (1 gram, 0.19 mmol), AEMABoc (522 mg, 2.28 mmol), 2,2'bipyridyl (62 mg, 0.40 mmol) and 5 mL methanol were added to a 25 mL schlenk flask equipped with a magnetic stir bar. The flask was frozen in liquid nitrogen and CuCl catalyst (21 mg, 0.21 mmol) was added. The reaction mixture was degassed with three freeze-pump-thaw cycles to remove the oxygen, and the polymerization was carried out at 40 ^{0}C for 15 h under an argon atmosphere. The reaction was stopped by opening the flask to air and the reaction mixture was then passed through a silica gel column to remove the copper catalyst using methanol as the solvent. On exposure to air the dark brown reaction mixture turned blue, indicating the areal oxidation of the Cu(I) catalyst. After removing most of the methanol by rotary evaporation the polymer was precipitated into excess cold diethyl ether. The product was isolated by filtration and dried under vacuum; PEG-*b*-PAEMA(Boc)Cl (1.1 g, 64%). ^{1}H NMR (300 MHz, $CDCl_3$) δ (ppm): 5.50 (broad s, -N**H**), 4.0 (broad s, -OC**H**$_2$CH$_2$NH), 3.63 (s, -C**H**$_2$C**H**$_2$O), 3.37 (broad s, -OCH$_2$C**H**$_2$NH, -OC**H**$_3$), 1.82 (broad s, -C**H**$_2$ backbone), 1.43 (s, -C(C**H**$_3$)$_3$), 1.11-0.81 (m, -C(C**H**$_3$)$_2$, -C**H**$_3$ backbone); FTIR (cm^{-1}): 3387, 2892, 1716, 1520, 1466, 1391, 1361, 1342, 1279, 1241, 1150, 1112, 1060, 996, 965, 843.

PEG-b-PAEMA(Boc)-b-PCMA(1): PEG-*b*-PAEMA(Boc)-Cl (1g, 0.11 mmol), 7-(2-Methacryloyloxyethoxy)-4-methylcoumarin (CMA) (2.6 g, 9.02 mmol), $CuCl_2$ (12 mg, 0.088 mmol), PMDETA (0.068 mL, 0.33 mmol), and 10 mL of DMF, were added to a 25 mL schlenk flask equipped with a magnetic stir bar. The flask was frozen in liquid nitrogen and CuCl catalyst (11 mg, 0.11 mmol) was added. The reaction mixture was degassed with three freeze-pump-thaw cycles to remove oxygen and the polymerization was carried out at 80 ^{0}C for 24 h under an argon atmosphere. The reaction mixture was concentrated under vacuum, polymer was precipitated into excess of cold methanol, filtered and dried; PEG-*b*-PAEMA(Boc)-*b*-PCMA (2 g, 56%). ^{1}H NMR (300 MHz, $CDCl_3$) δ (ppm): 7.40-5.90 (Coumarin **H**), 4.38-4.04 (-OC**H**$_2$C**H**$_2$O-Coumarin), 4.02-3.86 (-OC**H**$_2$CH$_2$NH), 3.58 (s, -C**H**$_2$C**H**$_2$O), 3.39-3.25 (-OCH$_2$C**H**$_2$NH), 2.22 (s, -C**H**$_3$ of coumarin), 2.04-1.55 (-C**H**$_2$ backbones of PAEMA and PCMA blocks), 1.39 (s, -C(C**H**$_3$)$_3$), 1.15-0.77 (-C**H**$_3$ backbones of PAEMA and PCMA blocks).

PEG-b-PAEMA-b-PCMA: PEG-*b*-PAEMA(Boc)-*b*-PCMA (500 mg, 0.016 mmol) was treated with 1:1 TFA:DCM mixture (8 mL) for 15 h at room temperature. After removing most of the solvent under rotary evaporation, the polymer was precipitated into excess cold diethyl ether, filtered and dried. The complete deprotection of tert-Butyloxycarbonyl (Boc) was confirmed by the disappearance of Boc signal at 1.39 ppm in ^{1}H NMR (300 MHz, $CDCl_3$).

PEG-*b*-PAEMA-*b*-PCMA micelle (3)

The amphiphilic triblock copolymer (PEG-*b*-PAEMA-*b*-PCMA) (100 mg, 0.0033 mmol) was dissolved in 20 mL DMF under stirring. To the solution under stirring was added 2 mL of MilliQ

water within the time interval of 30 minutes. The stirring was continued and additional 40 mL MilliQ water was added drop wise. The cloudy micelle solution was transferred to a dialysis tubing of MWCO 12 kDa and dialyzed against MilliQ water for three days. Final micelle concentration was 1.28 mg/mL. DLS showed a hydrodynamic diameter of (Dh) = 45±2 nm and zeta-potential (ξ) measurements showed ξ = 24±1 mV.

Photo core cross-linking of the micelle (4)

2 mL of PEG-*b*-PAEMA-*b*-PCMA aqueous micelle solution (0.03 mg/mL) in a quartz cuvette was irradiated from Omnicure UV photo curing system(S 2000) with UV intensity 2W/cm^2 (measured by the radiometer) through a standard filter (320-500 nm). The sample was irradiated at different time intervals and the decrease in absorption of coumarin moiety (*ca.* 320 nm) with time was monitored.

pH nanosensor fabrication (5)

PEG-*b*-PAEMA-*b*-PCMA micelle 3.9 mL (1.28 mg/mL) under stirring was exposed to UV radiation (2W/cm^2) from the photo curing system. Progress of the photo dimerization was monitored by UV spectra (at a concentration of 0.03 mg/mL). After 55% of photo dimerization (Dh = 40±1 nm and ξ = 22±2 mV), the sample was transferred to a dialysis tube of MWCO = 12 kDa and dialyzed against a carbonate buffer of pH 9.0. To this alkaline colloidal dispersion, was added activated BCECF (4 µl). BCECF (0.25 mg/mL) was activated with EDC·HCl and NHS in water. F_2FITC (1 µl) (1 mg/mL in dry DMSO), Alexa 633 (2 µl) (1mg/mL of dry DMSO) were also added and stirred at RT for 14 h. The reaction mixture was transferred to a dialysis tube of MWCO 12 kDa and dialyzed against buffer of pH 9 for three days and then against MilliQ water for another three days. The final nanosensor concentration was 1.26 mg/mL; Dh = 41±1 nm and ξ = 17±2 mV.

Photo de-core cross-linking of the micelle nanosensor (6)

The core cross-linked micelle nanosensor 3 mL (0.03 mg/mL) in a quartz cuvette was exposed to UV radiation (λ < 255 nm). The cuvette was placed vertically 16 cm away from the 6 W 254 nm UVGL-58 UV lamp. The progress of de-cross-linking was monitored by UV-Vis spectroscopy; Dh = 38±3 nm and ξ = 16±1 mV.

Results and discussion

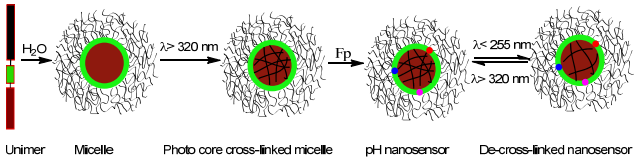

Figure 1. Schematic illustration of reversibly photo core cross-linked pH nanosensors fabrication, Fp = pH sensitive and reference fluorophore.

Figure 1 shows the synthesis of photo core cross-linked pH nanosensors. The amphiphilic triblock copolymer poly (ethylene-glycol)-*b*-poly(2-[N-(tert-Butoxycarbonyl)Amino]ethyl methacrylate)-*b*-poly(coumarin methacrylate) (PEG-*b*-PAEMA(Boc)-*b*-PCMA) (**1**) was synthesized by isolated macroinitiator ATRP (Scheme 1). Number-average molecular weight of the triblock measured by GPC was found to be lower than that calculated by ^{1}H-NMR ($CDCl_3$) peak integration. The polydispersity index (M_w/M_n = 1.21) shows narrow molecular weight distribution. These results are summarized in Table 1. The Boc-protection group was removed from PEG-*b*-PAEMA(Boc)-*b*-PCMA by treatment with trifluoroacetic acid to obtain the PEG-*b*-PAEMA-*b*-PCMA (**2**). Complete deprotection of the copolymer was confirmed by the disappearance of Boc-signal at 1.39 ppm by ^{1}H-NMR ($CDCl_3$) (Figure 2).

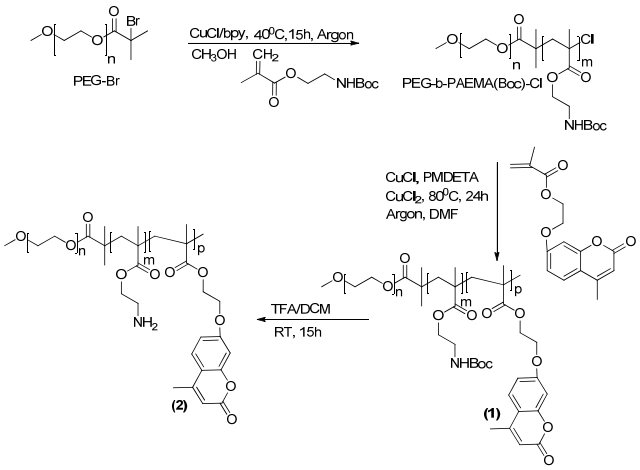

Scheme 1. Synthesis of amphiphilic triblock copolymer PEG-*b*-PAEMA-*b*-PCMA by isolated macrointiator ATRP. bpy = 2,2'bipyridine, PMDETA = N,N,N',N',N''-pentamethyldiethylenetriamine, DMF = N,N-Dimethylformamide, TFA = Trifluoroacetic acid, DCM = Dichloromethane.

Table 1. Molecular weight of PEG_{120}-*b*-$PAEMA(Boc)_9$-*b*-$PCMA_{80}$ (**1**)

M_n[a]	M_w[a]	M_w/M_n[a]	M_n[b]	n[c]	m[c]	p[c]
22100	26800	1.21	30390	120	9	80

[a] Determined by GPC, [b] Determined by NMR, [c] Number of repeating units of PEG block (n), PAEMA(Boc) block (m) and PCMA block (p).

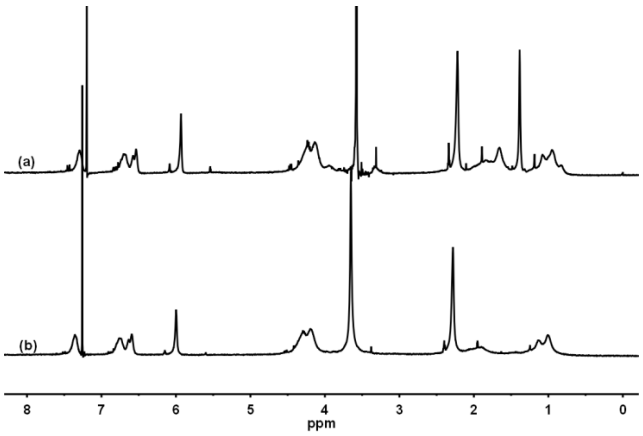

Figure 2. ^{1}H-NMR spectra of (a) PEG_{120}-*b*-$PAEMA(Boc)_9$-*b*-$PCMA_{80}$ (**1**), (b) PEG_{120}-*b*-$PAEMA_9$-*b*-$PCMA_{80}$ (**2**) in $CDCl_3$.

The amphiphilic triblock PEG-*b*-PAEMA-*b*-PCMA core-shell-corona functional micelle (**3**) having radially compartmentalized corona was prepared by dissolving PEG-*b*-PAEMA-*b*-PCMA in DMF followed by slow displacement of the common solvent (DMF) by a selective solvent for the hydrophilic block (water). The micelle was then kinetically trapped by complete replacement of the common solvent by the selective solvent *via* dialysis against MilliQ water. The presence of PEG corona and PCMA core may make the micelle biocompatible. Dynamic light scattering measurements (DLS) show number average hydrodynamic diameter (Dh) = 45±2 nm and zeta-potential (ξ) measurements show ξ = 24±1 mV (Table 2).

Table 2. Characterization data for micelle **3**, **4** and pH nanosensor **5**, **6**.

Micelle	DLS(D_h)[a] (nm)	Zeta(ξ)[b] (mV)
3	45±2	24±1
4	40±1	22±2
5	41±2	17±2
6	38±3	16±1

[a] Number average hydrodynamic diameter of aqueous micelle solution measured by DLS, [b] Zeta potential from 10 determination of 10 cycles.

The core cross-linked PEG-*b*-PAEMA-*b*-PCMA micelle (**4**) was synthesized by UV radiation induced photo core cross-linking at the PCMA core. The micelle solution (0.03 mg/mL) was exposed to UV radiation (2W/cm^2) (320 nm < λ < 500 nm) from a UV-Vis photo curing system and the decrease in coumarin absorption (*ca.* 320 nm) with respect to irradiation time was monitored by UV-Vis spectroscopy. The degree of coumarin photo dimerization (PD) at the PCMA core was also calculated from this UV-Vis spectrum. PD % = $(A_0\text{-}A_t)/A_0 \times 100$; where A_0 is the UV absorption of the coumarin core of the micelles before UV irradiation (t = 0) and after the time t, A_t (Figure 3).

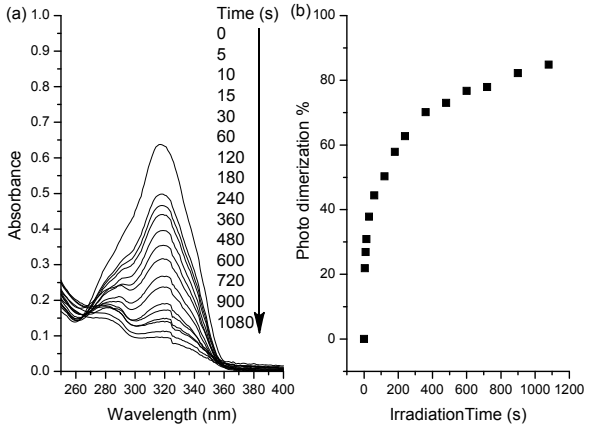

Figure 3. (a) Decrease in UV absorption of PEG-*b*-PAEMA-*b*-PCMA micelles during photo irradiation (λ>320 nm) measured by UV-Vis at different irradiation times, (b) the increase in photo dimerization degree during UV irradiation.

The micelle cross-linking by coumarin photo dimerization was further confirmed by FT-IR spectroscopy (Figure 4). Compared to the non-cross-linked micelles, the FT-IR spectra of the photo core cross-linked micelles show a shift in the carbonyl stretching absorption to higher energy with an increase in peak broadness. This indicates that as the photo cross-linking increases, the number of conjugated carbonyls in the pyrone subunits of the coumarins decrease due to the participation of the double bonds in dimerization at the micelle core. The broad absorption at 1729 cm^{-1} is due to the carbonyl groups presence at the shell region (PAEMA), and carbonyls at the PCMA core having increased -C=O character due to flexion of conjugation and decrease in double bond character caused by extension of conjugation. The alkenes C=C stretching at 1390 cm^{-1} decrease considerably after UV irradiation, which confirms the consumption of olefinic double bond in the cyclobutane ring formation. Additionally the cross-linked micelles show an increase in absorption around 1500 cm^{-1} and a broad absorption peak at 1150 cm^{-1} and 1240 cm^{-1}. These changes are also supporting the cyclobutane ring formation at the PCMA micelle core during photo irradiation of the aqueous PEG-*b*-PAEMA-*b*-PCMA micelle solution.

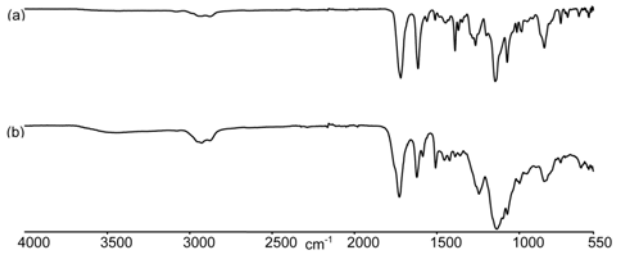

Figure 4 (a) IR spectra of non-cross-linked PEG-*b*-PAEMA-*b*-PCMA micelle (**3)** and (b) photo core cross-linked micelle,**4**.

Preparation of reversibly photo core cross-linked micelle nanosensor (**5**) is given in Scheme 2. The PEG-*b*-PAEMA-*b*-PCMA micelle (**3**) (1.28 mg/mL) was irradiated with λ > 320 nm using the same UV photo curing setup as explained above. After 55% of photo dimerization (determined from Figure 3), DLS and zeta potential measurements shows only slight decrease in hydrodynamic diameter and surface charge density of the micelles (Table 2, micelle **4**). This confirms that cross-linking occurred intramicellarly within the core rather than intermicellar cross-linking between the aggregates. The exclusive intramicellar cross-linking may be attributed to the steric stabilization mechanism offered by the PEG corona[29] The positive surface charge density further confirms the availability of free amino groups at the inner corona (shell) of the core cross-linked micelles. The photo core cross-linked micelle was then converted into a ratiometric pH nanosensor by covalently conjugating pH sensitive (F_2FITC and BCECF) and reference fluorophores (Alexa 633) at the inner corona of the micelle in an alkaline buffer (pH 9). The resulting nanosensor was purified by dialysis; DLS and zeta potential measurements show that the sensor (**5**) maintained the same size as that of the cross-linked micelle (**4**) however with a slightly decreased surface charge density due to the fluorophore attachments (Table 2). The free carboxylate groups present on the fluorophores attached to the micelle shell

may be responsible for the decrease in zeta potential.

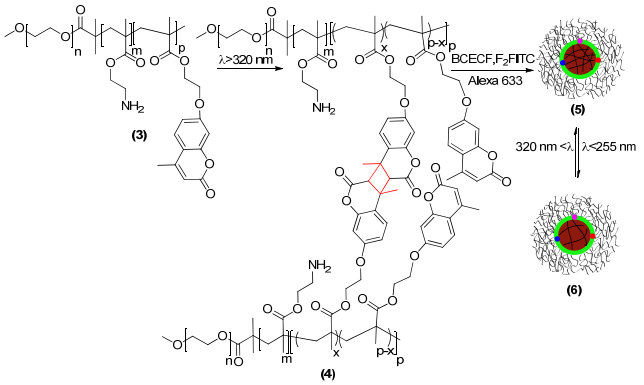

Scheme 2. Synthesis of core-shell-corona micelle based reversibly photo core cross-linked ratiometric pH nanosensors. BCECF = 2′,7′-bis- (2-carboxyethyl)-5-(and-6) carboxyfluorescein, F_2FITC (OG) = Oregon Green 488 isothiocyanate, Alexa 633 = Alexa Fluor; x is the extent of photo dimerization.

The pH sensitivity range of the pH nanosensor was determined by fluorescence measurements. The nanosensor (0.126 mg / mL)was excited (λ_{ex} = 490 nm for F_2FITC (OG) and BCECF; λ_{ex} = 561 nm for Alexa 633) in buffer of different pH. The pH dependent fluorescence emission spectra at 520 nm and pH independent reference spectra at 650 nm were recorded (Figure 5a). Fluorescence intensity (I) ratio ($I_{(F2FITC)} + I_{(BCECF)} / I_{(Alexa\ 633)}$) was plotted against the corresponding pH to obtain the pH calibration curves (Figure 5b). The pH calibration curve shows that the nanosensor is sensitive between the pH *ca.* 4 to 8. Since intracellular pH is generally between 6.8 and 7.4 in cytosol and 4.5 and 6 in the cell's acidic organelles, [30] the newly developed nanosensor will be capable of monitoring the intracellular pH in the cytosol and acidic organelles of the cells.

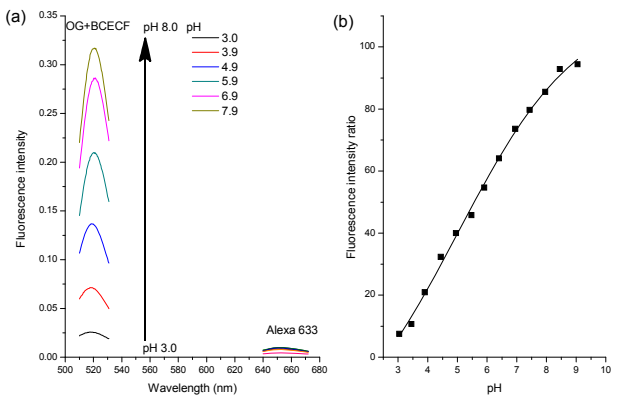

Figure 5. Representative fluorescence emission spectra for the pH nanosensor (a) and the pH calibration curve (b). Fluorescence intensity ratio = ($I_{(OG)} + I_{(BCECF)} / I_{(Alexa\ 633)}$)

Photo de-cross-linking of the micelle nanosensor was also performed. 3 mL of pH nanosensor dispersion (0.03 mg/mL) in a quartz cuvette was exposed to UV radiation (λ < 255 nm) from a 6 W 254 nm UVGL-58 UV lamp and the increase in UV absorption (*ca.* 320 nm) as a result of cyclobutane ring scission was monitored by UV-Vis spectroscopy (Figure 6a). The degree of photo de-dimerization was also calculated from the UV spectra (Figure 6b). The photo de-dimerization studies show that the complete sensor decross-linking was impossible, indicating the presence of dynamic dimerization de-dimerization equilibrium in the PCMA core of the micelle at λ < 255 nm. DLS and zeta potential measurements of the de-cross-linked micelle sensor show a slight decrease in number average hydrodynamic diameter (D_h) whereas the surface charge density remain unaltered during photo de-dimerization (Table 2). Though the complete de-cross-linking of the nanosensor was impossible, this reversibly core cross-linked micelle nanosensor may provide a platform for the development of nanosensors that are capable of monitoring intracellular pH during drug release from a de-cross-linked micelle core. Reversible micelle cross-linking strategy may also facilitate the dissociation and hence clearance of the nanosensor from the body *via* glomerular filtration; soon after its sensing applications are finished.

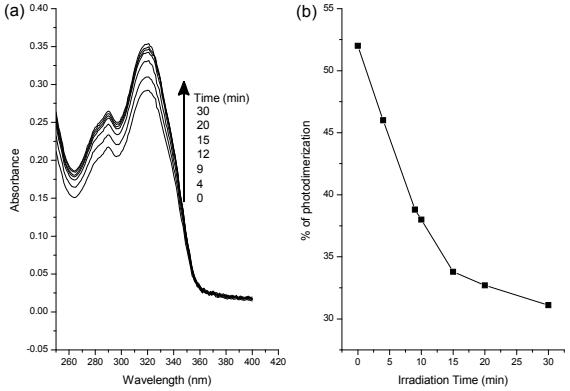

Figure 6. (a) Increase in UV absorption of core cross-linked micelle nanosensor (0.03 mg/mL) during exposure to UV radiation (λ < 255 nm) and (b) the corresponding photo de-dimerization degree of the nanosensor.

2D and 3D AFM images of the non-cross-linked and cross-linked micelle shows that the spherical micelle particles are more uniform after cross-linking (Figure 7). The narrow height distribution of the cross-linked micelle particles (histogram in Figure 7b) indicate that photo core cross-linking at the coumarin core reinforces the weak hydrophobic interactions and the resulting robust micelle shows less deformed and a more uniform spherical morphology on the hydrophilic silica surface.

Cite this: DOI: 10.1039/c0xx00000x

www.rsc.org/softmatter

PAPER

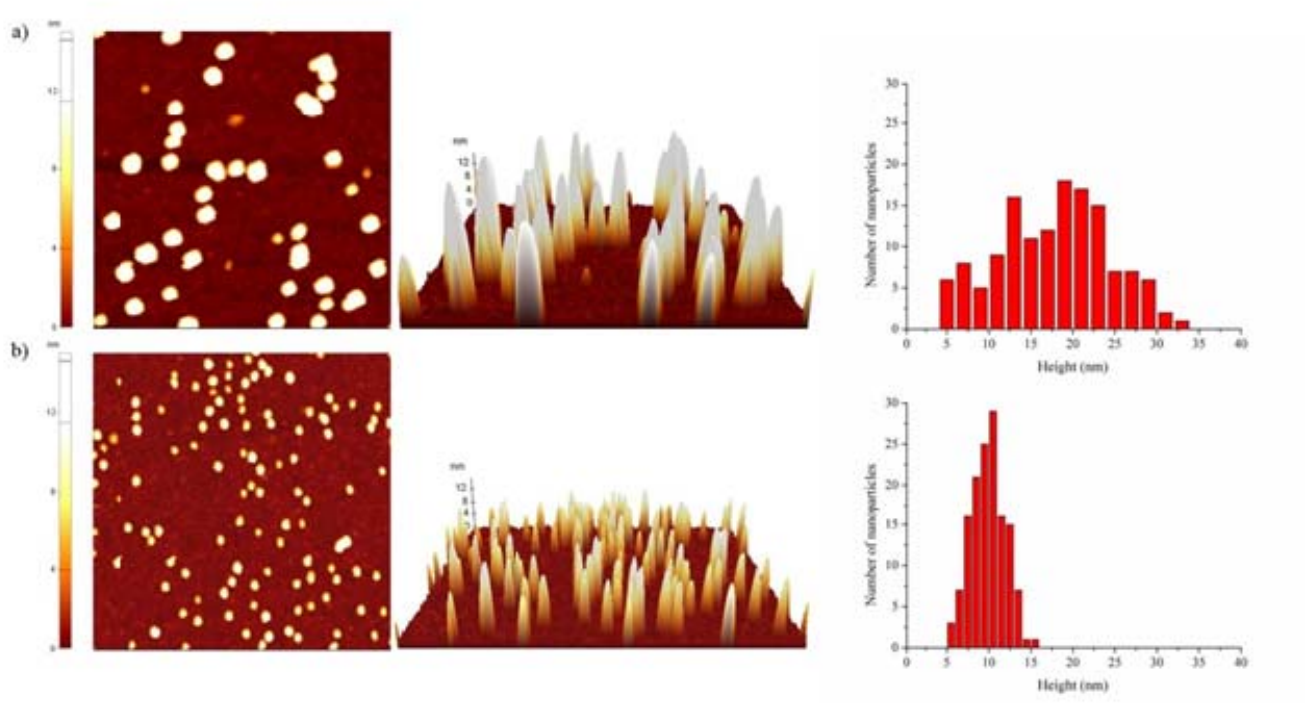

Figure 7. Tapping mode 2D and 3D AFM images and histogram representing height distributions of (a) non-cross-linked micelle, **3** and (b) cross-linked micelle, **4**. XY scan size is 1 μm x 1 μm

Conclusion

Polymeric core-shell-corona micelle based reversibly photo core cross-linked ratiometric pH nanosensors were synthesized. Wavelength dependent reversible photo dimerization of coumarin was the basis of the micelle cross-linking. Binding of pH sensitive and reference fluorophores at the shell region of the core cross-linked micelle resulted in ratiometric pH nanosensors having the pH sensitive shell protected from the external surrounding by the PEG corona. Due to the broad sensitivity range of the nanosensor (pH 4 to 8), this nanosensor may be capable of monitoring the pH in the cytosol and other intracellular organelles. The photo cross-linking may be able to prevent the disintegration of the nanosensors in biological environment under infinitely diluted condition; photo de-cross-linking may lead to disintegration of the nanosensors into unimers and hence may facilitate the excretion of the block copolymers from the body *via* renal route. The reversibly core cross-linked pH nanosensors may provide opportunity to monitor intracellular pH during drug release.

Notes and references

[a] *DTU Nanotech, Department of Micro-and Nanotechnology, Technical University of Denmark, Building 423, 2800 Lyngby, Denmark*
E-mail: thomas.andresen@nanotech.dtu.dk

Acknowledgements.

The authors would like to thank Kræftens Bekæmpelse and the Danish Research Council for Technology and Production (Grant 274-07-0172) for financial

1. R. V. Benjaminsen, H. Sun, J. R. Henriksen, N. M. Christensen, K. Almdal and T. L. Andresen, *ACS Nano*, 2011, **5**, 5864-5873.
2. E. Allard and C. Larpent, *Journal of Polymer Science Part A: Polymer Chemistry*, 2008, **46**, 6206-6213.
3. H. Sun, A. M. Scharff-Poulsen, H. Gu and K. Almdal, *Chemistry of Materials*, 2006, **18**, 3381-3384.
4. K. Almdal, H. Sun, A. K. Poulsen, L. Arleth, I. Jakobsen, H. Gu and A. M. Scharff-Poulsen, *Polymers for Advanced Technologies*, 2006, **17**, 790-793.

5. V. M. Chauhan, G. R. Burnett and J. W. Aylott, *Analyst*, 2011, **136**, 1799-1801.
6. H. Sun, K. Almdal and T. L. Andresen, *Chemical Communications*, 2011, **47**, 5268-5270.
7. A. Schulz, S. Hornig, T. Liebert, E. Birckner, T. Heinze and G. J. Mohr, *Organic & Biomolecular Chemistry*, 2009, **7**, 1884-1889.
8. J. Han and K. Burgess, *Chemical Reviews*, 2009, **110**, 2709-2728.
9. T. Vladimir P, *Journal of Controlled Release*, 2001, **73**, 137-172.
10. D. D. Lasic, *Nature*, 1996, **380**, 561-562.
11. A. L. Klibanov, K. Maruyama, V. P. Torchilin and L. Huang, *Febs Letters*, 1990, **268**, 235-237.
12. K. Matyjaszewski and N. V. Tsarevsky, *Nat Chem*, 2009, **1**, 276-288.
13. L. Lei, J.-F. Gohy, N. Willet, J.-X. Zhang, S. Varshney and R. Jerome, *Macromolecules*, 2003, **37**, 1089-1094.
14. E. S. Read and S. P. Armes, *Chemical Communications*, 2007, 3021-3035.
15. R. K. O'Reilly, C. J. Hawker and K. L. Wooley, *Chemical Society Reviews*, 2006, **35**, 1068-1083.
16. C. F. van Nostrum, *Soft Matter*, 2011, **7**, 3246-3259.
17. N. K. Mal, M. Fujiwara and Y. Tanaka, *Nature*, 2003, **421**, 350-353.
18. Y. Li, B. S. Lokitz, S. P. Armes and C. L. McCormick, *Macromolecules*, 2006, **39**, 2726-2728.
19. X. Xu, J. D. Flores and C. L. McCormick, *Macromolecules*, 2011, **44**, 1327-1334.
20. H.-i. Lee, W. Wu, J. K. Oh, L. Mueller, G. Sherwood, L. Peteanu, T. Kowalewski and K. Matyjaszewski, *Angewandte Chemie International Edition*, 2007, **46**, 2453-2457.
21. J. Jiang, B. Qi, M. Lepage and Y. Zhao, *Macromolecules*, 2007, **40**, 790-792.
22. S. R. Trenor, A. R. Shultz, B. J. Love and T. E. Long, *Chemical Reviews*, 2004, **104**, 3059-3078.
23. M. Lepage, L. Tremblay, J. Jiang, J. Babin, B. Qi and Y. Zhao, *Physics in Medicine and Biology*, 2007, **52,** 7423
24. J. Jiang, Q. Shu, X. Chen, Y. Yang, C. Yi, X. Song, X. Liu and M. Chen, *Langmuir*, 2010, **26**, 14247-14254.
25. Y. Zhao, J. Bertrand, X. Tong and Y. Zhao, *Langmuir*, 2009, **25**, 13151-13157.
26. S. Liu, J. V. M. Weaver, Y. Tang, N. C. Billingham, S. P. Armes and K. Tribe, *Macromolecules*, 2002, **35**, 6121-6131.
27. M.-H. Dufresne and J.-C. Leroux, *Pharmaceutical Research*, 2004, **21**, 160-169.
28. M. Obi, S. y. Morino and K. Ichimura, *Chemistry of Materials*, 1999, **11**, 656-664.
29. D. H. Napper, *Journal of Colloid and Interface Science*, 1977, **58**, 390-407.
30. J. Llopis, J. M. McCaffery, A. Miyawaki, M. G. Farquhar and R. Y. Tsien, *Proceedings of the National Academy of Sciences*, 1998, **95**, 6803-6808.

Appendix E

Pramod Kumar EK, Kristoffer Almdal and Thomas L. Andresen. ‘‘Synthesis and characterization of ratiometric nanosensors for intracellular pH quantification: A mixed micelle approach’’. *Chem. Commun*. **2012** (Submitted), supporting information.

Synthesis and characterization of ratiometric nanosensors for intracellular pH quantification: A mixed micelle approach

E.K. Pramod Kumar[a], Kristoffer Almdal[a], Thomas L. Andresen*[a]

Received (in XXX, XXX) Xth XXXXXXXXX 2011, Accepted Xth XXXXXXXXX 2011
First published on the web Xth XXXXXXXXX 2011
DOI: 10.1039/b000000x

Optical nanoparticle pH sensors designed for ratiometric measurements in living cells have previously been synthesized using post-functionalization approaches to introduce sensor molecules and to modify nanoparticle surface chemistry. This strategy often results in low control of the nanoparticle surface chemistry and is prone to batch-to-batch variations, which is undesirable for succeeding sensor calibrations and cellular measurements. Here we provide a new synthetic approach for preparing nanoparticle pH sensors based on self-organization principles, which in comparison to earlier strategies offers a much higher design flexibility and high control of particle size, morphology and surface chemistry.

Intracellular pH plays an important role in cellular processes, is highly regulated in cellular organelles,(RR)[1] and has been linked with cell cycle progression and programmed cell death.(RR)[4,5] Thus, quantification of pH in organelles of living cells is important for increasing our understanding of cellular processes. Furthermore, A high number of nanoparticle-based pH-sensitive drug delivery systems are being reported every year (REF Thompson, Kaasgaard exp opin 2010, Andresen, Prog. Lipid Res. 2005, A polymer micelle pH article), however, there is very limited knowledge on the intracellular trafficking of these systems, particularly regarding the pH that the particles are experiencing after internalization. At present, it is just assumed that the pH-sensitive drug delivery systems ends up in acidic compartments but this has not been tested and it is reasonable to hypothesize that their trafficking in cells depend on particle characteristics such as size, morphology and surface chemistry.

Nanoparticle-based pH sensors (nanosensors) for optical measurements could play an important role in enhancing our knowledge on how physicochemical characteristics of nanoparticles effect trafficking in cells, which could further improve our understanding of how to design better drug delivery systems that release their cargo in endosomes and/or lysosomes in a controlled manor. The methodology for conducting such measurements of pH in the endosome-lysosome system using nanoparticle-based pH sensors is not well developed, however, we recently reported new advancements in this area (REF ACS Nano). An additional challenge remains; we have to make nanoparticle sensor systems with precisely controlled physicochemical characteristics, with particular focus on controlling surface chemistry.

We and others have earlier synthesized nanoparticle pH sensors based on various matrices, e.g. by using microemulsion polymerization to obtain hydrocolloid-based nanosensors (REF Sun and Kopelman or Aylott). By coupling pH sensitive fluorophores (fluorescein and oregon green) and a pH insensitive dye (rhodamine B) to a polymeric nanoparticle, we recently reported a nanosensor allowing ratiometric measurement with a pH measurement range of 3.9 to 7.3 for measurement in living mammalian cells (REF ChemComm). In a later paper we further showed that the broad measurement range is highly important for live cell measurements of the endosome-lysosome pathway (REF ACS Nano). One of our main objectives in this research is to study the role of targeting ligands and surface chemistry of nanoparticles during endocytosis and trafficking in cells. However, we find that the nanoparticle post-functionalization procedure we and others have used, i.e. where the nanoparticles are synthesized before the desired functionalities are introduced, makes it difficult to control surface chemistry and targeting ligand density during synthesis. Furthermore, the succeeding characterization of the nanosensor surface is challenging.

Synthesis of nanoparticles by use of self-organization principles offers a way to build highly complex materials from simple building blocks.(RP)[1] In the present work, we have investigated polymer-based micelles as nanosensors where the desired functionality, morphology and surface chemistry is controlled by combining different polymer block copolymers (Fig. 1). The micelle nanosensor design is based on triblock copolymers where the middle block is used as a funcitonalizaiton region where fluorescent sensor dyes are attached.

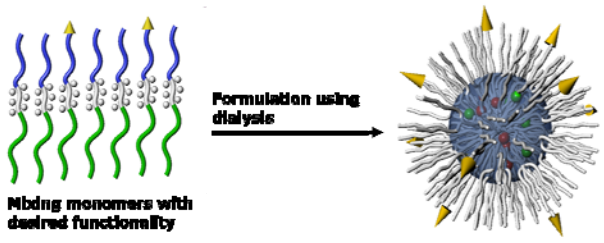

Figure 1. Polymer micelles are formed with high functionality by combining simple polymers with attached fluorescent dyes (red and green spheres) for pH measurements and targeting ligands (yellow cones) in organic solvent. Dialysis against a buffer solution results in formation of micelle based nanosensors with the desired functionality.

We have synthesized micelles with fluorescein and oregon green as pH sensor dyes and with rhodamine B as reference dyes to form nanosensors for ratiometeric pH measurements and with a cell penetrating peptide as targeting ligand. In order to obtain micelles with controlled size, functionality and morphology, well-defined triblock copolymer building blocks had to be synthesized and in the present work we have used atom transfer radical polymerization (ATRP),(RP)[2,26] which provides the necessary control with respect to polymer polydispersity and molecular architecture.

The amphiphilic triblock copolymers, poly(ethylene glycol)-b-poly(hydroxyethyl methacrylate)-b-poly(methyl methacrylate) (PEG-b-PHEMA-b-PMMA) (Mn=14500) and Boc-NH-poly(ethylene-glycol)-b-poly(hydroxyethyl methacr ylate)-b-poly(methyl methacrylate) (Boc-NH-PEG-b-PHEMA -b-PMMA) (Mn = 14400) were synthesized by ATRP (Scheme 1), see supporting information. From ^{1}H-NMR and GPC analysis, the average degree of polymerization and apparent molecular weight and polydispersity index (Mw/Mn) for each of the synthesized amphiphilic triblock copolymers was estimated and calculated (see table 1).

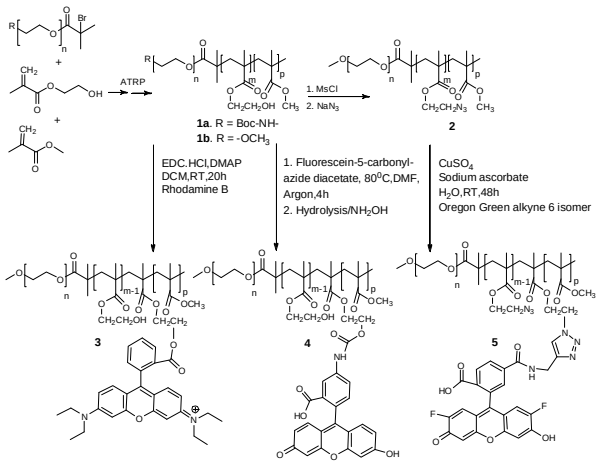

Scheme 1. Synthesis of fluorescently labelled amphiphilic triblock copolymers

Table 1. Molecular weight of Boc-NH-PEG$_{110}$-b-PHEMA$_5$-b-PMMA$_{71}$ (1a) and PEG$_{127}$-b-PHEMA$_7$-PMMA$_{80}$ (1b)

Polymer	Mn[a]	Mw[b]	Mn[b]	Mw/Mn[b]
1a	12810	19900	14400	1.38
1b	13000	19500	14500	1.34

[a] by ^{1}H-NMR, [b] by GPC measurements

The coupling of the fluorophores to the middle block of the copolymers to create pH nanosensors for optical measurements can be achieved in multiple ways. We used three different conjugation methods in the present work (Scheme 1). Hydroxyl groups in the triblock copolymer PEG-b-PHEMA-b-PMMA interface region (PHEMA) was converted into azido groups by nucleophilic substitution using mesyl chloride.(RP)[28] The formation of poly(ethylene glycol)-b-poly(2-azidoethyl methacrylate)-b-poly(methyl methacryl ate) (PEG-b-PAzEMA-b-PMMA) (2) was confirmed by ^{1}H-NMR and by IR spectroscopy (azide peak at 2107 cm^{-1}). Fluorescein conjugation was achieved by Curtius rearrangement (4),[29] oregon green by click chemistry (5), (RP)[30(Andresen)] and Rhodamine B by esterification (3).(REF)[Andresen] Conjugation of each of the fluorophores was confirmed by GPC analysis and fluorescence spectroscopy.

As a targeting ligand, a cysteine polyarginine cell penetrating peptide (cys-CPP) was introduced to the distal end of PEG in the triblock copolymers via a Michael addition to a pre-installed maleimide on the polymer (see supporting information).(REF)[Jølck,rev] In order to evaluate the CPP conjugation efficiency we derivatised the cys-CPP with Rhoadamine B (Rho-cys-CPP). Both peptides were prepared by solid phase synthesis. The Rho-cys-CPP allowed precise quantification of the coupling efficiency of the conjugation reaction by fluorescence spectroscopy. When introducing the peptide in 1:1 molar ratio between the peptide and polymer maleimide in water the coupling efficiency was 41%. By using excess CPP >90% conversion could be achieved. The same conditions were hereafter used to couple the cys-CPP without fluorophore to the distal end of PEG.

Micelle nanosensors for pH measurement could now be prepared by combining PEG-PHEMA-PMMA with four triblock copolymers conjugated to the pH sensitive fluorescein and oregon green, insensitive Rhodamine B, and one with the CPP. This was achieved by dissolving the polymers in a desired ratio in DMF succeeded by dialysis against MilliQ water or a buffer solution (e.g. PBS). This procedure resulted in polymeric micelle based ratiometric pH nanosensors with a very controllable size, which can be tuned by the molecular weight of the polymers, and with high control of surface chemistry and functionality depending on the polymer ratios (Fig. 1).

The polymer micelles are designed to have the reference and pH sensitive fluorophores in the interface region below the PEG corona where they are shielded against coordination effects of proteins and the biological environment in the cells. Förster resonance energy transfer (FRET) from fluorescein and oregon green to rhodamine B can be a challenge when using high fluorophore conentrations. This does not affect the actual pH measurements, as it is based on a ratiometric measurements and therefore accounted for by the calibration curve,(REF)[ACSNano] but it effects signal intensity and can be problematic from this point of view for cellular measurements. However, by controlling the polymer ratios and thereby the fluorophore concentrations, it is simple to prepare nanosensors with sufficient signal intensity to conduct reliable measurements in living cells using standard fluorescence microscopes.

The pH nanosensor was characterized by dynamic light scattering (DLS), and cryo-TEM measurements. DLS measurements showed that the sensor has a hydrodynamic diameter of 51±3nm. Cryo-TEM of the nanosensor shows "spherical" assemblies with high molecular density (Fig. 2a). Based on the size and previous experience, we believe that the PEG layer is not visualized well in the cryo-TEM and it is the core of the micelle we see as a dense structure. It is interesting that the interface area between the assembly and the water phase is not minimized indicating that the surface tension is

relatively low. Based on this, we hypothesize that the structures are highly flexible and interestingly we have observed that if CPP is not present on the micelle surface these micelles are only very poorly internalized by cells in comparison to other nanoparticle systems (data not shown).

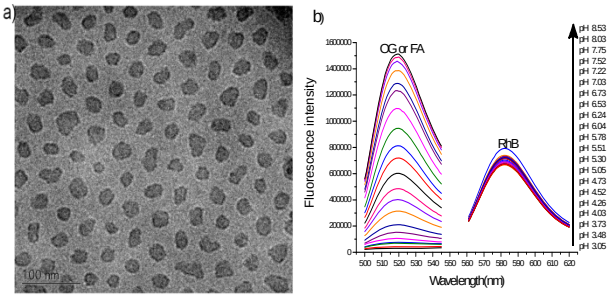

Figure 2. a) Cryo- Tem image of nanosensors, b) Fluorescence emission spectra at different pH of the nanosensors.

Next, pH calibration curves were constructed by fluorescence spectroscopy using buffer solutions of different pH, and an excitation wavelength of 490 to excite fluorescein and oregon green and 543 nm for rhodamine B. Fluorescence emission spectras of the nanosensors as a function of pH are plotted in Fig. 2b. From the fluorescence emission spectras maximum intensity was found for each of the individual fluorophore emmision spectras and the fluorescence intensity ratios (I_{OG} or I_{FA}/I_{RhB}) was calculated and plotted against pH to obtain the ratiometric calibration curves (Fig. 3). It is clear that the nanosensors are responsive to the change in pH and by using fluorescein, oregon green and rhodamine B, a measurement range from pH approximately 4,3 to 7,8 is obtained. Thus, the sensors behave as expected being responsive to a range that corresponds to the pKa value of fluorescein and Oregon green.(REF)[sun] Furthermore, response time and reversibility measurements of the nanosensors shows that the sensors are quickly responsive towards change in pH (within microseconds) and are reversible in their measurement, which shows that they are chemically stable in the conditions of the experiment (Fig. 4).

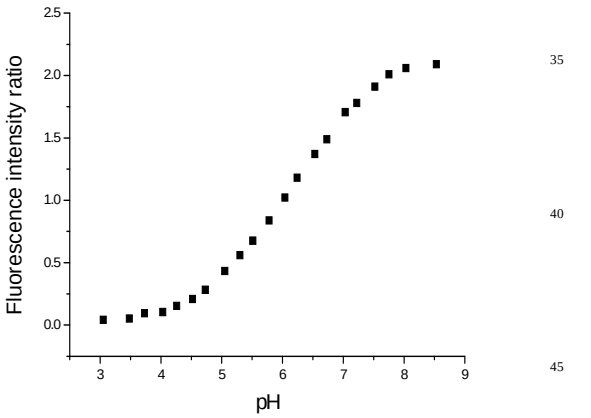

Figure 3. Ratiometric pH calibration curve for the nanosensor

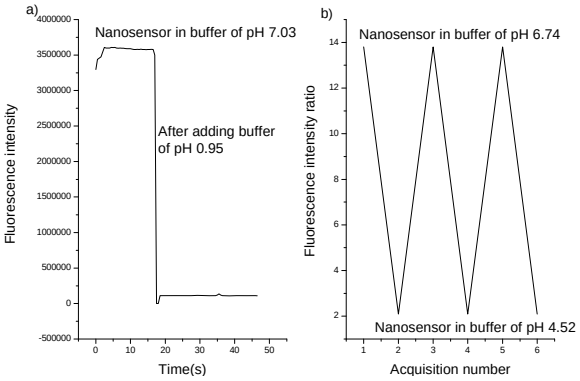

Figure 4. Response time (a) and reversibility (b) of nanosensor measurement evaluated by changing buffer pH of the nanosensor dispersion.

In conclusion, the mixed micelle approach for the preparation of nanoparticle sensors provides a flexibility in optimizing sensor properties that is not possible with previously reported nanosensors. The composition of pH sensitive and reference fluorophores in the nanosensors can be easily adjusted. By controlling the fluorophore-polymer density in the micelles it is possible maximize signal intensity and control the spectroscopic properties of the nanosensor. Furthermore, the surface density of the targeting ligands on the micelle surface is easily controlled by altering the amount of peptide bearing polymers in the nanosensors formulations. Thus, the mixed micelle approach provides a new method for preparing nanosensors for effective intracellular pH measurements.

Acknowledgement.
The authors would like to thank Kræftens Bekæmpelse and the Danish Research Council for Technology and Production (Grant 274-07-0172) for financial.

Notes and references

[a] *Technical University of Denmark, Department for Micro- and Nanotechnology, DTU Nanotech, 2800 Lyngby, Denmark. Fax: +45 4588 7762; Tel:+ 45 4525 8168; E-mail: thomas.andresen@nanotech.dtu.dk*

† Electronic Supplementary Information (ESI) available: [details of any supplementary information available should be included here]. See DOI: 10.1039/b000000x/

References will be added here

Synthesis and characterization of ratiometric nanosensors for intracellular pH quantification: A mixed micelle approach

E.K. Pramod Kumar[a], Kristoffer Almdal[a], Thomas L. Andresen*[a]

[a] Technical University of Denmark, Department for Micro- and Nanotechnology, DTU Nanotech, 2800 Lyngby, Denmark. Fax: +45 4588 7762; Tel:+ 45 4525 8168.

E-mail: thomas.andresen@nanotech.dtu.dk

Table of Contents

1. Materials and methods

2-Hydroxyethyl methacrylate (HEMA) (99%) and Methyl methacrylate (MMA) (99%) were obtained from Sigma Aldrich and radical inhibitors were removed by passing reagents through a column with basic alumina. Triethylamine (TEA) was distilled from calcium hydride and stored under molecular sieves (4Å). 2-Bromo-isobutyryl-bromide (98%), CuCl (99.995%), 2,2'bipyridyl (bpy) (99%), PMDETA (99%), $CuCl_2$ (99.995%) ,Methanesulphonyl chloride (MsCl) (99.7%), Anhydrous pyridine (99.8%), Sodium azide, Trifluroacetic acid (TFA), 3-maleimido-propionicacid-N-hydroxysuccinimide-ester, dialysis tubing (MWCO = 12kDa, 2 kDa), N-(3-Dimetyl amino propyl)-N'-ethylcarbodiimide hydrochloride (EDC.HCl) (98%), $CuSO_45H_2O$ (98%), (+)-Sodium L-ascorbate and DMAP (99%) were purchased from Sigma Aldrich and used without further purification. CH_3O-PEG-OH poly (ethylene glycol) monomethylether (Mn = 5000), and Rhodamine B were purchased from Fluka, Fluorescein-5-carbonyl azide diacetate and Oregon Green® 488 alkyne 6-isomer was from Invitrogen, Boc-NH-PEGOH from Iris Biotech GmbH. All solvents were purchased from Sigma Aldrich. Solvents used for Atom transfer polymerization (ATRP) were purified by distillation over drying agents as indicated, stored under molecular sieves and were transferred under argon. MeOH ($Mg(OMe)_2$), toluene (CaH_2), DMF (CaH_2). Other solvents were used as obtained.

^{1}H-nmr spectra were recorded on a Bruker 250 MHz in solvents as indicated. Chemical shifts (δ) are given in ppm relative to TMS. The residual solvent signals were used as reference and the chemical shifts converted in to TMS scale ($CDCl_3$: δ_H = 7.24 ppm, ^{6}d-DMSO: δ_H = 2.50 ppm). Infrared spectra's were recorded by Perkin Elmer FTIR Spectrometer (using KBr pellets). The wave numbers of recorded IR signals were quoted in cm^{-1}. The number average molecular weight (Mn) weight average molecular weight (Mw) and polydispersity (PD) (Mw/Mn) of block copolymers were determined by GPC analysis based on poly styrene calibration standards. Measurements were carried out by using Mixed-D GPC column from Polymer Laboratories (7.4 × 300 mm) and RID10A-SHIMADZU refractive index and UV detectors. DMF with 50mM LiCl solution was used as eluent. Hydrodynamic diameters (Dh) and size distributions of the amphiphilic colloidal suspension in MilliQ water at 25^0C were determined by Brookhaven ZETA PALS instrument. The calculation of the particle size distribution and distribution averages were performed by with the ISDA software package (from Brookhaven) through CONTIN particle size distribution analysis routines. All determinations were made in triplicate and duration of 2 minutes each. Zeta potential measurements were carried out by using Brookhaven ZETA PALS analyzer. The measurements were made in MilliQ water at 25^0C, and the zeta potential (ξ) was calculated using Smoluchowski equation. Electrophoretic mobility (μ) = $\boldsymbol{\xi\, \epsilon/\eta}$, where η and ϵ are the absolute viscosity and dielectric constant of the medium respectively. Mean value of ξ was chosen from 10 determinations of 10 data accumulations. Fluorescence measurements were carried out by using an Edinburgh instruments F-900 fluorometer. Peptide purification was done using a semipreperative Waters HPLC system equipped with a 2489 UV/Visible detector system and further characterized using Bruker Daltonics MALDI-TOF. Cryo-TEM measurements were carried out by using JEOM Transmission electron microscope.

2. Synthesis and characterization of amphiphilic triblock copolymers

2.1 Synthesis of PEG-b-PHEMA-b-PMMA

Synthesis of the macroinitiator PEG-Br

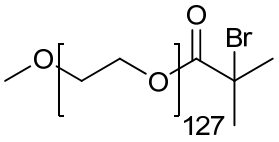

Following a modified procedure by Liu et al.,[1] CH_3O-PEG-OH, Mn = 5000 (5 gram, 1 mmol) was dissolved in 60 ml of toluene. After azeotropic distillation of 10 mL of toluene under reduced pressure to remove traces of water, TEA (0.278 mL, 2 mmol) was added and the solution was cooled to room temperature. 2-bromoisobutyryl bromide (0.185 mL, 1.5 mmol) was added drop wise and the reaction mixture was stirred at 40 ^{0}C for 2 days. The solution was filtered and most of the toluene was removed by rotary evaporation prior to precipitation into 10 fold excess of cold ether. The crude polymer was dried under vacuum, dissolved in water at pH 8-9 and then extracted with DCM. The organic layer was collected dried over anhydrous Na_2SO_4. The removal of the solvent under reduced pressure afforded the purified macro initiator in high yield: 5.5 g (99%). ^{1}H-NMR (250 MHz in $CDCl_3$): δ 3.6 (s, -C**H**$_2$C**H**$_2$O-), 1.9 (s, -C(C**H**$_3$)$_2$-); FTIR (cm^{-1}): 2887, 1737, 1466, 1359, 1342, 1279, 1241, 1148, 1107, 1060, 963, 841; GPC: Mn = 5630, Mw = 6320, PD (Mw/Mn) = 1.12.

Synthesis of diblock copolymer PEG-b-PHEMA-Cl

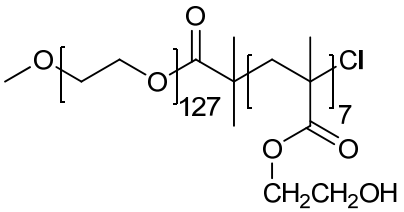

PEG-Br (1 gram, 0.1869 mmol), HEMA (0.226 mL, 1.86 mmol), 2,2'bipyridyl (61 mg, 0.39 mmol, 2.1 equiv) and 5 mL of dry methanol were added to a 25 mL Schlenk flask equipped with a stirrer bar. The solution was frozen in liquid nitrogen and CuCl catalyst (20 mg, 0.205 mmol) was added. The reaction mixture was then degassed with three freeze-pump-thaw cycles (each 15 minute long) to remove oxygen. The polymerization was hereafter carried out at 25^{0}C for 24 h under argon atmosphere. The resulting dark brown reaction mixture was passed through a silica gel column using methanol as solvent to remove the copper. After removing the methanol by rotary evaporation the polymer precipitated into excess cold diethyl ether and isolated by filtration The precipitate was dried under vacuum giving a good yield of 1 g (82%) of the diblock copolymer. ^{1}H-NMR (250 MHz in ^{6}d-DMSO): δ 4.9 (s, -OH), 3.9-3.4 (-COOC**H**$_2$CH$_2$-, -C**H**$_2$C**H**$_2$O-, -COOCH$_2$C**H**$_2$), 2.1-1.5 (-C**H**$_2$-backbone of PHEMA), 0.8((-C**H**$_3$ of PHEMA); FTIR (cm^{-1}): 3405, 2892, 2741, 1731, 1469, 1359, 1344, 1279, 1244, 1153, 1112, 1060, 964, 843; GPC: Mn = 6560, Mw = 8350, PD (Mw/Mn) = 1.27.

Synthesis of triblock copolymer PEG-b-PHEMA-b-PMMA

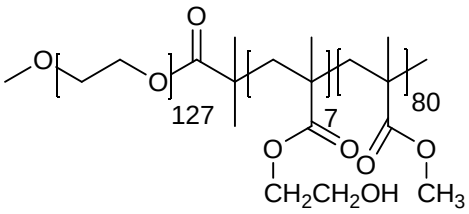

PEG-b-PHEMA-Cl (500 mg, 0.076 mmol), MMA (0.647 mL, 6.46 mmol), $CuCl_2$ (7.7 mg, 0.057 mmol), PMDETA (0.052 mL, 0.25 mmol) and 2 mL of DMF were added to a 25 mL schlenk flask containing a stirrer bar. The solution was frozen in liquid nitrogen, and CuCl catalyst (7 mg, 0.076 mmol) was added. After degassing using three freeze-pump-thaw cycles (each cycle 15 minute long) to remove oxygen, the polymerization was carried out at 35^0C for 25 h under argon atmosphere. The mixture was then concentrated under vacuum and the polymer was precipitated in petroleum ether. The crude triblock polymer was extracted with water to remove the possible existing water soluble PEG-b-PHEMA diblock copolymer. The purified water insoluble triblock copolymer was filtered and lyophilized giving 0.7 g (63%) of the desired compound. ^{1}H-NMR (250 MHz in DMSO): δ 4.9 (s, -OH), 4.0-3.4 (-COOC**H**$_2$CH$_2$, -C**H**$_2$C**H**$_2$O, -COOC**H**$_3$, -COOCH$_2$C**H**$_2$), 2.1-1.6 (-C**H**$_2$ backbone of PHEMA and PMMA), 1.1-0.5 (-C**H**$_3$ backbone of PHEMA and PMMA); FTIR (cm^{-1}) :3422, 2888, 1731, 1469, 1361, 1342, 1279, 1243, 1148, 1109, 1060, 965, 841; GPC: Mn = 14500, Mw = 19500, PD (Mw/Mn) =1.34, Mn (from ^{1}H-NMR) = 13000.

2.2 Synthesis and characterisation of Boc-NH-PEG-b-PHEMA-b-PMMA

Synthesis of the macroinitiator Boc-NH-PEG-Br

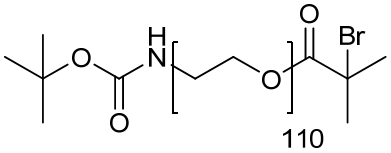

Following a modified procedure by Liu et al, Boc-NH-PEG-OH Mn = 4950 (1000 mg, 0.20mmol) was dissolved in 12 mL of toluene. After azeotropic distillation of 2 mL of toluene under reduced pressure to remove traces of water, TEA (0.053 mL, 0.4 mmol) was added and the solution was cooled to room temperature. 2-bromoisobutyryl bromide (0.038 mL, 0.3 mmol) added drop wise to the above solution and the reaction mixture was stirred at 40 ^{0}C for 2 days. The solution was filtered and most of the toluene was removed by rotary evaporation prior to precipitation into 10 fold excess of cold ether. The crude polymer was dried under vacuum, dissolved in water at pH 8-9 and then extracted with DCM. The organic layer was collected and dried over anhydrous Na_2SO_4. The removal of the solvent under vacuum afforded the purified macro initiator in high yield: 1 g (98%). ^{1}H-NMR (250 MHz in DMSO): δ 3.6 (s, -C**H**$_2$C**H**$_2$O), 1.9 (s, -C(C**H**$_3$)$_2$), 1.4 (s,-COOC(C**H**$_3$)$_3$); FTIR (cm^{-1}): 2896, 1974, 1737, 1640, 1469, 1361, 1342, 1279, 1243, 1150, 1112, 1060, 1060, 961, 841; GPC: Mn = 5100, Mw = 5151, PD (Mw/Mn) = 1.01.

Synthesis of diblock copolymer Boc-NH-PEG-b-PHEMA-Cl

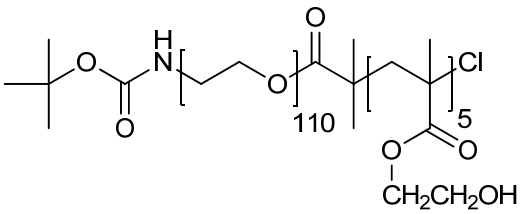

Boc-NH-PEG-Br (700 mg, 0.137 mmol), HEMA (0.178mL, 1.37 mmol), 2,2'bipyridyl (44 mg, 0.287 mmol) and 7 mL of methanol were added to a schlenk flask equipped with a stirrer bar. The flask was frozen in liquid nitrogen and added CuCl catalyst (14.9 mg, 0.151 mmol). The reaction mixture was degassed with three freeze-pump-thaw cycles (each 15 minute long) to remove the oxygen. The polymerization was hereafter carried out at 25^0C for 24 h under argon atmosphere. The resulting dark brown polymer solution was passed through a silica gel column to remove the copper catalyst using methanol as solvent. After removing most of the methanol by rotary evaporation the polymer was precipitated into excess cold diethyl ether and isolated by filtration. The precipitate was dried under vacuum giving a good yield of 0.66 g (77%). ^{1}H-NMR (250 MHz in DMSO): δ 4.9 (s, -OH), 4.0-3.4 (-COOC**H**$_2$CH$_2$,-C**H**$_2$C**H**$_2$O, -COOCH$_2$C**H**$_2$), 2.0-1.5 (-C**H**$_2$ backbone of PHEMA), 1.4 (s, -COOC(C**H**$_3$)$_3$), 0.8 (-C**H**$_3$ of PHEMA); FTIR (cm^{-1}): 3452, 2887, 2741, 1974, 1731, 1645, 1469, 1359, 1344, 1281, 1243, 1148, 1114, 1060, 963, 946, 841; GPC: Mn = 6300, Mw = 7430, PD (Mw/Mn) = 1.18.

Synthesis of triblock copolymer Boc-NH-PEG-b-PHEMA-b-PMMA

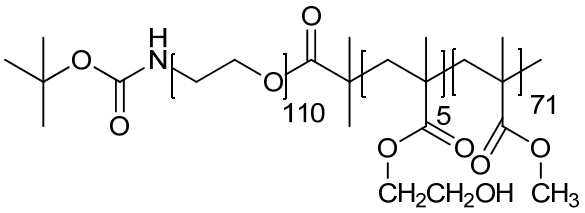

Boc-NH-PEG-b-PHEMA-Cl (500 mg, 0.079 mmol), MMA (0.72 mL, 6.74 mmol), $CuCl_2$ (8.5 mg, 0.0632 mmol) PMDETA (0.057 mL, 0.27 mmol) and 3 mL of DMF were added to a 25 mL schlenk flask equipped with a stirrer bar. The solution was frozen in liquid nitrogen and CuCl catalyst (7.8 mg, 0.079 mmol) was added. After degassing using three freeze-pump-thaw cycles (each cycle 15 minute long) to remove the oxygen, the polymerization was carried out at 35^0C for 25 h under argon atmosphere. The reaction mixture was then concentrated under vacuum and the polymer was precipitated in petroleum ether. The crude triblock copolymer was extracted with water to remove the possible existing water soluble BocNH-PEG-b-PHEMA diblock copolymer. The purified water insoluble triblock copolymer was filtered and lyophilized gives an yield 0.7 g (61%) of the desired polymer. ^{1}H-NMR (250 MHz in DMSO): δ 4.8 (s, -OH), 3.9-3.4 (-COOC**H**$_2$CH$_2$, -C**H**$_2$C**H**$_2$O, -COOC**H**$_3$, -COOCH$_2$C**H**$_2$), 2.0-1.5 (-C**H**$_2$ backbone of PHEMA and PMMA), 1.4 (s,-COOC(C**H**$_3$)$_3$), 1.1-0.5 (-C**H**$_3$ of PHEMA and PMMA); FTIR (cm^{-1}): 3439, 2952, 1967, 1733, 1634, 1488, 1451,

1352, 1277, 1247, 1195, 1150, 1107, 1060, 961, 912, 841; GPC: Mn = 14400, Mw = 19900, PD (Mw/Mn) = 1.38, Mn (from ^{1}H-NMR) = 12810.

3. Conjugation of fluorophores to the triblock copolymers

Conjugation of Fluorescein to PEG-b-PHEMA-b-PMMA

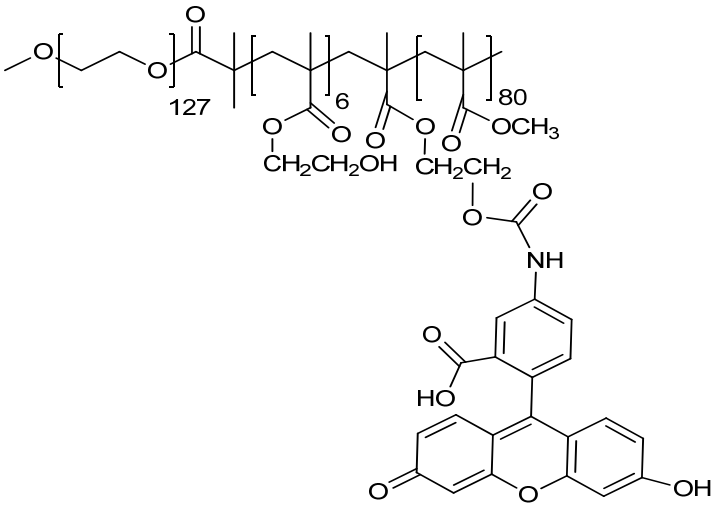

PEG-b-PHEMA-b-PMMA (100 mg, 6.8 µmol) and Fluorescein-5-carbonyl azide diacetate (3.63 mg, 13.6 µmol) were dissolved in 4ml of DMF in a 10 mL round bottom flask. After stirring the solution at 80^{0}C for 4h, two drops of hydroxyl amine aqueous solution (50% wt/V) and 2mL of ethanol was added and mixed well to hydrolyze the acetate groups. The yellow coloured solution was then cooled to room temperature and transferred into dialysis tubing of (MWCO 2kDa) and dialyzed against carbonate buffer of pH 9.2 for three days and then against MilliQ water for another three days .The micelle solution was then lyophilized to get the pure product. The binding of Fluorescein to the polymer was confirmed by GPC analysis (Figure S4) and also by fluorescence spectroscopy.

Conjugation of Rhodamine B to PEG-b-PHEMA-b-PMMA

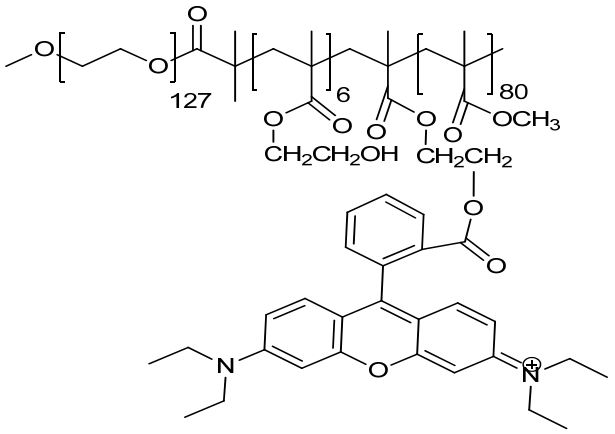

To an ice cold solution of PEG-b-PHEMA-b-PMMA (500 mg, 0.034 mmol) and Rhodamine B (17.9 mg, 0.0374 mmol) in 5 mL DCM, was added EDC.HCl (8 mg, 0.040 mmol) and DMAP (0.207 mg, 0.0017 mmol) which was stirred at 0^0C for 30 minutes. The reaction mixture was slowly warmed to room temperature and stirred at room temperature for another 20 h. After removing most of the solvent by rotary evaporation, the crude product was precipitated into excess of cold diethyl ether. The Rhodamine bounded polymer was further purified by dissolving it in DMF and using dialysis (MWCO = 2kDa) against MilliQ water for three days. After three days of continuous dialysis, solid RhB conjugated triblock copolymer was isolated by lyophilization. The binding of Rhodamine B to the polymer was confirmed by GPC analysis (Figure S4) and also by fluorescence spectroscopy.

Conjugation of Oregon Green 488 alkyne 6-isomer to PEG-b-PAzEMA-b-PMMA using click reaction

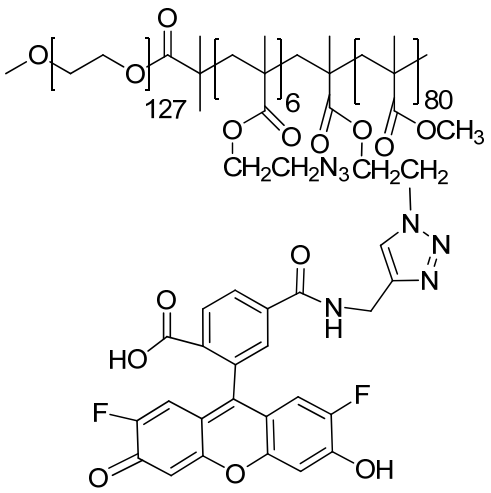

The triblock copolymer PEG-b-PHEMA-b-PMMA (0.5 g, 0.034 mmol) was dissolved in 15 mL dry pyridine and the solution was cooled to 0^0C. MsCl (0.130 mL, 1.7 mmol) in dry DCM (5mL) was added drop wise over several minutes. The resulting solution was warmed to room temperature and stirred over night. After filtration

of the solid precipitate, the filtrate was washed with saturated $NaHCO_3$ solution, extracted with DCM and dried over anhydrous Na_2SO_4. After removing most of the DCM by rotary evaporation, the mixture was precipitated into excess of cold diethyl ether to obtain yellow mesylated polymer. The mesylated polymer (200 mg, 0.013mmol) was dissolved in 3 ml DMF, and NaN_3 (45 mg, 0.689 mmol) was added .The solution was stirred at 90^0C for 5 h under argon atmosphere, then at room temperature for another 20 h. After removing most of the DMF under vacuum, the polymer was precipitated into an excess of cold diethyl ether followed by drying under vacuum giving PEG-b-PAzEMA-b-PMMA polymer. This triblock copolymer was further purified by dissolving it in DMF and using dialysis against MilliQ water for three days .The pure product was then recovered by lyophilization giving a yield of 0.136 g (72%). ^{1}H-NMR (250 MHz in DMSO): δ 4.1-3.4 (-C**H**$_2$CH$_2$N$_3$, -C**H**$_2$C**H**$_2$O, -COOC**H**$_3$, -CH$_2$C**H**$_2$N$_3$), 2.0-1.6 (-C**H**$_2$ backbone of PHEMA and PMMA), 1.0-0.6 (-C**H**$_3$ of PHEMA and PMMA); FTIR (cm^{-1}): 2952, 2896, 2107, 1729, 1486, 1451, 1385, 1350, 1275, 1243, 1191, 1148, 1109, 987, 963, 841, 748.

PEG-b-PAzEMA-b-PMMA (15 mg, 1.0 µmol) was dissolved in 3 mL DMF by stirring over night. To the solution under stirring was added 0.3 mL of MilliQ water with in the interval of 30 minutes, followed by 6 mL more MilliQ water drop wise. The cloudy micelle solution was transferred into a dialysis tubing (MWCO = 12 kDa) and dialyzed against MilliQ water for three days. The micelle solution was transferred into a 25 mL round bottom flask, was added 5 mL tertiary butanol, $CuSO_45H_2O$ (0.075 mg, 0.3 µmol), freshly prepared Sodium ascorbate solution (0.594 mg (as 5% aqueous solution)) and Oregon Green488 alkyne 6-isomer (0.449 mg, 1.0 µmmol) (in 0.2 mL of DMF). The solution was stirred for 48 h at room temperature. The crude reaction mixture was then transferred into the dialysis tubing of MWCO 2kDa and dialyzed against carbonate buffer (pH-9.2) for three days and then against MilliQ water for another three days. The micelle solution was then lyophilized to obtain the solid Oregon Green conjugated polymer. Binding of Oregon green was confirmed by GPC analysis (Figure S4) and also by fluorescence spectroscopy.

4. Conjugation of cell penetrating peptides (cys-CPP) to the triblock copolymers

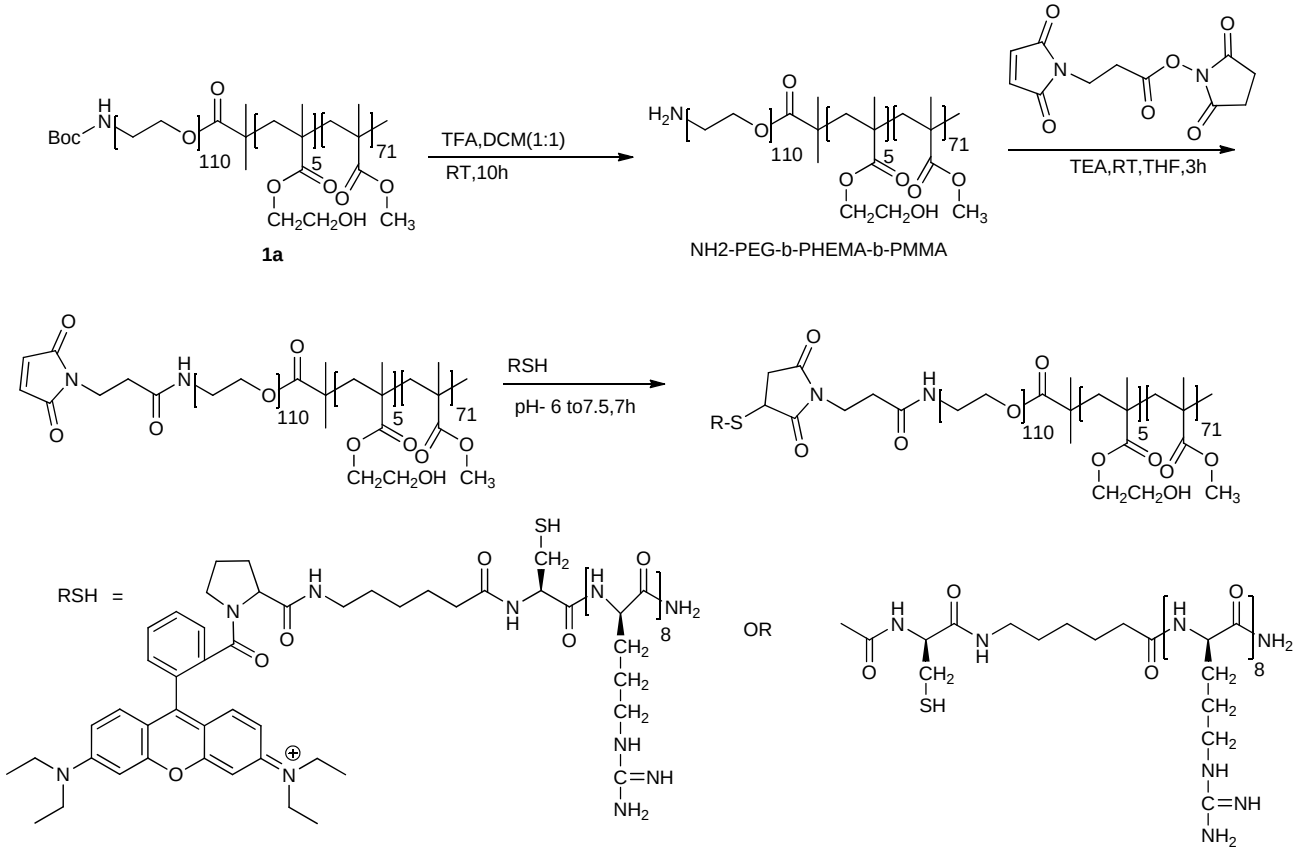

Scheme S1. Thioether bond formation between the peptide and triblock copolymer. TFA = trifluoro acetic acid, TEA = triethyl amine. DCM = Dichloromethane

Synthesis of RhB-Pro-Ahx-Cys-(Arg)$_8$-NH$_2$ peptide

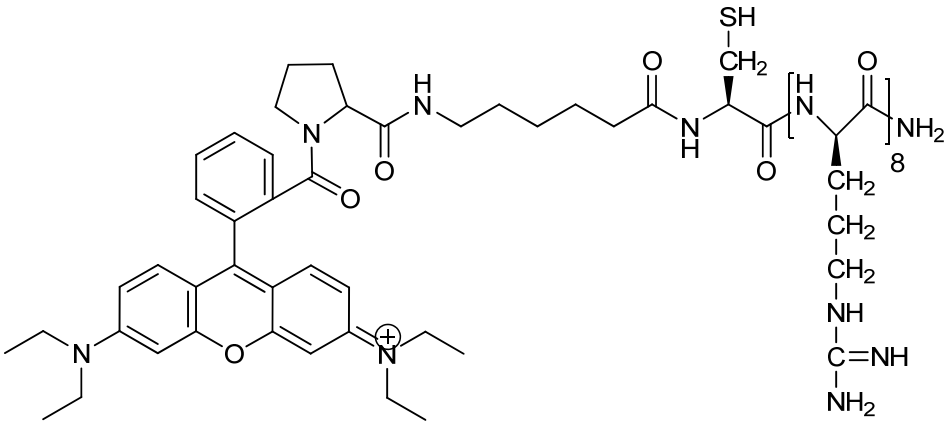

The C-terminal peptide amide was synthesized by solid phase peptide synthesis (based on Fmoc chemistry) using Rink amide resin as solid support. Each amino acid was coupled to the resin by HATU and DIPEA in DMF. 20% piperidine in DMF was used to cleave the Fmoc group in each step. The final peptide was cleaved from the resins using 95% TFA/water and triisopropylsiline in DCM. After evaporating the TFA under vacuum, the crude peptide was precipitated in to excess cold diethyl ether. The peptide was further purified by HPLC and characterized using MALDI-TOF, calculated mass $[M+H]^+$ 2005 and observed $[M+H]^+$ peak at 2005 Da, $[M+Na]^+$ peak at 2027 Da and $[M+K]^+$ at 2043 Da respectively.

Synthesis of Ac-(Cys)-Ahx-$(Arg)_8CONH_2$ peptide

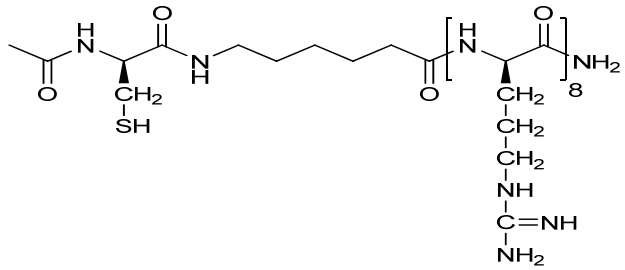

The peptide was synthesized by Fmoc based solid phase peptide synthesis using Novasyn TGR resin as solid support. For each coupling of the amino acid, HATU with 2,4,6 trimethyl pyridine was used as coupling agent. De-protection of the Fmoc group in each step was carried out using 20% piperidine in DMF. The final peptide was cleaved from the resin using 95% TFA/water and triisopropylsiline. After evaporating of TFA under vacuum, the peptide was precipitated in excess of cold diethyl ether. The peptide was further purified by preparative HPLC and characterized by MALDI-TOF, calculated mass $[M+H]^+$ 1524 and observed $[M+H]^+$ peak at 1524 Da and $[M+K]^+$ at 1562 Da respectively.

Modification of amino group of the polymer Boc-NH-PEG-b-PHEMA-b-PMMA with NHS ester

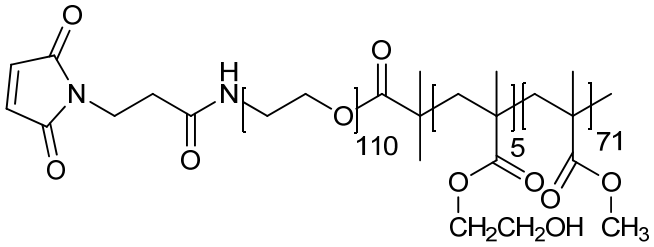

De-protection of Boc-NH-PEG-b-PHEMA-b-PMMA: The triblock copolymer Boc-NH-PEG-b-PHEMA-b-PMMA (300 mg, 0.020 mmol) was dissolved in 3 mL of DCM and 3 mL trifluoroacetic acid was added drop wise to the solution. The reaction mixture was stirred for 10 h at room temperature. After evaporating the solvent under reduced pressure, the polymer was precipitated into excess of cold diethyl ether and dried under vacum. The presence of free amino group was confirmed by NMR spectroscopy (disappearance of peak at δ 1.4 (s, 9H) and also by a positive Ninhydrin test [2].

NH_2-PEG-b-PHEMA-b-PMMA (120 mg, 0.0083 mmol) was dissolved in 2 mL of THF containing 50µl TEA. 3-maleimido-propionicacid-N-hydroxysuccinimide ester (2.2 mg, 0.0083 mmol) was added and the reaction mixture was stirred at room temperature for 3 h. Most of the solvent was removed by rotary evaporation; the crude product was precipitated into excess cold diethyl ether and dried under vacuum. The absence of free amino group was confirmed by a negative Ninhydrin test. (Instead of 3-maleimido-propionicacid-N-hydroxysuccinimide ester, water soluble sulfo-GMBS (N-gamma-Maleimidobutyryl-oxysulfosuccinimide ester) was also used for the peptide conjugation. The change in linker does not alter the yield of peptide conjugations.

d. Binding of RhB-Pro-Ahx-Cys-$(Arg)_8$-NH_2 and Ac-(Cys)-Ahx-$(Arg)_8CONH_2$ peptide to the polymer

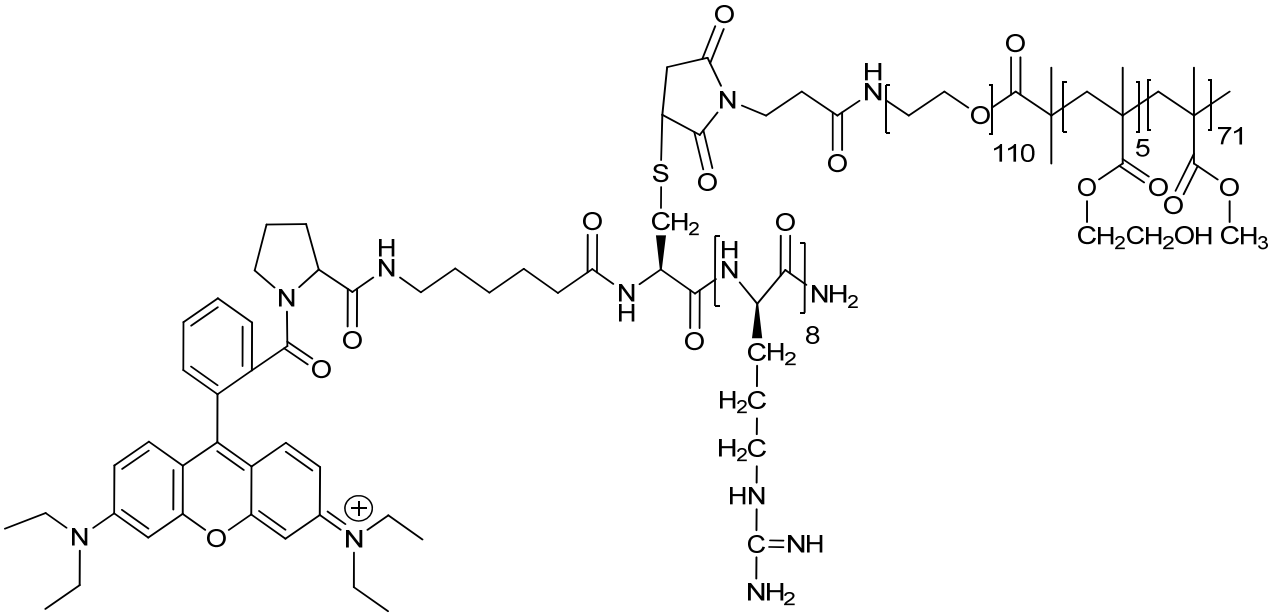

The polymer bearing the Maleimide group (25 mg, 0.0017 mmol) was dissolved in 5 mL of DMF, to the solution was added 0.5 mL of MilliQ water under stirring within a time interval of 30 minutes, followed by drop wise addition of another 10 mL of MilliQ water. The cloudy micelle solution was then transferred into a dialysis tubing (MWCO = 12kDa) and dialyzed against buffer of pH 6.75 for 6 h. The micelle solution in buffer of pH 6.75 was transferred into a round bottom flask, followed by peptide (3.4 mg, 0.0017 mmol) and the mixture was stirred at room temperature for 7 h. The Peptide conjugated polymer was dialyzed against MilliQ water for five days to remove un-reacted peptides. The concentration of peptide attached to the polymer was then determined from Rhodamine B calibration curve, and was found to be $7*10^{-7}$ M, 1.4 mg; yield (41%). The micelle solution was then lyophilized to obtain the solid peptide conjugated polymer. In contrast to the reactions of maleimides with amine, maleimides with thiol required a lower pH (6.5-7.5) to avoid the competitive reactions. It was reported[3] that once maleimide adducts formed above pH 8, they can hydrolyze into an isomeric mixture of maleamic acid adducts. Above pH 9, they can also undergo nucleophilic ring opening reactions with an adjacent amine to yield cross linked products. [4] The peptide Ac-(Cys)-Ahx-$(Arg)_8CONH_2$ was conjugated to the polymer using the exact same procedure. The reaction yield increased when excess peptide was used.

5. Fabrications of pH nanosensors

Synthesis of targeted nanosensor for the pH range 4.3 to 7.8 having (1%/weight) targeting peptides

Targeted ratio-metric pH nanosensors with a sensitive range between pH 4.3 to 7.8 was synthesized as follows. The amphiphilic triblock copolymer PEG-b-PHEMA-b-PMMA conjugated to Fluorescein (3.44 mg, 0.23 µmol), Oregon Green (1.48 mg, 0.10 µmol), Rhodamine B (0.0492 mg, 0.0033 µmol), and targeting peptide (0.098 mg, 0.0067 µmol) along with free PEG-b-PHEMA-b-PMMA (4.92 mg, 0.33 µmol) in the ratio (7 : 3 : 0.1 : 0.2 : 10) (total 10 mg) were dissolved in 2 mL of DMF by stirring overnight. Stirring was continued and 0.2 mL of MilliQ water was added over 30 minutes to the above solution. Additionally 4 mL of MilliQ water was added drop wise and the cloudy micelle solution was transferred to a dialysis tube (MWCO = 12kDa) and dialyzed against MilliQ water for five days. DLS measurement shows that hydrodynamic diameter (Dh) 51±3 nm and zeta potential measurement shows (ξ) = -7±3 mV.

6. Fluorescence measurements

pH calibration curves for the pH nanosensors

The pH calibration curves were constructed using fluorescence spectroscopy. 25 µl of the pH nanosensors were added to 1 mL of buffer having different pH and these nanosensor dispersions were excited at 490 and 543 nm respectively. Fluorescence emission spectra's of the nanosensors at different pH were plotted. From the fluorescence emission spectra's of Fluorescein (FA), Oregon Green (OG) and Rhodamine (RhB), $I_{OG\ or}\ I_{FA}\ /I_{RhB}$ were calculated. This fluorescence intensity ratio was plotted against different pH to obtain the ratio-metric pH calibration curves.

Response time measurement of the pH nanosensor

Response of nanosensors towards the change in pH was tested by measuring the variations of fluorescence intensity with respect to the time. 25 µl of the pH nanosensor was added to 1 mL of buffer solution and kinetic scan of the nanosensor dispersion was performed at 490 nm. pH of the nanosensor solution was changed suddenly by adding 1 mL of buffer having a different pH. The change in fluorescence intensity with respect to time gives the response time of the nanosensor. Measurements show that the sensors were responsive towards the change in pH within micro seconds.

Reversibility of the pH nanosensors

Reversibility of nanosensors was tested by repeatedly changing the fluorescence intensity ratio at two different pH. 25 µl of the pH nanosensor was added to 1 mL of buffer solution and the sample was excited at 490 nm and 543 nm. The fluorescence intensity ratio (I_{OG} or I_{FA})/I_{RhB} were calculated from the fluorescence measurement. The pH of the nanosensor was changed to another pH and fluorescence intensity ratio was measured again. The pH changes and measurements were repeated. The Reversibility curve for the pH nanosensors were constructed by plotting fluorescence intensity ratio against acquisition number. Measurements show that the sensors were reversible.

7. Selected spectra

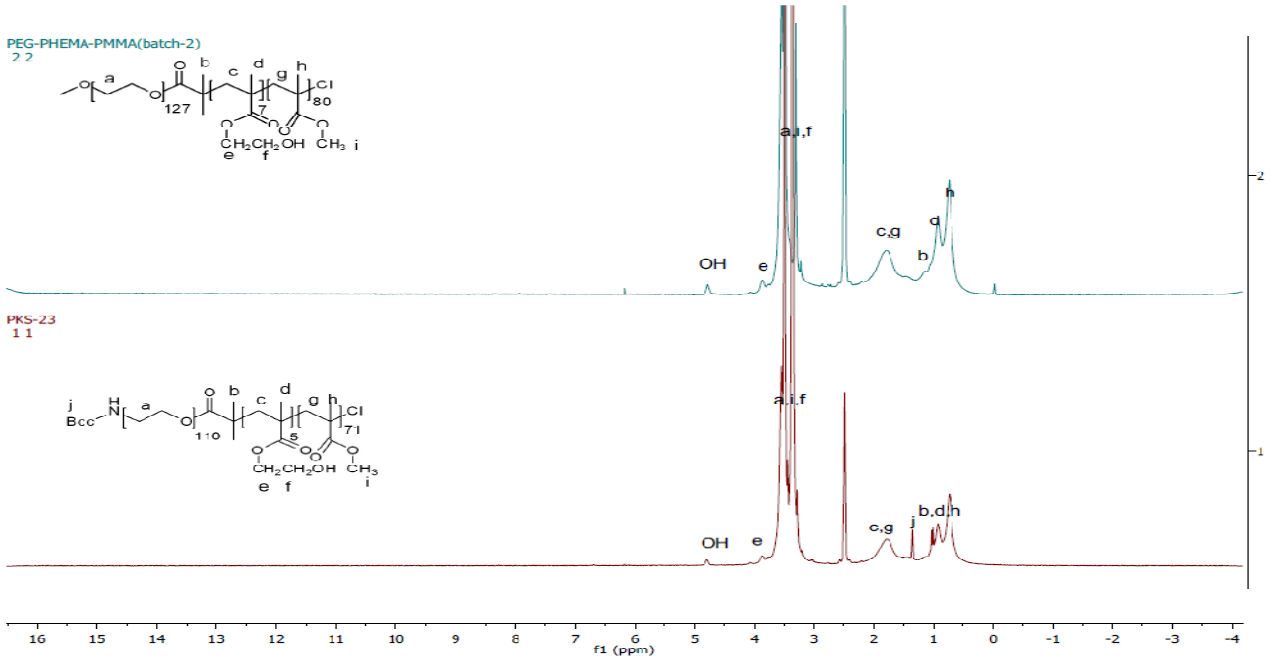

Figure S1. ^{1}H NMR spectra of the polymer PEG-b-PHEMA-b-PMMA and BocNH-PEG-b-PHEMA-b-PMMA in DMSO (^{6}d)

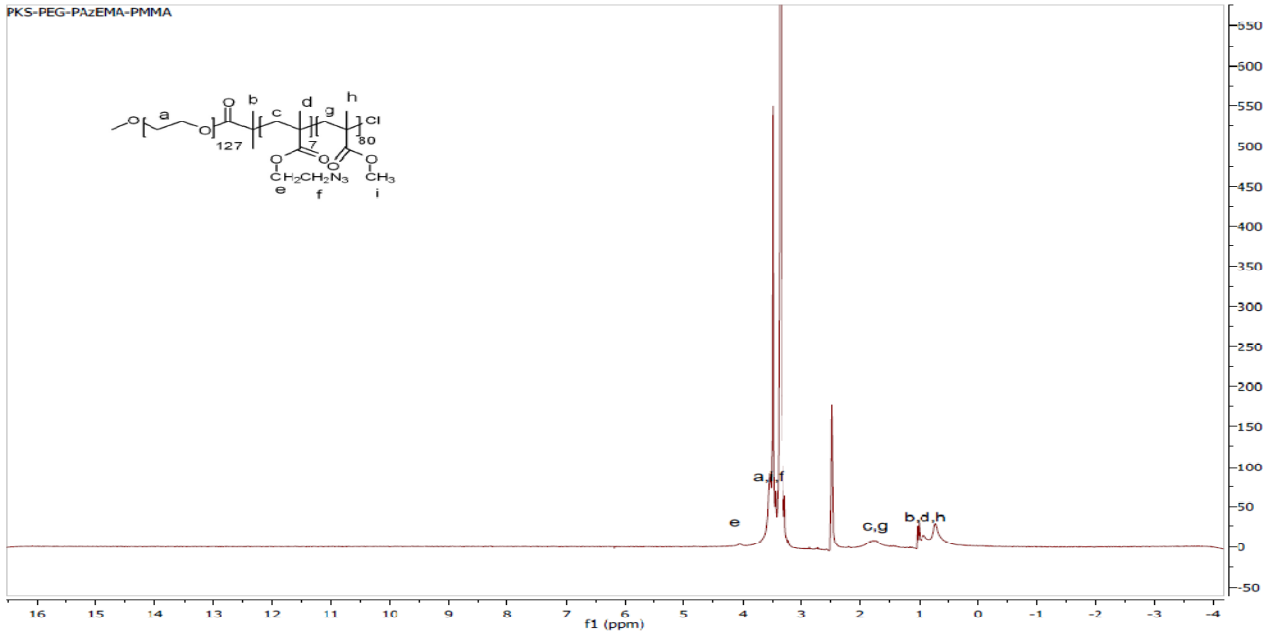

Figure S2. ^{1}H NMR spectra of the polymer PEG-b-PAzEMA-b-PMMA in DMSO (^{6}d), disappearance of -OH peak at 4.9 ppm indicates the complete conversion

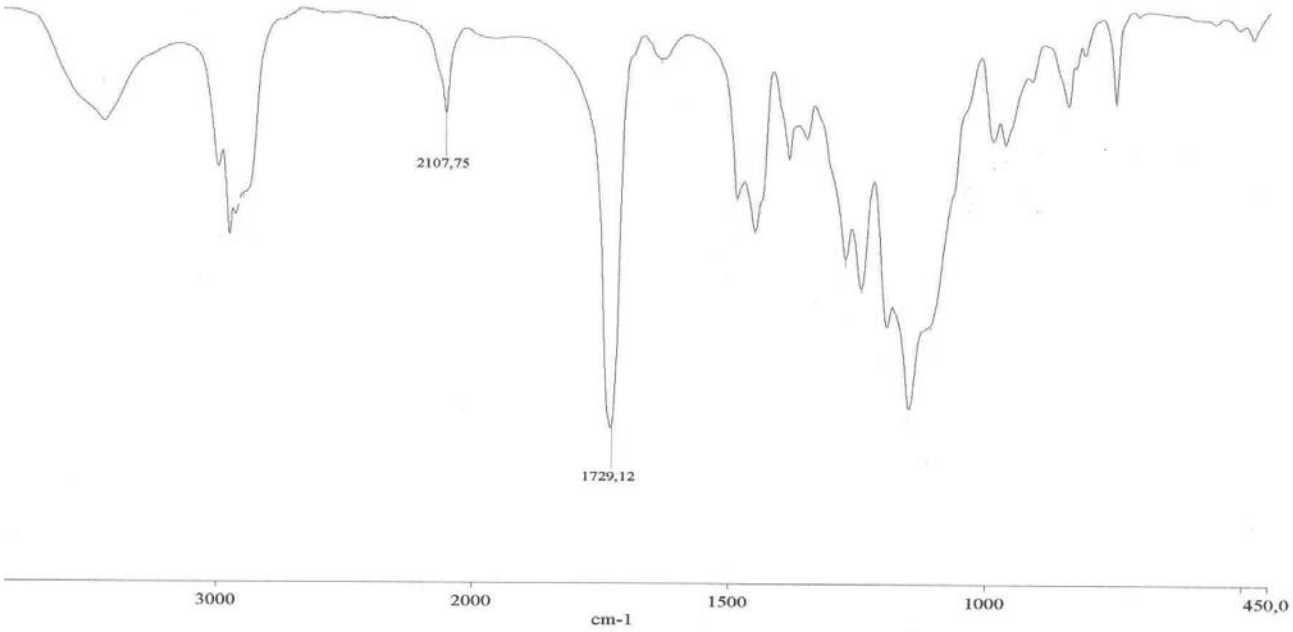

Figure S3. FTIR spectra of PEG-PAzEMA-PMMA, azide stretching vibration at 2107cm^{-1} and carbonyl stretching at 1729 cm^{-1}

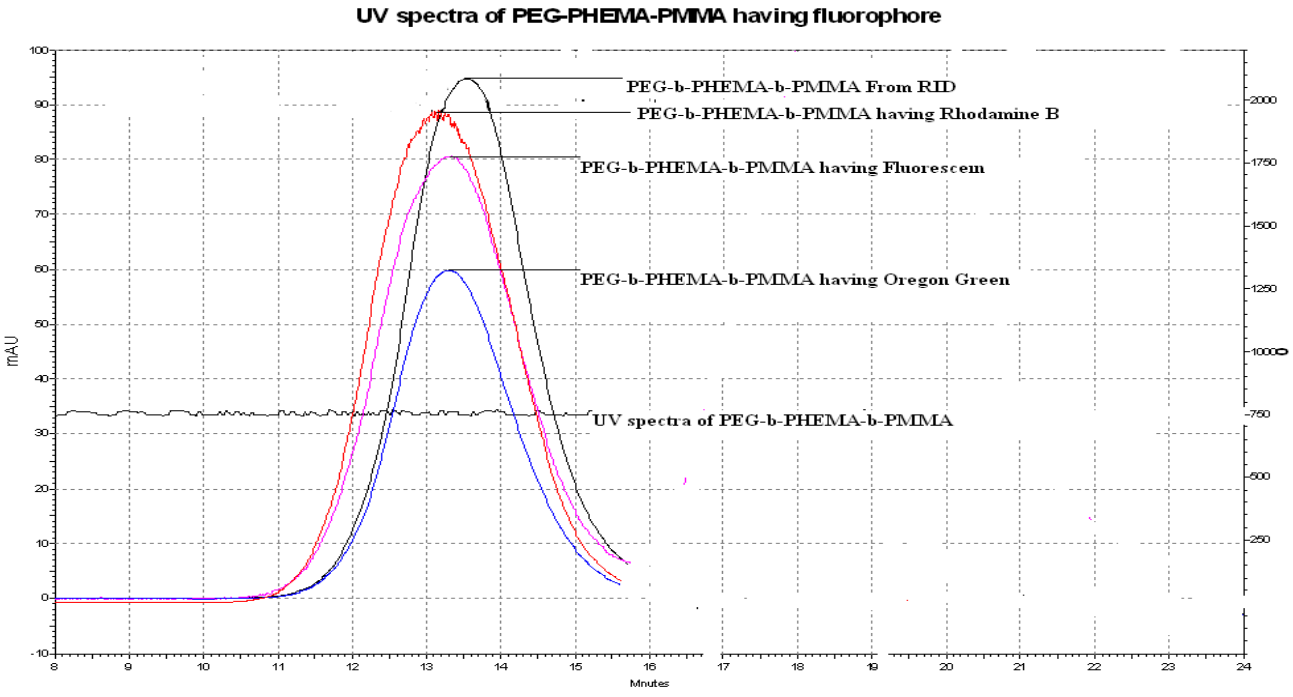

Figure S4. Covalent attachments of Fluorescein, Oregon Green and Rhodamine B to PEG-PHEMA-PMMA was confirmed by GPC analysis. Signals from refractive index detector (RID) and from UV detector (at 543 and 490 nm) were used for comparing and conforming the binding of fluorophores.

8. References

1. S. Liu, J. V. M. Weaver, Y. Tang, N. C. Billingham, S. P. Armes and K. Tribe, *Macromolecules*, 2002, **35**, 6121-6131.
2. E. Kaiser, R. L. Colescott, C. D. Bossinger and P. I. Cook, *Analytical biochemistry*, 1970, **34**, 595-598.
3. Y. Ishii and S. S. Lehrer, *Biophysical Journal*, 1986, **50**, 75-80.
4. C.-W. Wu, L. R. Yarbrough and F. Y. H. Wu, *Biochemistry*, 1976, **15**, 2863-2868.

Appendix F

Pramod Kumar EK, Lise N. Feldborg, Rasmus I. Jølck, Kristoffer Almdal and Thomas L. Andresen. ‘‘Synthesis of ratiometric, cRGDfK targeted and shell cross-linked core-shell-corona mixed micelle pH nanosensors having well defined surface and shell functionalization’’. *J. Am. Chem. Soc.* **2012** (Submitted), supporting information.

Synthesis of ratiometric, cRGDfK targeted and shell cross-linked core-shell-corona mixed micelle pH nanosensors having well defined surface and shell functionalization

Pramod Kumar EK, Lise N. Feldborg, Rasmus I. Jølck, Kristoffer Almdal, Thomas L. Andresen*

Department of Micro- and Nanotechnology, Technical University of Denmark, DTU Nanotech, Building 345B, DK-2800 Kongens Lyngby, Denmark

KEYWORDS core-shell-corona micelle, amphiphilic triblock, mixed micelle, shell cross-linking, pH nanosensors.

Supporting Information Placeholder

ABSTRACT: Post functional modifications of the amphiphilic triblock copolymers, PEG-b-PAzEMA-b-PMMA and NH_2-PEG-b-PAzEMA-b-PMMA were performed to introduce the pH sensitive and reference fluorophores as well as the targeting peptide, cRGDfK. Copper catalyzed azide-alkyne Huisgen 1,3-dipolar cycloaddition (CuAAC) reaction was used to bind the fluorophores to PEG-b-PAzEMA-b-PMMA, whereas cRGDfK was bound to NH_2-PEG-b-PAzEMA-b-PMMA by a diamide linker. Spontaneous self-assembly of these modified functional triblock copolymers along with free PEG-b-PAzEMA-b-PMMA resulted in non-cross-linked targeted mixed micelle nanosensors in aqueous media. Dendritic shell click cross-linking of the unimers of this nanoparticle scaffold resulted in robust intergrin targeted nanosensors. Thus, a new synthetic strategy has been developed for the fabrication of pH nanosensors. This pre-functional modification strategy reduces the role of dimensional synthetic organic chemistry on nanoparticle modifications and hence provides more precise knowledge about the functionalities to be introduced.

Intracellular pH controls the metabolic activities of enzymes,[1] ion channel conductivity,[2] cell cycle and cell divisions[3] of several cell types. Intracellular pH measurements could provide information about pH dependant drug release from engineered pharmaceutical carriers.[4, 5] In recent years, a number of polymeric nanoparticle based ratiometric sensor systems have been developed for the pH probing of microscopic environments, these including polystyrene,[6] polyacrylamide,[7-11] polysaccharide[12] based particles etc. These nanoparticles were converted in to pH nanosensors by post-functionalization. The main limitation of this approach is the uncertainty in predicting exact concentrations of fluorophores and degree of bioconjugation on the resulting nanosensors. Recent development in controlled radical polymerization techniques, especially the transition metal catalyzed atom transfer radical polymerization technique (ATRP),[13] could provide an easy and efficient way of synthesizing functional amphiphilic block copolymers with well defined compositions and narrow polydispersities. Post polymer modifications and co-micellisation [14, 15] of those functional unimers having similar composition with different functional characteristics could provide a platform for the synthesis of advanced polymeric nanosensors in simple and inexpensive procedures. It is well known that the cyclic RGD peptides could mimic the cell adhesion proteins and bind to the heterodimeric cell surface receptors, integrins.[16] In continuation with our interest to couple CuAAC[17, 18] chemistry and ATRP in to nanosensors fabrications, we describe in this communication the synthesis of polymeric micelle based, cyclic RGD peptide targeted, cross-linked and ratiometric pH nanosensor for intracellular pH measurements.

Figure 1 schematically illustrates the fabrication of shell cross-linked targeted and ratiometric pH nanosensors by the mixed micelle approach. The amphiphilic triblock copolymers Boc-NH-poly(ethylene-glycol)-*b*-poly(hydroxyethyl methacrylate)-*b*-poly(methyl methacrylate) (Boc-NH-PEG-b-PHEMA-b-PMMA)(**1**) and poly(ethylene-glycol)-*b*-poly(hydroxyethyl methacrylate)-*b*-poly(methyl methacrylate) (PEG-*b*-PHEMA-*b*-PMMA)(**2**) were synthesized by isolated macro-initiator atom transfer radical polymerisation techniques.[19] Post polymer modifications of the amphiphilic triblock copolymers were achieved by mesylation of the PHEMA hydroxyl groups followed by nuclephlic substitution by sodium azide resulting in Boc-NH-PEG-b-PAzEMA-b-PMMA (**3**) and PEG-b-PAzEMA-b-PMMA (**4**) (Scheme 1a). Disappearance of the –OH proton (^{1}H-NMR (DMSO-d^6) δ = 4.73 ppm) confirmed the complete conversion and the presence of *tert*-butoxycarbonyl (Boc) group on BocNH-PEG-b-PAzEMA-b-PMMA at δ = 1.36 ppm confirmed the stability of the protecting group under the reaction conditions. FTIR further confirmed the presence of azide groups on the polymers (ν = 2110 cm^{-1}). The Boc group from BocNH-PEG-b-PAzEMA-b-PMMA was removed by treatment with TFA/DCM. The complete de-protection was confirmed by the disappearance of Boc- signal at 1.36 ppm (Scheme 1b).

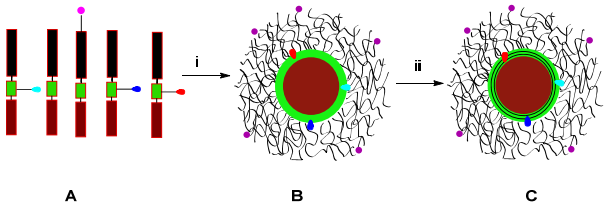

Figure 1. Fabrication of shell cross-linked targeted ratiometric pH nanosensors (**C**) from targeted mixed micelle nanosensors (**B**) formed by the spontaneous self assembly of amphiphilic functional triblock copolymers (**A**). i = self-assembly, ii = shell cross-linking

The targeting cyclic RGD peptide, c(RGDfK) was coupled to the chain end of the polymer by using *N,N'*-Disuccinimidyl carbonate linker (Scheme 1c). Binding of the peptide to the polymer was confirmed by FTIR spectroscopy (amide N-H stretch at 3277 cm^{-1} and amide -C=O stretch at 1670 cm^{-1}) in addition to a Kaiser test[20] which indicated the absence of free amino groups on the polymer.

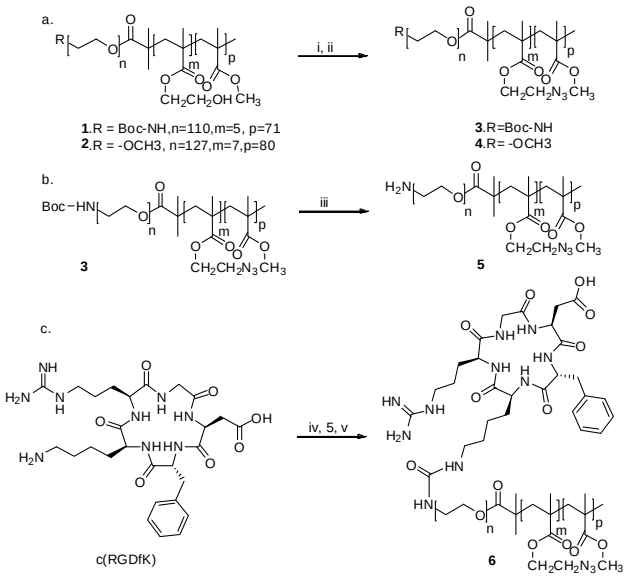

Scheme 1. Post functional modifications of the amphiphilic triblocks, at the side chain (a) and chain ends (b, c). i) CH_3SO_2Cl, Py, Ar atm, r.t, overnight; ii) NaN_3, DMF, Ar atm, 90^{0C} (5 h) to r.t (20 h); iii) TFA, CH_2Cl_2, r.t, 12 h; iv) N,N'-Disuccinimidylncarbonate, TEA, DMF (dry), Ar atm, r.t, 8 h; v) **5**, r,t, 24 h.

pH sensitive (Fluorescein and Oregon green alkyne) and pH insensitive reference fluorophore (Rhodamine B-alkyne) were attached separately to PEG-b-PAzEMA-b-PMMA by CuAAC reaction (Scheme 2). The catalysts and un-reacted fluorophores were removed by extensive dialysis against carbonate buffer and MilliQ water, followed by fluorescence measurements confirming the covalent attachment of fluorophores to the amphiphilic triblocks.

Effectiveness of dendritic shell cross-linking of PEG-b-PAzEMA-b-PMMA micelle (**10**) was investigated by click reaction. The dendritic benzyl ether cross linker, $(Alkyne)_4$-[G-1] was synthesised from dendritic alcohol $(OH)_4$-[G-1] and propargyl bromide by Williamson ether synthesis. The dendritic click shell cross-linking at the hydrophobic shell region of the micelles was performed by two different catalytic systems under otherwise identical conditions. $CuBr(PPh_3)_3$ / DIPEA in 1 : 4 (THF : Buffered H_2O) (Scheme 3) and $CuSO_4.5H_2O$ / Sodium ascorbate in 1:4 (*tert*-butanol : H_2O). After three days of reaction, subsequent dialysis and lyophilization, FTIR spectra of the cross-linked micelle (**11**) obtained by the $CuBr(PPh_3)_3$ / DIPEA approach showed complete disappearances of N≡N asymmetric stretching absorption of azide at 2100 cm^{-1} and the appearance of -C≡C-H and aromatic C=C stretching at 3260 cm^{-1} and 1593 cm^{-1} respectively. This indicate complete participation of the azide groups in the trazole ring formation, and the absorption at 3260 cm^{-1} and 1593 cm^{-1} confirms the presence of excess alkyne groups on the dendritic *benzyl* ether cross linker (Figure 2). Dynamic light scattering (DLS) and zeta potential measurements revealed that the cross-linking reaction did not affect the hydrodymanic diameter (Dh) or the zeta potential (ξ) of the nanoparticles. (Table 1, micelle **10**&**11**) thus indicating that the shell cross-linking of the well defined core-shell-corona micelle occurred intramicellarly even at high block copolymer concentrations (2.5 mg/mL). The dendritic shell cross-linking reaction using $CuSO_4.5H_2O$ / Sodium ascorbate in 1:4 *tert*-butanol : H_2O system was also effective but presence of azide peak at 2100 cm^{-1} (see supporting) indicated partialness. These optimization studies show that click reaction at the hydrophobic shell region of the PEG-b-PAzEMA-b-PMMA micelle give better results under more hydrophobic conditions.

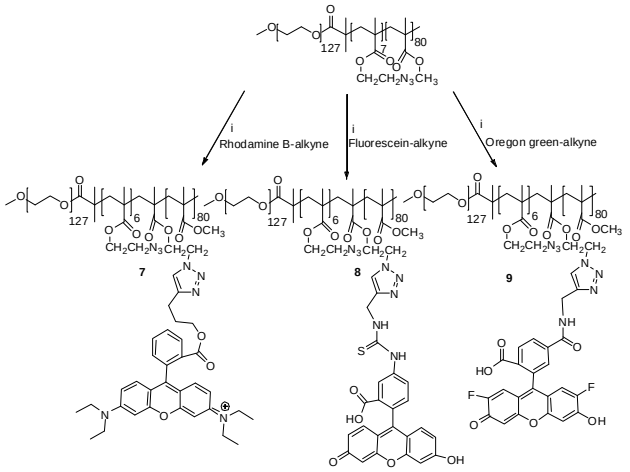

Scheme 2. Binding of fluorophores to the amphiphilic triblock copolymer (**4**) by click reactions. i = $CuSO_4.5H_2O$, Sodium ascorbate, H_2O : tBuOH (4:1), r.t, 72 h

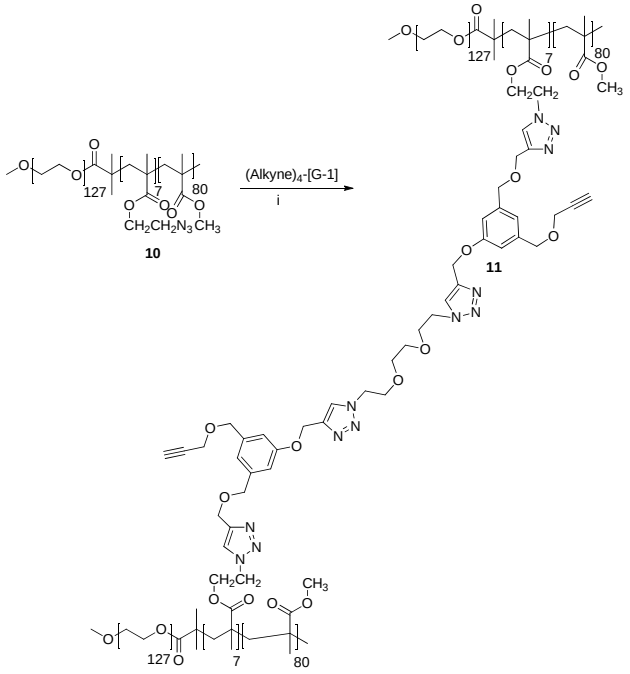

Scheme 3. Synthesis of dendritic click shell cross-linked core-shell-corona-micelle (**11**) using dendritic alkyne cross-linker. The minimum cross-linking possibility of the linker is shown in the figure. i) $CuBr(PPh_3)_3$, DIPEA, Cu wire, THF : Buffered water (1:4), r.t, 72h.

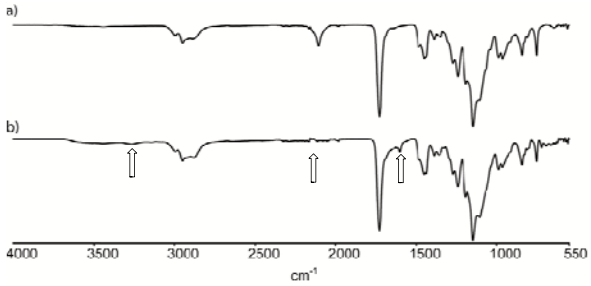

Figure 2. FTIR spectra of PEG-b-PAzEMA-b-PMMA micelle before cross-linking (a), **10** and after cross-linking (b), **11,** y-axis is % of transmittance (arbitrary units). Arrows in (b) indicates the presence of alkyne -C≡C-H and aromatic C=C stretching, and the absence of azide stretching absorptions.

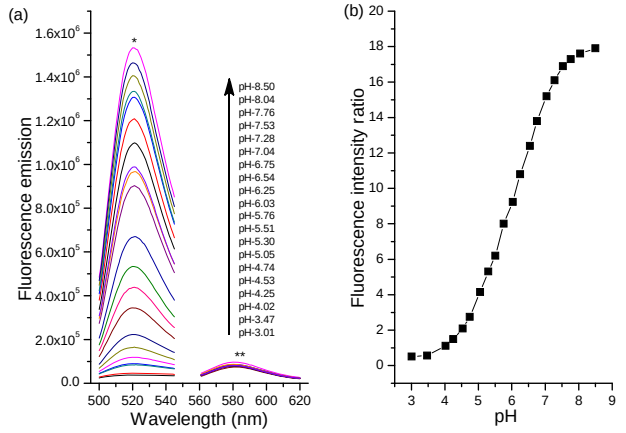

Figure 3.(a) Fluorescence emission spectra of the nanosensor. *Fluorescence intensity of pH sensitive fluorophores (excitation wavelength λ_{ex}= 488 nm), and **reference fluorophore (λ_{ex}= 543 nm), in buffer of different pH having sensor concentration 0.125 mg/mL. (b) pH calibration curve of the nanosensor. Curve made by plotting fluorescence intensity ratio ($I_{FA} + I_{OG} / I_{RhB}$) of the pH sensitive ($I_{FA} + I_{OG}$) and reference ($I_{RhB}$) fluorophores against pH. FA = Fluorescein, OG = Oregon green, RhB = Rhodamine B.

The targeted ratiometric and cross-linked pH nanosensor (**C**) was prepared by a two step procedure. The amphiphilic triblock copolymers attached to cRGDfK peptide (**6**), pH sensitive and reference fluorophores (**8, 9, and 7**) and the PEG-b-PAzEMA-b-PMMA (**4**) in the desired ratios were dissolved in DMF. Slow displacement of DMF by a selective solvent (water) resulted in non cross-linked but targeted ratiometric mixed micelle nanosensors (**B**). The targeted mixed micelle nanosensor was then cross-linked by dendritic benzyl ether cross linker using $CuBr(PPh_3)_3$/DIPEA catalyst under optimized reaction condition. After removing the catalyst and excessive reagents by extensive dialysis, the DLS and ζ-potential measurements showed that before and after shell cross-linking, the hydrodynamic diameter and zeta potential of the nanosensors were almost same, which confirmed the exclusive intramicellar cross-linking at the shell region of the nanosensors (Table 1. micelle **B**&**C**).

Table 1.Characterisation Data for the Micelle B, C, 10 and 11

Micelle	DLS (Dh)[a] (nm)	Zeta(ξ)[b] (mV)	H_{av}[c]
B	39±2	-19±2	15±4
C	38±1	-17±1	20±10
10	33±2	-13±2	---------
11	31±1	-12±2	---------

[a]Number averaged hydrodynamic diameters of aqueous micelle solutions by DLS. [b]ζ-potential from 5 determinations of 10 data sets.[c]Average heights of the micelles measured by tapping mode AFM and calculated from values of ca 100 particles

Nanosensors dispersion in MilliQ water was used for the construction of ratiometric in vitro pH calibration curve by fluorescence spectroscopy (Figure 3). The Covalent attachment of pH sensitive Oregon green and Fluorescein, and insensitive reference fluorophore, Rhodamine B at the shell region of the shell cross linked core-shell-corona micelle was confirmed by the pH calibration curve. The pH calibration curve shows that the nanosensors are sensitive between the pH ca.4.5 to 7.5 and confirm the broad pH sensitivity range of the triply labelled robust micelle sensor.

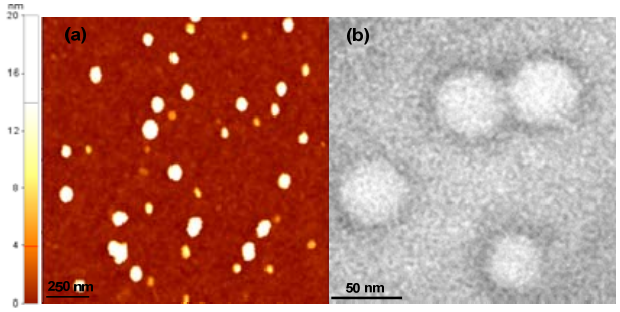

Figure 4 AFM (a) and TEM image (b) of the pH nanosensor, **C**.

The morphology of the cross-linked nanosensor (**C**) was analyzed by atomic force microscopy (AFM) and transmission electron microscopy (TEM) as shown in Figure 4. Both techniques showed spherical nanosensors in the 30 nm size range. The hydrodynamic diameter measured from DLS was slightly larger than diameter measured by TEM, indicating shrinking of the sensor during air dried sample preparation for TEM imaging. The average height of the sensor (H_{av}) calculated from AFM measurements (Table 1) shows that after cross linking, the height of the nanosensor do not changed considerably. This indicates that the shell cross-linking of the core-shell-corona micelle nanosensor do not considerably alter its interaction with the hydrophilic silica surface.

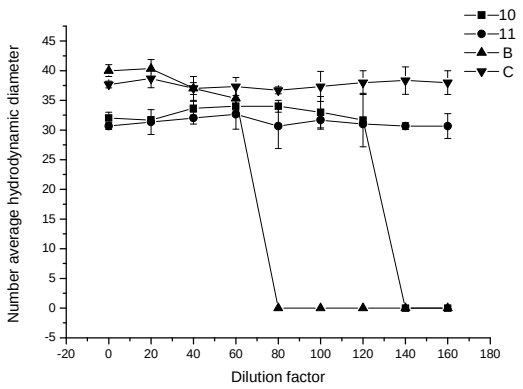

Figure 5. Number average hydrodynamic diameter (Dh) of the micelles measured by DLS as a function of dilution; for non-cross-linked mixed micelle sensor (**B**) (▲), micelle (**10**) (■), cross-liked mixed micelle sensor (**C**) (▼) and the cross-linked micelle (**11**) (●).

Effect of dilution on micelle stability was studied by DLS measurements (Figure 5). Under similar block copolymer concentration (1.2 mg/mL), the non-cross-linked micelle sensor (**B**) and non-cross-linked micelle (**10**) were not detectable after certain dilution. While at the same time the cross-linked micelle (**11**) and the nanosensor (**C**) were maintained their structural integrity throughout the experiments. Dissociation of mixed micelle nanosensor (**B**) was faster and occurred at concentration below ca. 20 mg/ L, whereas the non cross linked micelle showed much lower CMC (ca. 10 mg/L). This indicates the importance of covalent shell cross-linking between the unimers of these nanoparticle scaffolds during the mixed micelle nanosensor fabrications.

The self-assembly of amphiphilic functionalized unimers followed by covalent cross-linking at the shell region of the resulting core-shell-corona micelle provide an advanced micelle nanosensor. The covalent stabilization could prevent nanosensor dissociation below the critical micelle concentration (CMC) and thus enhances its applications in infinitely diluted biological conditions. Due to compatibility and orthogonality towards a wide range of functionalities, a dendritic click reaction was used for the covalent cross-linking at the shell domain. The presence of un-reactive PEG corona on the core-shell-corona micelle nanosensors could provide long circulating half life's for the sensors in blood by preventing the sensor recognition by the phagocytic cells and certain proteins (opsonization). The pH sensitive and reference fluorophores at the shell region are protected from the external surroundings by the PEG corona. The PEG corona also offers repulsive interaction between the micelle nanosensors, thus providing exclusive intramicellar cross-linking of the nanosensors even at high block copolymer concentrations (1.25 mg/mL). The cell surface adhesion proteins, $\alpha_v\beta_3$ integrins are responsible for tumor-induced angiogenesis. The binding of $\alpha_v\beta_3$ with the cyclic RGD peptide (c(RGDfK)) can reduces the rate of angiogenesis.[21] Thus the nanosensors with surface functionalized (c(RGDfK)) may provide an opportunity to monitor the intracellular pH during tumor regressions.

In conclusion, with the help of synthetic and dimensional synthetic organic chemistry and the principle of self-assembly, a ratiometric shell cross-linked and cRGDfK targeted mixed micelle nanosensor for intracellular pH measurement was fabricated. The ratiometric measurements eliminate the errors in fluorescence intensity due to excitation source fluctuations, fluorophore concentrations and environmental factors. The covalent dendritic shell cross-linking could make the nanosensor more robust and hence prevents sensor dissociations under diluted conditions The mixed micelle strategy allows the fine tuning of exact amount of fluorophores and targeting ligands present in the nanosensors. Thus a new strategy for nanosensor synthesis is developed which reduces the uncertainty in functional modification of nanoparticles during nanosensors fabrications. Further investigations of these nanosensors in a biological setting are currently in progress.

ASSOCIATED CONTENT

Supporting Information available: Synthesis, characterization and modifications of block copolymers, synthesis of dendritic cross-linker and cRGDfK and important spectra. This material is available free of charge via the Internet at http://pubs.acs.org.

AUTHOR INFORMATION

Corresponding Author

** E-mail: thomas.andresen@nanotech.dtu.dk*
(Word Style "FA_Corresponding_Author_Footnote"). Give contact information for the author(s) to whom correspondence should be addressed.

Present Addresses

†If an author's address is different than the one given in the affiliation line, this information may be included here.

Author Contributions

The manuscript was written through contributions of all authors. / All authors have given approval to the final version of the manuscript. / ‡These authors contributed equally. (match statement to author names with a symbol)

Funding Sources

The authors would like to thank Kræftens Bekæmpelse and the Danish Research Council for Technology and Production (Grant 274-07-0172) for financial

Any funds used to support the research of the manuscript should be placed here (per journal style).

Notes

Any additional relevant notes should be placed here.

ACKNOWLEDGMENT

The authors would like to thank Kræftens Bekæmpelse and the Danish Research Council for Technology and Production (Grant 274-07-0172) for financial

ABBREVIATIONS

CCR2, CC chemokine receptor 2; CCL2, CC chemokine ligand 2; CCR5, CC chemokine receptor 5; TLC, thin layer chromatography.

REFERENCES

(Word Style "TF_References_Section"). References are placed at the end of the manuscript. Authors are responsible for the accuracy and completeness of all references. Examples of the recommended formats for the various reference types can be found at http://pubs.acs.org/page/jacsat/submission/authors.html. Detailed

information on reference style can be found in The ACS Style Guide, available from Oxford Press.

BRIEFS (WORD Style "BH_Briefs"). If you are submitting your paper to a journal that requires a brief, provide a one-sentence synopsis for inclusion in the Table of Contents.

SYNOPSIS TOC (Word Style "SN_Synopsis_TOC"). If you are submitting your paper to a journal that requires a synopsis graphic and/or synopsis paragraph, see the Instructions for Authors on the journal's homepage for a description of what needs to be provided and for the size requirements of the artwork.

JACS Authors note: Authors are required to submit a graphic entry for the Table of Contents (TOC) that, in conjunction with the manuscript title, should give the reader a representative idea of one of the following: A key structure, reaction, equation, concept, or theorem, etc., that is discussed in the manuscript. The TOC graphic may be ***no wider than 9.0 cm*** and ***no taller than 3.5 cm*** as the graphic will be reproduced at 100% of the submission size. A surrounding margin will be added to this width and height during *Journal* production.

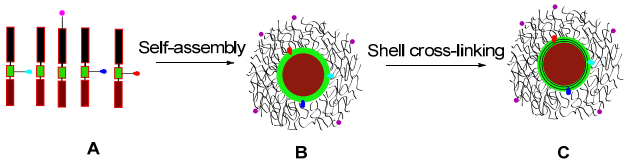

---

1. Ui, M., A role of phosphofructokinase in pH-dependent regulation of glycolysis. *Biochimica et Biophysica Acta (BBA) - General Subjects* **1966,** *124* (2), 310-322.
2. Moody, W., Effects of Intracellular H+ on the Electrical Properties of Excitable Cells. *Annual Review of Neuroscience* **1984,** *7* (1), 257-278.
3. Gillies, R. J.; Deamer, D. W., Intracellular pH changes during the cell cycle in Tetrahymena. *Journal of Cellular Physiology* **1979,** *100* (1), 23-31.
4. Wang, C. Y.; Huang, L., Highly efficient DNA delivery mediated by pH-sensitive immunolipo-somes. *Biochemistry* **1989,** *28* (24), 9508-9514.
5. Torchilin, V., Multifunctional and stimuli-sensitive pharmaceutical nanocarriers. *European Journal of Pharmaceutics and Biopharmaceutics* **2009,** *71* (3), 431-444.
6. Allard, E.; Larpent, C., Core-shell type dually fluorescent polymer nanoparticles for ratiometric pH-sensing. *Journal of Polymer Science Part A: Polymer Chemistry* **2008,** *46* (18), 6206-6213.
7. Sun, H.; Scharff-Poulsen, A. M.; Gu, H.; Almdal, K., Synthesis and Characterization of Ratiometric, pH Sensing Nanoparticles with Covalently Attached Fluorescent Dyes. *Chemistry of Materials* **2006,** *18* (15), 3381-3384.
8. Almdal, K.; Sun, H.; Poulsen, A. K.; Arleth, L.; Jakobsen, I.; Gu, H.; Scharff-Poulsen, A. M., Fluorescent gel particles in the nanometer range for detection of metabolites in living cells. *Polymers for Advanced Technologies* **2006,** *17* (9-10), 790-793.
9. Chauhan, V. M.; Burnett, G. R.; Aylott, J. W., Dual-fluorophore ratiometric pH nanosensor with tuneable pKa and extended dynamic range. *Analyst 136* (9), 1799-1801.
10. Benjaminsen, R. V.; Sun, H.; Henriksen, J. R.; Christensen, N. M.; Almdal, K.; Andresen, T. L., Evaluating Nanoparticle Sensor Design for Intracellular pH Measurements. *ACS Nano* 5 (7), 5864-5873.
11. Sun, H.; Almdal, K.; Andresen, T. L., Expanding the dynamic measurement range for polymeric nanoparticle pH sensors. *Chemical Communications 47* (18), 5268-5270.
12. Schulz, A.; Hornig, S.; Liebert, T.; Birckner, E.; Heinze, T.; Mohr, G. J., Evaluation of fluorescent polysaccharide nanoparticles for pH-sensing. *Organic & Biomolecular Chemistry* **2009,** *7* (9), 1884-1889.
13. Matyjaszewski, K.; Tsarevsky, N. V., Nanostructured functional materials prepared by atom transfer radical polymerization. *Nat Chem* **2009,** *1* (4), 276-288.

14. Webber, S. E.; Munk, P.; Tuzar, Z.; Division, N. S. A., *Solvents and self-organization of polymers / Proceedings of the NATO Advanced Study Institute, Antalya 1995*. Kluwer: Dordrecht, 1996; p 1-509 s.
15. Joralemon, M. J.; Smith, N. L.; Holowka, D.; Baird, B.; Wooley, K. L., Antigen-Decorated Shell Cross-Linked Nanoparticles:â€‰ Synthesis, Characterization, and Antibody Interactions. *Bioconjugate Chemistry* **2005,** *16* (5), 1246-1256.
16. Pierschbacher, M. D.; Ruoslahti, E., Cell attachment activity of fibronectin can be duplicated by small synthetic fragments of the molecule. *Nature* **1984,** *309* (5963), 30-33.
17. TornÃ¸e, C. W.; Christensen, C.; Meldal, M., Peptidotriazoles on Solid Phase:â€‰ [1,2,3]-Triazoles by Regiospecific Copper(I)-Catalyzed 1,3-Dipolar Cycloadditions of Terminal Alkynes to Azides. *The Journal of Organic Chemistry* **2002,** *67* (9), 3057-3064.
18. Kolb, H. C.; Finn, M. G.; Sharpless, K. B., Click Chemistry: Diverse Chemical Function from a Few Good Reactions. *Angewandte Chemie International Edition* **2001,** *40* (11), 2004-2021.
19. Nakagawa, Y.; Miller, P. J.; Matyjaszewski, K., Development of novel attachable initiators for atom transfer radical polymerization. Synthesis of block and graft copolymers from poly(dimethylsiloxane) macroinitiators. *Polymer* **1998,** *39* (21), 5163-5170.
20. Kaiser, E.; Colescott, R. L.; Bossinger, C. D.; Cook, P. I., Color test for detection of free terminal amino groups in the solid-phase synthesis of peptides. *Analytical biochemistry* **1970,** *34* (2), 595-8.
21. Brooks, P.; Clark, R.; Cheresh, D., Requirement of vascular integrin alpha v beta 3 for angiogenesis. *Science* **1994,** *264* (5158), 569-571.

Supporting information for :

Synthesis of ratiometric, cRGDfK targeted and shell cross-linked core-shell-corona mixed micelle pH nanosensors having well defined surface and shell functionalization

Pramod Kumar EK, Lise N. Feldborg, Rasmus I. Jølck, Kristoffer Almdal, Thomas L. Andresen*

Department of Micro- and Nanotechnology, Technical University of Denmark, DTU Nanotech, Building 345B, DK-2800 Kongens Lyngby, Denmark

1. Additional experimental information

1.1. Materials

2-Hydroxyethyl methacrylate (HEMA) (99%) and Methyl methacrylate (MMA) (99%) were obtained from Sigma Aldrich and radical inhibitors were removed by passing through the column filled with basic alumina. Triethylamine (TEA) was distilled from calcium hydride and stored under molecular sieves ($4A^0$). 2-Bromo-isobutyryl-bromide (98%), CuCl (99.995%), 2,2'bipyridyl (bpy) (99%), PMDETA (99%), $CuCl_2$ (99.995%), Methanesulphonyl chloride (MsCl) (99.7%), Anhydrous pyridine (99.8%), 4-Pentyn-1-ol (97%), Sodium azide, Trifluroacetic acid (TFA), dialysis tubing (MWCO = 12 kDa), Fluorescein isothiocynate (FITC) (90%), Propargylamine (98%), Propargyl bromide (80 wt.% in Xylene), KOH (90% flakes), N,N′-Disuccinimidyl carbonate (95%), N-(3-Dimetyl amino propyl)-N'-ethylcarbodiimide hydrochloride (EDC.HCl) (98%), $CuBr_2$ (99.999%), Triphenylphosphine (99%), N,N-Diisopropylethylamine (DIPEA) (99.5%), $CuSO_45H_2O$ (98%), (+)-Sodium L-ascorbate and DMAP (99%) were purchased from Sigma Aldrich and used as obtained. CH_3O-PEG-OH poly (ethylene glycol) monomethylether (Mn = 5000), and Rhodamine B were purchased from Fluka, Oregon Green® 488 alkyne 6-isomer was from Invitrogen, Boc-NH-PEGOH was from Iris Biotech GmbH. All solvents were purchased from Sigma Aldrich. Solvents used for Atom transfer polymerization (ATRP) were purified by distillation over the drying agents indicated in parentheses, stored under molecular sieves and were transferred under argon. MeOH ($Mg(OMe)_2$), toluene (CaH_2), DMF (CaH_2). Other solvents and commercially available chemicals were used as obtained.

1.2. Instrumentations

^{1}H-nmr spectra were recorded on Bruker 300 and 250 MHz in solvents as indicated. Chemical shifts (δ) are given in ppm relative to TMS. The residual solvent signals were used as reference and the chemical shifts converted into TMS scale ($CDCl_3$: δ_H = 7.24 ppm; ^{6}d-DMSO: δ_H = 2.50 ppm; CD_3OD: δ_H = 3.31 ppm). Infrared spectra's were recorded by Perkin Elmer Spectrum 100 FT-IR spectrometer and the wave numbers of recorded IR signals were quoted in cm^{-1}. The number average molecular weight (Mn) weight average molecular weight (Mw) and polydispersity (Mw/Mn) of block copolymers were determined by GPC analysis based on PEO/PMMA calibration standards. Measurements were carried out by using Mixed-D GPC column from Polymer Laboratories (7.4 × 300 mm) by using RID10A-SHIMADZU refractive index with DMF having 50 mM LiCl solution was used as eluent with a flow rate 0.5 mL / minutes at 25^0C. Dynamic light scattering: Hydrodynamic diameters (Dh) of the amphiphilic colloidal suspension in MilliQ water at 25^0C were determined by Brookhaven Zeta PALS instrument. All determinations were made in triplicate and duration of 2 minutes each. Zeta potential (ξ): Zeta potential measurements were carried out by using Brookhaven Zeta PALS analyzer. The measurements were made in MilliQ water at 25^0C. Fluorescence measurements were carried out by using The Olis Line of SLM based Spectrofluorimeter. Peptide purification was done by using Water 2489 UV/Visible HPLC detector and characterised by using Bruker Daltonics MALDI-TOF. Atomic force microscopy (AFM) images were obtained by PSIA XE-150 scanning force microscope using non-contact tapping mode close to resonance frequency of the silicon cantilever (Nanoworld, pointprobe type, force constant 42 N/m and tip radius <12 nm) of around 320kHz.All images were recorded under atmospheric conditions. TEM measurements were carried out by Tecnai T20G2 transmission electron microscope.

2. Experimental

2.1. Synthesis of PEG-b-PHEMA-b-PMMA and BocNH-PEG-b-PHEMA-b-PMMA

2.1.1. Synthesis of PEG-*b*-PHEMA-*b*-PMMA

2.1.1.1. Synthesis of the macroinitiator PEG-Br

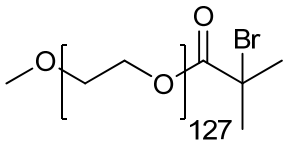

Following a modified procedure by Liu et al.,[1] CH_3O-PEG-OH, Mn = 5000 (5 gram, 1 mmol) was dissolved in 60 ml of toluene. After azeotropic distillation of 10 mL of toluene under reduced pressure to remove traces of water, TEA (0.278 mL, 2 mmol) was added and the solution was cooled to room temperature. 2-bromoisobutyryl bromide (0.185 mL, 1.5 mmol) was added drop wise and the reaction mixture was stirred at 40 ^{0}C for 2 days. The solution was filtered and most of the toluene was removed by rotary evaporation prior to precipitation into 10 fold excess of cold ether. The crude polymer was dried under vacuum, dissolved in water at pH 8-9 and then extracted with DCM. The organic layer was collected dried over anhydrous Na_2SO_4. The removal of the solvent under reduced pressure afforded the purified macro initiator in high yield: 5.5 g (99%). ^{1}H-NMR (250 MHz in $CDCl_3$): δ 3.6 (s, -C**H**$_2$C**H**$_2$O-), 1.9 (s, -C(C**H**$_3$)$_2$-); FTIR (cm^{-1}): 2887, 1737, 1466, 1359, 1342, 1279, 1241, 1148, 1107, 1060, 963, 841; GPC: Mn = 5630, Mw = 6320, PD (Mw/Mn) = 1.12.

2.1.1.2. Synthesis of diblock copolymer PEG-b-PHEMA

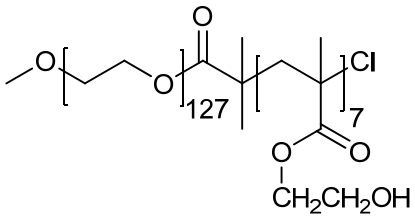

PEG-Br (1 gram, 0.1869 mmol), HEMA (0.226 mL, 1.86 mmol), 2,2'bipyridyl (61 mg, 0.39 mmol, 2.1 equiv) and 5 mL of dry methanol were added to a 25 mL Schlenk flask equipped with a stirrer bar. The RBF was frozen in liquid nitrogen and CuCl catalyst (20 mg, 0.205 mmol) was added. The reaction mixture was degassed with 3 freeze-pump-thaw cycles (each 15 minute long) to remove oxygen. Hereafter the polymerization was carried out at 25^{0}C for 24 h under argon atmosphere. The resulting dark brown polymer solution was passed through a silica gel column using methanol as solvent to remove the copper. After removing methanol by rotary evaporation the polymer precipitated into excess cold diethyl ether and isolated by filtration. The precipitate was dried under vacuum giving a good yield of 1 g (82%) of the diblock copolymer. ^{1}H-NMR (250 MHz in ^{6}d-DMSO): δ 4.9 (s, -OH), 3.9 -3.4 (-COOC**H**$_2$CH$_2$-, -C**H**$_2$C**H**$_2$O-, -COOCH$_2$C**H**$_2$), 2.1-1.5 (-C**H**$_2$- backbone of PHEMA), 0.8 ((-C**H**$_3$ of PHEMA); FTIR (cm^{-1}): 3405, 2892, 2741, 1731, 1469, 1359, 1344, 1279, 1244, 1153, 1112, 1060, 964, 843; GPC: Mn = 6560, Mw = 8350, Pd (Mw/Mn) = 1.27

2.1.1.3. Synthesis of triblock copolymer PEG-b-PHEMA-b-PMMA

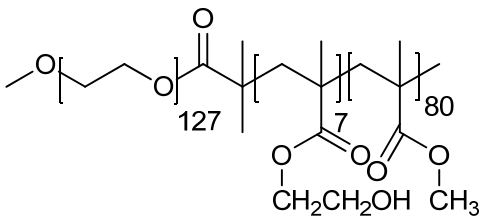

PEG-b-PHEMA-Cl (500 mg, 0.076 mmol), MMA (0.647 mL, 6.46 mmol), $CuCl_2$ (7.7 mg, 0.057 mmol), PMDETA (0.052 mL, 0.25 mmol) and 2 mL of DMF were added to a 25 mL schlenk flask containing a stirrer bar. The solution was frozen in liquid nitrogen, and CuCl catalyst (7 mg, 0.076 mmol) was added. After degassing using three freeze-pump-thaw cycles (each cycle 15 minute long) to remove oxygen, the polymerization was carried out at 35^0C for 25 h under argon atmosphere. The mixture was then concentrated under vacuum and the polymer was precipitated in petroleum ether. The crude triblock polymer was extracted with water to remove the possible existing water soluble PEG-b-PHEMA diblock copolymer. The purified water insoluble triblock copolymer was filtered and lyophilized giving 0.7 g (63%) of the desired compound. ^{1}H-NMR (250 MHz in DMSO): δ 4.9 (s, -OH), 4.0-3.4 (-COOC**H**$_2$CH$_2$, -C**H**$_2$C**H**$_2$O, -COOC**H**$_3$, -COOCH$_2$C**H**$_2$), 2.1-1.6 (-C**H**$_2$ backbone of PHEMA and PMMA), 1.1-0.5 (-C**H**$_3$ backbone of PHEMA and PMMA); FTIR (cm^{-1}) :3422, 2888, 1731, 1469, 1361, 1342, 1279, 1243, 1148, 1109, 1060, 965, 841; GPC: Mn = 14500, Mw = 19500, PD (Mw/Mn) =1.34, Mn (from ^{1}H-NMR) = 13000.

2.1.2. Synthesis and characterisation of Boc-NH-PEG-b-PHEMA-b-PMMA

2.1.2.1 Synthesis of the macroinitiator Boc-NH-PEG-Br

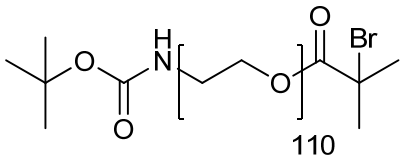

Following a modified procedure by Liu et al, Boc-NH-PEG-OH Mn = 4950 (1000 mg, 0.20mmol) was dissolved in 12 mL of toluene. After azeotropic distillation of 2 mL of toluene under reduced pressure to remove traces of water, TEA (0.053 mL, 0.4 mmol) was added and the solution was cooled to room temperature. 2-bromoisobutyryl bromide (0.038 mL, 0.3 mmol) added drop wise to the above solution and the reaction mixture was stirred at 40 ^{0}C for 2 days. The solution was filtered and most of the toluene was removed by rotary evaporation prior to precipitation into 10 fold excess of cold ether. The crude polymer was dried under vacuum, dissolved in water at pH 8-9 and then extracted with DCM. The organic layer was collected and dried over anhydrous Na_2SO_4. The removal of the solvent under vacuum afforded the purified macro initiator in high yield: 1 g (98%). ^{1}H-NMR (250 MHz in DMSO): δ 3.6 (s, -C**H**$_2$C**H**$_2$O), 1.9 (s, -C(C**H**$_3$)$_2$), 1.4 (s,-COOC(C**H**$_3$)$_3$); FTIR (cm^{-1}): 2896, 1974, 1737, 1640, 1469, 1361, 1342, 1279, 1243, 1150, 1112, 1060, 1060, 961, 841; GPC: Mn = 5100, Mw = 5151, PD (Mw/Mn) = 1.01.

2.1.2.2. Synthesis of diblock copolymer Boc-NH-PEG-b-PHEMA

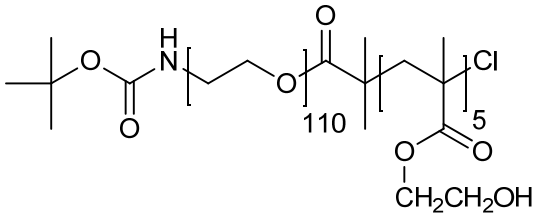

Boc-NH-PEG-Br (700 mg, 0.137 mmol), HEMA (0.178mL, 1.37 mmol), 2,2'bipyridyl (44 mg, 0.287 mmol) and 7 mL of methanol were added to a schlenk flask equipped with a stirrer bar. The flask was frozen in liquid nitrogen and added CuCl catalyst (14.9 mg, 0.151 mmol). The reaction mixture was degassed with three freeze-pump-thaw cycles (each 15 minute long) to remove the oxygen. The polymerization was hereafter carried out at 25^0C for 24 h under argon atmosphere. The resulting dark brown polymer solution was passed through a silica gel column to remove the copper catalyst using methanol as solvent. After removing most of the methanol by rotary evaporation the polymer was precipitated into excess cold diethyl ether and isolated by filtration. The precipitate was dried under vacuum giving a good yield of 0.66 g (77%). ^{1}H-NMR (250 MHz in DMSO): δ 4.9 (s, -OH), 4.0-3.4 (-COOC**H**$_2$CH$_2$,-C**H**$_2$C**H**$_2$O, -COOCH$_2$C**H**$_2$), 2.0-1.5 (-C**H**$_2$ backbone of PHEMA), 1.4 (s, -COOC(C**H**$_3$)$_3$), 0.8 (-C**H**$_3$ of PHEMA); FTIR (cm^{-1}): 3452, 2887, 2741, 1974, 1731, 1645, 1469, 1359, 1344, 1281, 1243, 1148, 1114, 1060, 963, 946, 841; GPC: Mn = 6300, Mw = 7430, PD (Mw/Mn) = 1.18.

2.1.2.3. Synthesis of triblock copolymer Boc-NH-PEG-b-PHEMA-b-PMMA

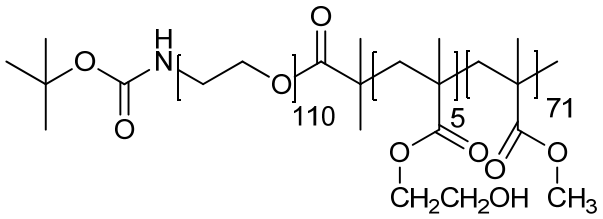

Boc-NH-PEG-b-PHEMA-Cl (500 mg, 0.079 mmol), MMA (0.72 mL, 6.74 mmol), $CuCl_2$ (8.5 mg, 0.0632 mmol) PMDETA (0.057 mL, 0.27 mmol) and 3 mL of DMF were added to a 25 mL schlenk flask equipped with a stirrer bar. The solution was frozen in liquid nitrogen and CuCl catalyst (7.8 mg, 0.079 mmol) was added. After degassing using three freeze-pump-thaw cycles (each cycle 15 minute long) to remove the oxygen, the polymerization was carried out at 35^0C for 25 h under argon atmosphere. The reaction mixture was then concentrated under vacuum and the polymer was precipitated in petroleum ether. The crude triblock copolymer was extracted with water to remove the possible existing water soluble BocNH-PEG-b-PHEMA diblock copolymer. The purified water insoluble triblock copolymer was filtered and lyophilized gives an yield 0.7 g (61%) of the desired polymer. ^{1}H-NMR (250 MHz in DMSO): δ 4.8 (s, -OH), 3.9-3.4 (-COOC**H**$_2$CH$_2$, -C**H**$_2$C**H**$_2$O, -COOC**H**$_3$, -COOCH$_2$C**H**$_2$), 2.0-1.5 (-C**H**$_2$ backbone of PHEMA and PMMA), 1.4 (s,-COOC(C**H**$_3$)$_3$), 1.1-0.5 (-C**H**$_3$ of PHEMA and PMMA); FTIR (cm^{-1}): 3439, 2952, 1967, 1733, 1634, 1488, 1451, 1352, 1277, 1247, 1195, 1150, 1107, 1060, 961, 912, 841; GPC: Mn = 14400, Mw = 19900, PD (Mw/Mn) = 1.38, Mn (from ^{1}H-NMR) = 12810.

2.2. Synthesis of PEG-b-PAzEMA-b-PMMA and BocNH-PEG-b-PAzEMA-b-PMMA

2.2.1. Synthesis of PEG-*b*-PAzEMA-*b*-PMMA

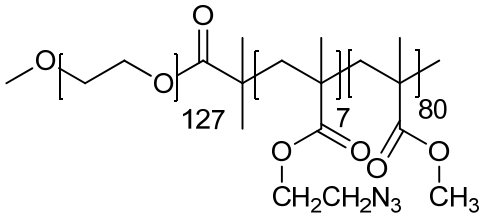

The triblock copolymer PEG-b-PHEMA-b-PMMA (1 g, 0.068 mmol) was dissolved in 15mL dry pyridine and the solution was cooled to 0^0C. To the solution MsCl (0.259 mL, 3.4 mmol) in dry DCM (5mL) was added drop wise over several minutes. The resulting solution was warmed to room temperature and stirred over night. After filtration of the solid precipitate, the filtrate was washed with saturated $NaHCO_3$ solution, extracted with DCM and dried over anhydrous Na_2SO_4. After removing most of DCM by rotary evaporation, the reaction mixture was precipitated into excess of cold diethyl ether to obtain yellow Mesylated polymer. The Mesylated polymer (200 mg, 0.013mmol) was dissolved in 3ml DMF, followed by NaN_3 (45 mg, 0.689 mmol) was added .The reaction mixture was stirred at 90^0C for 5 hours under argon atmosphere, then at room temperature for another 20 hours. After removing most of the DMF under vacuum, the polymer was precipitated into excess of cold diethyl ether followed by drying under vacuum gives PEG-b-PAzEMA-b-PMMA polymer. This triblock copolymer was further purified by dissolve in DMF and dialysis against MilliQ water for 3 d .The pure product was then recovered by lyophilization gives yield of 0.72 g (72%). ^{1}H-NMR (250 MHz in DMSO): δ 4.1-3.4 (-C**H**$_2$CH$_2$N$_3$, -C**H**$_2$C**H**$_2$O, -COOC**H**$_3$, -CH$_2$C**H**$_2$N$_3$), 2.0-1.6 (-C**H**$_2$ backbone of PHEMA and PMMA), 1.0-0.6 (-C**H**$_3$ of PHEMA and PMMA); FTIR (cm^{-1}): 2952, 2896, 2107, 1729, 1486, 1451, 1385, 1350, 1275, 1243, 1191, 1148, 1109, 987, 963, 841, 748.

2.2.2. Synthesis of NH_2-PEG-b-PAzEMA-b-PMMA

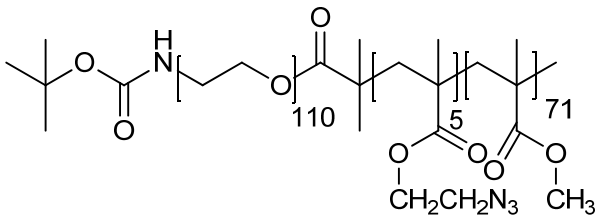

The triblock copolymer Boc-NH-PEG-b-PHEMA-b-PMMA (200 mg, 0.013 mmol) was dissolved in 3mL dry pyridine and the solution was cooled to 0^0C. MsCl (0.049 mL, 0.65 mmol) in dry DCM (1mL) was added drop wisely over several minutes to the above solution. The resulting solution was warmed to room temperature and stirred over night. After filtration of the solid precipitate, the filtrate was washed with saturated $NaHCO_3$, extracted with DCM and dried over anhydrous Na_2SO_4. After removing most of DCM by rotary evaporation, the yellowish mesylated polymer was precipitated into excess of cold diethyl ether and dried under vacum. The mesylated polymer (200 mg, 0.0132 mmol) was dissolved in 3ml DMF, followed by NaN_3 (45 mg, 0.689 mmol) was added. The reaction mixture was stirred at 90^0C for 5 hours under argon atmosphere, and then at room temperature for another 20 h. After removing most of the DMF under vacuum, the polymer was precipitated into excess of cold diethyl ether, filtered and dried under vacuum gives Boc-NH-PEG-b-PAzEMA-b-PMMA polymer. The copolymer was further purified by dissolved in DMF, subsequently dialyzed against MilliQ water for 3 d and recovered by lyophilisation. Isolated yield 0.13 g (70%). ^{1}H-NMR (250 MHz in DMSO): δ 4.1-3.4 (-C**H**$_2$CH$_2$N$_3$, -C**H**$_2$C**H**$_2$O, -COOC**H**$_3$, -CH$_2$C**H**$_2$N$_3$), 2.0-1.6 (-C**H**$_2$- backbone of PHEMA and PMMA), 1.36 (s, -COOC(C**H**$_3$)$_3$), 1.0-0.6 (-C**H**$_3$ of PHEMA and

PMMA); FTIR (cm^{-1}): 3439, 2952, 2896, 2107, 1731, 1486, 1449, 1389, 1348, 1273, 1243, 1193, 1148, 1109, 987, 961, 843, 750.

NH_2-PEG-b-PAzEMA-b-PMMA: The amphiphilic triblock copolymer Boc-NH-PEG-b-PAzEMA-b-PMMA (100 mg, 0.0069 mmol) was dissolved in 1 mL of DCM, followed by TFA (1 mL TFA in 1 mL DCM) was added and stirred at room temperature for 12 h. The solvent was removed under vacuum and the polymer was precipitated into excess of cold diethyl ether and dried. The complete de-protection was confirmed by disappearance of Boc- group signal at δ (1.36 ppm) ^{1}H-NMR (250 MHz in DMSO).

2.3. Synthesis of cyclic RGD peptide-c(RGDfK) and click reactive fluorophores

2.3.1. Synthesis of NH_2-Asp(tBu)-D-Phe-Lys(Boc)-Arg(Pbf)-Gly-OH

The immobilized linear pentapeptide NH_2-Asp(tBu)-D-Phe-Lys(Boc)-Arg(Pbf)-Gly-2-Chlorotrityl Resin was synthesized manually on 2-Chlorotrityl resin preloaded with NH_2-Gly-OH (330mg,1.1mmol/g) by standard Fmoc methodology. Each coupling was achieved by 4 equiv. Fmoc protected amino acid, 3.95 equiv. HATU and 8 equiv. 2,4,6-colidine in DMF. Cleavage of the Fmoc group was achieved by 20% piperidine in DMF for 2×5min. Each acylation and deprotection step was monitored by the Kaiser ninhydrin test. The peptide was cleaved from the solid support by addition of CH_2Cl_2/TFE/AcOH (7:2:1) for 30min after which the solvent was removed and the peptide lyophilized from a mixture of water and acetonitrile to give a white powder. The purity of the crude product was monitored by analytical HPLC (+95%) which was used in the next step without further purification.

Synthesis of c(RGDfK)

NH_2-Asp(tBu)-D-Phe-Lys(Boc)-Arg(Pbf)-Gly-OH (500mg, 0.485mmol) was dissolved in dry DMF (100mL) and NaHCO3 (204mg, 2.43mmol) and diphenyl phosphoryl azide (400mg, 1.46mmol) were added under stirring at RT and allowed to react overnight. The solvent was removed *in vacou* and and the crude product re-dissolved in EtOAc (75mL) and washed with sat. NH_4Cl (aq) (2×75mL) and brine (2×75mL). The organic phase was dried with $MgSO_4$, filtrated and reduced *in vacou* to give a white solid which was dissolved in TFA/H_2O/TIS (95:2.5:2.5) for 1h. The solvent was removed *in vacou* and the product lyophilized from a mixture of water and acetonitrile. Final purification was achieved by semi-preparative HPLC by employing a Knauer Eurospher 100-5 C_{18} 5µm (20*250mm) column. Eluent: (A) 5% CH_3CN + 0.1% TFA in H_2O, (B) 0.1% TFA in CH_3CN. Gradient profile; linear gradient from 0% B to 30% B over 10min, 30% B to 100% B from 10-20min. Flow rate; 20 mL/min. c(RGDfK) was isolated as a homogenous peak with retention time of 8.54 min. The solvent was removed in vacou and the product lyophilized from a mixture of water and acetonitrile to give a white fluffy powder (157mg, **54%**). The purity of the product was monitored by analytical HPLC using the same gradient profile and solvent mixtures as above but with a Waters C_{18} 5µm (4.6*150mm) column. Purity >98%. MALDI-TOF MS (m/z) (DHB+Na): Calcd. For $C_{27}H_{41}N_9O_7$ $(M+H)^+$ 604.32. Found:604.52.

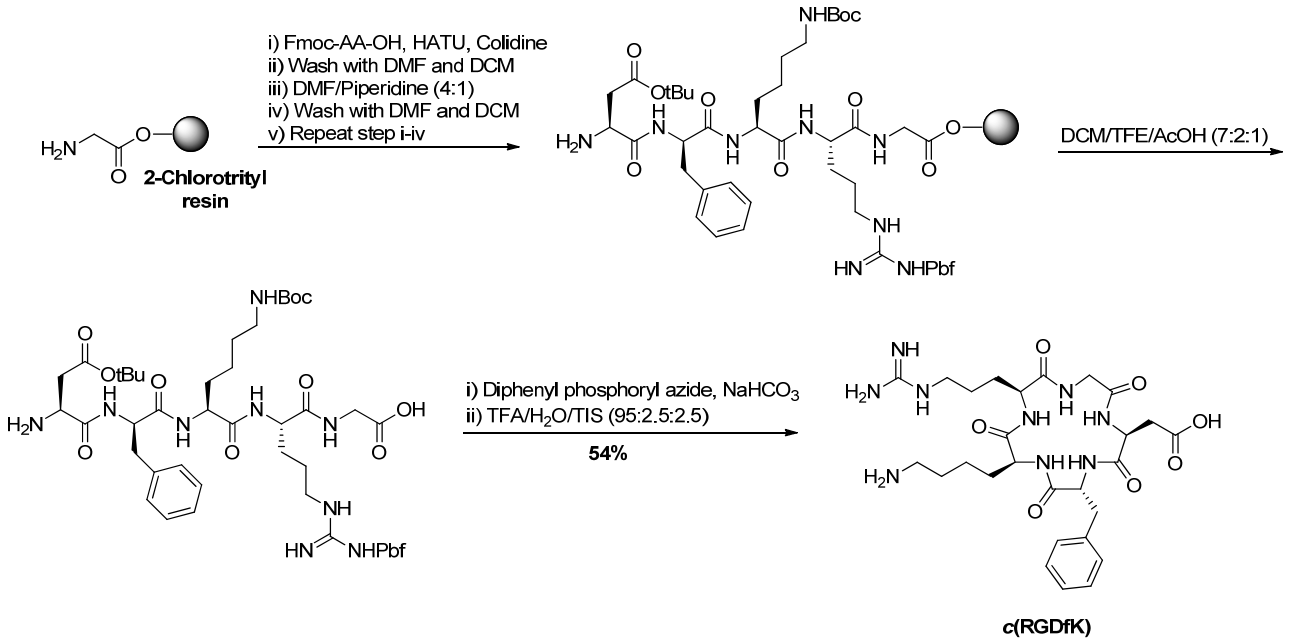

Scheme S1: Synthesis of c(RGDfK) by solid phase peptide synthesis.

2.3.2. Synthesis of 4-Pentynyl Rhodamine B ester (Rhodamine B- alkyne)

4-Pentynyl Rhodamine B ester was synthesized by the esterification reaction between Rhodamine B and 4-Pentyn-1-ol. 4-pentyn-1-ol (263 mg, 3.13 mmol) was dissolved in DCM (10mL) and cooled to 0^0C. Rhodamine B (500 mg, 1.04 mmol), EDC.HCl (550 mg, 2.87 mmol), and DMAP (508 mg, 4.16 mmol) were added under stirring and the reaction mixture was left at room temperature under N_2 atm. for 48 h in the absence of light. The reaction mixture was concentrated and purified by column chromatography gives 0.507 g (77%) mercury-shiny solid product. ^{1}H-NMR (300 MHz in $CDCl_3$): δ 9.44 (bs, 1H), 8.28 (dd, 1H, J = 1.1Hz, 7.8Hz), 7.81 (d, 1H, J = 1.5Hz, 7.5Hz), 7.73 (d, 1H, J = 1.4Hz, 7.6 Hz), 7.30 (dd, 1H, J = 1.1Hz, 7.5Hz), 7.06 (d, 2H, J = 9.5Hz), 6.87 (dd, 2H, J = 2.4Hz, 9.5Hz), 6.81 (d, 2H, J = 2.4Hz), 4.12 (t, 2H, J = 6.2Hz), 3.64 (q, 8H, J = 7.2Hz) 2.16 (s, 6H), 2.07 (d, 2H, J = 2.7Hz, 7.1 Hz), 1.90 (t, 1H, J = 2.7Hz), 1.69 (m, 2H), δ 1.31(t, 12H, J = 7.2Hz); ^{13}C NMR (75 MHz, $CDCl_3$): δ 165.2, 159.0, 157.9, 155.8, 133.7, 133.4, 131.6, 131.5, 131.5, 130.6, 130.5, 130.1, 114.4, 113.7, 96.6, 82.7, 69.5, 64.4, 54.7, 46.4, 27.5, 15.4, 12.9.

2.3.3. Synthesis of Fluorescein-Alkyne[2, 3]

Fluorescein isothiocyanate (FITC) (100 mg, 0.26 mmol) in THF (3mL) was added propargylamine (0.070 µL, 1.04 mmol) and 0.5 mL of TEA. The reaction mixture was stirred under argon atmosphere at room temperature in the absence of light. The progress of the reaction was monitored by TLC, after completion of the reaction (3h), the solvents and un-reacted propargylamine were removed under vacuum to yield a red-orange solid. ^{1}H NMR (300 MHz, DMSO): δ 9.93 (s, 1H), 8.37 (s, 1H), 7.71 (s, 1H), 7.11 (d, 1H, J = 8.4 Hz, ArH), 6.92–6.46 (m, 6H, ArH), 5.31 (s, 1H, ArH), 5.27 (s, 1H, ArH), 4.86 (s, 2H, CH2), 3.16 (s, 1H, C≡CH); ^{13}C NMR (75 MHz, DMSO): 169, 160,152, 147, 145, 142, 129, 125, 124, 112.6, 112, 109, 103, 102, 83, 79, 72, 68, 56; FTIR (cm^{-1}): 3060, 1736, 1636, 1590, 1496, 1464, 1386, 1315, 1270, 1207, 1180, 1109, 1044,995, 915, 848.

2.4. Conjugation of c(RGDfK) peptide to NH_2-PEG-b-PAzEMA-b-PMMA

The c(RGDfK) peptide (10 mg, 0.016 mmol) was dissolved in 1 mL dry DMF followed by anhydrous triethylamine (0.022 mL, 0.16 mmol) and disuccinimidylcarbonate (4 mg, 0.016 mmol) were added and stirred at room temperature under Argon for 8 h. After 8 h, NH2-PEG-PAzEMA-PMMA (200 mg, 0.016 mmol) was added and stirred at room temperature for 24 h. Most of the solvent was removed under vacuum and the product precipitated from excess of cold diethyl ether. The qualitative Kaiser test was performed, colourless solution indicate the absence of free amino groups. FTIR (cm^{-1}): 3277, 2105, 1721, 1670, 1639, 1535.

2.5. Conjugation of pH sensitive and reference fluorophores to PEG-b-PAzEMA-b-PMMA

2.5.1. Preparation of PEG-*b*-PAzEMA-*b*-PMMA micelle

The amphiphilic triblock copolymer PEG-*b*-PAzEMA-*b*-PMMA (500 mg, 0.034 mmol) was dissolved in 50 mL DMF by stirring overnight. To this clear solution under stirring, 5 mL of MilliQ water was added drop wise with in the time interval of 30 minute, followed by 100 mL more MilliQ water was added drop wise. The cloudy micelle solution was then transferred into dialysis tubing of molecular weight cut-off (MWCO) 12 kDa and dialysis against MilliQ water for 3 d. Final micelle concentration is 2.5 mg/mL. Hydrodynamic diameter (D_h) = 33 ± 2 nm and zeta potential (ξ) = -13 ± 2 mV.

2.5.2. Conjugation of Rhodamine B-alkyne to PEG-*b*-PAzEMA-*b*-PMMA

To the PEG-*b*-PAzEMA-*b*-PMMA micelle (40 mL, 100 mg, 0.0068 mmol), was added 10 mL tert.butanol and $CuSO_4.5H_2O$ (2.54 mg, 0.010 mmol). The mixture was allowed to stir at RT for 15 min, followed by freshly prepared aqueous solution of sodium ascorbate (4.0 mg in 1 mL MilliQ water, 0.020 mmol) and Rhodamine B-alkynes (dissolved in 0.2mL of MilliQ water) (4.27 mg, 0.0068 mmol) was added. The reaction mixture allowed to stirrer at room temperature for 3 d in the absence of light. The crude product was transferred into dialysis tubing of MWCO 12 kDa and dialysis against carbonate buffer (pH = 9) for 3 d and then against MilliQ water for another 3 d. The solution was then lyophilised to get the solid Rhodamine B bounded amphiphilic triblock.

2.5.3. Conjugation of Fluorescein-alkyne to PEG-*b*-PAzEMA-*b*-PMMA

The PEG-*b*-PAzEMA-*b*-PMMA micelle (40 mL, 100 mg, 0.0068 mmol), 10 mL tert.butanol and $CuSO_4.5H_2O$ (2.54 mg, 0.010 mmol) were allowed to stir at RT for 15 min. Freshly prepared aqueous solution of sodium ascorbate (4.0 mg in 1 mL MilliQ water, 0.020 mmol) and Fluorescein-alkyne (dissolved in 0.2mL of methanol) (2.91 mg, 0.0068 mmol) were added and the reaction mixture was stirred at room temperature for 3 d in the absence of light. The crude mixture was transferred into dialysis tubing of MWCO 12 kDa and dialysis against carbonate buffer for 3 d and then against MilliQ water for another 3 d. The solution was then lyophilised to get the solid Fluorescein bounded amphiphilic triblocks.

2.5.4. Conjugation of Oregon Green-alkynes to PEG-*b*-PAzEMA-*b*-PMMA

To the PEG-*b*-PAzEMA-*b*-PMMA micelle (40 mL, 100 mg, 0.0068 mmol), was added 10 mL tert.butanol and $CuSO_4.5H_2O$ (2.54 mg, 0.010 mmol). The mixture was allowed to stir at RT for 15 min, followed by freshly prepared aqueous solution of sodium ascorbate (4.0 mg in 1 mL MilliQ water, 0.020 mmol) and Oregon Green488 alkyne 6-isomer (dissolved in 0.2 mL of DMF) (3.05 mg, 0.0068 mmol) was added. After stirring at room temperature for 3 d in the absence of light, the reaction mixture was transferred into dialysis

tubing of MWCO 12 kDa and dialysis against carbonate buffer for 3 d and then against MilliQ water for another 3 d. The solution was then lyophilised to get the solid Oregon Green bounded polymer.

2.6. Synthesis of dendritic click cross-linker ((Alkyne)$_4$-[G-1]))

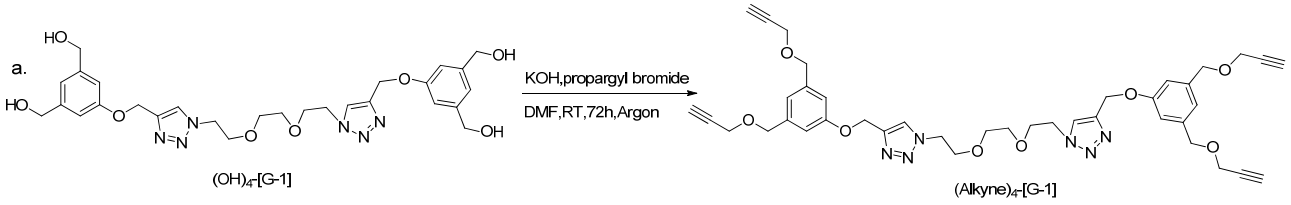

Scheme S2. Synthesis of dendritic alkyne click cross-linker

The dendritic alchol $(HO)_4$-[G-1] was synthesised by procedure described in the literature[4]. A solution of $(HO)_4$-[G-1] (500 mg, 0.73 mmol) in anhydrous DMF (5 mL) was stirred at 0 °C with propargyl bromide (80 wt.% in Xylene) (3 mL, 33 mmol). Portions of finely ground KOH (2490 mg, 44.5 mmol) was added over a period of 30 min. The reaction mixture was warmed to room temperature and stirred for 24h under argon atmosphere, the course of the reaction was monitored by TLC (10% MeOH in DCM $R_{f(product)}$ = 0.80). After completion of the reaction, the mixture was concentrated to dryness and the residue partitioned between DCM (100 mL) and brine (20 mL). The organic layer was washed with water and dried over anhydrous Na_2SO_4. The solvent was removed under reduce pressure to get the crude product, which was further purified by Column chromatography. The column was first run with the solvent system 1:1 Ethylacetate : Hexane to remove the traces of impurity, then changed to 1:1 Methanol : Ethylacetate, yield 450 mg (84%). ^{1}H-NMR (300 MHz in $CDCl_3$): δ 7.8 (s, 2H, triazole), 6.95 (s, 4H, Ar**H**), 6.94 (s, 2H, Ar**H**), 5.20 (s, 4H, triazole-C**H**$_2$O), 4.59 (s, 8H, -C**H**$_2$OCH$_2$C≡CH), 4.54 (t, 4H, -CH$_2$OCH$_2$C**H**$_2$-triazole), 4.1 (d, J = 2Hz, 8H, -CH$_2$OC**H**$_2$C≡CH), 3.84 (t, 4H, -CH$_2$OC**H**$_2$CH$_2$-triazole), 3.54 (s, 4H, -C**H**$_2$OCH$_2$CH$_2$-triazole), 2.45 (t, J = 2Hz, 4H, -CH$_2$OCH$_2$C≡C**H**); FTIR(cm^{-1}): 3282, 3138, 2111, 1600, 1459, 1352, 1290, 1078, 842, 641.

2.7. Synthesis of shell cross linked micelle using CuBr(PPh$_3$)$_3$/DIPEA catalyst

The PEG-b-PAzEMA-b-PMMA micelle solution in MilliQ water was dialysed (MWCO = 12 kDa) against THF : buffered water (1:4) for 3 d. The solution was transferred into 100 mL round bottom flask equipped with a stirrer bar. To the stirred solution of PEG-PAzEMA-PMMA micelle in 1:4 THF : buffered water (100 mg, 0.0069 mmol, 0.048 mmol of azide), was added $CuBr(PPh_3)_3$ (prepared by the literature procedure)[5] (13 mg, 0.014 mmol), DIPEA (0.025mL, 0.144 mmol), Cu wire (ca. 100 mg), and the dendritic cross linker $(Alkyl)_4$-[G-1] (in 0.5 mL of THF) (18 mg, 0.024 mmol). The reaction mixture was allowed to stirrer at RT for 3d. The crude product was transferred to dialysis tubing (MWCO = 12 kDa) and dialyzed against MilliQ water and THF (5 : 1) for 4d then against MilliQ water for another 4 d. Dh (DLS) = 31±1 nm, Zeta potential = -12±2 mV. FTIR (cm^{-1}): 3268, 1726, 1596, 1443, 1237, 1145, 983, 838, 747.

2.8. Synthesis of shell cross linked micelle using CuSO$_4$.5H$_2$O/Sodiumascorbate catalyst

The stirred solution of PEG-PAzEMA-PMMA micelle (100 mg (40 mL), 0.0069 mmol, 0.048 mmol of azide) in MilliQ water was added 10 mL of tert.butanol, $CuSO_4.5H_2O$ (3.6 mg, 0.014 mmol), Sodium ascorbate (28 mg, 0.144 mmol) (5%wt aqueous solution) and the dendritic cross linker $(Alkyl)_4$-[G-1] (in 0.5 mL of THF) (18 mg, 0.024 mmol). The reaction mixture was stirred at room temperature for 3 d. The crude product was transferred into dialysis tubing (MWCO = 12 kDa) and dialysis against MilliQ water and THF

(5 : 1) for 4 d and then against MilliQ water for another 4 d. Dh (DLS) = 33±2 nm, Zeta potential = -11±1 mV. FTIR (cm^{-1}): 3270, 2107, 1728, 1599, 1447, 1239, 1148, 988, 839, 748.

2.9. Fabrication of shell cross-linked targeted ratiometric mixed micelle pH nanosensors

The amphiphilic triblock copolymer PEG-b-PAzEMA-b-PMMA conjugated to Fluorescein (3.43 mg, 0.23 µmol), Oregon Green (1.47 mg, 0.10 µmol), Rhodamine B (0.049 mg, 0.0033 µmol), cRGDfK peptide (0.098 mg, 0.0067 µmol) and free PEG-PAzEMA-PMMA (4.9 mg, 0.33 µmol) in the ratio 7 : 3 : 0.1 : 0.2 : 10 (total 10 mg) were dissolved in 2 mL of DMF by stirring overnight. To the polymer solution under stirring, 0.2 mL of MilliQ water was added within the time interval of 30 minute followed by 4 mL more water added drop wise. The cloudy micelle solution was transferred into dialysis tubing of MWCO (12 kDa) and dialysis against MilliQ water for 3 d (Dh = 39±2 nm, Zeta potential = -19±2 mV) and then against buffered water : THF (4:1) for another 3 d.

The mixed micelle solution (10 mg, 0.68 µmol, 4.8 µmol of azide) was transferred into a round bottom flask equipped with a stirrer bar. To this solution was added $CuBr(PPh_3)_3$ (1.36 mg, 1.4 µmol), DIPEA (2.5 µL, 14.4 µmol), Cu wire (ca. 2 mg), and the dendritic benzylether cross linker $(Alkyl)_4$-[G-1] (in 100 µL of THF) (1.76 mg, 2.4 µmol). The reaction mixture was allowed to stirrer at RT for 3 d, transferred into dialysis tubing (MWCO 12 kDa) and dialyse against MilliQ water : THF (5 : 1) for 4 d and then against MilliQ water for another 4 d. Final sensor concentration in MilliQ water was = 1.25 mg/mL. Dh = 38±1 nm, Zeta potential = -17±1 mV.

3. Results in supporting informations

3.1. NMR spectra of PEG-b-PHEMA-b-PMMA and BocNH-PEG-b-PHEMA-b-PMMA

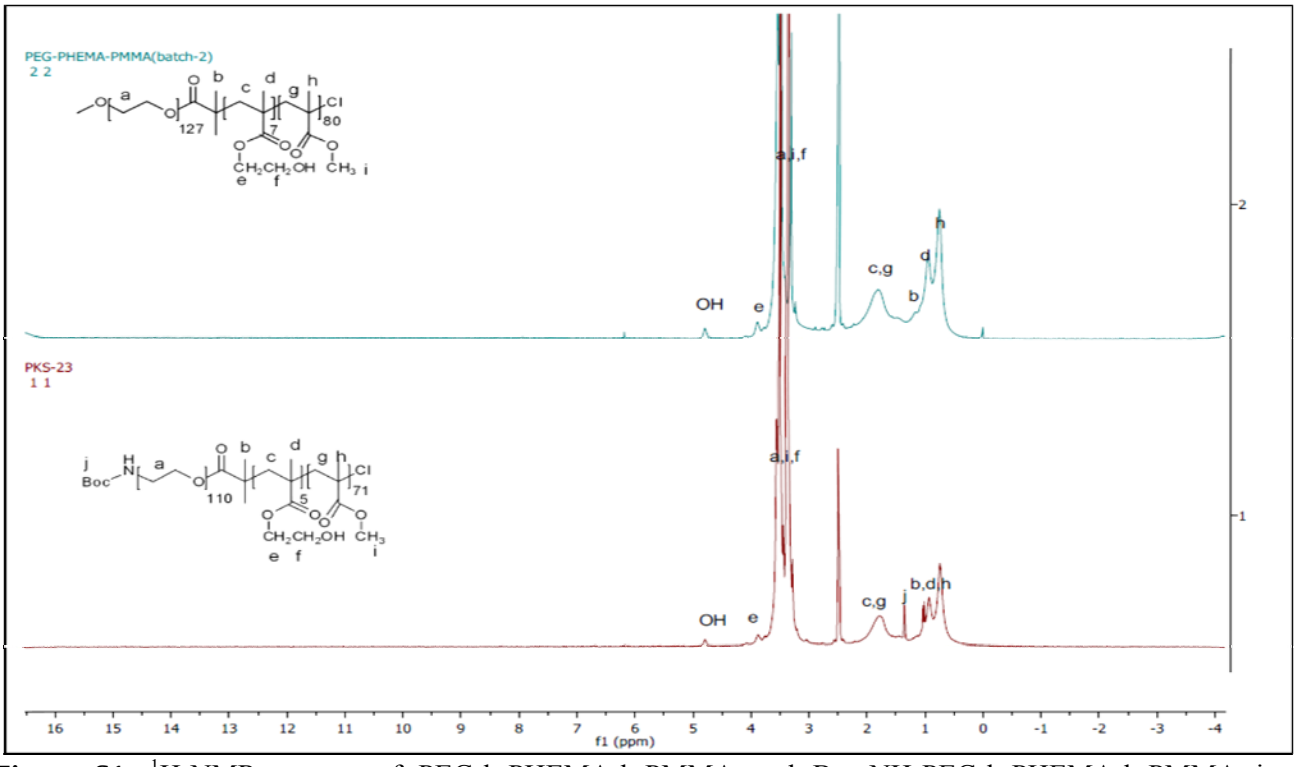

Figure S1. ^{1}H-NMR spectra of PEG-b-PHEMA-b-PMMA and Boc-NH-PEG-b-PHEMA-b-PMMA in ^{6}dDMSO

3.2. NMR spectra of PEG-b-PAzEMA-b-PMMA and BocNH-PEG-b-PAzEMA-b-PMMA

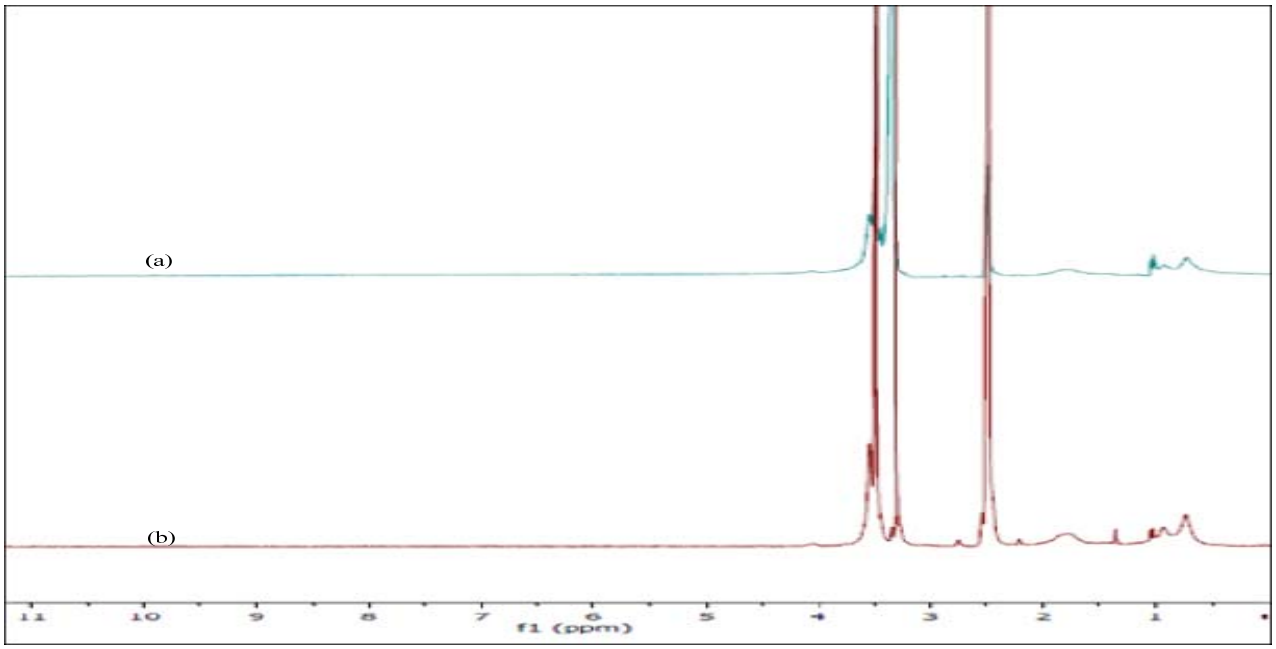

Figure S2.NMR spectra of PEG-PAzEMA-PMMA (a) and BocNH-PEG-PAzEMA-PMMA (b) in ^{6}d DMSO

3.3. IR spectra of c(RGDfK) conjugated PEG-b-PAzEMA-b-PMMA

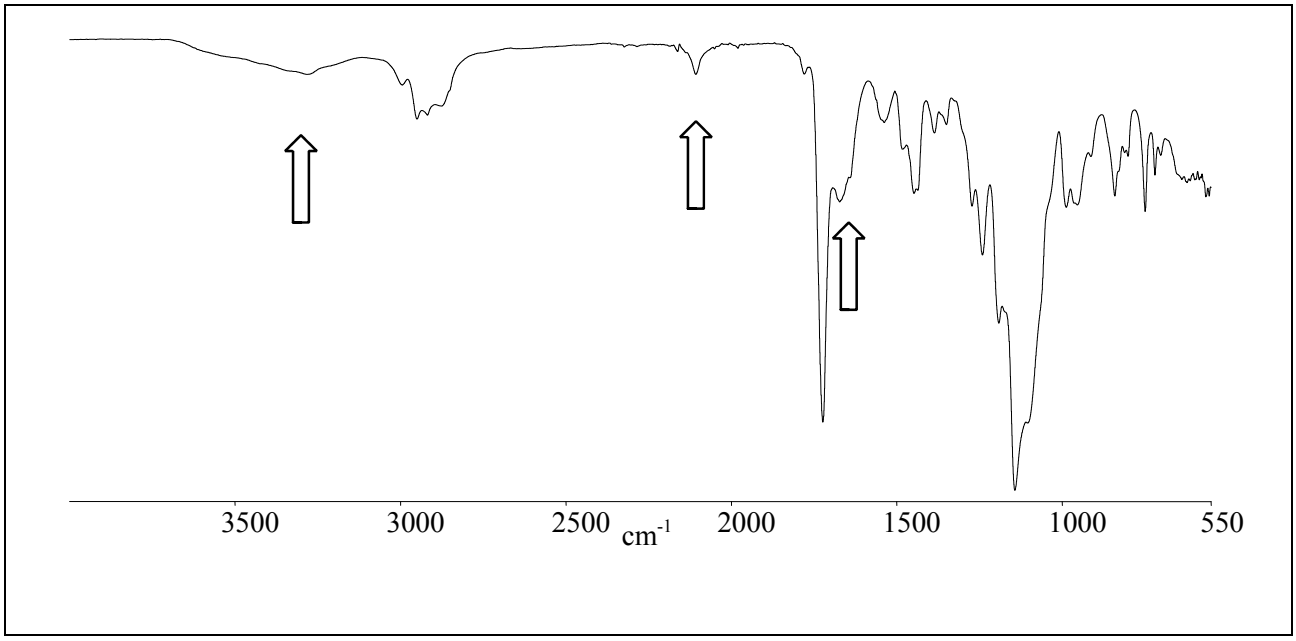

Figure S3. Arrows indicating the N-H, azide and amide CO stretching vibrations of c(RGDfK)NHCONH-PEG-b-PAzEMA-b-PMMA, y-axis % of transmittance (arbitrary unit).

3.4. IR spectra of CuSO4.5H2O/Sodiumascorbate catalysed click shell cross linking

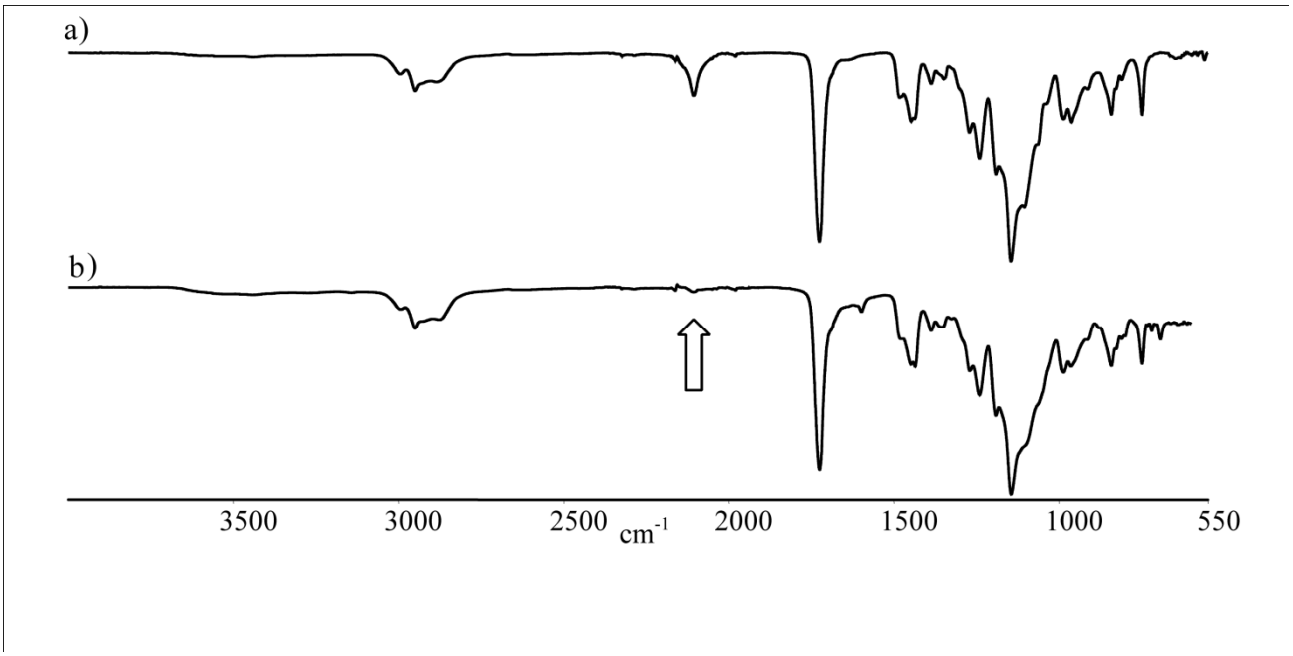

Figure S4. IR spectra of $CuSO_4.5H_2O$/Sodiumascorbate catalysed click shell cross linked PEG-b-PAzEMA-b-PMMA micelle (b) and the none cross linked micelle (a).The arrow in (b) indicate the presence of azide stretching at 2107 cm^{-1} due to the incomplete shell cross linking, y-axis % of transmittance (arbitrary unit)

References

[1] S. Liu, J. V. M. Weaver, Y. Tang, N. C. Billingham, S. P. Armes, K. Tribe, *Macromolecules* **2002**, *35*, 6121.

[2] B. P. Mason, S. M. Hira, G. F. Strouse, D. T. McQuade, *Organic Letters* **2009**, *11*, 1479.

[3] M. Ikeda, J. Minari, N. Shimada, M. Numata, K. Sakurai, S. Shinkai, *Organic & Biomolecular Chemistry* **2007**, *5*, 2219.

[4] M. J. Joralemon, R. K. O'Reilly, J. B. Matson, A. K. Nugent, C. J. Hawker, K. L. Wooley, *Macromolecules* **2005**, *38*, 5436.

[5] R. Gujadhur, D. Venkataraman, *Synthetic Communications* **2001**, *31*, 2865.